

Cononsolvency of Microgels: Equilibrium and Dynamics

Von der Fakultät für Mathematik, Informatik und Naturwissenschaften der
RWTH Aachen University zur Erlangung des akademischen Grades einer
Doktorin der Naturwissenschaften genehmigte Dissertation

vorgelegt von

Katja Nothdurft, M.Sc.

aus

Mobile (AL), USA

Berichter: Univ.-Prof. Dr. rer. nat. Walter Richtering
Univ.-Prof. Dr.-Ing. André Bardow

Tag der mündlichen Prüfung: 1. September 2021

Diese Dissertation ist auf den Internetseiten der Universitätsbibliothek verfügbar.

Die vorliegende Arbeit wurde zwischen Juni 2017 und April 2021 am Institut für Physikalische Chemie der RWTH Aachen unter der wissenschaftlichen Leitung von Prof. Dr. Walter Richtering angefertigt. Diese Arbeit entstand im Rahmen des Sonderforschungsbereiches 985 (Funktionale Mikrogele und Mikrogelsysteme).

Parts of the chapters in this dissertation were published previously. In the following, the contributions to the presented results are listed:

Chapter 1/4: Parts of the chapters were published. Adapted from: Nothdurft, K.; Müller, D. H.; Brands, T.; Bardow, A.; Richtering, W., Enrichment of methanol inside PNIPAM gels in the cononsolvency-induced collapse. *Phys. Chem. Chem. Phys.* **2019**, *21*, 22811-22818. with permission from PCCP Owner Societies.

I performed all experimental work, namely the synthesis of the macroscopic gels, the Raman measurements, and spectral evaluation. Raman experiments and modeling were done in cooperation with the Institute of Technical Thermodynamics in André Bardow's group. I wrote the whole manuscript. All coauthors acted as discussion partner for the experimental approach and proof-read the manuscript.

Chapter 5: The results concerning the solvatochromic microgels are unpublished.

The functionalized Nile Red label bearing a carboxylic acid group was provided by the group of Dr. Andrey Klymchenko at the Laboratoire de Biophotonique et Pharmacologie at the University of Strasbourg (France). I performed the microfluidic synthesis, the subsequent labeling, and characterization of the microgels. The fluorescence spectroscopy measurements and evaluation were conducted in collaboration with Dr. Silvia Centeno Benigno. Experimental approaches and results were mutually discussed. I wrote the whole chapter myself.

Chapter 6: Reproduced from: Kleinschmidt, D.; Nothdurft, K.; Anakhov, M. V.; Meyer, A. A.; Mork, M.; Gumerov, R. A.; Potemkin, I. I.; Richtering, W.; Pich, A., Microgel organocatalysts: modulation of reaction rates at liquid–liquid interfaces. *Mater. Adv.* **2020**, *1*, 2983-2993. – Published by The Royal Society of Chemistry.

Synthesis, catalytic testing, and other experiments for the characterization (NMR, TGA, ATR-FTIR) were conducted by Denise Kleinschmidt, Anna Meyer, and Matthias Mork. I performed the dynamic and static light scattering experiments and wrote the corresponding parts in the manuscript. Computer simulations were done by Mikhail Anakhov and Rustam Gumerov. All coauthors acted as discussion partner and proof-read the manuscript. Solely the results of the scattering experiments performed by myself are discussed in detail in this chapter. However, the remaining experimental part and results published are briefly presented in order to enable the placement in the context.

Chapter 7: The results of the osmotic pressure experiments are unpublished.

I performed all experimental work and the evaluation myself. Experimental approach and results were discussed with Dr. Andrea Scotti and Prof. Walter Richtering. I wrote the whole chapter myself.

Chapter 8: Parts of the chapter were published. Adapted with permission from: Nothdurft, K.; Müller, D. H.; Mürtz, S. D.; Meyer, A. A.; Guerzoni, L. P. B.; Jans, A.; Kühne, A. J. C.; De Laporte, L.; Brands, T.; Bardow, A.; Richtering, W., Is the Microgel Collapse a Two-Step Process? Exploiting Cononsolvency to Probe the Collapse Dynamics of Poly-N-isopropylacrylamide (PNIPAM). *J. Phys. Chem. B* **2021**, *125*, 1503-1512. Copyright 2021 American Chemical Society.

I synthesized microgels, designed the investigation setup, performed solvent-jump experiments, all Raman measurements and the data evaluation, and wrote the whole manuscript. The master for the microfluidic solvent-jump setup was printed by Arne Lüken. Raman experiments and modeling were done in cooperation with the Institute of Technical Thermodynamics in André Bardow's group. Experimental work, such as sample preparation and solvent-jump experiments, was supported by the students Sonja Mürtz and Anna Meyer under my supervision. Alexander Jans, Luis Busca Guerzoni, Prof. Laura De Laporte, and Prof. Alexander Kühne taught me microfluidics and were involved in very early-stage discussions on other investigation setups during my master thesis. David Müller, Dr. Thorsten Brands, Prof. André Bardow, and Prof. Walter Richtering acted as discussion partners for the experimental approach and interpretation and proof-read the manuscript.

Kurzzusammenfassung

Mikrogele sind dreidimensionale, vernetzte polymere Netzwerke, die in einem guten Lösungsmittel gequollen vorliegen. Poly-*N*-Isopropylacrylamid (PNIPAM)-basierte Materialien sind aufgrund ihres responsiven Verhaltens auf äußere Parameter, wie Temperatur und Lösungsmittelzusammensetzung, von großem Interesse. Obwohl PNIPAM-Mikrogele Gegenstand einer Vielzahl von anwendungsorientierten Studien sind, werden fundamentale Fragen immer noch diskutiert. Der Fokus dieser Arbeit liegt auf der Sensitivität von PNIPAM gegenüber der Zusammensetzung von Wasser-Methanol-Mischungen, der sogenannten Cononsolvency. Dabei sind die Gele in den reinen Lösungsmitteln gequollen, während Mischungen um 20 mol% Methanol ein Kollabieren der Gele bewirken.

Im ersten Teil dieser Arbeit wurden die Eigenschaften des Polymernetzwerks im Vergleich zu seiner Umgebung im Gleichgewicht untersucht. Massenbilanzexperimente in Kombination mit Raman-Mikrospektroskopie zeigten eine Anreicherung von Methanol im Inneren von makroskopischen PNIPAM-Gelen für ungünstige Wasser-Methanol-Gemische. Diese bevorzugte Adsorption von Methanol wurde durch Messergebnisse zur Fluoreszenzlebensdauer von solvatochromen Mikrogelen bestätigt. Darüber hinaus weisen die kollabierten PNIPAM-Mikrogele in ungünstigen Mischungen eine geringere Polarität auf als ihre Umgebung. Die Möglichkeit, die Eigenschaften der Mikrogele durch äußere Parameter zu steuern, wurde genutzt, um die katalytische Aktivität von PNIPAM-basierten Mikrogel-Katalysatoren zu modulieren. Des Weiteren wurden die mechanischen Eigenschaften von Mikrogelen durch Variation des externen osmotischen Drucks untersucht. Es wurde ein Übergang von einem weichen, verformbaren Polymernetzwerk zu einem steiferen, teilweise kollabierten Objekt beobachtet.

Im zweiten Teil wurde die Dynamik des Volumenphasenübergangs untersucht. Viele Anwendungen von responsiven Mikrogelsystemen beruhen auf der schnellen und reversiblen Anpassungsfähigkeit des Polymernetzwerks an die Umgebungseigenschaften. Um den Ablauf des Kollapses weiter aufzuklären, wurden fluoreszenzmarkierte Mikrogele im Mikrometerbereich untersucht. Ein speziell angefertigter Mikrofluidik-Aufbau ermöglicht einen schnellen Wechsel von reinem Wasser zu dem ungünstigen Gemisch aus 20 mol% Methanol in Wasser. Das Entquellungsverhalten wird durch einen zweistufigen Prozess beschrieben. Die größte Volumenänderung findet im ersten, schnellen Prozess statt, bei dem die Mikrogele noch porös sind. Im zweiten, langsameren Prozess werden nur geringe Größenänderungen beobachtet. Die Abhängigkeit der Relaxationszeiten vom Mikrogeldurchmesser wird unter Berücksichtigung der adhäsionsbedingten Verformung der Gele und der dem Kollaps zugrundeliegenden physikalischen Prozesse diskutiert.

Abstract

Microgels are three-dimensional, cross-linked polymeric networks swollen by a good solvent. Poly-*N*-isopropylacrylamide (PNIPAM)-based materials are of ongoing scientific interest due to their unique responsive behavior to external parameters such as temperature and solvent composition. Although PNIPAM microgels are the subject of a variety of application-oriented studies, fundamental aspects about the underlying processes of the responsive behavior are still under discussion. The present work focuses on the sensitivity of PNIPAM to the composition of water-methanol mixtures, the so-called cononsolvency effect. Here, the gels are swollen in either of the pure solvents, whereas water-rich mixtures around 20 mol% methanol cause deswelling of the gels.

In the first part of this thesis, the internal properties of the microgels in different swelling states in comparison to their surroundings were studied under equilibrium conditions. Mass balance experiments combined with Raman microspectroscopy revealed an enrichment of methanol inside the macroscopic PNIPAM gels for the cononsolvency-inducing water-methanol mixtures. This preferential adsorption of methanol was confirmed by measurements of the fluorescence lifetime of solvatochromic microgel beads. In addition, the collapsed PNIPAM microgel beads exhibit a lower polarity in unfavorable mixtures than the respective binary water-methanol mixtures. The possibility to control the properties of the microenvironment provided by microgels using external stimuli was exploited to modulate the catalytic activity of PNIPAM-based microgel-catalysts. Furthermore, the mechanical properties of microgel beads were investigated by variation of the external osmotic pressure. Upon compression, a transition from a soft, deformable polymer network to a stiffer, partially collapsed object was observed.

In the second part, the dynamics of the volume phase transition were studied. Many applications of responsive microgel systems rely on the fast and reversible adaptability of the polymer network to changes in the environment. To further elucidate the kinetics of the polymer response, fluorescently labeled PNIPAM microgel beads in the micrometer range were studied. A custom-made microfluidic setup allows a fast solvent exchange from pure water to the unfavorable mixture of 20 mol% methanol in water. The deswelling behavior is described by a two-step process. The major volume change occurs in the initial, rapid process where the microgels are still porous. In the second, slower process, only minor changes in size are observed. The dependence of the relaxation times on the microgel's diameter is discussed taking into account the adhesion-induced deformation of the gels and the physical processes underlying the collapse.

Contents

1. Introduction.....	1
1.1 Functional microgels	2
1.2 The cononsolvency effect	4
2. Scope of the thesis	9
3. Synthesis and characterization methods	11
3.1 Microfluidics	11
3.1.1 Droplet microfluidics	12
3.1.2 Synthesis of PNIPAM microgel beads by microfluidics	14
3.1.3 Differentiation between microgel beads and microgels from precipitation polymerization.....	16
3.2 Raman (micro)spectroscopy	18
3.2.1 The Raman effect.....	19
3.2.2 Indirect hard modeling (IHM)	21
3.2.3 Raman setup.....	23
3.2.4 Raman spectra of water, methanol and their mixtures.....	24
3.3 Fluorescence	25
3.3.1 Fluorescence microscopy.....	27
EQUILIBRIUM.....	29
4. Enrichment of methanol inside PNIPAM gels in the cononsolvency- induced collapse	29
4.1 Introduction	30
4.2 Swelling behavior of macroscopic PNIPAM gels	32
4.3 Mass balance experiments	32
4.4 Peak shift analysis	35
4.5 Variation of the cross-linker content	40
4.6 Conclusions	41
5. Probing the internal environment of solvatochromic microgel beads.....	43
5.1 Introduction	43

5.2	Synthesis of solvatochromic microgel beads	45
5.3	Probing the local polarity by fluorescence spectroscopy	47
5.4	Fluorescence lifetime imaging (FLIM)	48
5.5	Conclusions	51
6.	Modulation of the catalytic activity of microgel-catalysts by external triggers	53
6.1	Introduction	54
6.2	Characterization of the microgel-catalysts	55
6.3	Catalytic testing and simulations	59
6.4	Conclusions	61
7.	Mechanical properties of PNIPAM microgel beads.....	63
7.1	Introduction	63
7.2	Deswelling by osmotic pressure	65
7.3	Comparison of dextran (150 000 g/mol) and PEG (8000 g/mol)	70
7.4	Conclusions	71
	DYNAMICS.....	73
8.	Dynamics of the cononsolvency-induced collapse: A two-step process?	73
8.1	Introduction	74
8.2	Microfluidic platform.....	76
8.3	Setup characterization	78
8.3.1	Width of the solvent interface	79
8.3.2	Velocity of the solvent-jump.....	81
8.3.3	Visual appearance of the microgel beads	83
8.4	Solvent-jump experiments	84
8.4.1	Image evaluation	86
8.5	Size evolution after a solvent-jump	87
8.6	Dependence of deswelling kinetics on the size of the microgel bead.....	90
8.6.1	Influence of the adhesion	91
8.6.2	Discussion of the deviation from the Tanaka and Fillmore scaling law .	94
8.7	Conclusions	95

9. Summary and outlook	97
10. Experimental section	101
10.1 Materials	101
10.2 Macroscopic PNIPAM gels	102
10.2.1 Mass balance experiments	102
10.3 Microfluidics	102
10.3.1 Preparation of microfluidic devices	103
10.3.2 Microfluidic synthesis.....	103
10.3.3 PNIPAM microgel beads with varying size and cross-linker content ...	105
10.3.4 Nile Red-labeled microgel beads.....	106
10.3.5 Rhodamine-labeled microgel beads.....	106
10.4 Raman microspectroscopy measurements.....	107
10.4.1 Indirect hard modeling (IHM)	107
10.4.2 Raman measurements of macroscopic PNIPAM gels	108
10.4.3 Characterization of the solvent-jump setup	109
10.5 Fluorescence measurements	110
10.5.1 Fluorescence spectroscopy	110
10.5.2 Fluorescence lifetime imaging (FLIM).....	111
10.5.3 Time-resolved fluorescence microscopy	111
10.5.4 Spinning-disk confocal fluorescence microscopy	112
10.6 Synthesis and characterization of L-proline modified PNIPAM microgels.....	112
10.6.1 Dynamic light scattering (DLS).....	113
10.6.2 Static light scattering (SLS).....	114
10.7 Osmotic pressure experiments.....	114
References.....	115
List of symbols and abbreviations.....	139
Appendix.....	143

1. Introduction

Polymers are large macromolecules comprising multiple repeating units of low molecular mass known as monomers.^[1] One key goal of research in polymer sciences is to mimic the diversity and adaptability of systems found in nature by synthetic materials. Here, environmentally sensitive polymers that can adapt to changes, e.g. in temperature, solvent composition, or pH, are promising candidates.^[2] These polymers are often referred to as “smart” or “responsive” materials. The most prominent examples for responsive polymers are poly-*N*-isopropylacrylamide (PNIPAM)-based systems.^[3-7] Aside from linear polymers, advances in synthesis procedures enable the production of a variety of architectures such as stars, polymer brushes, (hyper)branched polymers, or three-dimensional, cross-linked polymer networks.^[8-13] The latter are generally termed as polymer gels or hydrogels when swollen by water.^[14] The covalent cross-links provide structural integrity and can be realized, e.g. by the addition of a cross-linking agent or by self-cross-linking.^[4,5] Microgels are a sub-category of polymer gels defined as gel particles of any shape with an equivalent diameter between 100 nm and 100 μm .^[14] All PNIPAM-based materials independent of their size exhibit a stimuli-responsive behavior. PNIPAM-based microgels are often used as a model system for soft materials as they can combine characteristics of flexible polymers and rigid particles.^[5,15] Additionally, they are surface-active and readily adsorb at interfaces similarly to surfactants. In general, microgels can adapt to environmental changes by a transition from a soft, porous polymer network to a collapsed particle resembling a hard colloid.^[4] This volume phase transition is accompanied by changes in size and physical properties. Furthermore, there is high flexibility in the synthesis procedures of microgels. Thereby, microgels with different sizes, compositions, morphologies, shapes, functionalities, and compartments can be produced.^[5] In combination with the possibility to reversibly tune their physicochemical properties by external stimuli, PNIPAM-based systems are interesting building blocks for a broad range of applications.^[15] To fully take advantage of the capabilities of responsive microgels, a fundamental and detailed understanding of the underlying physical processes and the timescales of their responsive behavior is crucial. A comprehensive knowledge allows for the systematic development of complex, functional microgel systems and the optimization for targeted applications.

1.1 Functional microgels

Microgels are three-dimensional, intramolecularly cross-linked polymer networks swollen by their surrounding medium in case of good solvent conditions.^[4,5] Typically, microgels are spherical, porous objects with an average size between 100 nm and 100 μm .^[14] Often microgels consist of adaptive polymer systems. These functional microgels show a unique swelling behavior as they change their physical properties, dimensions, structure, and interactions upon changes in the environment. Typical external triggers are temperature,^[3] pH,^[16,17] solvent composition,^[18-22] ionic strength,^[23] pressure,^[24-26] UV exposure,^[27-29] magnetic fields^[30,31] and electrochemical potentials.^[32] Size, shape, and properties such as cross-linking density can be adapted during the synthesis procedure. Furthermore, variation in the synthesis, e.g. by the choice of monomers, co-monomers, the integration of functional moieties or nanoparticles, allows combining multiple sensitivities in one system. Additionally, besides the conventional microgel morphology, a variety of microgel architectures such as hollow spheres,^[33-35] core-shell^[36] or anisometric microgels^[37-40] are accessible nowadays. The most common synthesis method is a free-radical precipitation polymerization,^[4,41] but also emulsion polymerizations^[42-44] and microfluidics^[39,45-50] can be applied to synthesize smart polymer networks.

The most prominent example of a stimuli-responsive polymer is poly-*N*-isopropylacrylamide (PNIPAM).^[3-7] PNIPAM-based systems are widely studied due to their sensitivity to temperature and solvent composition. Linear PNIPAM was already synthesized in 1968 by Heskins and Guillet.^[6] In 1986, the first preparation of a PNIPAM microgel, at that time referred to as aqueous latices of NIPAM, was reported.^[42] Here, the monomer, *N*-isopropylacrylamide (NIPAM), is polymerized in presence of a cross-linker bearing two functional groups such as *N,N'*-methylenebis(acrylamide) (BIS). Thus, cross-links between the linear PNIPAM chains are formed. The swelling ratio, i.e. the difference between the fully swollen and collapsed state of the microgels, is highly determined by the amount of cross-linker. The swelling ratio increases with decreasing amount of cross-links.^[51-53] The lowest degree of cross-linking is achieved by exploiting the self-polymerization of NIPAM without any additional cross-linking agent. These extremely soft and highly deformable microgels are called ultra-low cross-linked (ULC) microgels.^[54-56]

PNIPAM is most known for its reversible temperature-responsive behavior (Figure 1.1). It exhibits an entropy-driven and sharp change in size and other properties with temperature. For pure PNIPAM systems, this transition temperature, also known as the volume phase transition temperature (VPTT), is observed at 32 °C in water.^[3,4] Below the VPTT, the microgels present a swollen, soft and deformable polymer network. The amide groups of the

polymer form hydrogen bonds with the surrounding water molecules. When exceeding the VPTT, hydrophobic interactions between polymer chains predominate over the polymer-solvent interactions. Thus, water is expelled from the polymer network leading to a significant volume loss. The size change is accompanied by a different internal architecture with a more homogeneous polymer density and a sharp surface resembling a hard colloid.^[3] Even in the collapsed state, a significant water content of around 60 – 70% remains in the microgels.^[53,57] The transition temperature can be precisely tuned by the choice of monomer or the incorporation of suitable co-monomers.^[4,58]

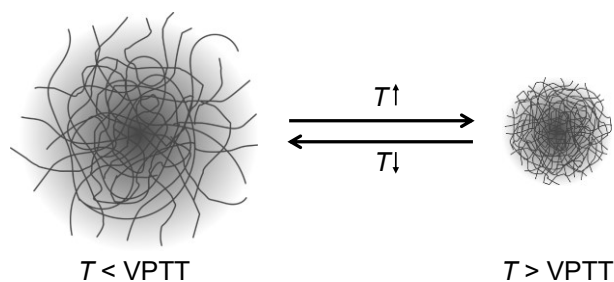


Figure 1.1: Scheme of the temperature-dependent swelling behavior of PNIPAM microgels: the water-swollen network below the VPTT (32 °C in water)^[3] collapses at high temperatures above the VPTT.

Overall, the responsive behavior to various external parameters and the possibility to tailor the properties of microgels during their synthesis make microgels appealing building blocks for a wide field of applications.^[15,59] Due to the transition temperature being close to the physiological temperature of 37 °C, PNIPAM-based materials exhibit a high potential for biomedical applications.^[15,60-62] Microgels have been explored as smart nano-carriers, e.g. in drug-delivery systems^[63-69] or catalysis.^[70-78] The tuneable swelling state and thus permeability of the polymer network allows controlling the uptake, encapsulation, and release of molecules.^[63-69] Also, microgels enable immobilization, stabilization, and easy recycling of catalysts.^[70-78] Due to their interfacially active character, microgels can generate smart emulsions that can be destabilized on demand by external triggers.^[79,80] Furthermore, applications as sensors,^[81-84] actuators,^[85] or switchable membranes for filtration^[86] have been discussed in the literature.

1.2 The cononsolvency effect

Some polymers are sensitive to the composition of solvent mixtures. In certain cases, either of the pure solvents acts as a good solvent, while mixtures of both cause a collapse of the polymer.^[19,87] The effect is referred to as cononsolvency and has been studied since the 1990s.^[87,88] The cononsolvency behavior of linear polymers, macroscopic gels, and microgels has been the subject of many experimental and theoretical investigations.^[19] PNIPAM is known for this effect in mixtures of water and methanol (MeOH),^[19] other alcohols,^[89,90] and other organic solvents such as dimethylformamide (DMF), tetrahydrofuran (THF), dimethyl sulfoxide (DMSO), acetone, acetic acid, or dioxane.^[20,89,91-95] Also, other polymer systems are sensitive to the solvent composition,^[96-98] e.g. polyvinylpyrrolidone (PVP),^[99] polyvinyl alcohol (PVA),^[100] poly-*N,N*-diethylacrylamide (PDEAAM),^[101,102] or copolymers of PNIPAM.^[103,104]

Figure 1.2 schematically depicts the cononsolvency of PNIPAM microgels in water and methanol.^[19] An example of the microgel diameter as a function of the methanol mole fraction is displayed in Figure 1.3. Pure water and pure methanol swell the polymer network. Upon addition of the respective other solvent to a pure solvent system, the microgels undergo a drastic volume loss. The microgels collapse in water-rich mixtures with the most unfavorable mixture at 20 mol% methanol.^[19,22] For the methanol-rich regime, the polymer network is already rather swollen by the solvent mixture. In comparison to the thermo-responsive behavior, PNIPAM microgels collapse less in an unfavorable mixture than at high temperatures in water.^[19] Mass transport of the cosolvent into the polymeric network is required for a cononsolvency-induced deswelling. For a temperature-induced deswelling, solely heat transfer is needed.

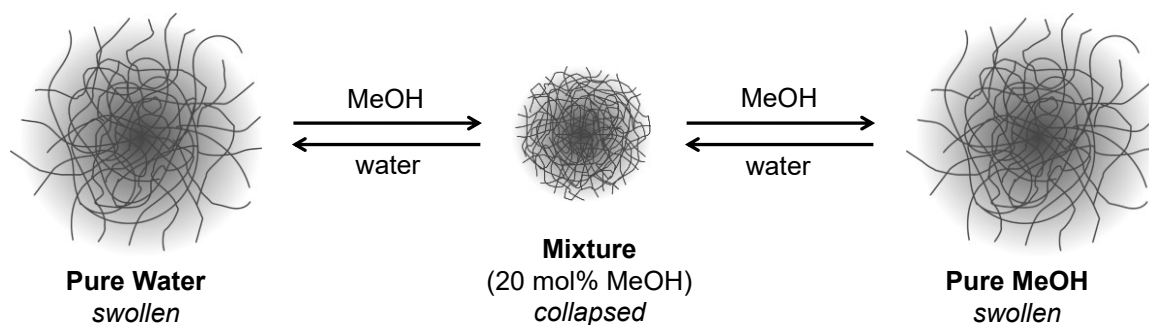


Figure 1.2: Scheme of the cononsolvency effect of PNIPAM microgels in water-methanol mixtures at room temperature: while the pure solvents, water and methanol, act as a good solvent for the microgels, their mixtures around 20 mol% methanol cause a drastic volume loss. Adapted from Scherzinger et al.^[19]

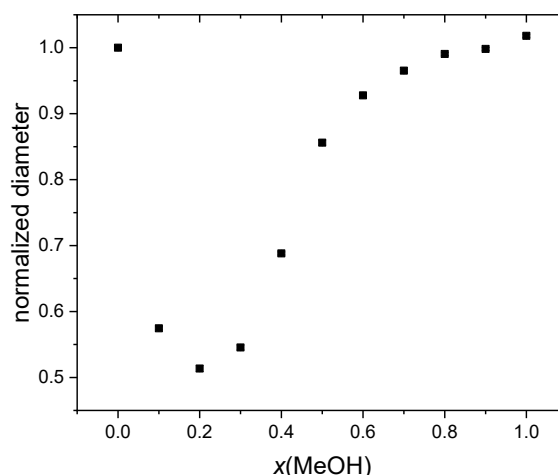


Figure 1.3: Typical course of the microgel diameter as a function of the methanol mole fraction in an aqueous solution. Here, representatively shown for a PNIPAM microgel bead with 5 mol% cross-linker and a diameter in water of 81 μm synthesized by microfluidics.

Multiple explanations regarding the origin of the cononsolvency effect are proposed and controversially discussed in the literature. There are various theories such as competitive hydrogen bonding,^[18,105-107] preferential adsorption,^[107-115] geometric frustration,^[116,117] and strong water-cosolvent interactions^[118] including the formation of water-methanol clusters.^[119] Tanaka et al.^[105] proposed that the cooperativity of hydration is reduced by competitive hydrogen bonding of methanol and water molecules with the polymer. As a result, the polymer undergoes a minimum of the total coverage and collapses. Related to these ideas, the concept of preferential adsorption of the cosolvent is discussed frequently. Here, methanol is assumed to be enriched within the polymer network. According to Dalgicdir et al.^[117] applying computational calorimetry, methanol obstructs the formation of hydrogen bonds between water and the peptide group of PNIPAM causing dehydration of the polymer. The importance of the amide proton to explain the cononsolvency behavior is stressed by Scherzinger and Hofmann et al.^[102,120] They compared the dependence on the solvent composition of PNIPAM, bearing a secondary amide group, to PDEAAM which is a tertiary amide and does not show cononsolvency. Walter et al.^[121] combined swelling experiments with molecular dynamic simulations. They proposed that the methanol molecules orient their methyl groups towards the bulk solvent generating an overall hydrophobic appearance to the water-rich bulk. Further studies by Mukherji et al.^[122] and Zhu et al.,^[94] using experimental data in combination with molecular dynamic simulations or mean-field approaches, suggested additional bridging of the cosolvent between polymer chains. In contrast, indirect mechanisms have been proposed without polymer-solvent interactions: In the work of Zhang and Wu,^[119] stoichiometric water-methanol complexes are formed through hydrogen bonds acting as a poor solvent for PNIPAM. Zuo et al.^[118] also recently supported the idea of strong water-cosolvent interactions exceeding the hydrogen

bonding to the polymer chains in combination with preferential adsorption as the origin of the cononsolvency. Here, results from neutron total scattering were combined with all-atom molecular dynamic simulations. Bischofberger et al.^[123] explained that hydrophobic hydration governs the phase behavior of amphiphilic polymers. The hydration of hydrophobes is decreased by the kosmotropic effect of the cosolvent which strengthens the hydrogen-bonded water network.

Besides studies on the origin of the cononsolvency, the impact of the solvent mixture composition on the physical properties of polymers and gels has been widely investigated. Predominantly, the swelling behavior as a response to a change in solvent composition has been described. Here, microgels have the great advantage that they are colloidally stable even in the collapsed state. Since they do not precipitate like linear chains, more experimental methods such as scattering techniques are applicable.^[19] Scattering methods have been used to determine the size and structure of microgels as a function of the solvent composition.^[18,21,22,104,124] It was found that the composition range in which cononsolvency occurs is almost independent of the cross-linking density of the PNIPAM gels.^[19,21,121] Furthermore, the influence of temperature on the cononsolvency behavior was investigated. Kojima et al.^[18] measured the temperature-dependent change of the hydrodynamic radius of PNIPAM microgels for various water-methanol mixtures. With increasing mole fraction of methanol, the volume phase transition becomes wider until no temperature dependence is detected in methanol-rich mixtures. The VPTT as a function of the solvent composition exhibits a minimum with a transition temperature below 0 °C at around 35 mol% of methanol.^[18] This observation is in concordance with early data from Winnik et al.^[87] for the lower critical solution temperature (LCST) of linear PNIPAM chains. Backes et al.^[125] studied PNIPAM microgels adsorbed on various surfaces compared to bulk solutions at different temperatures and in various water-ethanol mixtures by atomic force microscopy (AFM). The swelling behavior of the adsorbed microgels is influenced by the sample preparation and slight changes of the minimum microgel size were observed. Moreover, the cononsolvency behavior was studied as a function of pressure by small-angle X-ray or neutron scattering (SAXS, SANS).^[124,126,127] At high pressures, the typical cononsolvency behavior found at room temperature and ambient pressure vanishes.

The aforementioned preferential adsorption of one solvent species results in differences in the solvent composition between the polymer-rich phase, e.g. inside a gel, and the surroundings. The solvent partitioning in ternary PNIPAM-water-cosolvent systems was experimentally investigated by mass balance experiments and multiple spectroscopy measurement methods.^[89-91,110,128-131] Further details on these studies and the results from the

present work regarding the solvent composition inside PNIPAM gels are discussed in Chapters 4 and 5.

Furthermore, few investigations on the dynamics of the cononsolvency-induced collapse can be found in the literature. Recently, the time-resolved response of thin films in mixed water-methanol vapors was studied by spectral reflectance, time-of-flight neutron reflectometry and Fourier transform infrared (FTIR).^[132,133] For linear chains and microgels, a two-step process of the dynamics of the collapse after a sudden change of solvent composition has been proposed.^[22,134] In previous work by Keidel et al.^[22] using small PNIPAM microgels, structural changes of the microgels were revealed by time-resolved SAXS and mesoscale hydrodynamic computer simulations. However, the initial collapse could not be experimentally resolved with the time resolution of the SAXS experiments. The contribution of the present work to the understanding of the kinetics of the collapse behavior of PNIPAM microgels is presented in Chapter 8. In this chapter, further experimental and theoretical studies regarding the dynamics of the volume phase transition of responsive polymer systems are discussed in more detail.

2. Scope of the thesis

Smart polymer gels based on poly-*N*-isopropylacrylamide (PNIPAM) gained increasing interest over the past decades. The reversible responsiveness to external parameters such as temperature or solvent composition is essential for a variety of applications. However, fundamental aspects about the underlying processes of the responsive behavior are still under discussion. The main focus of this thesis lies on the cononsolvency effect of PNIPAM gels in water-methanol mixtures. The aim is to deepen the fundamental understanding of local properties depending on the swelling state and the response kinetics of microgels after a sudden external trigger.

Within the following work, different size ranges of gels are studied. The differences in their synthesis approaches, e.g. template synthesis for macroscopic gels, microfluidics for microgels of 20 to 100 μm (referred to as “microgel beads”), and precipitation polymerization for small microgels of several hundred nanometers, result in fundamental structural differences. Thus, Chapter 3 gives a theoretical description of microfluidics, the synthesis of microgel beads, and a comparison to small microgels. Furthermore, the two central characterization methods, Raman spectroscopy and fluorescence, are presented. The subsequent main scientific part of this thesis is divided into two sections: equilibrium (Chapter 4 – 7) and dynamic (Chapter 8) investigations. Each chapter includes an abstract and a short, more specific introduction into the approach and the main question addressed. All experimental details are described in Chapter 10. The first chapters concern equilibrium studies to gain insights on the kind of microenvironment the PNIPAM gels provide compared to their surroundings. Chapter 4 reports on macroscopic PNIPAM gels which were equilibrated in water-methanol mixtures. A mass balance approach was combined with Raman spectroscopic measurements to study the solvent partitioning and molecular interactions. Chapter 5 describes the synthesis of solvatochromic microgel beads labeled with Nile Red. The polarity and hydrogen-bonding environment was probed using fluorescence spectroscopy and lifetime imaging. Chapter 6 presents the impact of the previously studied polarity and swelling state of microgels on a model catalysis system using small L-proline modified PNIPAM microgels. The last equilibrium study (Chapter 7) focuses on the mechanical properties of PNIPAM microgel beads. Here, microgel beads with different cross-linking and sizes were immersed in solutions with varying osmotic pressure exerted by high molecular weight dextran to calculate the bulk moduli. In the second part (Chapter 8), the dynamics of the volume phase transition of PNIPAM gels were investigated. A previous study using small microgels and time-resolved small-angle X-ray scattering

proposed a two-step collapse after a sudden solvent-jump. The polymer collapse could not be resolved entirely, especially with regard to the rapid initial deswelling. Therefore, larger PNIPAM microgel beads, thus with slower kinetics, were exposed to a solvent-jump in a custom-made microfluidic device in the present work. The response was visualized by fluorescence microscopy. The size evolution and the dependence of the kinetics on the microgel bead size are discussed.

3. Synthesis and characterization methods

The following sections provide an overview of the theoretical background of the primarily used synthesis method, microfluidics including a differentiation from precipitation polymerization. Furthermore, the two main characterization approaches, Raman spectroscopy and fluorescence methods, are briefly introduced.

3.1 Microfluidics

Microfluidics has emerged as a new technology since the beginning of the 1990s. It describes the controlled manipulation of small volumes (nano- to attoliter) by microfluidic devices with channel dimensions of tens to hundreds of micrometers.^[135] The origin of microfluidics emerged from the motivation to create small analysis platforms for (bio)chemical purposes.^[135-139] Nowadays, microfluidics is applied in a vast amount of applications such as analysis, screening assays, biomedical research, material synthesis, microreactors, sensors, to name a few.^[39,135,140-144] Due to the miniaturization of dimensions, only small volumes and thus, quantities of reagents are necessary. The miniaturization leads to a reduction of the ecological footprint, time, and costs. The large surface-to-volume ratio and low thermal mass in these systems facilitate heat transfer and temperature control. Microfluidic devices allow controlled flow manipulation through miniaturized channels, valves, pumps, mixers, filters, separators, etc.^[145,146] To characterize the fluid behavior in confined spaces, various dimensionless quantities are available.^[147] The Reynolds number (Re) relates the inertial forces to viscous forces and is defined as

$$Re = \frac{vl\rho}{\eta} \quad (1)$$

where v is the fluid velocity, l a characteristic length, ρ the density, and η the viscosity of the fluid. At low Reynolds numbers, the flow is laminar as the viscous forces overwhelm inertial forces. Above a critical, high Reynolds number ($Re > 2000$), the flow becomes turbulent.^[147] The flow regime encountered in the dimensions of microfluidic devices at common fluid velocities usually remains within the laminar flow regime. Other typical dimensionless numbers are the capillary number, relating viscous forces to surface tension, and the Péclet number, relating convection and diffusion.^[147]

3.1.1 Droplet microfluidics

Microfluidics is a powerful tool to generate highly monodisperse emulsion droplets from two immiscible phases. The droplet formation is affected by various parameters such as channel geometry and surface properties of the channels, flow rates of the fluid phases, their viscosities, densities, and interfacial tension.^[148] Typical microfluidic designs for droplet generation are shown in Figure 3.1, namely co-axial flowing stream, T-junction, and flow-focusing geometries.^[46,148] Each design carries intrinsic features leading to a precise droplet formation.

In general, the droplet formation is based on the balance between the interfacial tension and the shear forces posed on the dispersed phase by the continuous phase.^[149] Droplet microfluidic devices can be operated in the dripping or jetting regime. In the dripping regime, droplets of the dispersed phase are generated, whereas the dispersed phase does not break into individual droplets but forms an even stream in the jetting regime. A dimensionless number important to understand and predict the droplet formation is the capillary number.^[148] It describes the balance between local shear stresses and capillary pressure. For droplet generation, capillary numbers are typically between 10^{-3} and 10. In case of the flow-focusing geometry, the ratio of the capillary numbers of the continuous and dispersed phase controls the transition between dripping and jetting.^[148]

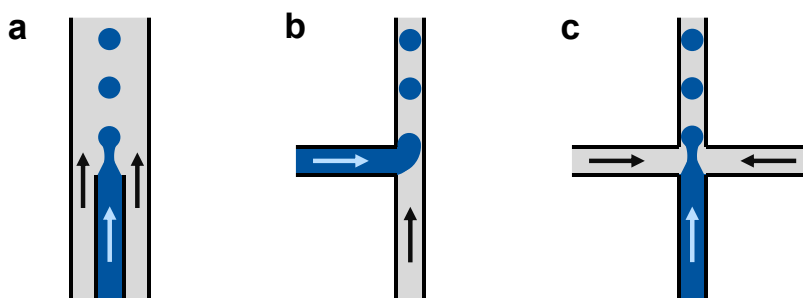


Figure 3.1: Schematic drawings of microfluidic designs for droplet generation: (a) co-flowing stream (b) T-junction, and (c) flow-focusing geometry. The dispersed and continuous phases are depicted in blue and grey, respectively. Arrows indicate the flow direction. Adapted from ref. [148].

Microfluidic devices for droplet generation can be fabricated from different materials. The two most common ones are glass capillaries and elastomeric polymers such as polydimethylsiloxane (PDMS).^[150,151] Glass capillary devices are coaxially arranged glass capillaries that have to be aligned with high precision by hand to achieve optimal performance. This time-consuming, filigree process is compensated by the high solvent resistance of glass.^[150] Additionally, the wettability can be easily adjusted by treatment with appropriate surface modifiers to render the surface hydrophobic or hydrophilic. In the case

of double emulsions, different surface properties are desired for the different channels. Here, glass capillary devices offer the advantage that each capillary can be modified individually before assembling the device as well as there are low wetting constraints due to the three-dimensional setup.^[152] In contrast, the modification of individual channels on a PDMS chip is more complicated.^[153] However, the fabrication of PDMS microfluidic devices by soft lithography is easy and inexpensive.^[154] The preparation of a PDMS-based device is described in detail in Figure 10.1 of section 10.3.1. Briefly, a silicon master patterned with any desired design is covered by a PDMS precursor. After curing, the PDMS is peeled off exhibiting the inverse pattern of the master, and holes for the tubing are punched. By oxygen bonding, e.g. to a microscope slide, the microchannels of the microfluidic setup are fabricated. The structured master is reusable and a numerous amount of identical microfluidic devices can be replicated.^[151]

The main restriction of PDMS-based microfluidics is the limited solvent compatibility of PDMS.^[155] Certain organic solvents swell, deform or dissolve the PDMS reducing the number of possible reaction systems. For emulsions, the channels of the microfluidic device are modified to prevent wetting by the dispersed phase.^[156] The surface modification can be achieved by physical modification such as plasma treatment^[157] or chemical modification. Chemical derivatization can be realized by covalent attachment of hydrophobic or hydrophilic molecules,^[158-160] physi-/chemisorption,^[161,162] or polymer grafting.^[163,164] A common treatment for single water-in-oil emulsions is the silanization with a fluoroalkyl silane.^[165] Another approach is the deposition of Parylene C.^[166] Here, several micrometers of Parylene C can be deposited onto the channels using chemical vapor deposition to increase hydrophobicity and prevent swelling of the PDMS.^[167] The longevity of a surface treatment depends on the modification method and usage conditions.^[156] The modification of the channel surfaces adjusted to the desired application is crucial to prevent wetting of the channel walls by the dispersed phase which would lead to non-uniform droplet formation. In addition to wetting, there are multiple further phenomena causing droplet failure or polydispersity such as satellite droplet formation, coalescence, or fouling of the device.^[156]

Emulsion droplets fabricated by droplet microfluidics can be exploited as templates for the polymerization of a variety of monomers to obtain monodisperse microgel beads. This strategy gives control over microgel sizes, shapes, morphologies, and compositions.^[39,46-50] Optimized systems reach polydispersities below 2 – 3 %.^[46] There are numerous synthetic methods for the polymerization of the droplets.^[148] For a free-radical polymerization, a typical initiator system is ammonium persulfate (APS) in one of the immiscible phases and the accelerator *N,N,N',N'*-tetramethylethylenediamine (TEMED) in the other phase.^[168,169] After droplet formation, the TEMED diffuses into the droplet where their redox reaction

leads to the formation of radicals starting the polymerization on-chip. Furthermore, photo- or thermo-initiators, or pre-polymer systems with cross-linkable side groups can be used.^[38,39,170] Here, the microdroplets can be polymerized directly on-chip or collected and polymerized off-chip in a collection vial or another microfluidic device. For on-chip polymerization, it is crucial to precisely limit the external trigger, e.g. the irradiation, to the outlet channel to prevent clogging of the inlet channels by prematurely polymerized reagents.^[38,150,171] Furthermore, a reaction system with rapid polymerization kinetics, adjusted channel dimensions and flow rates allow the synthesis of anisometric particles. Here, the droplets formed at the cross-junction are squeezed and/or elongated in the outlet channel determining their shape.^[39] Before leaving the outlet channel, the droplets have to be sufficiently polymerized so that their shape remains and relaxation into spheres off-chip is prevented. Krüger et al.^[38] presented another approach where the flow-focusing microfluidic chip was operated in the jetting regime. To receive anisometric microgels, Krüger et al. applied a strong, pulsed laser for a segmented polymerization of the polyethylene glycol (PEG) precursor solution. Despite single emulsions, droplet microfluidics can be modified to create double or high-order multiple emulsions, microcapsules or even multi-core capsules, Janus-like particles, or microbubbles.^[50,152,153,172-177]

3.1.2 Synthesis of PNIPAM microgel beads by microfluidics

PNIPAM microgels or microcapsules in the micrometer range can be synthesized via droplet microfluidics.^[35,149,168,169,178] Within this thesis, these larger microgels are referred to as “microgel beads”. The easiest synthesis approach is a free-radical polymerization (Figure 3.2): The aqueous phase contains the monomer *N*-isopropylacrylamide (NIPAM), the cross-linker *N,N'*-methylenebis(acrylamide) (BIS), and an initiator such as APS. A comonomer can be added to the aqueous phase, e.g. to render the microgel beads fluorescent or integrate functional side groups for post-modification. The continuous phase is immiscible with water and comprises a surfactant to stabilize the interface of the droplets preventing coalescence. Typical combinations for the continuous phase are a fluorocarbon oil (Novec 7500) with a fluorinated surfactant (Krytox),^[169] kerosene with polyglycerol polyricinoleate (PGPR 90),^[149,179] n-hexadecane with Span 80,^[180] or paraffin oil with a silicone-based surfactant such as ABIL EM 90.^[179,181] Additionally, the reaction accelerator TEMED is added to the continuous phase. TEMED is soluble in both the continuous and aqueous phases. Upon emulsification, TEMED diffuses into the aqueous droplets. Here, a redox reaction with APS takes place initiating the formation of radicals and thus the polymerization. The aqueous droplets act as a spatial limitation for the microgel gelation. Therefore, the final size of the microgel beads can be modified by controlling the droplet

size by adjusting the relative flow rates of the aqueous and continuous phases. After polymerization inside the templating microdroplets, the microgel beads are washed and redispersed in water.^[169]

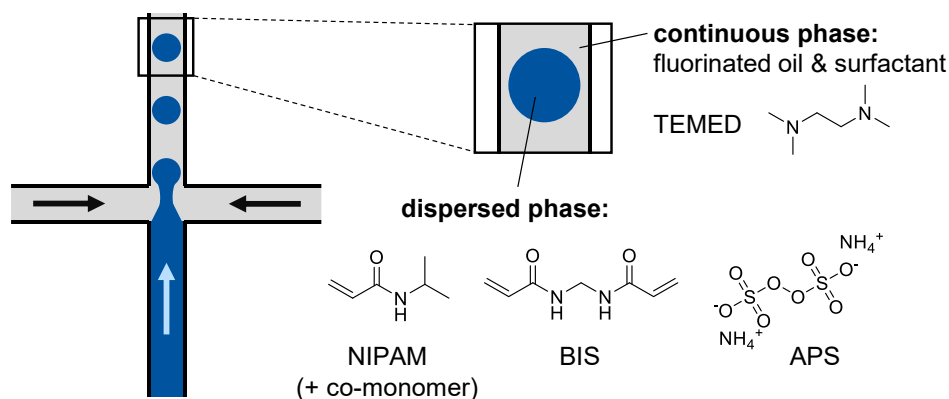


Figure 3.2: Schematic illustration of the PNIPAM microgel beads synthesis using flow-focusing microfluidics. The aqueous phase containing NIPAM, if desired a co-monomer, BIS and APS is dispersed at the cross-junction of the microfluidic device by the oil phase comprising a fluorocarbon oil, fluorinated surfactant, and TEMED. TEMED diffuses into the aqueous droplet, triggers a redox reaction with APS, and thereby initiates the free-radical polymerization.

The microgel bead fabrication starting with low molecular weight monomers has some drawbacks. The uncontrolled polymerization mechanism causes the formation of inhomogeneities on the nano- and micrometer length scale. In addition, the control over cross-linking, copolymerization of functional moieties, or the overall degree of polymerization is limited to adjustments prior to synthesis.^[170,182] Thus, synthesis strategies have been developed separating the polymer synthesis from the microgel bead formation. One method is the polymer-analogous gelation from a pre-polymer solution.^[172,183] Such an approach was realized for cross-linked alginate or gelatin microspheres^[46,184-186] and has been adapted for PNIPAM microgel beads by Seiffert and Weitz.^[170,172] To this end, a photo-cross-linkable pre-polymer comprising linear PNIPAM chains with dimethylmaleimide (DMMI) side groups was synthesized under controlled conditions. A semidilute solution of this pre-polymer is emulsified using microfluidics. Upon UV irradiation in presence of a triplet sensitizer, the DMMI groups transform into dimers leading to permanent interconnections between polymer chains.^[183] The DMMI moieties only slightly influence the thermo-responsive behavior of PNIPAM. The microgel bead synthesis by such a polymer-analogous gelation allows higher control over composition, chain architecture, and homogeneity.

The group of Seiffert studied the influence of the inhomogeneity of PNIPAM microgel beads from microfluidics on their thermoresponsive behavior.^[182] A fast polymerization, e.g. realized by a high amount of initiator or high temperatures, results in a strongly inhomogeneous network. Seiffert et al.^[182] observed an inhomogeneity on the micro- and nanometer

scale. Microgel beads synthesized under mild reaction conditions were found to be more homogeneous. The lowest degree of network inhomogeneity was achieved by the aforementioned controlled polymer-analogous gelation of photo-cross-linkable PNIPAM. Comparing these three systems, no influence of the network inhomogeneity on the temperature-dependent behavior under equilibrium was observed. However, the kinetics of the polymer response varied depending on the synthesis conditions.^[182] Microgel beads with micrometer-sized inhomogeneities showed a continuous and faster deswelling. Furthermore, Huang et al.^[187] reported that the porosity of the polymer network influences the response of microgels. An approach to significantly increase the porosity of PNIPAM microgel beads is the addition of polyethylene glycol (PEG) chains as porogens to the aqueous phase.^[187] Phase separation and the spatial hindrance due to the PEG molecules during polymerization result in a porous morphology of the PNIPAM network. The PEG chains are removed during purification of the microgel beads after synthesis. Chain length and concentration of the PEG additive can be varied to tune the morphology and thereby the volume change and the thermal response rate of the microgel beads.

3.1.3 Differentiation between microgel beads and microgels from precipitation polymerization

Within this thesis, microgels resulting from different synthesis methods are discussed and compared. Formally, the gels synthesized via microfluidics are considered microgels, as are the microgels from precipitation polymerization. However, their structure and accessible size range are fundamentally different due to different synthesis characteristics. To simplify the distinction where necessary, the larger microgels from microfluidics are referred to as “microgel beads” and the ones from precipitation polymerization as “small microgels”. In the following, differences in size and structure of the microgels due to the synthesis method are outlined.

Microgel beads synthesized by droplet microfluidics can reach sizes in the range of ten to several hundred micrometers as they rely on a stable droplet formation in the microfluidic chips.^[149,169] Temperature-responsive microgels in the size range between 100 nm and 3 μm are accessible by free-radical precipitation polymerization above the lower critical solution temperature (LCST).^[4] Here, the water-soluble monomer(s), e.g. NIPAM or *N*-vinylcaprolactam (VCL), a cross-linking agent, and an initiator are dissolved in water. These water-soluble initiators such as peroxide- or azo-based compounds decompose at the reaction temperature producing free radicals. These free radicals attack the monomers followed by radical propagation and chain growth. Reaching a critical molecular weight, the temperature-sensitive polymer chains collapse at the synthesis temperature forming precursor particles.

These polymer-rich phases can grow upon aggregation, deposition on the surface of existing polymer particles, or monomer addition.^[4] The resulting microgel particles are deswollen at the reaction temperature and are electrostatically stabilized by the remaining charges from the initiator.^[3] LCST-type polymers and their microgels swell upon cooling down to below the critical temperature. Here, the microgels are also stabilized by steric mechanisms.^[4] The incorporation of cross-links secures the structure of the polymer network upon swelling. As aforementioned, the softness and swelling behavior is strongly influenced by the amount of cross-linker. Low cross-linker contents correlate with a soft polymer network and a high swelling ability. The size can be controlled by the addition of surfactants, e.g. sodium dodecyl sulfate (SDS), the initiator or monomer concentrations, or the reaction temperature.^[52,188-190] Temperature-ramp or seed and feed protocols allow the preparation of microgels in the intermediate size range up to 5 μm .^[191,192]

A characteristic feature of many polymer gels is a certain degree of spatial inhomogeneity of their cross-linking density. The origin of nano- to microstructural spatial inhomogeneity in polymer gels has been studied since the 1990s.^[193,194] In 2004, Stieger et al.^[195] studied the structure of small temperature-sensitive PNIPAM microgels synthesized by precipitation polymerization. Small-angle neutron scattering revealed an inhomogeneous distribution of the cross-linking density. The radial density profile gradually decreased towards the periphery of the microgel. Thus, small microgels have a highly cross-linked core and a less cross-linked outer region with dangling chains.^[195-197] This characteristic morphology results from the faster consumption of the cross-linker in comparison to the monomer during the synthesis.^[3,193,198,199] However, structural changes occur upon heating to above the volume phase transition temperature (VPTT). The collapse of the polymer chains sharpens the particle surface and an almost box-like radial density profile is found.^[195] Ultra-low cross-linked (ULC) microgels exhibit a similar structural behavior with a fuzzy core-shell structure in the swollen state and a sharp homogeneous structure in the collapsed state.^[54,56] In comparison to conventional microgels, the fuzziness is reduced but still significant.^[54,200]

The microfluidic synthesis of PNIPAM-based microgel beads is fundamentally different from the precipitation polymerization at elevated temperatures. Accordingly, it is not surprising that the internal structure of the resulting microgel beads differs. From a polymer physical point of view, microgel beads from microfluidics resemble more macroscopic hydrogels.^[182] Furthermore, one should keep in mind that a conventional precipitation polymerization and a microfluidic synthesis are typically carried out at different temperatures. The relaxed state of a microgel from precipitation polymerization is the collapsed state as they are synthesized at elevated temperatures well above the VPTT. The microgels experience stress upon swelling at room temperature.^[19,201] In contrast, a

microfluidic synthesis using the APS/TEMED system is carried out at room temperature. The resulting microgel beads are synthesized in a spatially restricted water droplet but not in their collapsed state. Thus, in the more or less swollen conformation, the polymer network is relaxed, whereas stress is exerted on the microgel bead as it collapses.

3.2 Raman (micro)spectroscopy

Raman spectroscopy is a laser-spectroscopic method that allows for in-situ and non-invasive characterization of substances and mixture compositions.^[202-205] It can be applied to any physical state (solid, liquid, and vapor) and offers a wide range of sizes of the probe volume (bulk, microscopic particles, etc.). Furthermore, the main advantages of Raman spectroscopy are that the intensity of the scattered light is proportional to the concentration and that the peak positions within the spectrum represent a kind of fingerprint of the individual molecules and their structure. Thus, quantitative evaluation of the amount of every single compound in a mixture sample is possible. However, the evaluation can become tricky when bands of different components strongly overlap or when nonlinear effects occur. Raman scattering is less widely applied than infrared spectroscopy due to problems, e.g. with fluorescent background signal or degradation.^[202] However, advances in the technology of detectors, lasers, and processing devices simplified the application of the method. Modern setups allow the automatic recording of spectra in real-time due to short exposure times. Furthermore, the combination of Raman spectroscopes with additional optical devices, often referred to as Raman microspectroscopy, provides high spatial resolution.^[202-205]

In literature, Raman spectroscopy has been applied for various studies exceeding the sole identification of substances. For example, the hydrogen bonding between water and alcohols for various mixtures^[206-208] or the influence of the temperature on the water structure^[209] was studied. Another example is the determination of diffusion coefficients in multicomponent systems. Peters et al.^[210,211] created a laminar co-flow of miscible solvents in a microfluidic chip. The channel geometry corresponds to a spiral with a Y-shaped inlet. Measurement points at different positions of the channel equal different contact times between the solvents. Thus, temporally and spatially resolved concentration profiles can be extracted from the Raman spectra. In combination with a multicomponent convection-diffusion model, diffusion coefficients were calculated. Others used Raman spectroscopy to analyze the production or properties of soft matter materials such as polymer systems.^[212] For example, Meyer-Kirschner et al.^[213] used in-line Raman spectroscopy to study the polymerization kinetics of microgels. The progress of the polymerization can be followed by the quantitative evaluation of time-resolved Raman data. The conversion of the monomers and production

of polymer is revealed by the decrease and increase of their Raman signals. Tsuboi et al.^[214] studied the laser-induced volume phase transition of rod-shaped PNIPAM gels. They qualitatively compared the Raman signals from PNIPAM at various photon pressures and different positions in the gel to gain information on the hydration state of the polymer. In this thesis, Raman microspectroscopy was applied to study the cononsolvency behavior of PNIPAM gels in water-methanol (MeOH) mixtures in equilibrium^[128] and the kinetics of a sudden solvent exchange. Both are discussed in detail in Chapters 4 and 8. In the following, the basic principles behind Raman (micro)spectroscopy and the quantitative evaluation of Raman spectra are presented. More detailed information can be found in textbooks on Raman, e.g. by Smith et. al.^[202] or Ferraro et al.^[215]

3.2.1 The Raman effect

The Raman effect was first experimentally observed by Raman and Krishnan in 1928.^[216] It describes the inelastic scattering of electromagnetic radiation by matter leading to an energy transfer between the photons and the molecular vibrations.^[202,203,217] The light interacts with the molecule and polarizes and distorts the electron cloud around the nuclei. Thereby, an unstable virtual state is formed and the photon is quickly reradiated (Figure 3.3). Here, the

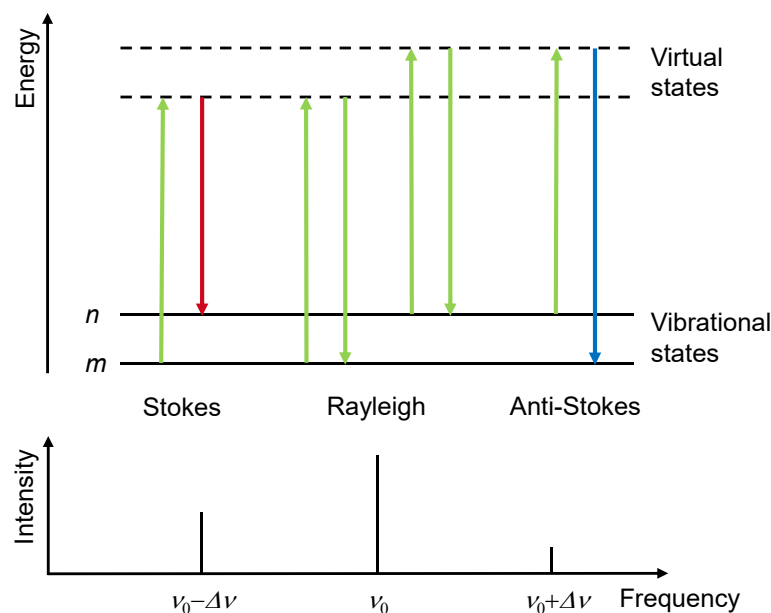


Figure 3.3: Principle of Rayleigh and Raman scattering. Molecules can be excited from their vibrational ground states (m and n) into virtual states by interaction with electromagnetic radiation. For Rayleigh scattering, the excitation energy (upward arrows) equals the scattered energy (downward arrows). During Stokes Raman scattering, the scattered photons have less energy leading to a red shift ($\nu_0 - \Delta\nu$). Oppositely, anti-Stokes Raman scattering means that the scattered photons have more energy leading to a blue shift ($\nu_0 + \Delta\nu$). Usually, the intensity of Stokes Raman scattering is stronger than anti-Stokes scattering. Adapted from ref. [202] and [203].

molecule predominantly returns from the virtual level to the ground level. This process is called elastic scattering or Rayleigh scattering. In case of an energy transfer either from the photon to the molecule (Stokes scattering) or from the molecule to the photon (anti-Stokes scattering), the scattering is inelastic. In both cases, the energy of the incident photon deviates from the scattered photon. This comparably rare process is defined as Raman scattering. At room temperature, Raman Stokes scattering is dominant because most molecules are present in the ground state, the lowest energy vibrational state (m). Anti-Stokes scattering requires molecules already in the excited vibrational state (n). The ratio between Stokes and anti-Stokes scattering is influenced by temperature. Higher temperatures increase the number of molecules in excited states and thus, increase anti-Stokes scattering. Although Raman scattering is a rare process (only one in every $10^6 - 10^8$ photons^[202]), modern setups allow high sensitivity at low laser power.

All Raman active molecules, i.e. with a polarizable electron shell, exhibit characteristic vibrations. The scattered light forms a component-specific spectrum. Each component shows characteristic bands at certain positions in this spectrum depending on the vibrational degrees of freedom of the molecules. The number of vibrational degrees possible for a nonlinear molecule is given by $3N - 6$ with N the number of atoms. For example, water has three modes of vibration (Figure 3.4): the symmetric and asymmetric stretch and the bending mode.^[202]

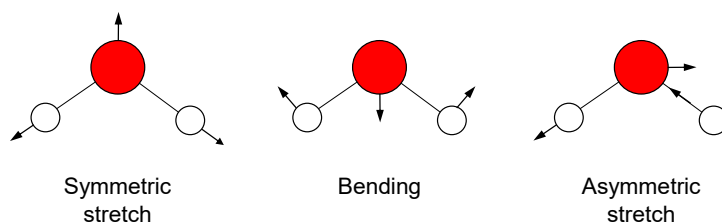


Figure 3.4: The three vibrational modes of water (O: red. H: white). Adapted from ref. [202].

In complex molecules, there are many Raman-active intramolecular vibrations. It was found that if two or more bonds are close together and of similar energy, they interact as a group. For example, in the methyl group $-\text{CH}_3$, the C-H bonds are treated as a group differentiating between a symmetric and an asymmetric stretching vibration rather than separate CH stretches.^[202] The energy of the vibration is defined by the mass of the atoms or groups and the strength of the bond: the lighter the atoms and stronger the bonds, the higher the frequency. In vibrational spectroscopy, the intensity of the vibrations is typically depicted in dependence of the relative wavenumber. In Raman spectra, the terms “wavenumber” and “Raman shift” are often used as synonyms. The Raman shift refers to the difference in energy and therefore the difference in frequency between the incident and

scattered radiation.^[204] This has the advantage that the Raman shift is independent from the excitation wavelength.^[202] The relation of wavenumber ($\tilde{\nu}$), frequency (ν) and wavelength (λ) is given in equation (2). The unit of the wavenumber is historically specified in cm^{-1} .

$$\tilde{\nu} = \frac{\nu}{c} = \frac{1}{\lambda} \quad (2)$$

The intensity of Raman scattering from a sample is proportional to the number of atoms in the investigated sample volume (i.e. concentration of the component). This proportionality is basis for most quantitative analysis. For multicomponent systems without nonlinear effects, the spectrum is a simple, linear superposition of the spectra of each pure component.^[205] Nonlinear effects can occur due to intermolecular interactions, e.g. hydrogen bonding, in liquid mixtures.^[218] These interactions cause changes of the spectral position or shape of certain bands depending on the composition of the mixture. The accuracy of the quantitative analysis of the mole fractions in multicomponent system is typically 0.1 to 1 mol%.^[128,211,218-220] Nonlinear effects and/or an overlap of peaks of different components complicate the quantitative evaluation of data. However, the nonlinear features can be exploited to gain other information from the spectra as will be demonstrated in detail in Chapter 4.

3.2.2 Indirect hard modeling (IHM)

Raman spectra of multicomponent mixtures are usually evaluated by fitting a weighted sum of pure component spectra to the mixture spectrum referred to as classical least squares (CLS) method.^[205] The peak area of a component scales with its concentration at the measurement point. However, as aforementioned, especially multicomponent systems are prone to exhibit nonlinear effects. To achieve a precise, quantitative evaluation, a variable spectral analysis is needed. To this end, Alsmeyer et al.^[218,221] presented an analysis method called indirect hard modeling (IHM). In IHM analysis, every peak in a spectrum of a pure component is modeled with peak-shaped pseudo-Voigt functions. The sum of these peak functions forms the pure component model (\mathcal{A}_i^*). Each peak function has four degrees of freedom such as peak position, full width at half maximum (FWHM), the area of the peak and Gaussian part of the peak shape. To account for nonlinear effects, these parameters can be assigned as fixed or flexible. For example, a degree of freedom regarding the peak position enables the modeling of peak shifts. In IHM, it is usually assumed that the peak area within each component spectrum is unaffected by molecular interactions.^[203,205] Therefore, the area of a pseudo-Voigt function is a fixed parameter during spectral fitting.^[222] In addition, a baseline can be explicitly included to compensate for spectrometer and sample errors^[221] or a background model (\mathcal{B}) to account, e.g. for the glass signal of the analysis

platform (for example cuvette or microfluidic device). All pure component models needed for the investigated system are weighted by factors (ζ_i , with $\zeta_i \geq 0$) and combined to a mixture model \mathcal{A} . Here, n_C is the number of components.

$$\mathcal{A} = \zeta_B \mathcal{B} + \sum_{i=1}^{n_C} \zeta_i \mathcal{A}_i^* \quad (3)$$

To evaluate multicomponent spectra, the residuals between the mixture spectrum and the mixture model are minimized in a least-squares procedure. Within this spectral fitting step, the parameters set as flexible can be adjusted to address nonlinear effects. The results of the spectral fitting step are the weights of each component which are proportional to the area below each pure component model.^[222] As aforementioned, the peak areas and thus weights are proportional to the concentrations of the components. To convert the weights into mole fractions, a calibration is required. A ratiometric calibration considers the ratio of weights as the ratio is not dependent on experimental parameters such as laser intensity or refractive index.^[222] For two components i and j , the ratio of the weights correlates with the ratio of the mole fractions.

$$\frac{\zeta_i}{\zeta_j} = k_{i,j} \frac{x_i}{x_j} \quad (4)$$

$k_{i,j}$ denotes the calibration factor of the binary system in mole fractions. Furthermore, the closure condition that the sum of the mole fractions of all components must equal 1 applies. Therefore, the mole fraction of one component in a mixture spectrum can be calculated using the following equation.^[218]

$$x_i = \frac{1}{\sum_{j=1}^{n_C} \frac{\zeta_j}{\zeta_i} k_{i,j}} \quad (5)$$

The calibration factors are previously determined from the analysis of mixture spectra with known composition in a further least-squares procedure. For a binary mixture, one mixture spectrum with known composition (x_{true}) in addition to the pure component spectra is technically sufficient. However, usually multiple spectra are used to assess the quality of the calibration by calculating the root-mean-square error (RMSE).^[223]

$$RMSE_{\text{cal}} = \sqrt{\left(\frac{1}{n_{\text{cal}} n_C} \sum_{s=1}^{n_{\text{cal}}} \sum_{i=1}^{n_C} (x_{\text{pred},s,i} - x_{\text{true},s,i})^2 \right)} \quad (6)$$

Here, n_{cal} is the number of calibration spectra and $x_{\text{pred},s,i}$ the mole fraction of component i that is predicted from equation (5).

3.2.3 Raman setup

A typical Raman setup consists of a laser, focused onto a probe volume by a suitable mirror and lens.^[202,204] The scattered light can be observed at 90° of the incident beam or backscattered light is detected depending on the setup. A notch or band-pass filter must be installed to suppress the Rayleigh scattering. The Raman signal from the sample is then focused on the entrance slit of a spectrometer. Here, the scattered light is decomposed into different wavelengths, e.g. by a diffraction grating, and detected by a two-dimensional charge-coupled device (CCD). In modern setups, Raman spectrometers are often coupled to confocal microscopes as schematically shown for an inverted setup in Figure 3.5.^[202] In a combined setup, the microscope objective is used as focusing lens and the backscattered Raman signal is detected. To receive a confocal resolution, the entrance slit of the spectrometer serves as a pinhole to spatially filter the incident light. Thus, only scattering of a specific plane of the sample is collected and any signal from the surroundings which is out of focus is eliminated. Such setups combine the precise spatial resolution at distinct measurement points and the in-situ identification and quantification of the present compounds.^[202]

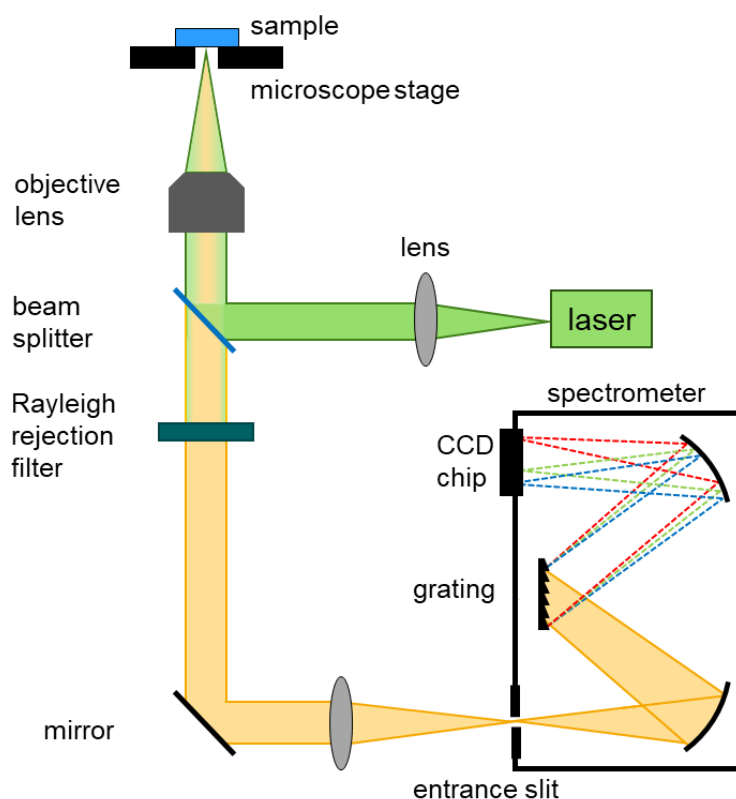


Figure 3.5: Schematic setup of an inverted confocal Raman microscope similar to the one used for the Raman measurements in the present work.

3.2.4 Raman spectra of water, methanol and their mixtures

Within this thesis, Raman spectroscopy was utilized to study water-methanol systems. Therefore, a closer description of their Raman signals and special features of their mixtures is given here. Figure 3.6 shows the Raman spectra of pure water (black) and pure methanol (red). The Raman spectrum of water exhibits a broad O-H stretching region at $2800 - 3750 \text{ cm}^{-1}$. Additionally, a very weak contribution of the bending vibration is visible near 1645 cm^{-1} .^[224] Methanol has strong contributions due to the symmetric and asymmetric stretching of the methyl group at 2837 cm^{-1} and around 2946 cm^{-1} , respectively. A weak and broad contribution of the O-H stretching overlaps with the water signal. In the fingerprint region, further distinct bands are visible. The CH_3 deformation is located around 1451 cm^{-1} and the CO stretching around 1037 cm^{-1} .^[225]

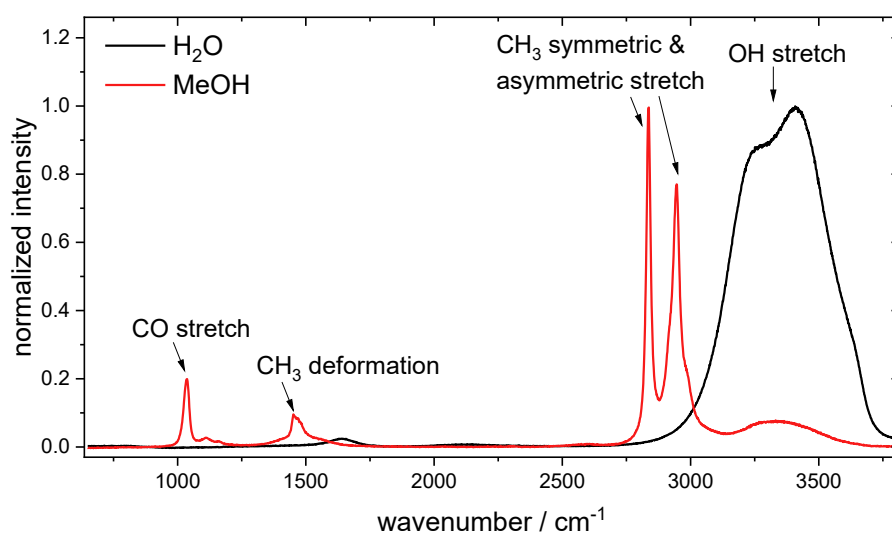


Figure 3.6: Raman spectra of pure water (black) and pure methanol (red).

Mixtures of water and methanol exhibit strong nonlinear effects in their Raman spectra. Figure 3.7 shows the methanol CO stretching and CH_3 symmetric stretching bands in dependence of the methanol mole fraction in water-methanol mixtures. While the CO band shifts to lower wavenumbers with decreasing methanol fraction, the CH_3 band shifts towards higher wavenumbers. These methanol peak shifts reveal information on the hydrogen-bonding environment.^[207,226] The peaks shifts occurring in water-methanol mixtures and the information content received from a peak shift analysis are discussed in more detail in section 4.4.

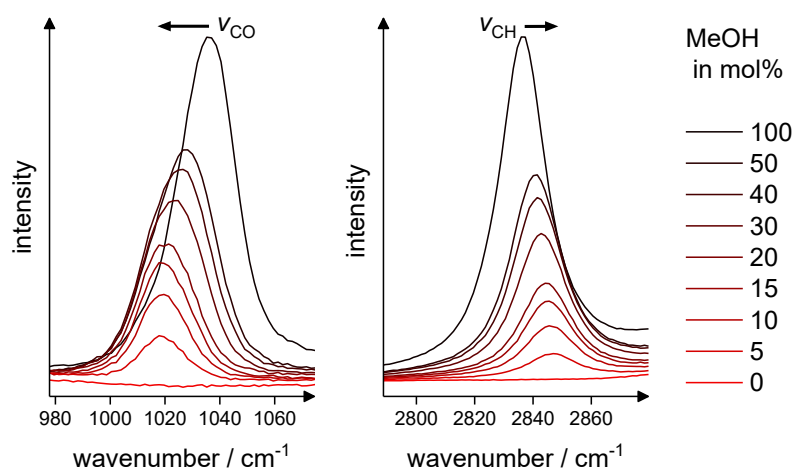


Figure 3.7: Nonlinear effects in water-methanol mixtures: peak shift of the CO and CH₃ symmetric stretching band of methanol depending on the methanol mole fraction.

3.3 Fluorescence

Fluorescence techniques are essential tools for studies of biological systems and in material sciences.^[227-230] In the following, a brief introduction to the basic principle and experimental methods is given. More detailed information can be found in textbooks on fluorescence, e.g. by Lakowicz^[229] or Kubitschek et al.^[230] The first observation of fluorescence was described for a quinine solution in sunlight by Herschel in 1845.^[231] Molecules emitting fluorescence are called fluorophores and often bear aromatic groups. Typical examples are quinine, rhodamine, and fluorescein.^[229] The common processes taking place between the light absorption and emission are illustrated in the Jablonski diagram (Figure 3.8).^[229,232]

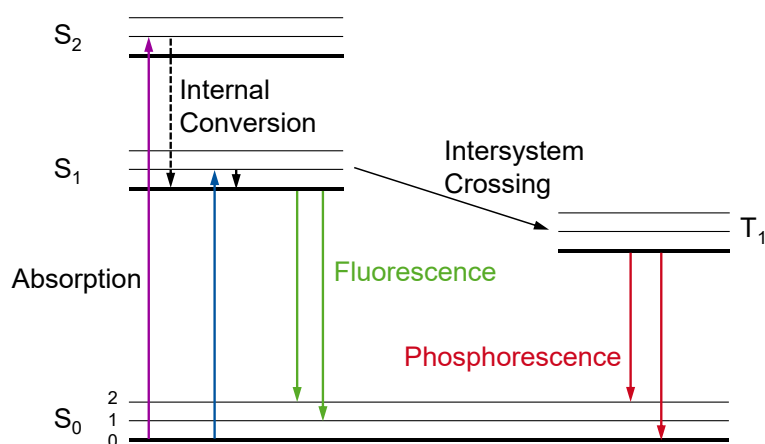


Figure 3.8: Illustration of a simplified Jablonski diagram. Adapted from ref. [229].

There are various electronic states such as the singlet ground state (S_0) and the first and second excited states (S_1 or S_2). Each electronic state comprises a number of vibrational energy levels, depicted by 0, 1, 2, etc. Upon irradiation with light of an appropriate

wavelength, the fluorophores absorb photons. Thereby, a fluorophore is excited from the singlet ground state to one of the higher energy states of S_1 or S_2 . In the subsequent internal conversion process, the molecules rapidly relax to the lowest vibrational state of S_1 . The internal conversion occurs within 10^{-12} s or less. As fluorescence lifetimes are typically close to 10^{-8} s, the internal conversion usually completes prior to emission.^[229] Therefore, fluorescence results from the lowest energy vibrational state of S_1 . In general, the fluorophore returns to a higher excited vibrational ground state. The emission of fluorescence is shifted to a longer wavelength, i.e. lower energy, than the excitation. This energy loss is typically due to the thermal relaxation to the first vibrational state of S_1 during the internal conversion and the decay to a higher vibrational level of S_0 . The decay from S_1 to S_0 may also result from a collision with solvent molecules. Here, the excess energy is lost without fluorescence emission. Furthermore, molecules in the S_1 state can undergo a conversion to the first triplet state (T_1). This process is called intersystem crossing. Emission from T_1 is known as phosphorescence. As the relaxation from T_1 to S_0 is spin forbidden, the intensity is comparably low. For phosphorescence, the energy loss between excitation and emission is even larger than in case of fluorescence.^[229]

Each fluorophore has characteristic excitation and emission spectra with one or more bands depending on its atomic structure, electron resonance properties, as well as chemical environment.^[233] Due to the aforementioned energy loss between excitation and emission, a shift of the absorption and emission maximum can be observed. This difference in wavelength is referred to as Stokes shift. Depending on the fluorophore, the shift can range from a few to several hundreds of nanometers.^[233] The Stokes shift is highly important for fluorescence microscopy as the emitted light can be separated from the excitation light using appropriate filters.^[229] Furthermore, the properties of the fluorophores depend on their local environment. Factors such as the solvent polarity and viscosity need to be considered as they can influence the position, intensity, and shape of the absorption bands.^[234] Pronounced changes of position and intensity of an absorption band and/or an emission band due to a change in the polarity of the surrounding medium are termed solvatochromism.^[234,235] One prominent example of a hydrophobic solvatochromic dye is Nile Red (NR). The emission wavelength exhibits a red shift with increasing polarity of the solvent (see Chapter 5). In contrast, other dyes, e.g. rhodamine derivatives, only show a negligible shift with solvent polarity.^[232] Therefore, solvatochromic dyes can be exploited for fluorescence imaging and sensing of local properties, e.g. in biological or polymer systems.^[234,236,237]

In addition to common steady-state measurements, time-resolved methods measure intensity decays or anisotropy decays.^[229] Here, the sample containing the fluorophore is exposed to a light pulse shorter than the decay time of the sample. This excitation results in

an initial population of fluorophores in the excited state which subsequently decays with time. In an experiment, the fluorescence intensity decay of the sample is recorded with a high-speed detection system on the nanosecond timescale.^[229] The time-dependent intensity decay is typically fitted to a multi-exponential model, i.e. the sum of individual single exponential decays. Often, a distribution of decay times is expected due to a range of environments. The time-resolved data contains information lost during the averaging processes in steady-state measurements. For example, the existence of more than one lifetime (or decay time) reveals the presence of more than one conformational state or microenvironment. Similar to the emission wavelength, the fluorescence lifetime of NR is sensitive to its environment. In the literature, this sensitivity was used to probe the local hydrogen-bonding strength.^[238] Furthermore, advances in technology allow to create spatially resolved lifetime images, also referred to as fluorescence lifetime imaging (FLIM). Here, the contrast of the image is based on the lifetime in each region of the sample. For visualization, the lifetime components are commonly depicted in different colors.^[229]

3.3.1 Fluorescence microscopy

Fluorescence microscopy is widely applied to examine and image specimens. In contrast to bright-field microscopy, fluorescence microscopy offers high contrast and specificity.^[230] In conventional fluorescence microscopy, the sample is illuminated with light of a specific wavelength matching the excitation wavelength of the fluorophore. Several light sources, such as arc lamps along with an excitation filter, lasers, or high-power light-emitting diodes (LEDs), are commonly used.^[230] The light emitted by the sample is much weaker and separated from the incident light using an emission filter with a beam-splitter. Subsequently, the emitted light is focused onto a detector, e.g. a CCD camera. The major drawback of conventional fluorescence microscopy is that light emitted from out-of-focus regions also reaches the detector leading to blurry images.^[239]

Confocal imaging allows better observation of fine details with a high spatial resolution compared to conventional fluorescence microscopy. The principle was developed by Minsky et al.^[240] in 1961 and is still applied in modern setups.^[239,241] In confocal microscopy, a focused beam scans across the sample point by point. Emitted light that does not originate from the focal plane is excluded by introducing a narrow aperture, the confocal pinhole. Thus, only a thin cross-section of the sample in the focal plane is perceived. To provide high intensities, a laser is used as excitation source which scans the sample using a dichroic mirror and lenses. With this setup, only a single spot of the sample is imaged at once and the final image is constructed one pixel at a time. This leads to high resolution and a sharp, high-contrast image, but is a time-consuming procedure.^[239] This limitation can be overcome

using a spinning-disk confocal microscope. Its principle was invented by Nipkow in 1884 and was later adopted for confocal microscopy by Petrán et al.^[242] Here, the single pinhole is replaced by a rotating disk with multiple pinholes and an additional disk with multiple micro-lenses. The pinholes are arranged in a spiral so that the entire field of view is covered when the disk rotates. Upon imaging, the micro-lenses focus the excitation light onto the pinholes increasing the intensity reaching the sample. The light that goes through the pinholes creates a set of confocal mini-beams scanning the sample.^[241] The detection of the emitted light is usually realized by means of a photomultiplier tube (PMT) or a CCD camera providing high detection efficiencies. A confocal image is formed almost immediately. Commercial spinning-disk confocal microscopes can reach framerates of > 50 fps, however, usually less confocality is reached in comparison to single beam setups.^[239,241] In modern confocal systems, several laser systems are combined with acousto-optical devices to precisely control the wavelength (ranging from 400 – 750 nm) and excitation intensity. Additionally, it is possible to construct three-dimensional images of the specimen by stacking a series of thin slices taken along the vertical z -axis.^[239,243]

EQUILIBRIUM

The following part concerning equilibrium studies of PNIPAM gels is structured in four subsections. Each subsection includes an abstract and a short, more specific introduction into the approach and the main question addressed. In the first two sections, the distribution of the solvent and cosolvent in the ternary system with PNIPAM was examined. On the one hand, macroscopic gels are studied by mass balance experiments and Raman microspectroscopy. On the other hand, PNIPAM microgel beads were modified with solvatochromic, covalently bound moieties and investigated using fluorescence spectroscopic methods. The third part depicts the relevance of detailed studies of the collapse behavior and the resulting environment provided by PNIPAM microgels for applications such as catalysis. The last part deals with another trigger, namely the osmotic pressure. Instead of penetration into the polymer network as for cononsolvency, large linear polymer chains are excluded from the network increasing the external osmotic pressure. These studies reveal insights into the mechanical properties of the microgel beads. The results from the osmotic pressure experiments are relevant for the interpretation of the dynamics of the polymer collapse in the second part of the thesis.

4. Enrichment of methanol inside PNIPAM gels in the cononsolvency-induced collapse

Parts of the following chapter were published. Adapted from: Nothdurft, K.; Müller, D. H.; Brands, T.; Bardow, A.; Richtering, W., Enrichment of methanol inside PNIPAM gels in the cononsolvency-induced collapse. *Physical Chemistry Chemical Physics* **2019**, *21*, 22811-22818. with permission from PCCP Owner Societies – *for contributions of authors see page V*

ABSTRACT: Cross-linked poly-*N*-isopropylacrylamide (PNIPAM) gels adapt to their environment by a unique transition from a flexible, swollen macromolecular network to a collapsed particle. PNIPAM gels are swollen in both, pure water and pure methanol (MeOH). However, a drastic volume loss is observed in mixtures of water and methanol

over a wide composition range. This effect is referred to as cononsolvency. Cononsolvency couples the volume phase transition to the transport of the cosolvent into the polymeric network. So far, the mechanisms underlying cononsolvency have not been fully elucidated. To obtain insights on cononsolvency, Raman microspectroscopy was applied to capture spatially resolved spectra distinguishing between the surroundings and the inside of the gel. Here, indirect hard modeling (IHM) was used for the spectral analysis. Mass balancing allowed the calculation of the solvent composition inside the PNIPAM gel. The results show an increased methanol fraction inside the collapsed gel as compared to its surroundings. Furthermore, the sensitivity of the vibrational bands of methanol to its local hydrogen-bonding environment allows to derive information about the molecular interactions. The methanol peak shifts measured inside the gel point towards donor-type hydrogen bonds between methanol and the peptide group of PNIPAM in the cononsolvency-induced collapse. The presented data should enhance our understanding of cononsolvency.

4.1 Introduction

Environmentally sensitive polymer gels are three-dimensional, cross-linked polymeric networks that are reversibly affected by changes in their surroundings, e.g. temperature, pH, or solvent composition.^[5,59] In particular, water-based systems are of great interest for variable applications.^[15,62,66,70,71,82] The most prominent example of a stimuli-responsive gel is based on poly-*N*-isopropylacrylamide (PNIPAM) in combination with the cross-linker *N,N'*-methylenebis(acrylamide) (BIS).^[3] Besides the well-studied thermoresponsive behavior, PNIPAM is sensitive to the solvent composition, e.g. of water-alcohol mixtures.^[19,87] Either of the respective pure solvent swells the polymer network. However, a drastic, very fast volume loss is caused by changing the solvent mixture to a certain intermediate range.^[22] This volume change is similar to the volume phase transition induced by temperature. For water and methanol (MeOH), a minimum in size is found around the most unfavorable mixture of about 20 mol% of methanol. This effect is referred to as cononsolvency. Cononsolvency is an intriguing phenomenon whose underlying processes are controversially discussed since the 1990s (see section 1.2).^[87,244,245] For PNIPAM, cononsolvency behavior was found in mixtures of water and methanol^[87,246] or other alcohols^[21,89,247,248] and water-organic solvent mixtures.^[91,93,108,248-250]

The understanding of the cononsolvency is essential for the optimal design of new functional materials for applications such as catalysis, actuators, sensors, or extraction and separation processes.^[9,251-254] One example is the system developed by Wang et al.^[252] who designed bilayer hydrogel actuators made of PNIPAM and poly(*N*-hydroxyethylacrylamide)

with controllable actuation performance combining the temperature and solvent-dependent behavior of the PNIPAM layer. Another application of cononsolvency has been demonstrated for double hydrophilic block copolymers composed of PNIPAM and poly(*N*-vinylimidazole) that exhibit an enhanced catalytic performance in esterolysis reactions within the cononsolvency-induced micellization.^[255] Moreover, greater insights about the collapse behavior of polymers in cononsolvency mixtures will be of interest for the usage of PNIPAM-based brushes as a transfer system for nanoparticles that would be prone to aggregation otherwise.^[9] Another theoretical study was presented by Li et al.^[254] concerning a system with polymer brushes forming cylindrical nanopores switchable by a cosolvent.

Along with publications regarding the origin of the cononsolvency of PNIPAM in binary water-alcohol mixtures, several studies have investigated the difference in solvent composition within the PNIPAM gel compared to the surrounding fluid. As discussed in section 1.2, various theoretical studies and molecular dynamics simulations have suggested preferential adsorption of alcohol by strong interactions with the PNIPAM chain in the collapsed region.^[107,111,113,117,121] Wang et al.^[110] performed high-resolution ¹H MAS NMR experiments on PNIPAM microgels in pure water and in binary water-alcohol mixtures. Solely mixtures with low alcohol contents (2.5 or 5 mol%) were investigated. They determined preferential adsorption of alcohol molecules within the collapsed microgel network by quantification of the free and confined solvent species. Similar results were found by Mukae et al.^[90] and H  ther et al.^[89] performing indirect mass balancing experiments with macroscopic PNIPAM gels. Maeda et al.^[129] investigated linear PNIPAM in water-isopropanol mixtures by Raman microspectroscopy. They distinguished between polymer-rich domains of adsorbed chains and the solvent-rich matrix. Preferential adsorption of isopropanol in the polymer-rich regions was observed. The opposite behavior was found for linear PNIPAM in water-DMSO mixtures, where the cosolvent is excluded from the collapsed, polymer-rich phase.^[91] Regarding water-methanol mixtures, Maeda et al.^[129] briefly stated that methanol was not enriched in the polymer-rich phase. Yang et al.^[130] proposed that methanol molecules interact solely with water molecules in the first solvation shell of the PNIPAM chains up to $x(\text{MeOH}) < 0.75$.

In this chapter, the cononsolvency of PNIPAM gels in water-methanol mixtures was explored over a wide composition range. The experimental approach of a mass balance pursued by H  ther et al.^[89] was combined with Raman microspectroscopic measurements. For the quantitative evaluation of the Raman spectra, the method of indirect hard modeling (IHM) was used.^[218] The spatial resolution of the Raman microscope in combination with a polymer gel allows a clear distinction between the polymer and its surroundings. The mass balancing method was applied to determine the solvent composition within a macroscopic

gel in comparison to the surrounding solution over a wide range of water-methanol mixtures. Subsequently, the PNIPAM-solvent interactions were elucidated by direct Raman microspectroscopy measurements inside the gel. Here, the sensitivity of the methanol peaks on the methanol molecules' local hydrogen-bonding environment is discussed.

4.2 Swelling behavior of macroscopic PNIPAM gels

Macroscopic PNIPAM gels with 5 mol% cross-linker were synthesized by a cooled molding approach (details in section 10.2). The swelling behavior of these gels was evaluated in binary water-methanol mixtures between 0 and 70 mol% methanol. Figure 4.1 shows the dependence of the swelling degree on the methanol mole fraction. The swelling degree is defined as the weight of the gel equilibrated in the mixture divided by the dry mass. In water, the gel is fully swollen at ambient temperature. Upon addition of methanol, the polymer network collapses with a significant volume loss, also observable in the decreasing swelling degree. The smallest swelling degrees are reached for 15, 20, and 30 mol% methanol. Subsequently, a further increase in methanol fraction leads to reswelling of the gel. The results are in agreement with previous experiments of PNIPAM microgel, macrogels, or linear chains in water-methanol mixtures.^[19]

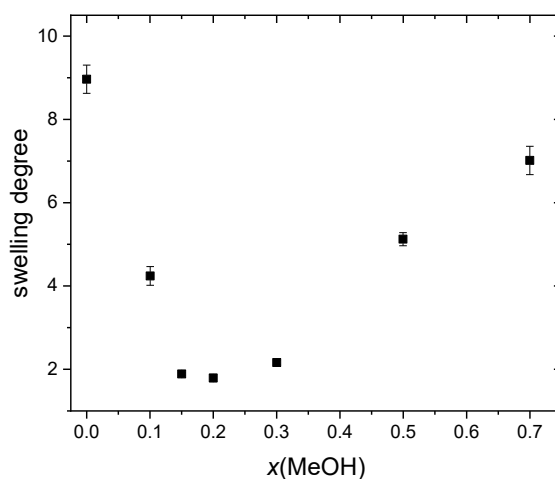


Figure 4.1: Swelling degree ($q_{\text{swell}} = m(\text{gel})/m(\text{gel,dry})$) of PNIPAM gels as a function of the methanol mole fraction in water-methanol mixtures.

4.3 Mass balance experiments

The approach for the mass balancing experiments is depicted in Figure 4.2 (for experimental details, see sections 10.2.1 and 10.4.2): The dried PNIPAM gels were equilibrated in known water-methanol mixtures. For the mass balance, Raman microspectroscopy measurements were performed for the surrounding solution. Afterwards, the gels were removed from their

vial and weighed. The solvent composition of the surrounding solution was evaluated by IHM. Previous to the removal of the gel, Raman spectra were captured inside the equilibrated PNIPAM gel to perform a peak shift analysis (section 4.4).

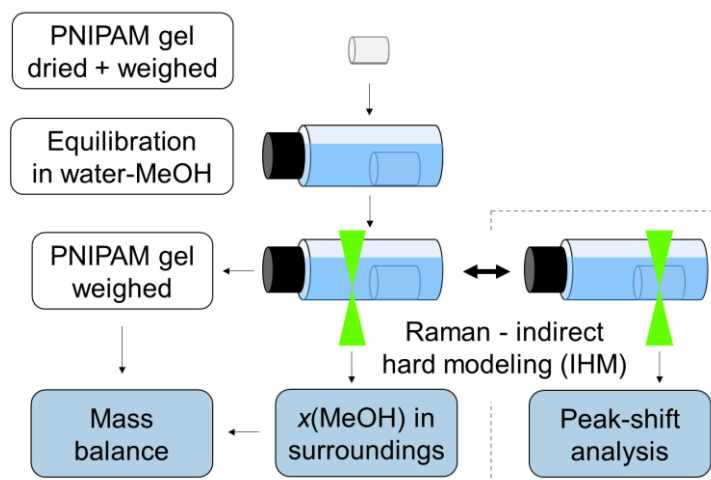


Figure 4.2: Approach for the equilibrium investigations of macroscopic PNIPAM gels in water-methanol mixtures.

The composition of the surrounding solution was evaluated by spectral analysis of the component areas using IHM.^[218] To this end, measurements were performed for binary mixtures of water and methanol of known compositions beforehand for calibration. The calibration yields a root-mean-square error (RMSE) of 0.36% for the mole fractions (Figure 4.3a). An exemplary fit of the mixture model to the measured spectra including the corresponding residuals is shown in Figure 4.3b for 20 mol% methanol in water.

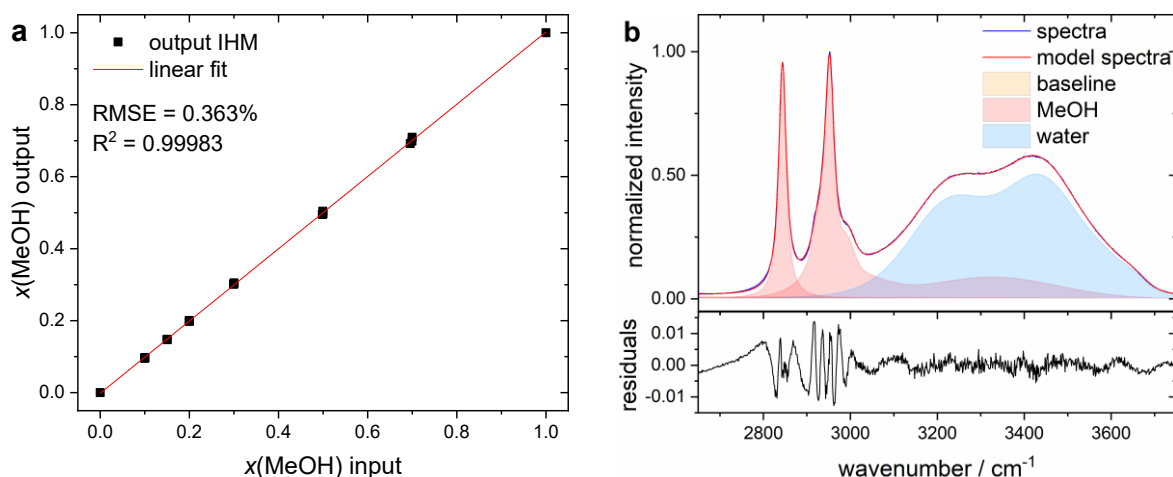


Figure 4.3: (a) Calibration of the applied indirect hard model using various binary water-methanol mixtures. (b) Exemplary fit of the Raman spectrum of 20 mol% methanol in water (used for calibration) with the modeled (pure component) spectra and the residuals.

From the IHM analysis, the methanol mole fraction in the surrounding fluid is obtained as a function of the overall methanol concentration. The mole fractions are converted into

mass fractions $\omega_{\text{MeOH}}^{\text{sol}}$. In combination with the weight m_{gel} of the gel swollen in the respective mixture, the solvent composition inside the gel is calculated using the mass balance of methanol:^[256]

$$\omega_{\text{MeOH}}^{\text{gel}} = \frac{m_{\text{MeOH}}^0 - \omega_{\text{MeOH}}^{\text{sol}} (m_{\text{MeOH}}^0 + m_{\text{water}}^0 - m_{\text{gel}} + m_{\text{gel}}^{\text{dry}})}{m_{\text{gel}} - m_{\text{gel}}^{\text{dry}}} \quad (7)$$

Here, m_i^0 denotes the known initial masses of the components in the system. The weight fraction ($\omega(\text{MeOH})$) is afterwards converted to the corresponding mole fraction ($x(\text{MeOH})$).

Figure 4.4 displays the comparison of the methanol concentration inside the gel to that in the surroundings as a function of the overall concentration. An accumulation of the alcohol within the polymer network is found for solvent compositions that induce the gel collapse (15 – 30 mol% MeOH). The highest deviation (7.4 mol%) from the overall composition is found for the most unfavorable mixture of 20 mol% methanol. For the partly swollen states at 10, 50, and 70 mol% methanol, no difference from the overall or surrounding solvent composition is measured.

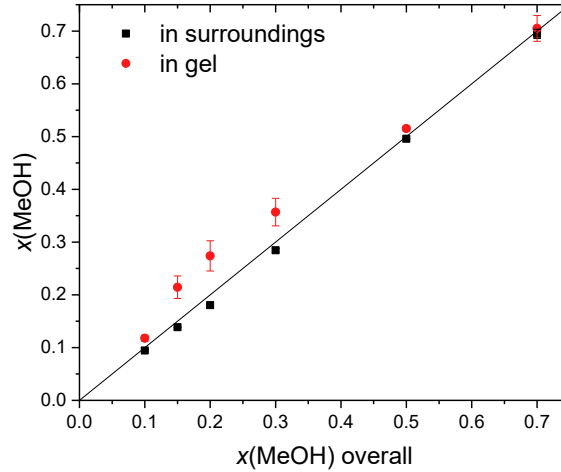


Figure 4.4: Methanol distribution inside the gel (red) compared to its surroundings (black) after equilibration in various water-methanol mixtures. The diagonal line represents the case of a uniform distribution of the solvent mixture within the whole system.

Comparable results were found for various aqueous mixtures inducing cononsolvency.^[89,110,129] Wang et al.^[110] compared the preferential adsorption of methanol and ethanol to PNIPAM in binary water-alcohol mixtures using ^1H MAS NMR. Here, Wang et al. could separate confined and free alcohol species due to peak splitting. For comparatively low overall concentrations of 2.5 and 5.0 mol% of alcohol, they determined an increased mole fraction of confined binary solvents. They ascribed this effect to a preferential interaction of the polymer with the alcohols and observed a more pronounced effect for the more hydrophobic ethanol compared to methanol. For 2.5 and 5.0 mol% overall alcohol

concentration, 5.7 and 7.4 mol% was found inside the gel in case of ethanol, while methanol only reached values of 3.3 and 5.8 mol%. Hüther et al.^[89,256] conducted mass balancing experiments using PNIPAM gels in combination with water-ethanol mixtures over the whole composition range. An increased fraction of the cosolvent inside the gel is suggested – more precisely, within the collapsed region of PNIPAM in water-ethanol mixtures (between 11 and 50 wt% of ethanol). The greatest difference (15.2 wt%) between the inside of the gel and the overall mixture was evaluated for an initial concentration of 28.9 wt% ethanol. Wang et al. concluded for low alcohol fractions that the enrichment of alcohol inside the gels increases with the hydrophobicity of the alcohol. This conclusion is confirmed by the presented data on water-methanol mixtures over a wider composition range in comparison to the results of Hüther et al.^[89] for water-ethanol mixtures. The accumulation of ethanol (15.2 wt%) found by Hüther et al. is higher than the accumulation of methanol found in this work (7.4 mol% methanol corresponding to 12.5 wt%).

Besides the preferential adsorption of alcohol species, other aqueous mixtures inducing cononsolvency show an accumulation of the cosolvent in the polymer network. Hüther et al.^[89] also investigated water-acetone mixtures and found that acetone was less enriched than ethanol. Additionally, preferential interaction of acetone with PNIPAM was found using high-resolution ¹H MAS NMR spectroscopy^[250] and molecular dynamic simulations.^[108] Zhu et al.^[94] recently used a local-bulk partitioning model to quantify the distribution of dimethylformamide (DMF) molecules between the chain surface and the surrounding bulk solution to study PNIPAM microgels in water-DMF mixtures. The number of DMF molecules adsorbed to the chain, in particular the number of DMF bridges, is increased in the collapsed structure.

4.4 Peak shift analysis

In addition, it was tested whether Raman microspectroscopy can be applied to directly determine the solvent composition inside the gel. To this end, Raman was additionally measured inside the PNIPAM gels (Figure 4.5). However, the PNIPAM peaks in the spectra strongly overlap with the methanol peak in the CH-stretching region between 2850 – 3050 cm⁻¹. Furthermore, nonlinear effects appear, such as peak shifts of all components, changes in the Gaussian part of the pseudo-Voigt peak shape and width, complicating the evaluation of the peak area during the spectral analysis by IHM. Although there is less overlap in the fingerprint region at low wavenumbers, no water signal is present to determine the water-methanol ratio. As no quantitative evaluation of the solvent

composition can be achieved using the peak area, the sensitivity of the methanol peak positions to the hydrogen-bonding environment is exploited.

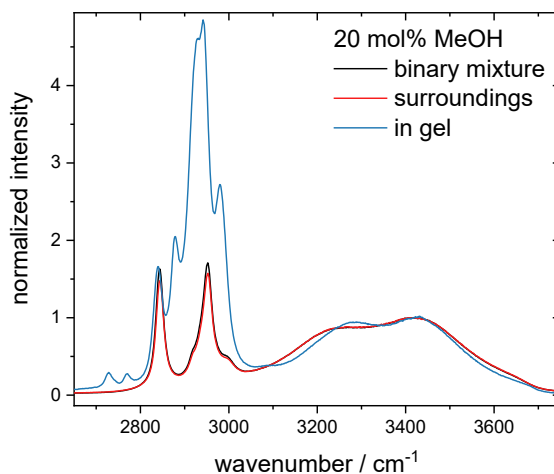


Figure 4.5: Raman spectra captured at 20 mol% initial methanol concentration in the binary reference solution, next to the PNIPAM gel and inside the gel. The intensity is normalized to the water signal at 3415 cm^{-1} .

For the binary mixture of water and methanol, it is well known that a significant shift occurs for the methanol CO- and CH-stretching band located at 1035.3 and 2836.5 cm^{-1} in pure methanol, respectively.^[207,257] A reference solution consisting solely of the binary mixture of water and methanol ($0.1 < x(\text{MeOH}) < 0.7$) was measured and a linear dependence of the peak shifts on the methanol concentration was found over a wide composition range. The CO band experiences a red shift by 16.2 cm^{-1} upon decreasing the methanol fraction to 10 mol%, whereas the CH band experiences a blue shift by 8.5 cm^{-1} . The opposite direction and difference in the strength of the CO and CH shift were observed experimentally before and supported by ab initio calculations.^[225] Investigations focusing on the dependence of the methanol peak position on the methanol hydration were published by Dixit et al.^[207] In this context, a linear shift was observed in the intermediate composition range ($0.7 > x(\text{MeOH}) > 0.25/0.15$). In the outer regions (for $x(\text{MeOH}) > 0.7$, $x(\text{MeOH}) < 0.25/0.15$), a deviation from this linear dependence was found. Different hydrogen-bonding configurations of methanol and water are proposed to explain the behavior. These configurations are discussed in more detail further below.

Evaluating the same methanol CO- and CH-stretching band and their shifts in the ternary system from the spectra captured inside the PNIPAM gel, a different correlation with the methanol fraction is found. A comparison of the spectra and the peak shifts for the binary and ternary system is displayed in Figure 4.6 and Figure 4.7: As aforementioned, the binary water-methanol mixtures exhibit a linear dependence of peak position and solvent composition (black symbols in Figure 4.7). In contrast, the peak shift is strongly reduced inside the gel compared to the value expected for a uniform distribution of solvent molecules

in the whole system, especially in the region of the cononsolvency-induced collapse (red full symbols in Figure 4.7). The peak positions found inside the gel are always closer to their original positions in pure methanol. The highest deviation of the peak shift inside the gel compared to the pure binary solvent mixture is again visible for the collapsed polymer region between 15 and 30 mol% methanol. If the peak shift would still be linearly correlated to the methanol fraction, as for the binary system, the measurements would indicate a higher amount of methanol inside the polymer network.

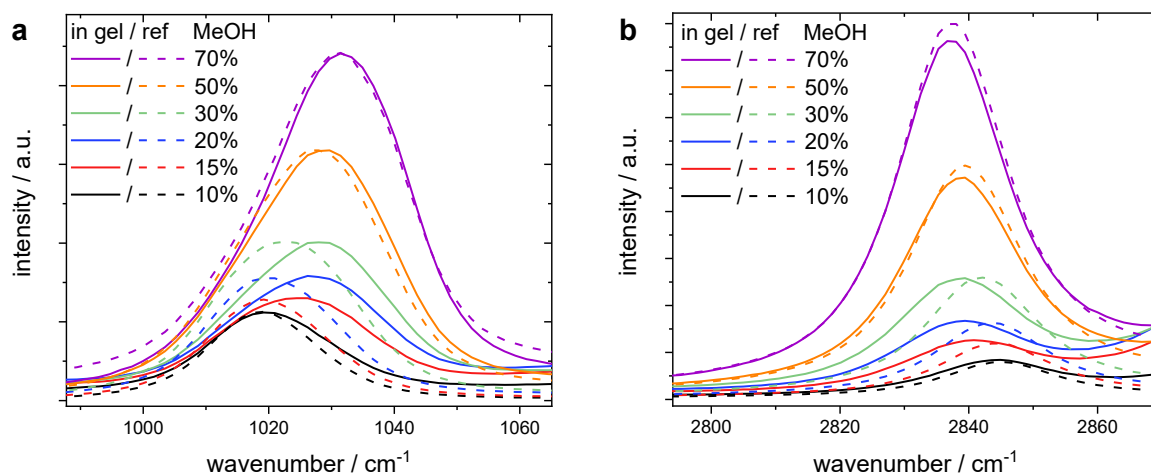


Figure 4.6: Comparison of the CO-peak position (a) and the CH-stretching region (b) of reference binary solutions (dashed lines) and inside a PNIPAM gel (solid lines) for different water-methanol mixtures.

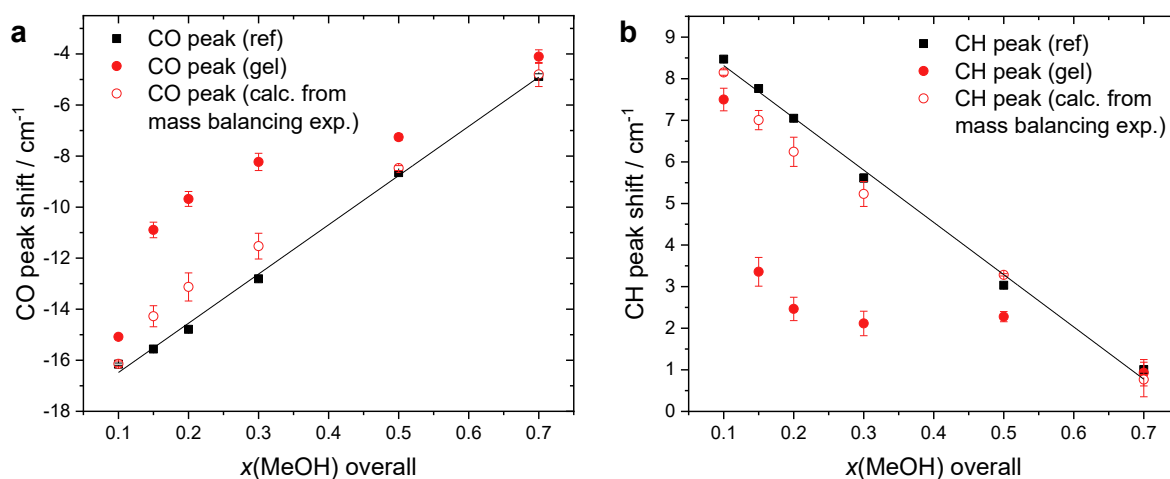


Figure 4.7: Methanol CO-peak shift (a) and CH-peak shift (b) extracted from spectra measured in a binary reference solution of solely water and methanol (black) and inside the gel (full red). The open red symbols represent the peak shifts corresponding to the methanol fraction obtained in the mass balancing experiment which were calculated using the linear fit (black line) of the binary reference solution.

To correlate the aforementioned enrichment of methanol inside the gel with the sensitivity of the peak positions, the mole fraction of methanol calculated in the mass balancing experiment is transferred to the corresponding peak shift. Here, a linear fit of the binary reference solution is used to convert $x(\text{MeOH})$ in the gel to peak shifts (red open symbols in Figure 4.7): In principle, the same trend is found that peak shifts are reduced inside the gel compared to the initial solution. However, the effect is significantly weaker. The peak shift caused by the enrichment of methanol inside the gel is much smaller than the peak shift actually measured. Thus, it is not possible to simply evaluate peak shifts to obtain the methanol concentration in the ternary system due to additional effects on the methanol peak positions. Most likely, methanol-polymer interactions affect the vibrational bands in addition to the solvent composition.

To elucidate the origin of the methanol peak positions inside PNIPAM gels, the results are compared to the literature by Gruenloh et al.^[226] and Dixit et al.^[207] on the binary mixture and molecular simulations. First, the effect of various hydrogen-bonding options on the methanol peak position is described for binary solvent mixtures. For facilitation, the discussion is focussed on the CH-peak position:

Gruenloh et al.^[226] derived trends for the shift of the CH-peak position by evaluating well-known benzene-methanol clusters measured with resonant ion-dip infrared spectroscopy: When methanol acts as a hydrogen-bond donor (D), the wavenumber of the CH peak decreases. In contrast, the peak position increases to higher wavenumbers when methanol is an acceptor (A) of a hydrogen bond or is existent in an acceptor-acceptor-donor (AAD) configuration. The strength of this increase is similar for both configurations. This behavior is explained by the compensating effects of the combination of acceptor and donor hydrogen bonding. In pure liquid methanol (Figure 4.8a), the solvent molecules form chain-like clusters where each methanol molecule acts as a single acceptor/single donor (AD). As aforementioned, Dixit et al. explained the shift of the CH- and CO-methanol-peak bands by the change in the hydrogen-bonding environment. If only little water is added to pure methanol (Figure 4.8b), water molecules coordinate at the end of the chain-like methanol clusters. Here, the chain-end methanol molecules act as hydrogen-bond acceptors. Upon further hydration (Figure 4.8c), water breaks/shortens the methanol chains and, in addition, individually solvated methanol molecules are formed. Each methanol molecule can accept two and donate one hydrogen bond leading to an AAD configuration. These explanations align with Gruenloh's findings that A and AAD methanol molecules cause a blue shift of the CH band in the spectra. The different hydrogen bonds have the opposite effect on the CO-peak position and a red shift occurs. These trends are applied to interpret the peak shifts inside the PNIPAM gel shown before.

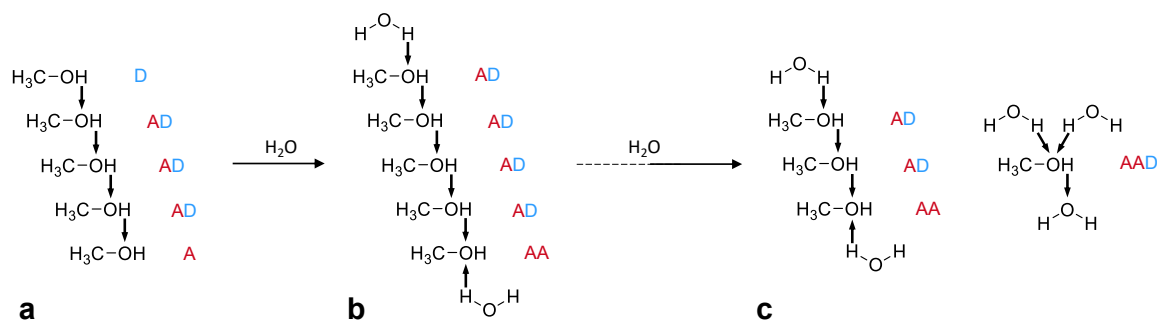


Figure 4.8: Acceptor (A) and donor (D) hydrogen bonding of methanol molecules in pure methanol (a) and in mixtures with increasing water fraction (b, c). Adapted from Dixit et al.^[207]

One factor decreasing the peak shift of the CH band is the increased methanol fraction inside the PNIPAM gels in the region of the cononsolvency-induced collapse. Here, the AAD hydrogen bonding is reduced compared to that in the binary solvent mixture. As mentioned in the discussion of Figure 4.7, only a part of the peak shift is caused by this increased methanol fraction. The remaining difference in peak shift arises from interactions with the polymer. Various studies show that there is a strong preference for the PNIPAM chains to form hydrogen bonds.^[117,121,122] In pure water, hydrogen bonds predominantly exist between PNIPAM-CO and water. These bonds are broken upon the addition of methanol and are partly replaced by hydrogen bonds to methanol. As aforementioned, Dalgicdir et al.^[117] debated that the methanol molecules geometrically frustrate the ability of water to form hydrogen bonds with the PNIPAM peptide group. The total number of hydrogen bonds decreases in the cononsolvency-induced collapse, however, the number of PNIPAM-methanol hydrogen bonds is enlarged. According to Mukherji et al.^[122] hydrogen bonds between the oxygen of the carbonyl group of PNIPAM and the hydrogen of methanol are expected to be most prominent. Here, methanol acts as a donor. Other hydrogen-bonding options involve the PNIPAM-NH group. In this case, methanol can act either as an acceptor or donor. With respect to the trends established by Gruenloh et al.,^[226] donor-type hydrogen bonding causes a decrease in the wavenumber of the CH-peak position. Thus, to align with the decrease in CH-peak shift measured inside the PNIPAM gel, donor-type hydrogen bonding between methanol and either the oxygen or nitrogen of the PNIPAM peptide group is indicated.

As previously mentioned, the effect of different hydrogen bonds on the CH-peak position is opposite compared to the effect of the CO peak position. Therefore, the red shift of the CO peak indicates donor-type hydrogen bonds as well.

4.5 Variation of the cross-linker content

In addition to the samples with 5 mol% cross-linker discussed in the previous sections, macroscopic gels with varying BIS content were prepared. When the amount of cross-linker in the synthesis was increased to 10 or 20 mol%, the macrogels became opaque and more brittle when dried. Therefore, such high cross-linked gels are not further discussed in the following. Instead, macroscopic gels with only 1 mol% BIS were investigated. The inset in Figure 4.9a shows a photograph comparing two gels swollen by water, one with 5 mol% BIS (black) and the other with 1 mol% BIS (red). Although both gels were prepared in the same mold, the lower cross-linked gel is significantly larger, i.e. its polymer network swelled more upon washing with water after the synthesis procedure. Additionally, Raman spectra were measured inside both gel types swollen in water (Figure 4.9a). The spectra are normalized to the highest intensity of the water signal. For the less cross-linked gel, a lower intensity of the PNIPAM bands between 2700 and 3025 cm^{-1} is found. Hence, inside the same confocal volume, the amount of polymer relative to the water content is smaller, which aligns with the visual comparison of the gels. For both gel types, the swelling ratio defined as $q_{\text{swell}} = m(\text{gel, swollen})/m(\text{gel, dried})$ is determined in various water-methanol mixtures (Figure 4.9b). Within the synthesis procedure, solely the ratio of NIPAM and BIS was varied, but the overall mass fraction of the monomer solution was kept at 1 g/mL in both cases. Therefore, the weights of the dried gels are similar, independent from the cross-linker content. For the most unfavorable mixtures between 15 and 30 mol% methanol in water, no difference in the swelling ratio is found. However, significant differences are observed for the gels in their swollen or partly swollen states. Here, the swelling degree of the samples with 1 mol% BIS is larger, i.e. more solvent could be retained inside the gel. These observations are in concordance with findings for small PNIPAM microgels^[53] and medium-sized PNIPAM microgel beads from microfluidics (Chapter 7).

Mass balancing experiments (Figure 4.10a) and peak shift analysis (Figure 4.10b) were also conducted with the gels containing only 1 mol% BIS and compared to the previously presented higher cross-linked samples. The peak shift analysis for the CO stretching band is shown in the Appendix (Figure A1). Both the enrichment of methanol and the correlation between peak shift and methanol fraction are found to be almost quantitatively the same for the differently cross-linked systems.

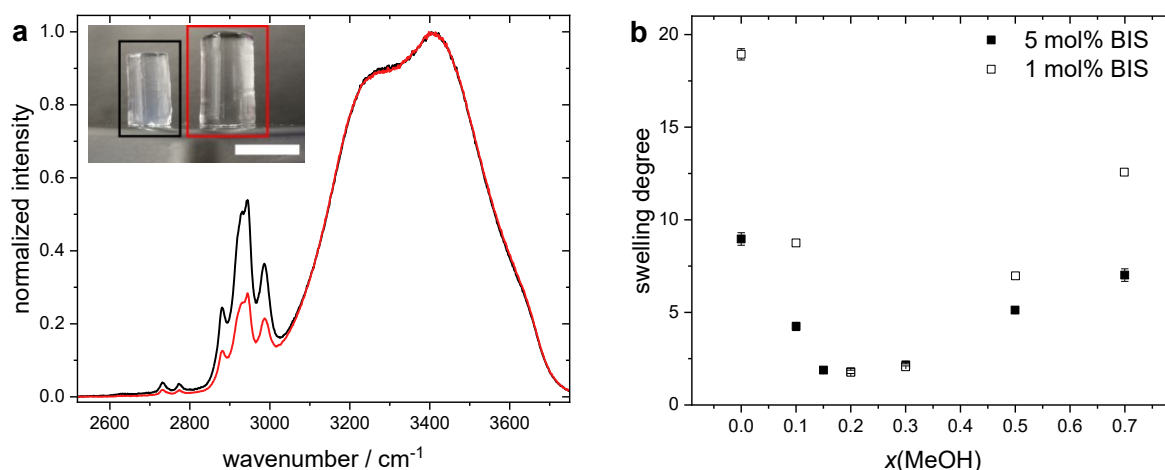


Figure 4.9: (a) Raman spectra and photograph of a gel with 5 mol% BIS (black) and a gel with 1 mol% BIS (red). For both, a 96 well plate was used as mold. Scale bar 1 cm. (b) Swelling ratio ($q_{\text{swell}} = m(\text{gel, swollen})/m(\text{gel, dried})$) of macroscopic gels with different cross-linker contents.

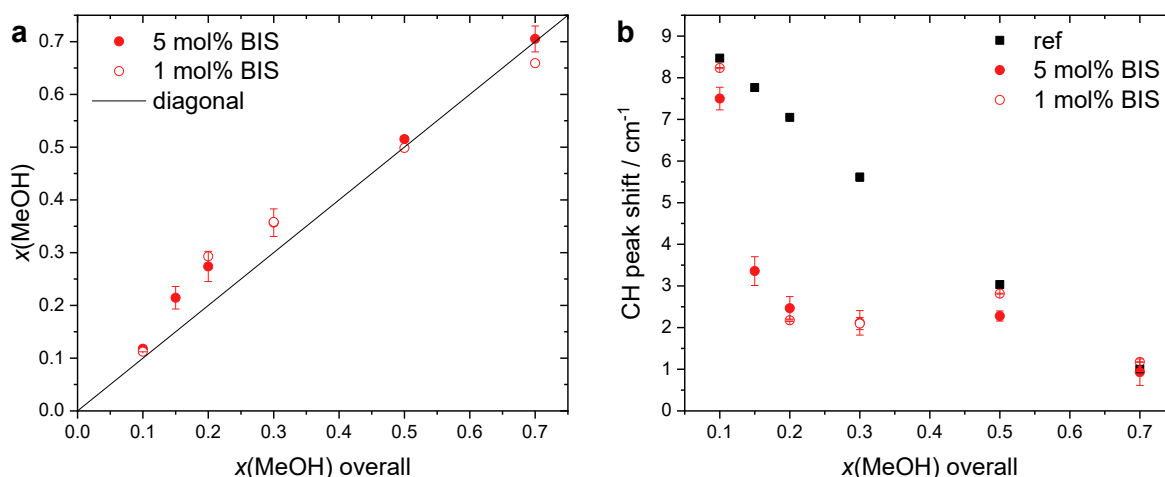


Figure 4.10: Comparison of PNIPAM macrogels with 5 mol% (red, full) or 1 mol% (red, open) cross-linker: (a) Methanol distribution inside the gel after equilibration in various water-methanol mixtures. The diagonal line represents the case of a uniform distribution. (b) Methanol CH-peak shift extracted from spectra measured in a binary reference solution of solely water and methanol (black) and inside the gels (red).

4.6 Conclusions

In the region of the cononsolvency-induced collapse, an increased fraction of methanol inside PNIPAM gels is found compared to the surrounding liquid. However, less methanol is observed in the PNIPAM gel compared to the same system with ethanol presented by H  ther et al.^[89] Thus, the accumulation of the alcohol species inside the polymer network in its collapsed region is more pronounced with increasing hydrophobicity of the alcohol moiety.

For more detailed information on molecular interactions, the sensitivity of the methanol vibrational bands to the local environment of methanol was exploited. More explicitly, the impact of acceptor/donor hydrogen bonding of methanol is taken into account. The binary water-methanol mixture exhibits a linear dependence of the methanol peak positions on the methanol fraction over a wide composition range. However, a deviation from this trend is found for the ternary system with water-methanol-PNIPAM which is ascribed to two effects: Firstly, a small shift is caused by the different solvent composition inside the gel leading to a change in water-methanol hydrogen bonding. Secondly, a major part of the peak shift is due to interactions between methanol and PNIPAM. Based on literature findings, donor-type hydrogen bonding can be responsible for a decrease in wavenumber of the methanol CH-peak position (and an increase of the methanol CO-peak position).^[207,226] Therefore, the presented results suggest that methanol predominantly donates its hydrogen for interactions with the oxygen of the carbonyl group of PNIPAM within the cononsolvency-induced collapse. In general, no distinct difference is found between gels with different cross-linker contents. Both, 1 and 5 mol% BIS-gels exhibit the accumulation of methanol accompanied by similar shifts of the CO- and CH-peak positions.

The obtained results regarding the cononsolvency behavior, the enrichment of methanol inside the gel, and the molecular interactions can provide further understanding of the performance of new functional materials. For applications in catalysis, drug delivery systems, or extraction and separation processes, information on the local structure and polarity within the gels are valuable.^[258,259] For example, the properties of the environment during catalysis impact the catalytic activity and selectivity.^[72,75,260] Hydrophobic substrates and/or catalysts will prefer the increased hydrophobicity of the collapsed, methanol-enriched polymer network (see Chapter 6). Furthermore, Mukherji et al.^[251] recently pointed out the importance of a detailed understanding of the cononsolvency to create design principles for new materials. Here, molecular information about the local arrangement of the solvent molecules can support the setup or verification of simulations predicting, e.g. properties and structures of PNIPAM-based systems in cononsolvency mixtures. In this respect, further detailed insights regarding the kinetics of the volume phase transition induced by cononsolvency should be pursued (see Chapter 8).^[22,261,262]

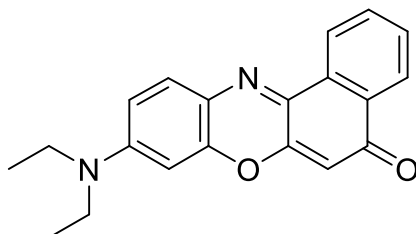
5. Probing the internal environment of solvatochromic microgel beads

ABSTRACT: Many applications of microgels rely on their unique adaptability, and therefore variable physical properties of the polymer network. Especially for drug-delivery systems, uptake and release, or catalysts, the environment provided by the microgels in contrast to the surroundings is crucial. Poly-*N*-isopropylacrylamide (PNIPAM) microgels are mostly known and studied due to their thermoresponsive behavior. Other external stimuli, such as the solvent composition, are less understood. Here, the internal properties of the microgels at different compositions still require further detailed investigations. This work contributes to this question by taking a close look at the polarity of PNIPAM microgel beads in various water-methanol (MeOH) mixtures. To this end, PNIPAM microgel beads were synthesized by microfluidics and subsequently covalently labeled with Nile Red (NR). NR is a solvatochromic dye that can probe the polarity of its microenvironment. Its emission maximum and lifetime correlates with the solvent composition. Confocal fluorescence spectroscopy was employed to resolve the polarity inside the microgels in comparison to the polarity of binary water-methanol mixtures. Significant differences are found for the cononsolvency-inducing mixtures. Here, the polymer network presents a lower polarity than the respective binary mixture. This deviation can be attributed to the combined effect of the deswollen polymer network and a higher methanol concentration inside the gels. Fluorescence lifetime imaging of microgel beads shows high potential to give quantitative and spatially resolved insights into the enrichment of methanol inside the microgel beads.

5.1 Introduction

Microgels are often discussed in terms of a versatile functional material for various applications, e.g. as nano-carriers in drug-delivery systems, sensors, and catalysts.^[15,63,72,81] In these applications, the environment inside the polymer network in comparison to the surrounding fluid is crucial as the environment inside the microgel should often be favored. Consequently, it is important to understand and investigate the differences, e.g. in polarity. A powerful tool to probe the polarity is the solvatochromism of fluorescent dyes. Solvatochromic dyes change their color in response to a change in their microenvironment and are widely applied for fluorescence sensing and imaging.^[234,236,237] One prominent example of a hydrophobic solvatochromic dye is Nile Red (NR, Scheme 5.1). NR exhibits an intensive fluorescence emission in methanol (MeOH) around 638 nm. In contrast, water causes a

significant red shift to 661 nm and the emitted fluorescence intensity decreases.^[263] Thus, the emission wavelength shifts to higher values with increasing polarity of the solvent. Therefore, a common approach to obtain insights into the local polarity is the evaluation of the position of the emission maximum of NR (λ_{max}). The fluorescence lifetime poses another parameter influenced by the hydrogen-bonding ability of the surrounding solvent.^[237,238]



Scheme 5.1: Chemical structure of Nile Red (NR).

NR has been used to stain and examine the polarity of biological structures,^[234,237,264-266] as a probe for hydrogen bonding,^[238] and for uptake^[95] and release studies.^[267] Furthermore, it has been utilized to observe structural changes of linear polymers, highly-branched polymers, or gels.^[95,258,268,269] In super-resolved fluorescence microscopy, NR has been exploited to gain information about environmental properties in addition to positional information.^[258,265,266] Moon et al.^[266] used the polarity-dependent emission shift of NR to reveal a compositional inhomogeneity in the membranes of live mammalian cells. Purohit et al.^[258] investigated the local polarity inside poly-*N*-isopropylacrylamide (PNIPAM)-based core-shell microgels with super-resolved fluorescence microscopy. PNIPAM is an intensively studied functional polymer that can change its physical properties in response to external triggers. It is most known for its temperature-dependent behavior.^[3] Increasing the temperature above a critical value causes a transition from a swollen, flexible polymer network to a hard, collapsed sphere. Purohit et al. exploited the sensitivity of NR without covalent binding to gain spatially resolved information on the hydrophobicity of the core-shell microgels at various temperatures. The polarity decreased with the collapse of the respective microgel compartment. Pietsch et al.^[236] reviewed the combination of the thermoresponsive behavior of smart polymers and the solvatochromism of dyes to create “fluorescent thermometers”.

Despite the well-investigated thermoresponsive behavior, PNIPAM can additionally exhibit a distinct sensitivity to the solvent mixture composition, the so-called cononsolvency effect (see section 1.2). Here, PNIPAM attains a swollen structure in either of the two pure solvents, whereas certain mixtures lead to a collapse of the polymer chains. Typical examples are water-alcohol mixtures but cononsolvency can also occur in mixtures of water and other organic solvents such as dimethylformamide (DMF) or tetrahydrofuran (THF).

Thivaïos and Bokias^[95] studied PNIPAM gels in water-THF mixtures and observed the adsorption of NR by the gels using indirect measurements of the surrounding solution. Depending on the swelling state of the polymer network, a different affinity of NR to diffuse into the gels was found. Due to the deswelling of the gels in water-rich mixtures, the polymer network offers a hydrophobic environment favored by the hydrophobic dye. In contrast, no significant adsorption of NR in the THF-rich regime, and thus by a swollen polymer network in a less polar solvent, was observed.^[95]

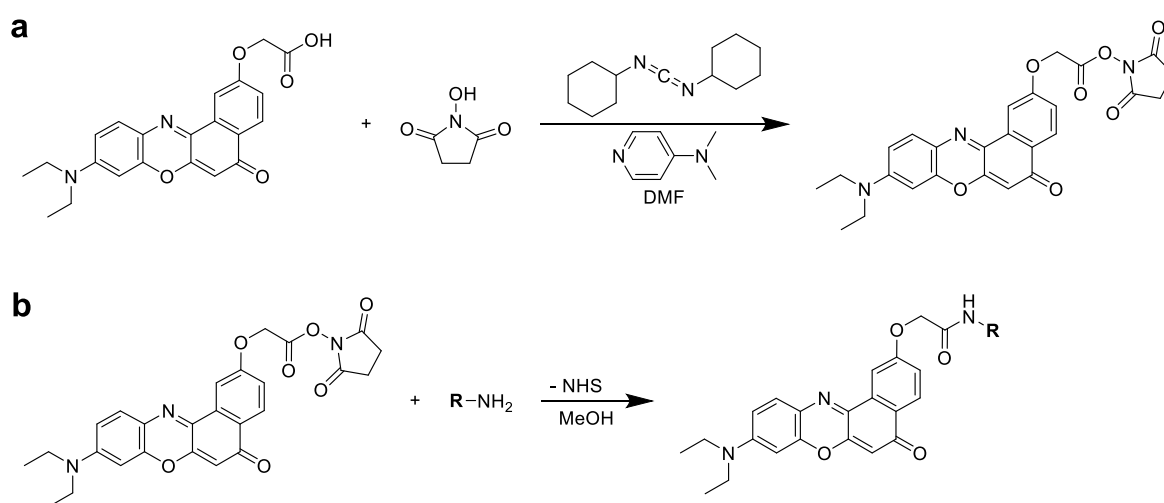
In the present work, the cononsolvency behavior of PNIPAM microgel beads with covalently bound NR moieties in water-methanol mixtures was investigated. To allow spatially resolved measurements without needing a highly complex measurement method, microgel beads with a diameter of around 26 μm in water were synthesized by microfluidics. In a second step, these microgel beads were covalently labeled with a NR derivative. The size of the microgel beads allows to resolve the change of the NR emission and lifetime directly inside the gels as a function of the methanol fraction using confocal fluorescence spectroscopy. Here, pronounced differences between the polarity inside the microgel beads and the polarity of a binary methanol-water system were found for the cononsolvency-inducing mixtures. Furthermore, the high potential of fluorescence lifetime imaging (FLIM) to obtain spatially resolved and quantitative information on the microenvironment was shown in first experiments.

5.2 Synthesis of solvatochromic microgel beads

Solvatochromic microgel beads were prepared in several steps (for experimental details, see section 10.3.4). Microfluidics was used to synthesize PNIPAM microgel beads with a primary amine group by introducing *N*-(3-aminopropyl) methacrylamide (APMA) as a co-monomer in the aqueous phase. Here, 1 or 3 mol% APMA was used. Both samples exhibited a mean diameter around 25 μm in their swollen state in water: for MG-PNIPAM-APMA-1 (1 mol% APMA), a diameter of $26 \pm 2 \mu\text{m}$ was measured, and for MG-PNIPAM-APMA-3 (3 mol% APMA), a diameter of $25 \pm 3 \mu\text{m}$. For the subsequent labeling step (Scheme 5.2), a NR derivative with an *o*-carboxylic group (NR-O-C-COOH) was activated with *N*-hydroxysuccinimide (NHS) (Scheme 5.2a). The NHS-activated ester group then reacted with the primary amine of the APMA-modified microgel beads (Scheme 5.2b).

In the first approach of the labeling step, the concentration of MG-PNIPAM-APMA-1 was adjusted to approximately 1 mg/mL in phosphate buffer (pH 8) and the NR derivative was added. After purification, the microgel beads were imaged by fluorescence microscopy. Here, an inhomogeneous distribution of the NR-labels was observed (Figure A2 in the

Appendix). The cause of this uneven labeling might be the nonpolar character of the NR derivative. If added to the rather polar buffer solution, the NR catches onto the more hydrophobic microgel beads as soon as possible without a uniform distribution throughout the solution and polymer network. As a consequence, the labeling step was conducted in methanol instead of the phosphate buffer solution. To additionally increase the fluorescence intensity, the MG-PNIPAM-APMA-3 sample, i.e. with more primary amine groups, was labeled in parallel to the MG-PNIPAM-APMA-1. For both samples, a uniform fluorescence was imaged after labeling, mixing, and washing (Figure 5.1). As higher labeling is desirable for the following fluorescence spectroscopy, experiments proceeded with the MG-PNIPAM-APMA-3-NR sample.



Scheme 5.2: (a) Activation of the NR derivative (NR-O-C-COOH) with NHS. (b) Labeling reaction: the NR-O-C-COO-NHS reacts with the primary amine groups present in the APMA-modified microgel beads (simplified as R-NH₂).

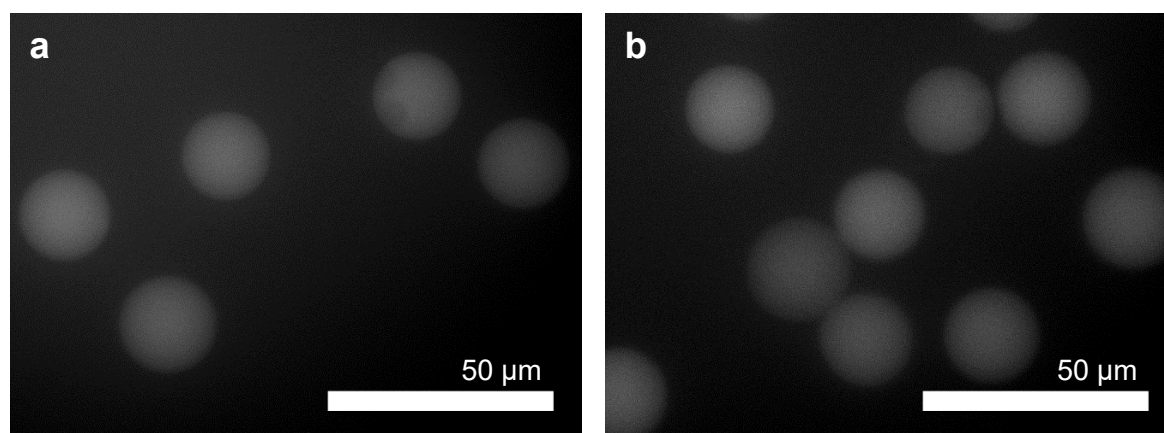


Figure 5.1: Images of the NR-labeled PNIPAM microgel beads in methanol using a conventional fluorescence microscope: (a) MG-PNIPAM-APMA-3-NR ($d(\text{MeOH}) = 23 \pm 3 \mu\text{m}$) and (b) MG-PNIPAM-APMA-1-NR ($d(\text{MeOH}) = 22 \pm 2 \mu\text{m}$).

5.3 Probing the local polarity by fluorescence spectroscopy

In the following, the results from the fluorescence spectroscopic measurements in various water-methanol mixtures are discussed (for experimental details, see section 10.5.1). The measurements were performed by Dr. Silvia Centeno Benigno. First, reference measurements with free NR-O-C-COOH were conducted for various water-methanol mixtures. The black points in Figure 5.2 represent the position of the emission maximum of NR-O-C-COOH ($\lambda_{\text{max}}(\text{ref})$) in the respective mixture. Depending on the solvent composition, values between 638.4 nm in pure methanol and 661.5 nm in pure water were extracted from the fluorescence spectra. A linear dependence of $\lambda_{\text{max}}(\text{ref})$ and $x(\text{MeOH})$ is found: the higher the methanol mole fraction the lower the wavelength of the maximum emission. Hence, the position of the maximum emission gives insights into the polarity and solvent composition of the system. As water is more polar than methanol, a higher wavelength correlates with higher polarity.

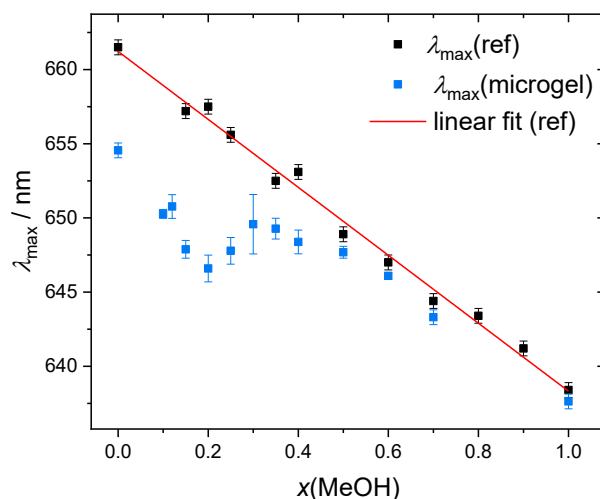


Figure 5.2: Wavelength of the maximum emission of NR as a function of the methanol mole fraction in the reference system (NR-O-C-COOH, black) and the NR-labeled PNIPAM microgel beads (blue, MG-PNIPAM-APMA-3-NR).

Secondly, comparative experiments were performed in similar mixtures using the NR-labeled PNIPAM microgel beads. The values of $\lambda_{\text{max}}(\text{microgel})$ were extracted as described in the experimental section (blue points Figure 5.2). For high methanol fractions (> 50 mol% methanol), the values for the position of the maximum emission inside the gel are found to be similar to those of the reference experiments. However, a significantly different dependence of $\lambda_{\text{max}}(\text{microgel})$ on the solvent composition is obtained in the water-rich region (< 50 mol% methanol). In pure water, the emission maximum inside the microgel beads is lower than in the reference solution due to the hydrophobic character of the polymer network. Upon addition of methanol, the wavelength strongly decreases up to 20 mol% of

methanol in water. Subsequently, a slight increase of the wavelength for methanol fractions up to 30 mol% occurs before it decreases again for higher methanol fractions. The “bump” around the most unfavorable mixture of 20 mol% methanol in Figure 5.2 correlates with two overlaying effects. As known from temperature-dependent investigations, collapsed microgels present a higher hydrophobicity of the polymer network.^[258] Water-methanol mixtures around 20 mol% methanol also lead to a collapse of the microgel beads. Additionally, the results in Chapter 4 show that methanol accumulates inside PNIPAM gels in the region of the cononsolvency-induced collapse. Both effects cause a less polar environment inside the PNIPAM microgel beads in the collapse-inducing solvent mixtures, nicely captured by the locally decreased emission wavelength of the NR-label. When exceeding a methanol concentration of 20 mol%, the partial reswelling of the microgel beads lead to a small increase of the wavelength of the NR band. At methanol fractions > 30 mol%, the effect of the reswelling of the polymer network on the local polarity is exceeded by the higher apolarity due to the overall increased methanol fraction. Consequently, $\lambda_{\text{max}}(\text{microgel})$ decreases and follows the linear course of the reference above 50 mol% methanol.

5.4 Fluorescence lifetime imaging (FLIM)

The potential of fluorescence lifetime measurements (FLIM) to obtain further detailed insights was tested in first experiments (for experimental details, see section 10.5.2). Measurements were conducted by Dr. Silvia Centeno Benigno. First of all, a reference system comprising the NR derivative (NR-O-C-COOH) in different solvent mixtures was investigated. The average arrival times of emitted photons after excitation by a laser pulse were detected and evaluated with a multi-exponential decay function to extract the lifetime components τ . In the case of the reference system, a mono-exponential model was sufficient to describe the decay curves, and therefore one lifetime component was extracted for each composition. The dependence of the lifetime on the methanol mole fraction is shown in Figure 5.3. Similar to the shift in the position of the maximum emission, there is a linear correlation between the lifetime and the solvent composition. The longer the lifetime, the less polar is the environment of the NR-derivative. In comparison, the lifetime determined for the NR-derivative (3.0 ns) in the present measurements is slightly higher than the 2.80 ns Cser et al.^[238] measured for pristine NR in methanol.

Furthermore, FLIM measurements of NR-labeled microgel beads under different conditions were performed: directly after being spin-coated from a methanol dispersion, swollen by methanol, or immersed in an unfavorable mixture of 20 mol% methanol. For the

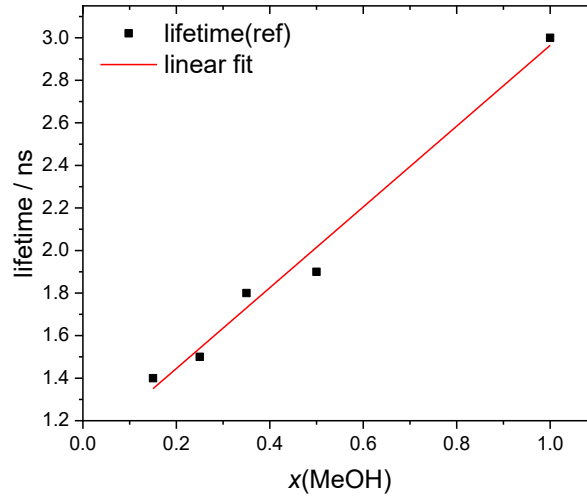


Figure 5.3: Fluorescence lifetime of the reference system (NR-O-C-COOH) as a function of the methanol mole fraction in water-methanol mixtures fitted with a linear function. For all binary mixtures, only one lifetime component was required to describe the fluorescence decay.

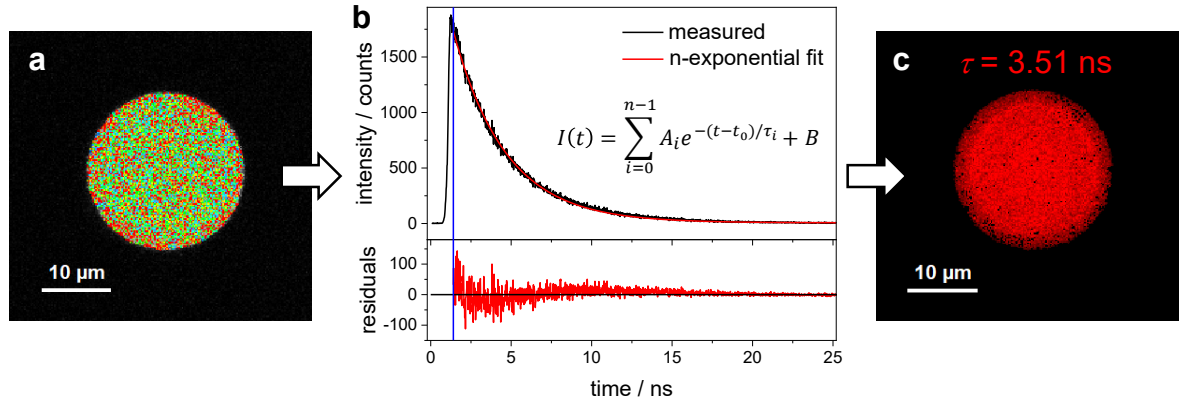


Figure 5.4: Fluorescence lifetime measurements of a NR-labeled microgel bead (MG-PNIPAM-APMA-3-NR) immersed in pure methanol after spin-coating. The average arrival times visible in the FastFLIM image (a) are analyzed using a multi-exponential tail fit with n lifetime components (b). The lifetime components obtained from the fit are applied to the FastFLIM image to construct the final FLIM image (c). Each pixel containing a certain lifetime is indicated in the corresponding color. In this case, only one lifetime of 3.51 ns was found and the respective pixels are marked in red.

case of using the microgel beads swollen by methanol, the data acquisition and processing is illustrated in Figure 5.4. An area of around $115 \times 115 \mu\text{m}^2$ of the sample was imaged and the arrival times of the photons emitted by the sample were detected for each pixel resulting in a color-map image of the average arrival times (FastFLIM image). Then, a region of interest, i.e. a single microgel bead, was defined (a). As before, the time-dependent photon count was plotted and fitted with a multi-exponential fit to determine the lifetime components (b). Depending on the decay curve, one, two, or more exponential terms were required for an adequate description of the data. Finally, the multi-exponential decay model was applied to each pixel in the FastFLIM image to build up the FLIM image (c). Every pixel was colored in the color assigned to the corresponding lifetime component. In the case

of the microgel bead swollen by methanol, one lifetime component was sufficient. Therefore, only one color (red) is visible in the final FLIM image. A lifetime distribution with its maximum at 3.51 ns for the NR-labeled microgel beads in methanol was observed. As aforementioned, in the reference measurements of NR-O-C-COOH in methanol, a lifetime of 3.0 ns was obtained. Thus, the microenvironment of the NR-label inside the microgel bead is more hydrophobic than the one without the polymer network.

An exemplary FLIM image of the microgel beads solely spin-coated from a methanol dispersion, without addition of any further solvent, is shown in Figure 5.5a. Here, two lifetime components were necessary to fit the fluorescence decay. Specifically, $\tau_1 = 4.5$ ns (red pixels) and $\tau_2 = 3.1$ ns (green pixels). Yellow pixels result from the combination of both. The longer lifetime corresponds to an ethylacetate-like environment or a poor hydrogen-bonding solvent.^[238] The second lifetime can be assigned to a methanol environment. The less polar environment is mainly detected at the outer region of the microgel beads. In the core of the microgel beads, yellow, thus the combination of both lifetimes, is predominantly found. This distribution suggests that only the periphery of the microgel beads dried during the spin-coating process leaving a hydrophobic, polymer-rich shell. In the interior of the gel, some methanol molecules were entrapped resulting in regions with a smaller lifetime.

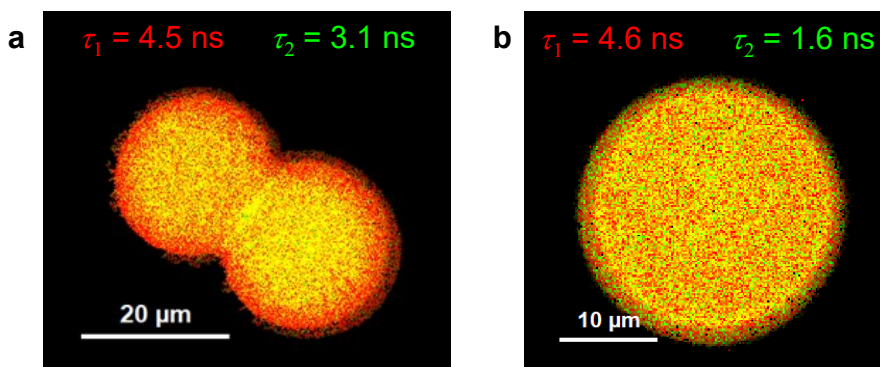


Figure 5.5: FLIM images of NR-labeled microgel beads (MG-PNIPAM-APMA-3-NR): (a) spin-coated from a methanol dispersion without additional solvent, and (b) immersed in 20 mol% methanol in water.

Figure 5.5b gives an example of a microgel bead immersed in the most unfavorable water-methanol mixture with 20 mol% methanol. Again, a bi-exponential function was required to properly describe the fluorescence decay. Both components are nearly evenly distributed throughout the microgel bead resulting in numerous yellow pixels. Interestingly, some pixels are exclusively green or red. Thus, heterogeneity of the polymer network on the length scale of one pixel (between 150 and 179 nm) is suggested. The first lifetime exhibits a value of 4.6 ns (red) and is comparable to the lifetime found for the spin-coated sample ascribed to the hydrophobic polymer network. The second lifetime of 1.6 ns (green) is significantly

shorter and is assigned to the solvent mixture. Using the linear fit from the reference measurements (Figure 5.3), 1.6 ns correspond to a water-methanol mixture with 28 mol% methanol. Thus, in this cononsolvency-inducing mixture, an enrichment of methanol can be observed. This aligns almost quantitatively with the results from the mass balance experiment using macroscopic PNIPAM gels presented in Chapter 4 (Figure 4.4). These first experiments already demonstrate the high potential of FLIM. The measurement method and size of the microgel beads enable the spatially resolved and quantitative evaluation of the internal environment and solvent composition. Further measurements and data evaluation for more microgel beads are ongoing to achieve better statistics.

The diameter of the microgel bead in the unfavorable mixture is strikingly close to the size measured for the swollen state. In the 20 mol% methanol sample, microgel beads with a significantly smaller diameter were found as well ($\sim 13 \mu\text{m}$). Fluorescence spectroscopy measurements and FLIM of these smaller microgel beads revealed a smaller wavelength of the emission maximum and longer lifetimes for the solvent mixture environment compared to larger microgel beads. These observations hint towards an even higher accumulation of around 40 mol% methanol inside the microgel beads. Further investigations are needed to elucidate where these differences originate from. Spreading and adhesion due to the spin-coating during the sample preparation presumably influence the contact area of the microgel beads with the glass slide.

5.5 Conclusions

PNIPAM microgel beads containing primary amine groups were successfully synthesized by microfluidics and subsequently covalently labeled with a NR-derivative. Due to the apolar nature of NR, homogeneously labeled microgel beads are only obtained when the labeling step is conducted in methanol instead of phosphate buffer. The labeling density can be adjusted by the concentration of co-monomer APMA during the synthesis, i.e. the number of primary amine groups in the polymer network.

The evaluation of the shift in wavelength of the maximum emission band of NR revealed a linear dependence on the solvent composition for the reference measurements with free NR-O-C-COOH. In contrast, there was a clear deviation from this linear correlation in the case of the NR signal emitted by the NR-labeled microgel beads. The wavelength of the emission maximum of the NR-label represents the local polarity inside the modified microgel beads: in the water-rich regime, the water-methanol mixtures act as bad solvents for the polymer network. The resulting collapse of the microgel beads increases the local hydrophobicity, therefore reducing the wavelength of maximum emission. Additionally, the

wavelength was lowered even further by the enrichment of methanol inside the beads in these cononsolvency-inducing mixtures. For methanol fractions above the most unfavorable mixture of 20 mol% methanol, the partial reswelling of the microgel beads lead to a small increase of the wavelength of the NR band. Subsequently, for the methanol-rich regime, the position of the NR band is mainly governed by the apolarity due to the methanol fraction in the surrounding mixture.

First spatially resolved measurements of the fluorescent lifetime of the NR-label provided further and quantitative insights. Similar to the position of the emission maximum, the lifetime of the reference (NR-O-C-COOH) exhibits a linear dependence on the solvent composition. For the NR-labeled microgel beads in pure methanol, one lifetime component evenly distributed across the microgel bead was evaluated. The hydrophobic polymer network slightly increased the lifetime component in comparison to the lifetime of free NR in methanol. In contrast, the evaluation of FLIM for microgel beads immersed in a 20 mol% methanol in water mixture required two lifetime components. The longer lifetime corresponds to the hydrophobic polymer network. The shorter lifetime correlates to an enrichment of methanol inside the polymer network. These findings align with the enrichment found for the macroscopic PNIPAM gels discussed in Chapter 4. Open questions regarding the degree of deswelling and quantitative enrichment of methanol in the unfavorable mixture remain and require further investigations.

6. Modulation of the catalytic activity of microgel-catalysts by external triggers

The following chapter was reproduced from: Kleinschmidt, D.; Nothdurft, K.; Anakhov, M. V.; Meyer, A. A.; Mork, M.; Gumerov, R. A.; Potemkin, I. I.; Richtering, W.; Pich, A., Microgel organocatalysts: modulation of reaction rates at liquid-liquid interfaces. *Materials Advances* **2020**, *1*, 2983-2993. Published by the Royal Society of Chemistry. – *for contributions of authors see page V – Solely the results of the scattering experiments performed by myself are discussed in detail. The remaining results are briefly presented to enable the placement in the context.*

ABSTRACT: Smart and responsive nano-carriers for catalysis show high potential to systematically investigate and control the catalytic activity. Within this chapter, a colloidal microgel-catalyst comprised of poly-*N*-isopropylacrylamide (PNIPAM) with covalently-bound L-proline moieties is presented. The work focuses on the modulation of the catalytic activity due to the responsiveness of PNIPAM to temperature and solvent composition. Here, the aldol reaction of cyclohexanone with 4-nitrobenzaldehyde was studied in water, methanol (MeOH), and various mixtures of these two solvents. Previous to catalytic testing, the microgel-catalysts and their swelling behavior were characterized by dynamic and static light scattering (DLS, SLS). Additionally, the experimental results were combined with dissipative particle dynamics (DPD) simulations providing insights into the structure of the reaction system in different solvents. Here, a grave difference with respect to the surrounding solvents was found. In methanol, reagents and microgel-catalysts form a homogeneous system. In contrast, the system is heterogeneous in an aqueous solution where the microgel-catalysts adsorb at the liquid-liquid interface between water and the hydrophobic reagents. When increasing the temperature to above the volume phase transition temperature (VPTT) of PNIPAM, the collapsed polymer network immerses more into the reagents phase. As a result, the reaction rate increases. In water-methanol mixtures, overlaying effects occur. The collapse of the microgels and enrichment of methanol inside the microgels at 20 mol% methanol increases the catalytic activity for mixtures around this composition. In general, a higher methanol fraction positively influences the reaction rate. The different micro-environments provided by the polymer network depending on its swelling state and the general solvent quality modulate the catalytic behavior.

6.1 Introduction

Microgels are usually spherical, cross-linked polymer networks with a porous and soft structure. One outstanding property of microgels is their responsiveness to their surroundings. Depending on the monomer or combination of monomers, the physical properties, such as size or stiffness, can be modulated by external stimuli, e.g. temperature, pH, or solvent composition.^[5] The most intensively studied microgels are based on poly-*N*-isopropylacrylamide (PNIPAM) and *N,N'*-methylenebis(acrylamide) (BIS) as the cross-linker.^[3] Additionally, functional co-monomers for fluorescent labeling, protein sequences, or catalytically active sites can be easily incorporated during the free-radical precipitation polymerization.^[4,5] Due to their versatile compositions and properties, microgels have become an important material class in recent studies of polymer science. Microgels find application, e.g. in drug-delivery, biomaterials, smart emulsion (de)stabilization, sensors, or catalysis.^[15,59] In catalysis, microgels have been explored as smart nano-carriers, e.g. for metal nanoparticles, enzymes, metallic complexes, or organocatalysts.^[73-78] Microgels enable the immobilization and stabilization of the catalysts in the reaction medium. For instance, the incorporation of metal nanoparticles into the polymer network prevents their aggregation and leaching.^[270,271] Additionally, microgels simplify the recycling and reuse of catalysts.^[75,270] In the case of functional microgels, their responsiveness to the surroundings can be exploited to modulate the catalytic activity.^[74,271,272] Lu et al.^[272] reported a nano-composite system comprising a polystyrene core with a PNIPAM shell carrying Ag nanoparticles for the model reaction of 4-nitrophenol to 4-aminophenol by sodium borohydride. Due to the thermoresponsive behavior of PNIPAM, the catalytic activity of the nanoparticles could be controlled. At high temperatures, the collapsed polymer network caused a significant diffusion limitation and thus, a deviation from the conventional Arrhenius-type dependence on temperature. Ferguson et al.^[74] also studied PNIPAM-based nanogels but additionally copolymerized a photocatalytic co-monomer. These dual-responsive photocatalytic polymer nanogels can be repetitively quenched and reactivated by changes in temperature. Photocatalysis only takes place at low temperatures in the swollen state of the microgel-catalysts.

In a recent study by Kleinschmidt et al.,^[75] the amino acid L-proline was incorporated in PNIPAM microgels. L-proline is an example of an organocatalyst, i.e. an inexpensive and nontoxic small organic molecule, that can be used instead of metal-based catalysts or enzymes for asymmetric catalysis. Free L-proline is water-soluble, however, most organic reagents are only poorly soluble in water. Thus, only a slow reaction rate and low catalyst turnover number at high catalyst loading can be achieved.^[273] To overcome this problem, polymer-supported L-proline systems^[273-276] such as the L-proline modified PNIPAM

microgels^[75,277] were explored. Kleinschmidt et al.^[75] focused on the optimization of the enantioselective aldol reaction of 4-nitrobenzaldehyde and cyclohexanone. For this purpose, the influence of the localization of the L-proline within the microgel was compared. In all cases, the microgel-catalysts allowed catalytic reactions in an aqueous reaction system by creating a hydrophobic environment, while free L-proline is inactive in an aqueous solution. In water, this hydrophobic environment surrounding the catalytically active sites is more effective when the L-proline moieties are localized in the microgel core. The hydrophobic reagents locally accumulate in the L-proline-rich core minimizing unfavorable contacts with water leading to higher reaction rates. In methanol (MeOH), the reagents are well soluble. Here, easily accessible L-proline moieties are favored resulting in the highest reaction rate for the microgel-catalysts with L-proline in the outer shell of the microgels. Finally, recycling of the catalysts with stable conversion and selectivity values was reported.^[75]

Within the following chapter, the same microgel-catalysts composed of L-proline modified PNIPAM microgels for the aldol-reaction of 4-nitrobenzaldehyde and cyclohexanone are discussed. However, while these microgel-catalysts served only as passive carriers in the previous study, the focus now lies on the catalysis and especially its modulation due to the responsiveness of the microgels. On the one hand, PNIPAM exhibits a distinct thermoresponsive behavior in water with a volume phase transition temperature (VPTT) around 32 °C.^[3] On the other hand, PNIPAM shows a cononsolvency behavior: In pure water and pure methanol, the polymer network is swollen, whereas a drastic volume loss occurs around 20 mol% methanol.^[19] The influence of these two external triggers, temperature and solvent composition, on the catalytic properties of the microgel-catalysts was evaluated. In order to gain deeper insights, the experimental results from scattering methods and catalytic testing were combined with dissipative particle dynamics (DPD) simulations.

6.2 Characterization of the microgel-catalysts

The precipitation polymerization of NIPAM, BIS, and the copolymerizable L-proline derivative achieved a good yield of 92%. Attenuated total reflection Fourier transform infrared (ATR-FTIR) spectroscopic measurements confirmed the presence of 6.69 mol% effectively incorporated L-proline groups. The catalytic activity of these microgel-catalysts was tested and compared as a function of temperature and various water-methanol mixtures. Previous to catalytic testing, the swelling behavior of the microgel-catalysts was characterized by dynamic and static light scattering (for experimental details, see section 10.6).

The hydrodynamic radius (R_h) of the microgel-catalysts was investigated as a function of the temperature in water (20 – 50 °C), methanol (20 – 50 °C), and 20 mol% methanol (10 – 40 °C) (Figure 6.1a). Additionally, the temperature dependence is compared to the behavior of pure PNIPAM microgels (5 mol% BIS) (Figure 6.1b). For the microgel-catalysts, a reversible temperature-responsive behavior is found in all three solvents. The heating and cooling cycle overlap (Figure 6.1a). In water, the typical, distinct temperature dependence is found between 20 and 50 °C. The microgel-catalysts are swollen in water at low temperatures. At the VPTT, a large decrease in size is observed. The hydrodynamic radius of 167 ± 2 nm at 25 °C decreases by 34% to 110 ± 1 nm at 45 °C. The transition temperature of the microgel-catalysts is slightly shifted to a higher value (35 °C) compared to pure PNIPAM microgels (32 °C). In the case of pure PNIPAM microgels, a plateau is reached for higher temperatures around 40 °C. In contrast, the microgel-catalysts show a further significant decrease in size above 45 °C (see Figure 6.1b). The minimum size was measured at 70 °C with a hydrodynamic radius of 68 nm corresponding to a decrease in size of about 60% compared to 25 °C. A further increase of the temperature up to 75 °C did not induce further deswelling. This suggests that the microgel-catalysts are fully collapsed at 70 °C which is coherent with the synthesis temperature. Normalized to the size measured at the highest temperature in water (45 °C for the PNIPAM microgels, 75 °C for the microgel-catalysts), it becomes obvious that the swelling ratio of the microgel-catalysts is higher than that of the PNIPAM microgels. The difference can be explained by the lower cross-linker concentration during the microgel-catalyst synthesis (~ 2 mol%). In methanol, no distinct temperature dependence is visible for the microgel-catalysts or the pure PNIPAM microgels.

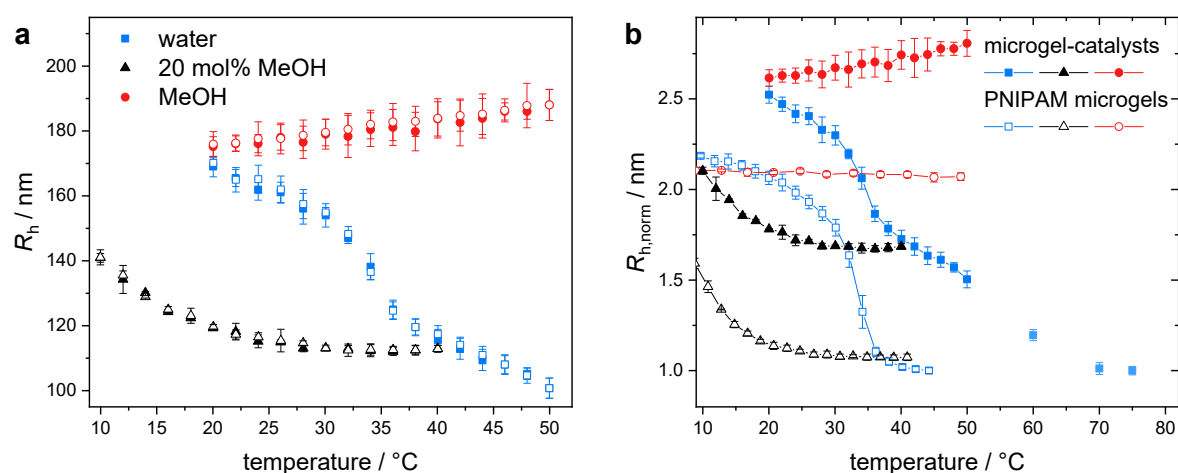


Figure 6.1: (a) Temperature-dependent measurements of R_h of the microgel-catalysts in water (blue), methanol (red), and 20 mol% methanol (black) (full symbols – heating cycle, open symbols – cooling cycle). (b) Comparison of the temperature dependence of R_h of the microgel-catalysts and pure PNIPAM microgels (5 mol% BIS). R_h was normalized to the fully collapsed state at the highest measured temperature. The data of the pure PNIPAM microgels were taken from Kojima et al.^[18]

While pure PNIPAM microgels in methanol do not display any response to the temperature, the radius of the microgel-catalysts seems to slightly increase with increasing temperature (approx. 10 nm). This increase in size suggests that methanol becomes a better solvent for the L-proline PNIPAM network with increasing temperature. The water-methanol mixture with 20 mol% methanol acts as a poor solvent for the microgels and the microgels are in their collapsed state at room temperature. Cooling the samples to below room temperature results in a partial reswelling. Both systems, the microgel-catalysts and pure PNIPAM microgels, are less collapsed in the mixture at room temperature than in water at high temperatures. However, the difference between the radius of the fully collapsed state in water at high temperature and in the 20 mol% mixture above 25 °C is significantly higher in the case of the microgel-catalysts.

Figure 6.2 displays the dependence of the hydrodynamic radius on the composition of the water-methanol mixture at 25 °C. As already shown in the temperature-dependent measurements, the microgel-catalysts are slightly larger in methanol (175 ± 7 nm) than in water (167 ± 2 nm) and exhibit the lowest hydrodynamic radius for the 20 mol% methanol mixture (116 ± 2 nm). At low methanol contents, the size decreases significantly, whereas the polymer network reswells at methanol mole fractions > 20 mol% until it is rather swollen for methanol fractions > 50 mol%. The solvent-dependent swelling shows a minimum at 20 mol% methanol which is similar to pure PNIPAM systems. Surprisingly, no influence of the incorporation of the L-proline on the position of this minimum was detected.

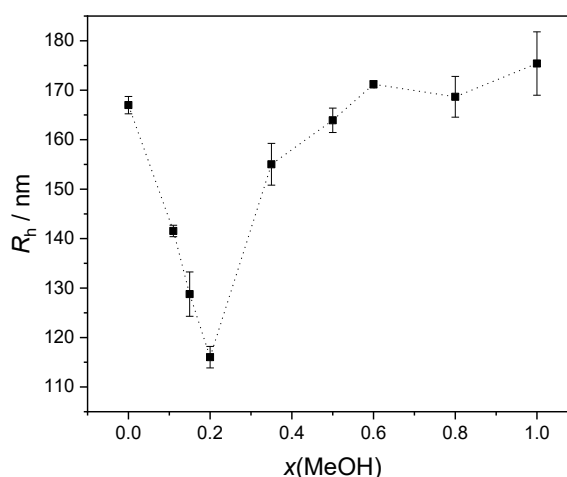


Figure 6.2: R_h of the microgel-catalysts as a function of the water-methanol composition at 25 °C.

In addition to the DLS measurements, the swelling behavior was characterized using SLS (Figure 6.3). SLS measurements were performed in water (25 and 45 °C), methanol (25 °C), and 20 mol% methanol (10 and 25 °C). The corresponding scattering curves are shown in Figure 6.3a. The microgel-catalysts are too small to exhibit any minima in the measured

q -range. Therefore, the Guinier region ($qR_g < 1$) was evaluated to obtain the radius of gyration (R_g).^[278] Here, very low measurement angles were discarded as the solvent background increases significantly in that regime. The Guinier plots and linear fits are shown in Figure 6.3b-d.

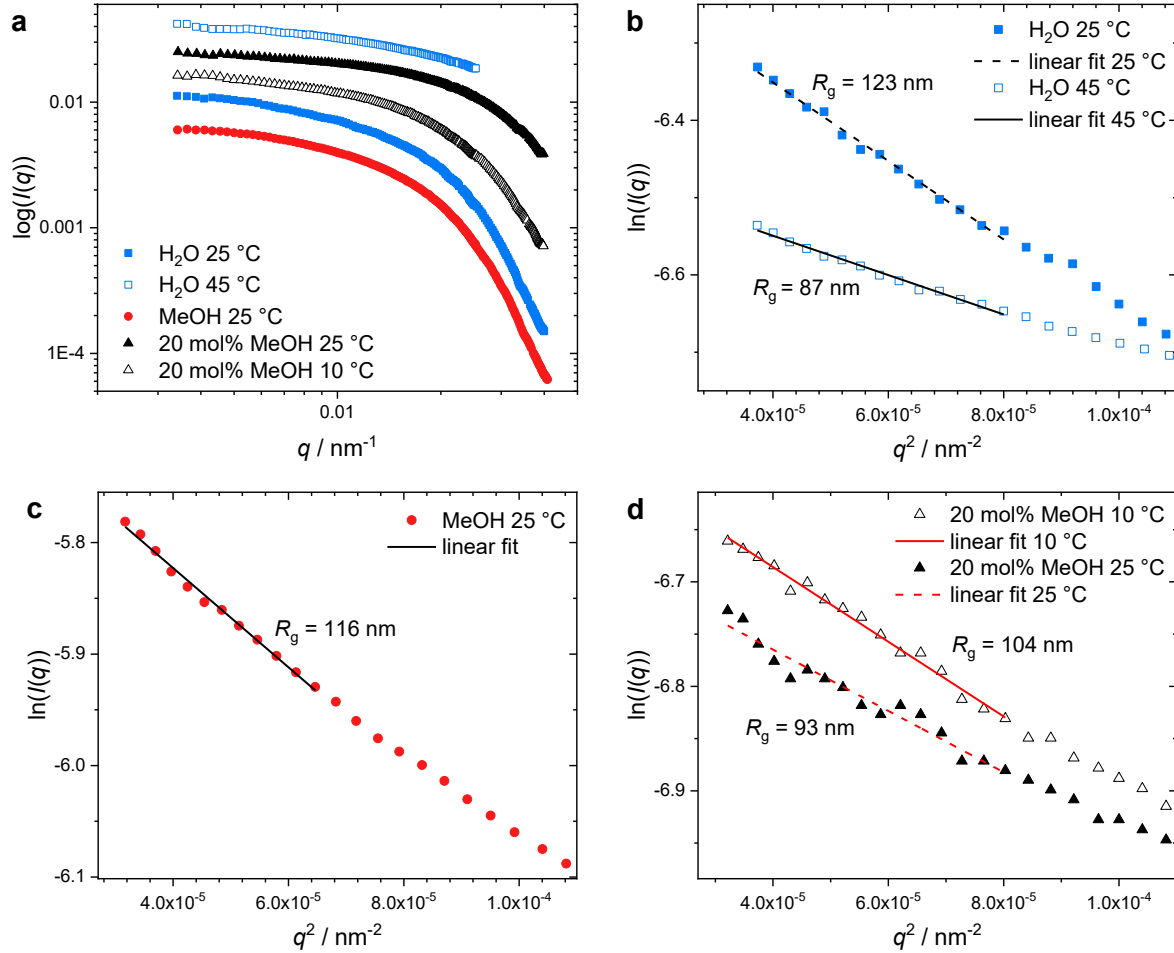


Figure 6.3: Scattering curves (a, shifted for visibility) of the microgel-catalysts in various solvents at different temperatures and the corresponding Guinier plots in water (b), methanol (c), and 20 mol% methanol (d).

Table 6.1 displays an overview of R_h , R_g , and their ratio R_g/R_h . In principle, R_h and R_g exhibit a comparable trend regarding the swelling state of the microgel-catalysts. For the ratio R_g/R_h , it is known that a homogeneous sphere has a value of 0.78. For pure PNIPAM microgels in their swollen state in water, ratios between 0.55 – 0.6 are documented.^[279] In comparison, higher ratios close to the one of a hard sphere were found in the case of the microgel-catalysts. Here, the R_g/R_h -ratios lie between 0.66 and 0.81. The smallest ratios are determined for the swollen microgel-catalysts in methanol and water, as well as for the partly swollen state at 10°C in the 20 mol% methanol mixture. The R_g/R_h -ratios close to 0.78 indicate a less fuzzy, more homogeneous structure of the microgel-catalysts compared to pure PNIPAM microgels.

Table 6.1: Comparison of the R_h , R_g , and their ratio of the microgel-catalysts in different swelling states in water, methanol, and 20 mol% methanol.

Solvent	$T / ^\circ\text{C}$	R_h / nm	R_g / nm	R_g/R_h
Water	25	167 ± 2	123 ± 2	0.74 ± 0.012
	45	110 ± 1	87 ± 2	0.79 ± 0.02
20 mol% MeOH	10	141 ± 1	104 ± 2	0.73 ± 0.012
	25	116 ± 2	93 ± 3	0.81 ± 0.03
MeOH	25	175 ± 7	116 ± 2	0.66 ± 0.04

6.3 Catalytic testing and simulations

The catalytic activity of the microgel-catalysts was investigated at various temperatures as well as in various water-methanol mixtures.

Temperature-dependent catalytic testing was performed between 25 and 45 $^\circ\text{C}$ in steps of 5 $^\circ\text{C}$ in water and methanol, thus comparing the responsive microgel-catalysts in water and the non-responsive system in methanol. In general, the apparent reaction rate constant (k_{app}) is significantly higher in methanol. To improve the comparability, the values of k_{app} were normalized to the corresponding value at 25 $^\circ\text{C}$ and the relative change due to temperature was analyzed (Figure 6.4a). For both solvents, the apparent reaction rate constant increased with the reaction temperature. In methanol, the microgel-catalysts only showed a linear correlation with a 2.5-fold increase between 25 and 45 $^\circ\text{C}$. In contrast, the temperature-dependent change of the reaction rate constant in water significantly differs and highly resembles the temperature-dependent change of the radius. The deswelling of the microgels in water with increasing temperature led to a 5-fold increase in the apparent reaction rate constant. Therefore, the deswelling of the microgels seems to be the predominant factor governing the catalytic activity. From the literature, it is known that the target aldol reaction requires a certain hydrophobic environment close to the L-proline moieties.^[75,280] The higher hydrophobicity of the collapsed microgel-catalysts at high temperatures provides a favorable environment for the hydrophobic reagents. Additional temperature-dependent effects like a limited diffusion due to the deswollen network could not be verified. A possible explanation lies within the swelling behavior of the microgel-catalysts in water. From DLS measurements (Figure 6.1b), it was obtained that the microgel-catalysts are not fully collapsed at 45 $^\circ\text{C}$ but at the synthesis temperature of 70 $^\circ\text{C}$. The incomplete collapse at 45 $^\circ\text{C}$ allows the diffusion of the reagents inside the polymer network at this temperature. More detailed insights on the temperature-dependent catalytic behavior were obtained by DPD simulations. The simulations of the reaction in methanol showed a homogeneous system with no significant changes in the number of contacts with increasing temperature. In contrast, a

heterogeneous system is present in the aqueous system where the microgel-catalysts adsorb at the interface between water and the hydrophobic reagents. Depending on the temperature, the microgels either immerse more into the water or the reagents. Increasing the temperature to above the VPTT, the microgel-catalysts collapse and immerse more in the reagent phase. This leads to a higher average number of contacts between the reagents and the catalytically active L-proline sites. As a consequence, the reaction rate increases.

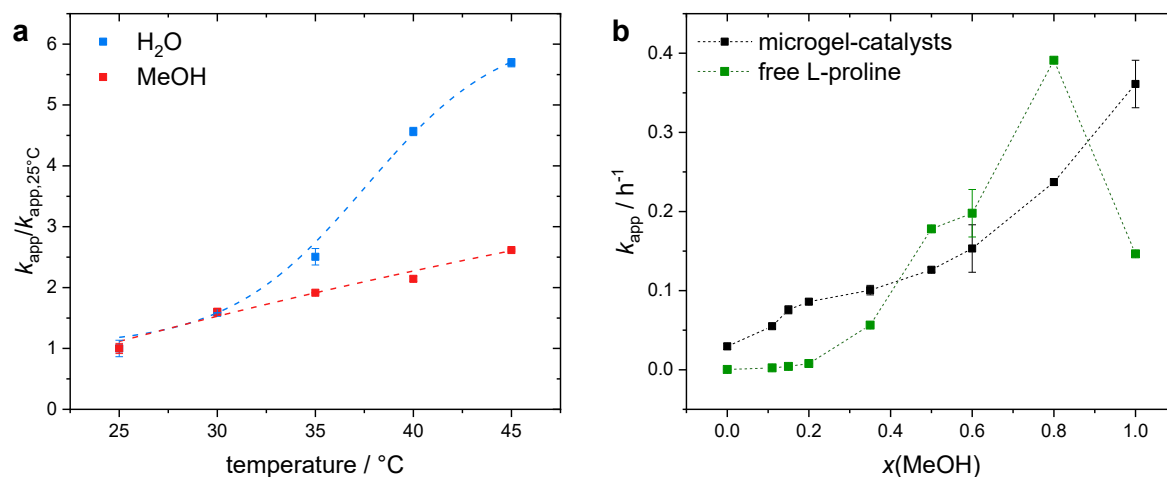


Figure 6.4: Catalytic testing of the microgel-catalysts in the aldol reaction of 4-nitrobenzaldehyde and cyclohexanone: (a) Temperature dependence of the normalized apparent reaction rate constant ($k_{app}/k_{app,25^{\circ}\text{C}}$) of the microgel-catalysts in pure water (blue) and methanol (red). (b) The apparent reaction rate constant of the microgel-catalysts (black) and free L-proline (green) as a function of the methanol fraction in the water-methanol mixtures.

Regarding the catalytic activity in various water-methanol mixtures at room temperature (Figure 6.4b), overlapping effects were revealed. In general, a high methanol fraction is favorable for the catalysis due to the higher solubility of the reagents. Water has an ambivalent role in the enamine-type reaction mechanism.^[281] On the one hand, the formation of key intermediates is suppressed, but on the other hand, water also suppresses reversibly and irreversibly formed spectator species. These two effects have an opposite impact on the reaction rate and a fine balance between them is necessary. Consequently, in the reference experiment with free L-proline, only a slow increase of the reaction rate was found in the water-rich regime up to 20 mol% methanol. Then, a large increase of the reaction rate occurred up to 80 mol% methanol. As a certain amount of water is favorable to suppress spectator species, the reaction rate dropped in pure methanol. In contrast, a slightly different behavior was observed using the microgel-catalysts: In the water-rich regime, the reaction rate increases up to 20 mol% methanol before the growth of the reaction rate becomes more steady, similar to the reaction rate of the unbound L-proline. In the region around 20 mol% methanol, the microgel-catalysts are in their collapsed state. The collapsed polymer network is less polar than the respective binary water-methanol mixtures as demonstrated in

Chapter 5 (Figure 5.2). Thus, the microgel-catalysts provide a more hydrophobic environment favorable for the reaction. Additionally, methanol is enriched in the collapsed polymer network as shown in Chapters 4 and 5.^[128] The higher methanol fraction is additionally favorable for the aldol reaction and further accelerates the reaction rate.

6.4 Conclusions

Responsive PNIPAM microgels modified with catalytically active L-proline can be applied to catalyze the enantioselective aldol reaction of 4-nitrobenzaldehyde and cyclohexanone in an aqueous solution. The modulation of the catalytic behavior by external triggers and its interpretation were supported by DPD simulations. Scattering experiments demonstrated the easily addressable responsiveness to temperature and solvent composition. As expected, no distinct temperature dependence was found in methanol, while the typical collapse in water above the VPTT was observed. The incorporation of L-proline led to a shift of the VPTT to a slightly higher value (35 °C) than known for pure PNIPAM microgels. Strikingly, the collapse did not reach a plateau below the synthesis temperature of 70 °C. In contrast, the cononsolvency behavior is not noticeably influenced by the L-proline groups and the minimum in size remains at 20 mol% methanol. SLS measurements revealed a more homogeneous structure compared to pure PNIPAM microgels.

In catalysis experiments, the microgel-catalysts and reagents form a hetero-phased system in water and a homogeneous system in methanol. Catalytic testing was performed at various temperatures between 25 and 45 °C. The temperature-induced deswelling of the microgel-catalysts in water correlate with an increasing catalytic reaction rate. The collapsed polymer network provides a suitable and more hydrophobic environment for the hydrophobic reagents. Even at 45 °C, no hint towards a diffusion limitation was observed. Presumably, this can be attributed to the incomplete collapse of the polymer network at this temperature. An acceleration of the aldol reaction was achieved with increasing temperature. In contrast, the system in methanol shows a homogeneous distribution of the components and only a weaker, linear increase of the reaction rate with temperature. Regarding the catalysis experiments in various cononsolvency-inducing mixtures of water and methanol at room temperature, overlaying effects were identified. In general, methanol is the better solvent for the reagents. Therefore, the aldol reaction is accelerated by an increasing methanol share. However, additional effects occur in water-rich mixtures. The microgel-catalysts are collapsed around 20 mol% of methanol in water. Moreover, methanol accumulates inside the polymer network in the region of the cononsolvency-induced collapse. The resulting more hydrophobic, collapsed, and methanol-enriched polymer network leads to an increase

of the catalytic reaction rate up to 20 mol% methanol. For methanol-rich mixtures and therefore (partially) swollen microgel-catalysts, the improved solvent quality for the reagents due to the methanol governed the catalytic activity.

7. Mechanical properties of PNIPAM microgel beads

ABSTRACT: Poly-*N*-isopropylacrylamide (PNIPAM) microgel beads have been the subject of numerous fundamental and application-oriented studies. While most of them investigate the reversible responsive behavior to different environmental triggers, this chapter focuses on the mechanical properties of microgel beads of different sizes and cross-linking densities. The bulk modulus can be determined by measuring the volume change of the microgel beads due to external osmotic pressures. To this end, multiple PNIPAM microgel beads were synthesized by microfluidics and immersed in solutions with high molecular weight dextran ($M_w = 150\,000$ g/mol, 1 – 30 wt%). The compression-dependent size of the microgel beads was simply visualized using an optical microscope. The correlation between the size of the microgel beads and the external osmotic pressure is used to calculate the bulk modulus. In agreement with the literature, an increasing bulk modulus is found with increasing cross-linking density. Furthermore, a transition from a soft to a stiffer polymer network is observed after compression to ~ 0.72 of the diameter in water.

7.1 Introduction

Responsive microgels have been attracting wide attention in recent decades as they exhibit promising properties for multiple applications, especially in the biomedical field.^[15,60,61] Here, the mechanical properties strongly affect the biological response and acceptance of synthetic materials.^[282,283] Depending on the field of application, e.g. the cell types, a careful adjustment of the softness of the material is important to mimic the target system's environment. In addition to the compatibility with the biological material, the handling and resulting mechanical stresses have to be tolerated by the material. During the synthesis, the mechanical properties of a single microgel can be controlled by variation of the monomer concentration, the cross-linking density, or additives.^[284] Just like the size and internal morphology of the microgels, the stiffness also depends on the swelling state of the respective system. The mechanical properties on the single-particle level influence the properties of microgel suspensions at the macroscopic scale.^[284,285] However, despite the widespread use of microgels in applications and especially fundamental studies, their mechanical properties have still not been fully understood.

In the literature, there are various approaches to define and understand micromechanical properties. For example, atomic force microscopy (AFM) has been applied to determine the

Young's modulus of hydrogels or microgels in the nanometer and micrometer range.^[286-289] Force-distance curves have been measured across the sample to spatially resolve the stiffness of microgels.^[287] However, AFM measurements require specialized equipment and sophisticated knowledge about the appropriate measurement settings, type of AFM probe, and data processing. For larger, micron-sized microgels, Abate et al.^[290] presented a less complex procedure to estimate the elastic modulus by encapsulation of two polyacrylamide microgels in a micro-drop. Yuan et al.^[291] used a simple micro-compression technique where a hydrogel microsphere is compressed in a controlled manner between a flat surface and a large, flat probe. For both methods, the forces acting on the gels were determined and correlated with the elastic response of the microgels. Moreover, Wyss et al. developed a capillary micromechanical method to characterize the elastic properties of PNIPAM microgel beads on the single-particle level.^[292,293] A microgel bead is trapped in the tapered end of a glass capillary and different pressures are applied. The pressure-dependent deformation provides access to the shear as well as the bulk elastic modulus of the gels. Later, a similar approach using a polydimethylsiloxane (PDMS)-based microfluidic chip has been developed by the same group for kinetic measurements after a sudden increase in osmotic pressure.^[294] Furthermore, multiple studies can be found exploiting the osmotic pressure exerted by high molecular weight polymer chains to probe the mechanical properties of microgels.^[295-298] Above an external osmotic pressure comparable to the bulk modulus, deswelling of the microgels is induced. Osmotic compression is the most direct way to obtain the bulk modulus as it results in a fully isotropic compression of the soft particles without any shear component. Sierra-Martin et al.^[295,296] determined the bulk modulus of small polyvinylpyrrolidone (PVP) and PNIPAM-polyethylene glycol (PEG) microgels by evaluating the pressure-dependent deswelling. Dynamic light scattering (DLS) was used to measure the hydrodynamic radius of microgels in solutions where the concentration of dextran was increased to exert osmotic pressure. Recently, Ruscito et al.^[297] studied the response of core-shell-type microgels to osmotic pressure variations. Distinct cross-linker differences and different stainings were chosen for the core and shell of the microgels. They combined DLS and confocal fluorescence imaging to visualize and measure the compression of the microgels.

In this chapter, the mechanical properties, more precisely the bulk moduli, of PNIPAM microgel beads in the micrometer range were determined by their compression-dependent deswelling behavior. To this end, microgel beads of three different sizes were produced using droplet microfluidics. Additionally, the amount of cross-linker introduced into the system was varied while keeping the droplet size and therefore the microgel bead size in the collapsed state constant. To probe the mechanical properties, the microgel beads were

exposed to various osmotic pressures exerted by high molecular weight dextran ($M_w = 150\,000$ g/mol). Here, a wide range of dextran concentrations (1 – 30 wt%) was tested. By direct optical visualization and size evaluation, the deswelling as a function of the external osmotic pressure was extracted. The correlation of osmotic pressure and microgel volume gives access to the bulk modulus. Here, a transition from a soft to a stiffer network is observed after a certain deswelling ratio is reached. Furthermore, the bulk modulus increases with increasing cross-linker content. Finally, a striking difference in the deswelling behavior was found depending on the linear polymer (dextran or PEG ($M_w = 8000$ g/mol)) used to increase the osmotic pressure.

7.2 Deswelling by osmotic pressure

Microgels are porous networks that are swollen by their surrounding solvent. High molecular weight molecules or particles in the surrounding fluid with larger sizes than the mesh size of the polymer network cannot penetrate the pores. As a consequence, the osmotic pressure of the interior of the microgel and that of its surroundings differ. A uniform compression acts on the polymer network. From the literature, it is known that an external osmotic pressure (Π) larger than the bulk modulus (K) leads to a deswelling of the microgels. The bulk modulus is defined by equation (8). Measuring the osmotic pressure and microgel size independently allows the calculation of the bulk modulus using the slope of the linear dependence between the osmotic pressure and the microgel volume (V).^[284,295]

$$K = -V \left(\frac{d\Pi}{dV} \right) \quad (8)$$

To this end, microgel bead samples with two different amounts of cross-linker and different diameters in water were investigated (for experimental details, see section 10.3.3). In total, five microgel samples were prepared. Their sample codes, distinguishing between small, medium, and large microgel beads, cross-linker content, and mean diameter in water are listed in Table 7.1.

Table 7.1: Microgel samples synthesized by microfluidics. For each, the sample code, N,N' -methylenebis(acrylamide) (BIS) content, and diameter in water are listed.

Sample abbreviation	BIS / mol%	$d(\text{H}_2\text{O})$ / μm
MG-5-S	5	22 ± 2
MG-5-M	5	39 ± 2
MG-5-L	5	79 ± 4
MG-1.2-M	1.2	49 ± 2
MG-1.2-L	1.2	109 ± 6

First of all, the three microgel samples with 5 mol% BIS but different diameters in water are compared. The microgel beads were imaged in solutions containing increasing concentrations of dextran using an optical microscope (for experimental details, see section 10.7). Figure 7.1a shows the change in diameter as a function of the external osmotic pressure. For comparison, the diameters are normalized to their size in water. The initial diameters of the microgel beads in water were 22, 39, and 79 μm for MG-5-S, MG-5-M, and MG-5-L, respectively (see Table 7.1). Increasing the osmotic pressure above 4 kPa (~ 5 wt% dextran), a first slight deswelling is observed for all three samples. Any further increase in pressure leads to further, significant deswelling until the lowest value of a normalized diameter around 0.55 is reached for the highest measured osmotic pressure. At this highest osmotic pressure (~ 30 wt% dextran), the microgel beads partly aggregated due to depletion forces. Depletion-induced flocculation was also reported for small microgels at high osmotic pressure which impeded the size measurements by scattering methods.^[296,299] In contrast, the present visualization allows the size evaluation of the remaining single microgel beads. Subsequently, the osmotic pressure was plotted against the volume for each sample (Figure 7.1b, Figure 7.2). From the log-log plots (Figure 7.1b), the onset of the deswelling was evaluated. The volume in water is indicated by small vertical lines. For all three samples, the three data points corresponding to low osmotic pressures (below the dashed lines) are considered as constant and neglected in the following linear fitting.

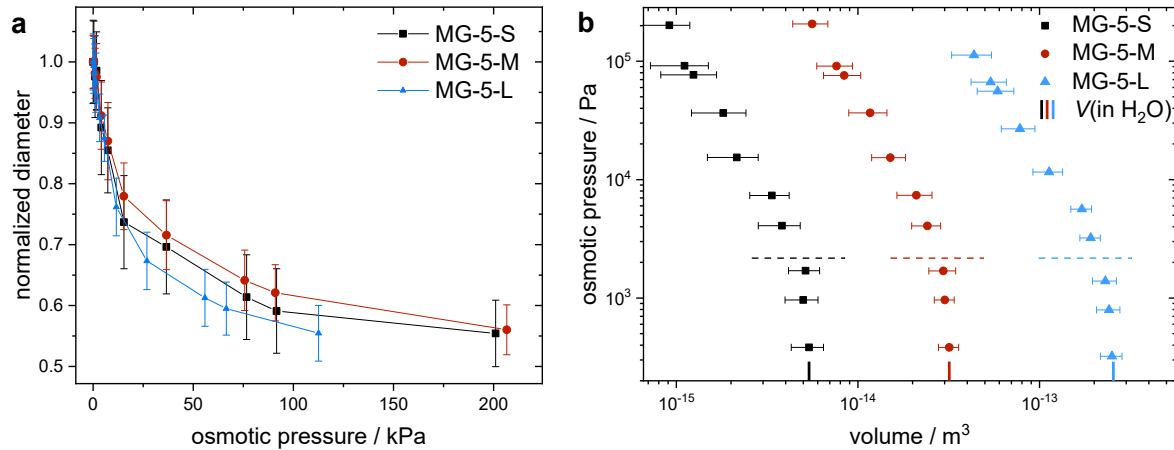


Figure 7.1: (a) Normalized microgel bead diameter as a function of the osmotic pressure exerted by different amounts of dextran. Three microgel bead samples with 5 mol% BIS but different sizes in water are compared. (b) External osmotic pressure in relation to the microgel volume in a log-log plot. The dashed horizontal lines roughly indicate the critical osmotic pressure above which a noticeable deswelling was measured. The three small vertical lines on the x -axis correspond to the volume in water of the respective color-coded sample.

The Π - V plots are depicted in Figure 7.2. The correlation of osmotic pressure and volume does not follow a single linear behavior. Instead, two linear fits are tested. For each, the bulk modulus is calculated using equation (8). The error of the bulk modulus results from the

error of the slope and the standard deviation of the microgel bead volume. The linear fits indicated in red correspond to low compressions and exhibit a small slope. Bulk moduli of 36.3 ± 0.5 kPa, 40 ± 2.5 kPa, and 27.0 ± 0.9 kPa are determined for MG-5-S, MG-5-M, and MG-5-L, respectively. In this regime, the polymer network is soft and shows strong deswelling with osmotic pressure. After deswelling of the polymer network to around 0.72 ± 0.02 of the diameter in water, a second linear dependence is observed and fitted (blue). Here, significantly larger bulk moduli of 152 ± 13 kPa, 155 ± 14 kPa, and 153 ± 11 kPa with increasing microgel size are found. This transition between a soft and a stiffer polymer network agrees with the assumption that a partially collapsed microgel bead is stiffer than the swollen network. Overall, no distinct dependence of the bulk moduli on the diameter in water is found. All investigated samples with 5 mol% cross-linker exhibit qualitatively comparable mechanical properties. The bulk modulus of the MG-5-L sample at small osmotic pressures points towards a softer network for the largest sample in its swollen state. In the size dependence in Figure 7.1a, the relative deswelling of MG-5-L is slightly larger than for the smaller samples at the same osmotic pressure, however, the differences are in the range of error.

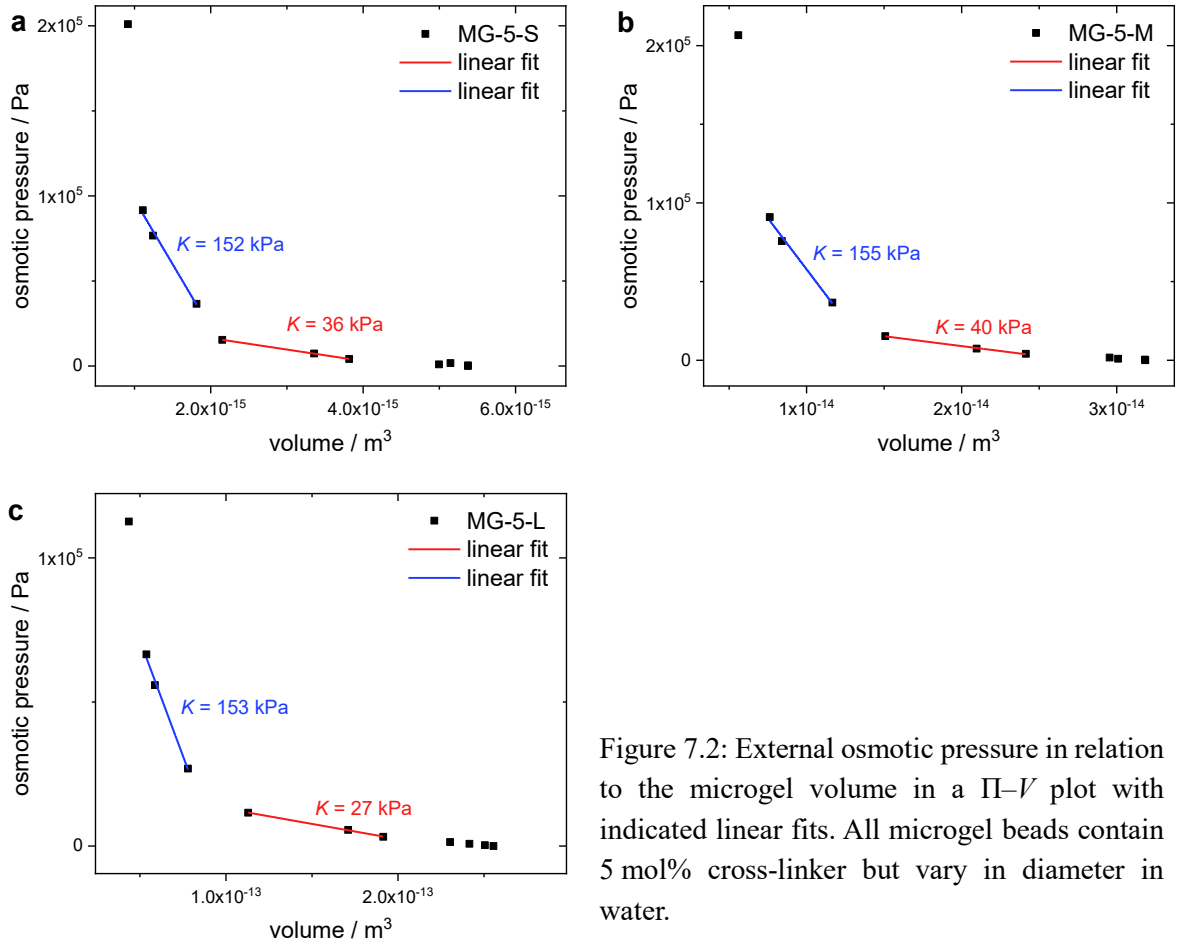


Figure 7.2: External osmotic pressure in relation to the microgel volume in a Π - V plot with indicated linear fits. All microgel beads contain 5 mol% cross-linker but vary in diameter in water.

Additionally, microgel beads with a lower cross-linker content (1.2 mol% BIS) were investigated and compared to their higher cross-linked counterparts. To this end, the droplet size during the microfluidic synthesis was kept similar and only the BIS concentration was varied. Both pairs, MG-5-M/MG-1.2-M (Figure 7.3a) and MG-5-L/MG-1.2-L (Figure 7.3b), reach nearly the same diameter at high osmotic pressures. For osmotic pressures higher than 5 – 7 kPa, the correlation of size and osmotic pressure is almost identical, independent of the degree of cross-linker. However, as expected, the swelling in water is significantly larger for the less cross-linked samples. Deswelling ratios of around 0.55 and 0.41 were measured for the 5 and 1.2 mol% samples, respectively. As before, a log-log plot of Π – V is shown (Figure 7.3d). Here, the initial change at low osmotic pressures appears more gradual. The critical osmotic pressure where the microgel beads start to collapse seems to be lower than for higher cross-linked samples.

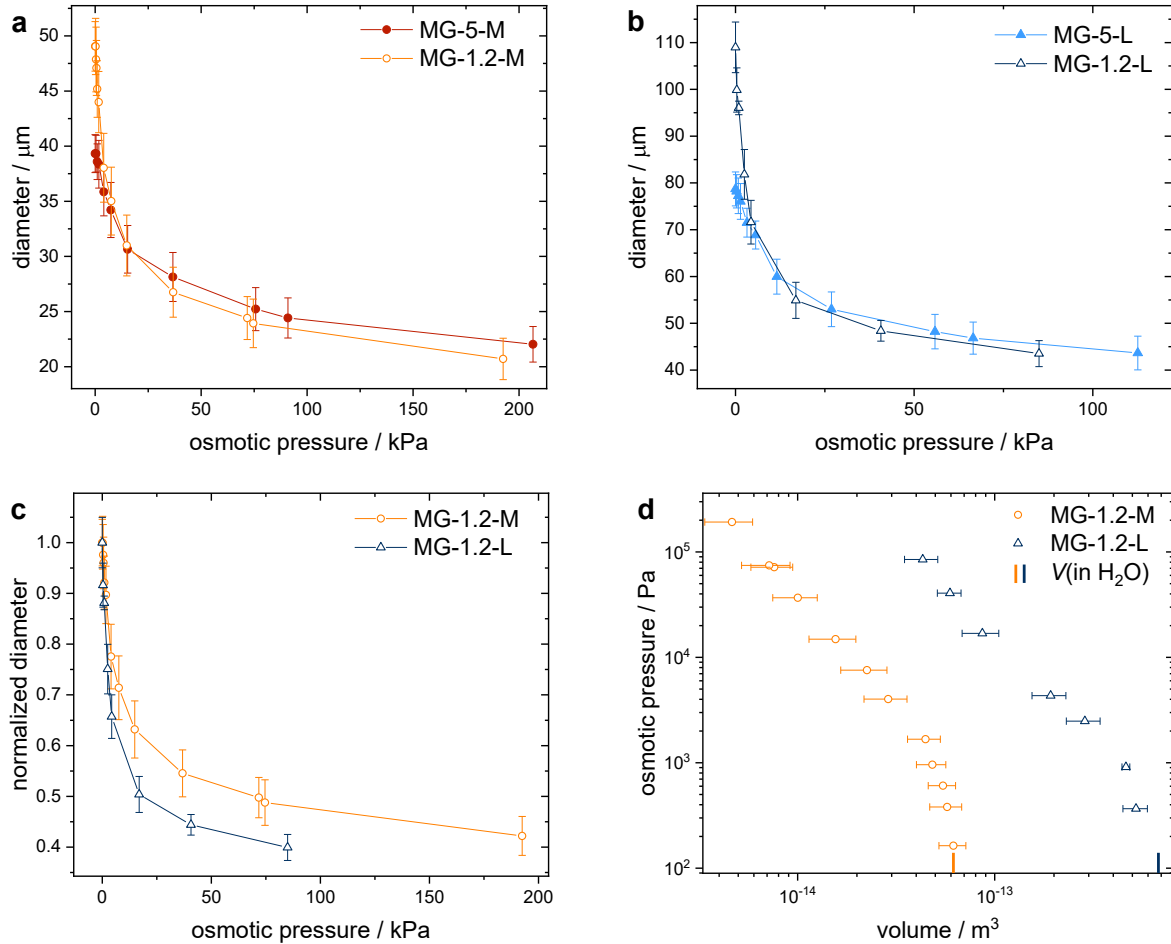


Figure 7.3: Comparison of the osmotic pressure-induced deswelling of (a) MG-5-M and MG-1.2-M and (b) MG-5-L and MG-1.2-L. (c) Comparison of the deswelling curves of MG-1.2-M and MG-1.2-L. The diameter was normalized to the diameter in water. (d) Log-log plot of Π – V for the two samples with 1.2 mol% BIS. The two small vertical lines correspond to the volume in water of the respective color-coded sample.

For the linear fitting (Figure 7.4), only the size in water is excluded. Bulk moduli of around 8 ± 1 kPa were calculated from the slopes of the linear fits. In comparison to the higher cross-linked microgel beads, they are clearly softer. In concordance with the progression of the 5 mol% BIS samples, the less cross-linked microgel beads become significantly stiffer after deswelling down to 0.66 – 0.72 of their initial size in water (also see Figure A3 in the Appendix). No clear second linear regime is found.

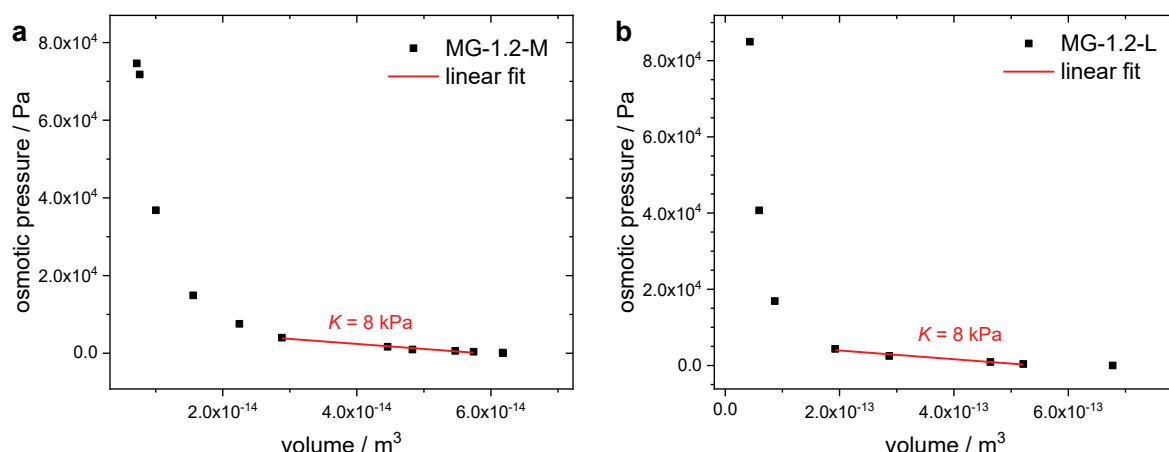


Figure 7.4: External osmotic pressure in relation to the microgel bead volume in a Π - V plot with indicated linear fit. Both microgels contain 1.2 mol% cross-linker but vary in diameter in water.

To conclude, microgel beads with the same cross-linker concentration show similar bulk moduli independent of the initial diameter in water. Furthermore, less cross-linked microgel beads exhibit smaller bulk moduli due to their softer polymer network. Guo et al.^[298] used the same experimental approach and found a bulk modulus of 17.3 kPa for PNIPAM microgel beads with 1.8 mol% BIS. Using the capillary micromechanics technique, a bulk modulus of 18.5 kPa^[298] was obtained for the same microgel beads, whereas microgel beads with cross-linker-to-monomer molar ratios of 1/36 (2.7 mol%) and 1/14 (6.7 mol%) reached bulk moduli of 30 kPa and 43 kPa, respectively.^[292] The increase in the bulk modulus was smaller than the authors had expected and close to the standard deviation of 10% for these experiments.^[292] The size range of the moduli and the qualitative trend between the mechanic properties and cross-linker content correlates with the findings in the present work. The quantitative difference might result from the slightly deviating synthesis parameters. In comparison, Sierra-Martin et al.^[295] determined the bulk moduli of small PNIPAM microgels cross-linked with PEG-diacrylate (700 g/mol, 1 mol%) and a diameter around 360 nm in their swollen state. Below the transition temperature at 28 °C, a bulk modulus of 3.3 ± 0.2 kPa was obtained. The longer cross-links created by the PEG700 in comparison to BIS cross-links explain the smaller bulk modulus of the PNIPAM-PEG microgels in comparison to the MG-1.2-M/L in the present work. Microgels with PEG700 are softer and

show a higher degree of swelling than microgels with the same concentration of BIS as cross-linking agent.^[300]

In the present work, all samples exhibit a transition from a softer to a stiffer polymer network after being compressed to around 0.72 of the diameter in water. Other studies usually investigate only a smaller range of osmotic pressures.^[295,296,298] However, similar curve progressions were found by Ruscito et al.^[297] for their core-shell microgels with distinct morphologies which were described using a Flory-Rehner modified model.

7.3 Comparison of dextran (150 000 g/mol) and PEG (8000 g/mol)

For one microgel bead sample (MG-5-S), identical experiments were conducted using PEG with an average molecular weight of around 8000 g/mol. The correlation between PEG concentration and osmotic pressure was taken from Stanley and Strey.^[301] The comparative plot of the pressure-dependent deswelling is shown in Figure 7.5. A striking difference in the extent of deswelling depending on the type of linear polymer is found. A considerable deswelling of the microgel beads is already observed at low concentrations of dextran. In contrast, the microgel beads collapse significantly less at theoretically the same osmotic pressure when applied by PEG. At very high osmotic pressures (~ 1800 kPa) using 30 wt% PEG, a diameter of about 10 μm is found which is slightly smaller than the 12 μm measured for the highest osmotic pressure exerted by dextran (30 wt%, 200 kPa).

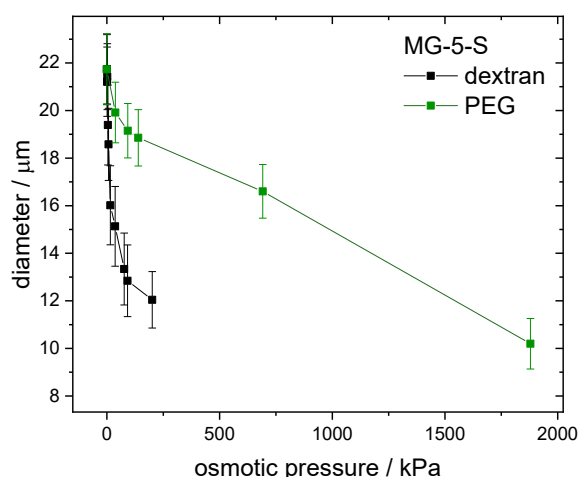


Figure 7.5: Comparison of the microgel bead diameter (MG-5-S) with increasing external osmotic pressure exerted by either dextran (150 000 g/mol) or PEG (8000 g/mol).

In the literature, the effect of osmotic pressure on microgels has been tested using PEG chains of different molecular weights, ranging from 200 up to 50000 g/mol for some studies.^[299,302] For the lowest molecular weight (~ 200 g/mol) no deswelling occurred at low

concentrations. Instead, slight swelling of the PNIPAM gels was observed. Saunders et al.^[299] and Ishida et al.^[302,303] concluded that these low molecular weight PEG chains can freely enter the polymer network. Ishida et al. investigated a large range of concentrations of the PEG chains and found a re-entrant swelling behavior for PEG200 similar to the cononsolvency effect.^[303] Ishida et al.^[302] also reported a small uptake of PEG with a molecular weight of 1000 and 6000 g/mol into the macroscopic PNIPAM gels with 1 mol% cross-linker at low concentrations. In the work of Saunders et al. using higher cross-linked microgels (3.5 mol%), PEG chains with molecular weights above 1080 g/mol compressed the polymer network already at low concentrations as the chains were effectively excluded from the network.^[299] However, there were still differences in the extent of deswelling depending on the molecular weight for low volume fractions. At the same PEG concentration, the swelling ratio becomes smaller with increasing molecular weight.^[303] In an uptake and release study, it was found that poly(styrene sulfonate) chains with hydrodynamic radii of 3 nm and 10 nm were adsorbed by polyampholyte core-shell microgels.^[304] The length of the polyelectrolyte chains determined the penetration depth. The short polyelectrolyte was adsorbed into the core, while the long chains were mainly confined in the shell at the surface of the core.

In the present comparison of dextran and PEG, the different molecular weights and thereby the size of the chains are probably responsible for the difference in deswelling. The smaller PEG chains might partly diffuse into the interior of the microgel beads, while the dextran is completely excluded. Another aspect might be the empirical relations between the weight fraction of the polymer and the osmotic pressure currently taken from the literature. These relations should be verified for the chemicals used in the present experiments.

7.4 Conclusions

PNIPAM microgel beads of different sizes and with different amounts of cross-linker were synthesized by microfluidics. The mechanical properties, namely the bulk moduli, were determined, exploiting the correlation between the deswelling of the microgel beads and the external osmotic pressure exerted by high molecular dextran. The pressure-dependent deswelling could easily be measured by optical visualization. Cross-linker contents of 5 and 1.2 mol% were compared. The smaller amount of BIS results in a looser cross-linked polymer network with a higher swelling ability. Therefore, microgel beads with 1.2 mol% cross-linker exhibit lower bulk moduli than the microgel beads with 5 mol% cross-linker. For the same amount of cross-linker but different sizes, no clear impact on the bulk modulus was found. The results align with the literature taking differences in the synthesis procedure

and type of cross-links into account. Furthermore, a transition between a soft and a stiffer polymer network when the microgel beads collapsed to ~ 0.72 of the diameter in water was revealed. Moreover, the use of dextran (150 000 g/mol) or PEG (8000 g/mol), respectively, to increase the osmotic pressure was compared. Large differences in the deswelling of the microgel beads at (theoretically) the same osmotic pressure were detected depending on the polymer. This hints towards a partial uptake of the smaller PEG chains while dextran is fully excluded from the polymer network. In the next step, the empirical relations between osmotic pressure and weight concentration of polymer found in the literature should be verified.

In the future, a comparison between the microgel beads and small microgels from precipitation polymerization should be pursued to elucidate the impact of size and different cross-linking distribution (see section 3.1.3). Additionally, AFM measurements can be used to further characterize the mechanical properties of the microgel beads.

DYNAMICS

The following part presents the investigation of the dynamics of the cononsolvency-induced volume phase transition. After an introduction to the state of the art, the custom-made microfluidic setup and its characterization are described including the requirements for the microgels in the solvent-jump experiments. Finally, the experimental results and their evaluation are discussed and compared to theory.

8. Dynamics of the cononsolvency-induced collapse: A two-step process?

Parts of the following chapter were published. Adapted with permission from: Nothdurft, K.; Müller, D. H.; Mürtz, S. D.; Meyer, A. A.; Guerzoni, L. P. B.; Jans, A.; Kühne, A. J. C.; De Laporte, L.; Brands, T.; Bardow, A.; Richtering, W., Is the Microgel Collapse a Two-Step Process? Exploiting Cononsolvency to Probe the Collapse Dynamics of Poly-N-isopropylacrylamide (PNIPAM). *Journal of Physical Chemistry B* **2021**, *125*, 1503-1512. Copyright 2021 American Chemical Society. – *for contributions of authors see page VI*

ABSTRACT: Many applications of responsive microgels rely on a fast adaptation of the polymer network. However, the underlying dynamics of the deswelling/swelling process of the gels have not been fully understood. The present work focuses on the collapse kinetics of poly-*N*-isopropylacrylamide (PNIPAM) microgel beads due to cononsolvency. Cononsolvency means that either of the pure solvents, e.g. pure water or pure methanol (MeOH), act as a so-called good solvent leading to a swollen state of the polymer network. However, in mixtures of water and methanol, the previously swollen network undergoes a drastic volume loss. To further elucidate the cononsolvency transition, PNIPAM microgel beads with diameters between 20 and 110 μm were synthesized by microfluidics. To follow the dynamics, pure water was suddenly exchanged with an unfavorable mixture of 20 mol% methanol (solvent-jump) within a microfluidic channel. The dynamic response of the microgel beads was investigated by optical and fluorescence microscopy and Raman microspectroscopy. The experimental data provide unique and detailed insight into the size-

dependent kinetics of the volume phase transition due to cononsolvency. The change in the microgel's diameter over time points to a two-step process of the microgel collapse with a bi-exponential behavior. Furthermore, the dependence between the two time constants of this bi-exponential behavior and the microgel's diameter in the collapsed state deviates from the square-power law proposed by Tanaka and Fillmore.^[305] The deviation is discussed considering the adhesion-induced deformation of the gels and the physical processes underlying the collapse.

8.1 Introduction

Adaptive microgels are three-dimensional polymer networks swollen by their surrounding solvent. Their structure, size, and thus physical properties can adjust to changes in their environment. The volume change transition between the swollen microgel and its collapsed state can be controlled by external stimuli, such as temperature, pH, light, solvent composition, or pressure.^[5,15] For all stimuli, the response of the microgels relies on the transport of the trigger into the polymer network and the subsequent (partial) expulsion of solvent out of the gel. Collapse-inducing stimuli weaken the polymer-solvent interactions and strengthen polymer-polymer interactions. Many potential applications, e.g. drug delivery systems,^[63-65] sensors,^[81,82] actuators,^[85] switchable membranes,^[86] or catalysis,^[71,72] rely on the adaptability and the response kinetics of the polymer network to these external triggers.^[59,306] Many well-studied functional microgels are based on poly-*N*-isopropylacrylamide (PNIPAM). While the equilibrium properties of hydrogels have been extensively examined, the volume change kinetics have been less studied. Mostly, temperature-jump investigations are reported. Here, all size ranges are covered – starting with linear chains, small microgels, larger gels of several 100 μm up to macroscopic hydrogels.^[182,307-312] But also investigations on pH-jumps^[313-315] or, more recently, pressure-jumps using time-resolved small-angle neutron scattering (SANS)^[24] have been published. A more application-oriented study focused on the deswelling/swelling kinetics of microgels due to the uptake and release of an amphiphilic drug.^[65] Theoretical studies and simulations report more generic descriptions of the dynamic processes.^[22,316] All these publications discuss the exponential relaxation times (time constants, τ) for the swelling and deswelling processes and their dependence on the gel size.

However, while some studies suggest one time constant, others propose up to three processes including a plateau region: Tang et al.^[307] observed the temperature-induced collapse of PNIPAM chains using fluorescence and Rayleigh scattering and suggested a two-stage process for the deswelling starting with the growth of pearls which then merge to a

globule. In contrast, Wang et al.^[308] studied PNIPAM microgels of 40 to 200 nm in radius after a temperature-jump. Time-dependent transmittance data were fitted with a mono-exponential function. Also, the generic description of a collapse of neutral polymer networks using dissipative particle dynamics simulations by Nikolov et al.^[316] proposed a single-exponential evolution of the size with time. In contrast, Sato Matsuo et al.^[309] defined three processes for the deswelling of larger PNIPAM gels after a temperature-jump imaged with an optical microscope. Subsequent to an initial shrinking to a certain radius and a plateau region with no visible size change, a skin layer and hence bubble formation was observed.

Additionally, the dependence of the time constants on the gel sizes was thoroughly discussed. The prominent theory of Tanaka and Fillmore^[305] suggests a scaling law of the relaxation time (τ) to the square of the final radius ($R(\text{final})^2$). Although there are experimental and theoretical studies supporting the square-power law,^[305,314,316,317] others reported no correlation^[308] or a deviation from the exponent of two.^[309,310]

To further elucidate the dynamics of the deswelling process, the present study focuses on the sensitivity of PNIPAM to the composition of water-methanol (MeOH) mixtures.^[19,87] The polymer network is swollen in either of the good solvents, pure water or methanol, and collapsed in a mixture of water and methanol. The most pronounced collapse occurs at approximately 20 mol% methanol. Cononsolvency has been studied since the 1990s (see section 1.2). The focus has been on theoretical and equilibrium studies to elucidate the origin of this phenomenon that were controversially discussed.^[105,116,117,119,122,123,128,318,319] In contrast, the kinetics of the cononsolvency has only been rarely studied in literature:^[18,22,120,134] For the cononsolvency-induced collapse, an initial mass transport of the cosolvent into the polymer network is needed to trigger the collapse. In contrast, e.g. during a temperature-jump, the water molecules are already present in the polymer network and solely heat transfer is required. However, in kinetic studies an instantaneous stimulus is considered, i.e. the velocity of the stimulus must be faster than the polymer response. Then, the mass transport of solvent molecules out of the microgel and the microgel response are the essential factors for the kinetics. Xu et al.^[134] investigated pyrene-labeled PNIPAM chains during a solvent-jump from water to 50 vol% methanol. They propose a two-step collapse with characteristic relaxation times of around 12 and 270 ms. In a more complex, application-oriented setup, namely microgel-based etalons, significantly larger time-scales have been reported.^[320] The system comprised a layer of PNIPAM-co-acrylic acid microgels with 1.7 μm in diameter with a thin gold layer on either side. The response to a solvent-jump from water to 30 vol% methanol for a gold overlayer thickness of 5 nm took between 50 to 100 s. Recently, the time-resolved response of thin films consisting of a diblock copolymer of polymethyl methacrylate (PMMA) and PNIPAM after a change from water to mixed

water-methanol vapors was reported.^[132] Interestingly, a two-step response with an initial swelling and subsequent deswelling of the films was found. Keidel et al.^[22] studied the collapse kinetics of small PNIPAM microgels with a diameter around 1.8 μm using time-resolved small-angle X-ray scattering (TR-SAXS). In their work, the collapse was theoretically described by mesoscale hydrodynamic computer simulations. The microgel structure was analyzed during the transition from a swollen state in pure water or methanol to the collapsed state in a 20 mol% methanol-water mixture. The authors proposed a two-step process: The initial fast collapse is ascribed to the cluster formation at the cross-links. The second, significantly slower process, corresponds to the relaxation of the polymer chains to form a compact globule. However, the initial fast process of the volume phase transition could not be resolved for the studied small microgels with the time resolution of the TR-SAXS experiments.

In this chapter, deeper insights into the kinetics of the solvent-induced deswelling of PNIPAM microgels in water-methanol mixtures are presented. To circumvent the limitation by a very fast initial process, larger μm -sized microgels (microgel beads) are investigated in the present work as they overall have slower collapse kinetics. For the experiments, fluorescently labeled PNIPAM microgel beads with a diameter between 20 and 110 μm were synthesized via microfluidics. To analyze the collapse kinetics, a custom-made microfluidic design was developed. The microfluidic design allowed a fast and reproducible solvent-jump from water to the most unfavorable mixture of 20 mol% methanol. The response of the microgel beads could easily be captured by fluorescence microscopy. For the characterization of the investigation setup, Raman microspectroscopy, light microscopy, and confocal fluorescence microscopy were combined. The investigation of microgel beads with various initial diameters in water (swollen state) indicates two main conclusions: the deswelling induced by cononsolvency proceeds in a two-step process and the dependence of the corresponding characteristic times on the microgel bead's diameter in the collapsed state deviates from the square-power law. Explanations for this deviation are proposed based on the deformation of the gels due to the adhesion to the wall and the physical processes underlying the collapse.

8.2 Microfluidic platform

To study the kinetics of the cononsolvency transition of PNIPAM microgel beads in the micrometer size range, a solvent-jump is required. A solvent-jump is defined as a sudden exchange from one to another solvent. In the present case, a fast change from pure water to the most unfavorable mixture of 20 mol% methanol in water is desired. To achieve a fast

and reproducible solvent-jump, a custom-made microfluidic chip was designed. Figure 8.1a depicts the design of the investigation chip with the corresponding measures. The main feature is the Y-shaped inlet present on both sides of a straight channel. The design was printed with a multiphoton 3D printer (Nanoscribe, Photonic Professional GT) with slight variation in the dimensions: two heights (100 or 150 μm) and two widths (700 or 1000 μm) were chosen. The channels with a height of 150 μm were solely used for the largest microgel beads. The microfluidic chips were fabricated by soft lithography (see section 10.3.1) allowing the replication of identical devices. An easy replication was highly important as numerous channels were required for the solvent-jump experiments. Figure 8.1b shows assembled optical micrographs of an actual microfluidic polydimethylsiloxane (PDMS) chip. Both water and methanol are compatible with PDMS and do not significantly swell the material.^[155] However, for the Raman investigations, a comparable microfluidic setup fully made of borosilicate glass from Micronit was used because the Raman signal of PDMS overlaps with the methanol bands in the spectra. This overlap would have complicated the quantitative spectral analysis.

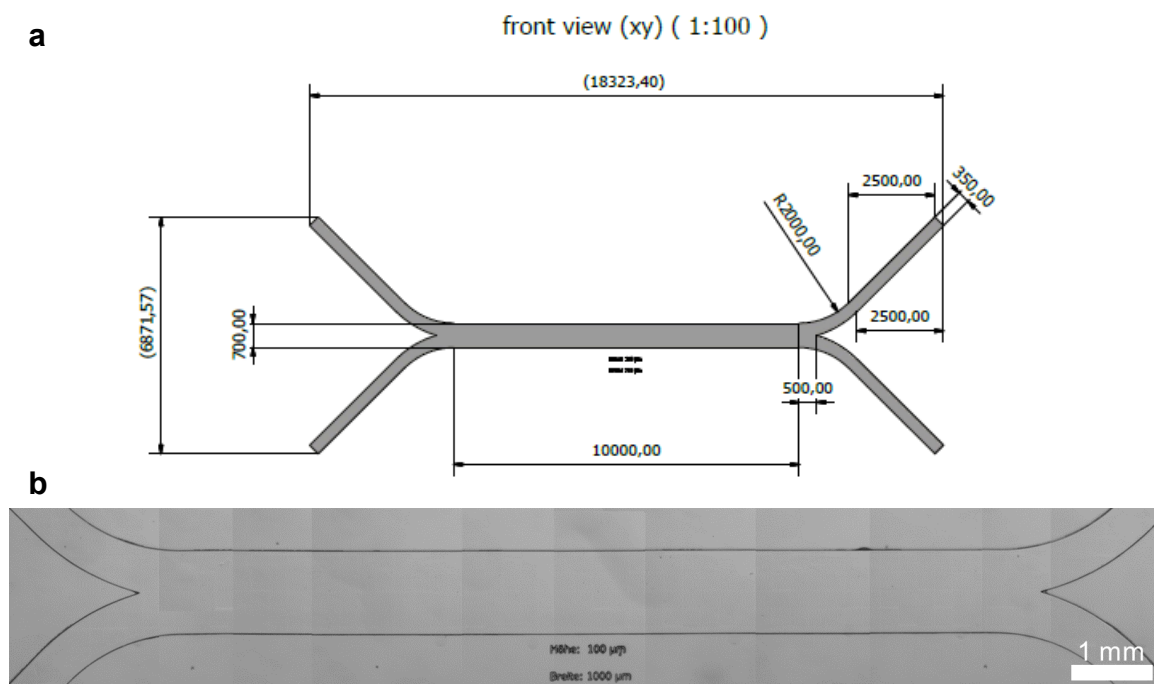


Figure 8.1: (a) Design for printing the Y-shaped inlet chip for the dynamic cononsolvency experiments. All values are in μm . Two different widths (700 or 1000 μm) and two different heights (100 or 150 μm) were produced. (b) Assembled optical images of an actual microfluidic PDMS chip with height 100 μm and width 1000 μm .

During initial tests of the microfluidic channels, it was observed that the microgel beads after purification exhibit the tendency to adhere to the glass bottom of microfluidic devices. The adhesion of the microgel beads is exploited as it simplifies the observation and imaging of one individual gel during the collapse. To set up the solvent-jump experiments, a diluted

aqueous microgel dispersion is inserted into the channel until one microgel bead adhered to the channel bottom at a suitable position. Then, as illustrated in Figure 8.2 top, each inlet is connected to a syringe and pump with either water (blue) or the mixture of 20 mol% methanol (red) to generate a co-flow of the two solvents. The interface between this co-flow can easily be shifted across the channel's width by adjusting the flow rate ratio of the two volume flows (90:10 $\mu\text{L}/\text{min}$) as exemplarily shown in the bottom part of Figure 8.2. The slightly whitish horizontal line in the micrographs corresponds to the interface between the solvents. This shift of the interface can be repeated as often as desired. The fast switching relies on the laminar flow of the two solvent streams in the dimensions of the microfluidic setup. Laminar flow theory states that two parallel streams only mix by diffusion at their interface.^[321,322] Recently, a comparable setup and experimental operation were found to be highly efficient for fast reagent exchanges in single-molecule studies.^[323]

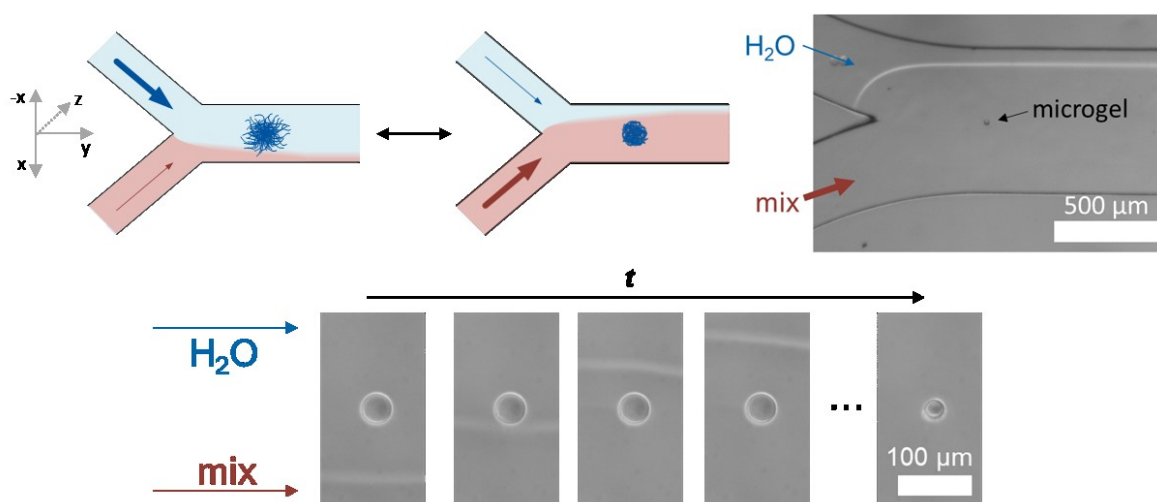


Figure 8.2: Approach and images of the microfluidic platform to observe the volume change transition. To realize a fast solvent-jump in this setup, a co-flow of pure water (blue) and the most unfavorable mixture of 20 mol% methanol in water (red) is created. A microgel bead adhered to the channel bottom can then be collapsed by adjusting the ratio between the respective solvent flow rates.

8.3 Setup characterization

For the kinetic investigations, it is important to generate a solvent-jump that is faster than the reaction of the microgel bead to the change in its environment. To verify the suitability of the microfluidic platform, the solvent-jump setup was characterized as follows: First, the width of the interface between the two solvents was investigated for various positions and flow rate ratios using Raman microspectroscopy. Knowing the interface width is important to ensure that the microgel bead sees the desired solvent composition. Second, time-resolved light microscopy and Raman measurements were performed during a solvent-jump to

characterize the dynamics of the system. In addition, optical microscopy was applied to examine the velocity of the solvent interface and the visual appearance of the microgel beads.

The details of the setup characterization are discussed in detail in the following sections 8.3.1 – 8.3.3. Briefly summarized: To obtain comparable results, microgel beads close to the inlets exposed to an undisturbed interface between the two solvents, thus, without any hindrance upstream, were chosen for the dynamic experiments. Otherwise, the interface between water and mixture would not be sharp enough to enable a fast and complete solvent-jump. Furthermore, the interface crosses the microgel beads within 50 to 100 ms and the solvent-jump is faster than the polymer response. All measurements characterizing the solvent-jump experiment demonstrate that the setup is suitable to investigate the volume change kinetics of the microgel beads. Additionally, the visual appearance of the microgel beads was checked to ensure a precise size evaluation. The microgel beads must have a sharp edge in the swollen and collapsed state. Furthermore, microgel beads with 5 mol% cross-linker were chosen for the experiments as lower cross-linked microgel beads presented a strongly inhomogeneous collapse behavior.

8.3.1 Width of the solvent interface

The width of the interface was evaluated from Raman spectra across the channel width (x) at different distances from the inlets (y) and at different heights (z), thus, distances from the glass surface (Figure 8.3). For experimental details, see section 10.4.3.

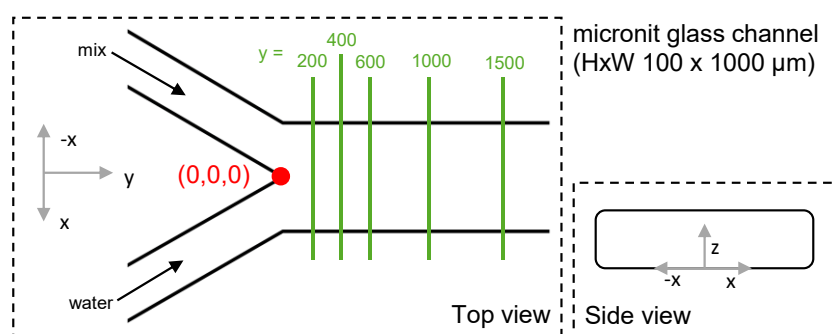


Figure 8.3: Sketch of the Y-shaped microfluidic design with an indication of directions and measurement positions to determine the width of the solvent interface.

Figure 8.4 shows exemplary curve progressions for a flow rate of 50 $\mu\text{L}/\text{min}$ of pure water and 50 $\mu\text{L}/\text{min}$ of 20 mol% methanol in water at a distance of 1500 μm from the inlets and at three different heights. The width of the interface is defined by the difference in x -position when the solvent composition deviates by approx. 0.05 from the initial or final solvent composition, i.e. ideally $0.195 > x(\text{MeOH}) > 0.005$ (inset Figure 8.4).

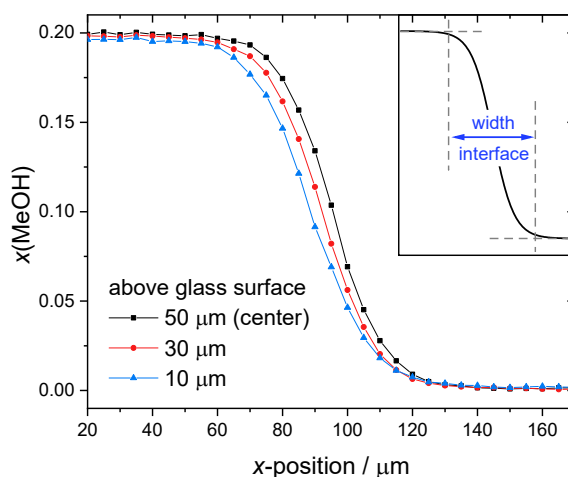


Figure 8.4: Change of the methanol mole fraction across the channel width for three different z -positions (10, 30, or 50 μm above the glass surface of the channel, 50 μm being the center) at a distance of 1500 μm from the inlets. The inset schematically shows how the width of the solvent interface was determined.

The results (Figure 8.5a) reveal the sharpest interface at the center of the height of the channel close to the inlets ($y = 200 \mu\text{m}$, $z = 50 \mu\text{m}$). This position corresponds to the shortest contact time between the two solvents. For a 50/50 flow rate ratio between water and mixture, the smallest width is around 40 μm . However, even in the worst case, hence far away from the inlets ($y = 1500 \mu\text{m}$) and close to the glass surface ($z = 10 \mu\text{m}$), a width of only 62 μm was determined. Thus, the overall channel dimensions with at least 700 μm channel width allow a full solvent exchange from water to the unfavorable mixture. Similar

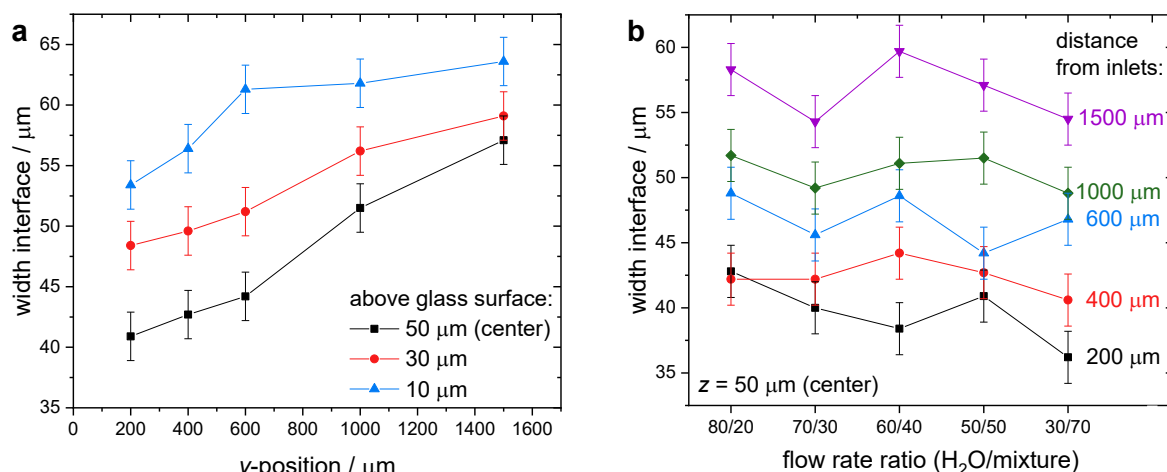


Figure 8.5: (a) Evaluation of the width of the interface between pure water and 20 mol% methanol in water using Raman microspectroscopy for a 50/50 flow rate ratio in dependence of the distance from the inlets (y). Measurements were performed 10, 30, or 50 μm above the glass surface of the channel. 50 μm corresponds to the center of the channel height. (b) The width of the interface at the center of the channel ($z = 50 \mu\text{m}$) at different distances from the inlets for different flow rate ratios between water and 20 mol% methanol.

results are found for the width as function of height and distance for other flow rate ratios (Figure A4 in the Appendix). In Figure 8.5b, the influence of the flow rate ratio on the width of the interface at the center above the glass bottom ($z = 50 \mu\text{m}$) is plotted. For all flow rate ratios, the trend of a slightly greater width with increasing distance from the inlets is more or less true. But, for the same distance from the inlets, no trend between width and different flow rate ratios is found.

Furthermore, it was observed that microgel beads can disturb the interface between the two solvents. An example is shown in the Appendix (Figure A5). The interface can be strongly bent by microgel beads, especially when several beads are gathered at one position, preventing the interface from switching completely to the other channel side. When two single microgel beads are (slightly) in front of or next to each other even without any contact, the response of the second microgel bead is impaired. As a consequence, only microgel beads without any hindrance upstream were chosen for the dynamic experiments.

8.3.2 Velocity of the solvent-jump

Time-resolved Raman microspectroscopy was used to follow the change in solvent composition during a typical solvent-jump experiment (for experimental details, see section 10.4.3). To this end, a comparable solvent-jump was performed in an empty investigation channel without any microgel beads. As shown in Figure 8.6a, the setup allows solvent-jumps to any desirable mixture, e.g. 20, 30, and 50 mol% methanol, within the same time scale. Figure 8.6b displays a threefold repetition of the solvent-jump to 20 mol% methanol which confirms the reproducibility of a solvent-jump at the same position. Additionally, one measurement far away from the inlets at the other side of the investigation channel ($y \approx 7 \text{ cm}$) was conducted (Figure 8.6c). At very far distances, the two solvent phases are already partly mixed. As a result, no jump from pure water would be possible anymore.

In addition, the solvent-jump from water to 20 mol% methanol was performed and measured inside a microgel bead. Here, the change in methanol mole fraction and PNIPAM peak area are compared (Figure 8.6d). One should keep in mind that the methanol and PNIPAM peaks highly overlap in the recorded spectral region. As a result, the accuracy of the quantitative results from the modeling of the spectra is reduced. However, the results can be interpreted qualitatively: Due to the solvent-jump, indicated by the sudden increase of the methanol mole fraction to 0.2, the peak area ascribed to the PNIPAM gel increases. After an initial, fast increase, the peak area increases only slowly and no plateau is reached within the investigated time. In contrast, the solvent composition scatters around its final value of 20 mol% methanol a second after initiation of the solvent-jump. Thus, the investigation setup allows the observation of the polymer response to a fast solvent-jump.

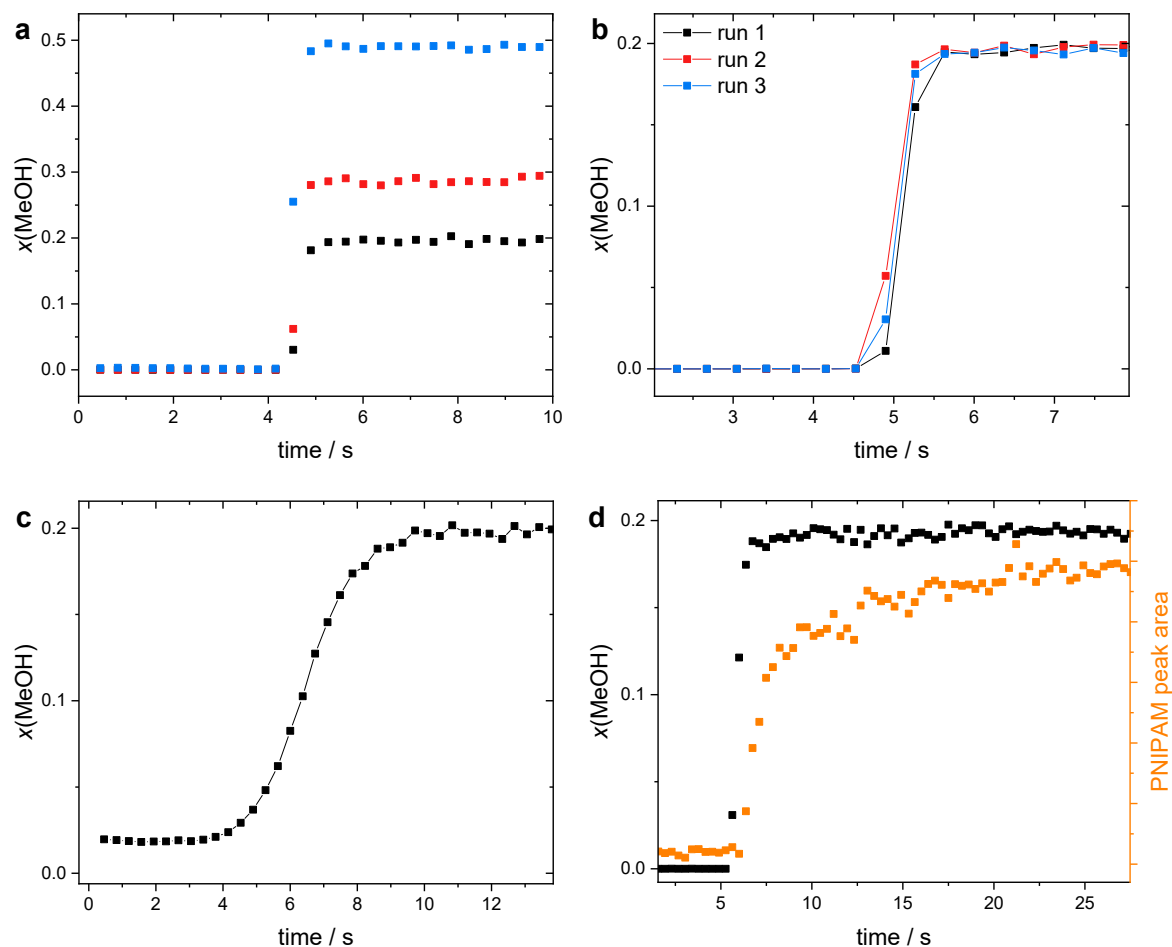


Figure 8.6: Characterization of the solvent-jump experiment using time-resolved Raman micro-spectroscopy. The mole fraction of methanol was evaluated with indirect hard modeling (IHM). (a) Change in solvent composition in the surroundings during a solvent-jump from water to different mixtures: 20 mol% (black), 30 mol% (red), and 50 mol% (blue) methanol. (b) Threefold repetition of the solvent-jump from water to 20 mol% methanol close to the inlets. (c) Change in solvent composition for a solvent-jump from water to 20 mol% methanol far away from the inlets (7 cm). (d) Change in solvent composition inside a microgel bead ($d(\text{H}_2\text{O}) = 78 \mu\text{m}$) in comparison to the change of the PNIPAM peak area in the Raman spectra.

Furthermore, light microscopy was used to estimate the velocity of the interface. To this end, the solvent exchange was repetitively performed and imaged at various positions in an empty investigation channel. An average of $1.0 \pm 0.17 \text{ mm/s}$ was determined. Additionally, the time for the solvent interface to cross over a microgel bead was determined for each microgel bead size range (Figure 8.7). It can be concluded that it took less than 50 – 100 ms and, thus, was faster than the microgel bead collapse.

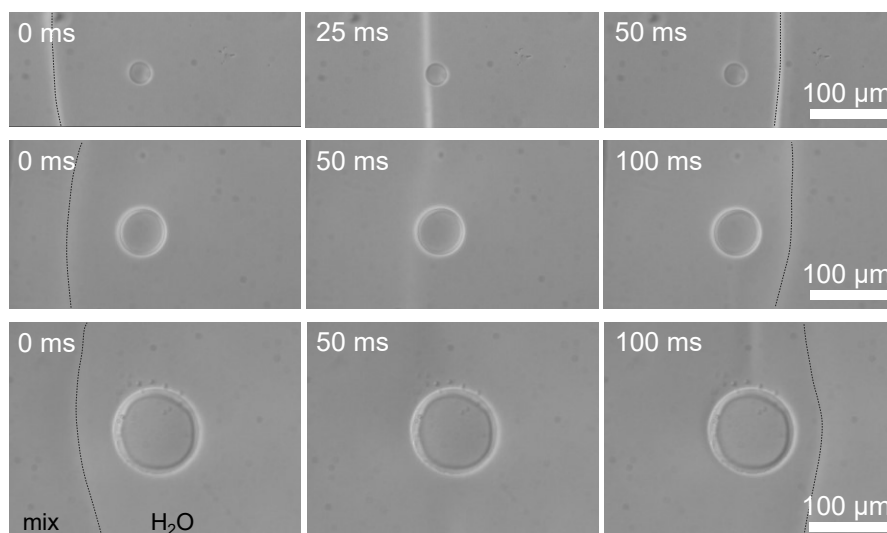


Figure 8.7: Velocity of the solvent interface observed by light microscopy. Snapshots of the solvent-jump from water to 20 mol% methanol for three different microgel bead sizes. The interfaces are indicated by dashed black lines in the left and right images.

8.3.3 Visual appearance of the microgel beads

In addition to the position of the microgel beads in the channel, their visual appearance plays an important role for their suitability for dynamic investigations. While their adhesion is crucial to hold the microgel beads at the same position during imaging, excessive adhesion is undesired. Figure 8.8 shows optical images of two different microgel beads in water and in 20 mol% methanol. In water, both of them looked similar. However, the one in Figure 8.8b exhibited a strong adhesion and deformation when the surrounding solution was switched to the 20 mol% methanol mixture. As a result, no clear edge is visible for the collapsed microgel bead and, thus, no image evaluation would be possible. In contrast, the microgel bead in Figure 8.8a had a clear and measurable edge in water as well as in the water-methanol mixture. The visual appearance of the microgel beads in the unfavorable mixture was always checked previously to a solvent-jump experiment.

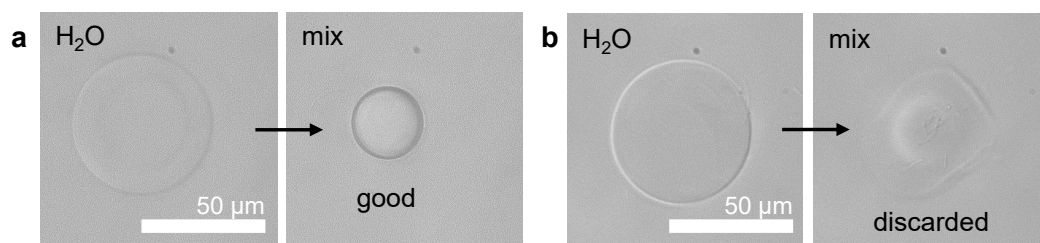


Figure 8.8: Optical micrographs of two microgel beads (a,b) in water and in 20 mol% methanol in water. The strongly adhering gel (b) with no sharp edge visible in the mixture was excluded from solvent-jump experiments.

Kinetic deswelling studies on macroscopic gels often exhibit the formation of an impermeable skin layer. As a result, the internal osmotic pressure increases, leading to “bubbles” of lower polymer density emerging on the surface of the gels. Sato Matsuo et al.^[309] described the appearance of bubbles after a temperature-jump due to an impermeable, collapsed gel surface layer for spherical PNIPAM gels with a diameter of around 200 μm to 2.0 mm at 30 $^{\circ}\text{C}$ in water. The deformation of the surface layer depends on the amount of cross-linker.^[324,325] Low cross-linker amounts favor the formation of bubbles at the gel’s surface. In the preliminary tests of this thesis, microgel beads with 1 and 2 mol% cross-linker were exposed to a solvent-jump to an unfavorable mixture. In those cases, a skin layer formation and an inhomogeneous collapse with bubble formation were observed (Figure 8.9). With increasing initial size, a more pronounced inhomogeneous skin layer was formed. As a result, no size evaluation was possible. Therefore, experiments were carried out with microgel beads with 5 mol% cross-linker. These microgel beads collapse without any visible inhomogeneities and no clear skin layer formation was observed. This suggests that, if at all, a semipermeable layer is formed at the surface. A semipermeable or no skin layer formation has also been proposed in literature for small microgels in the nm or low μm range.^[22,308]

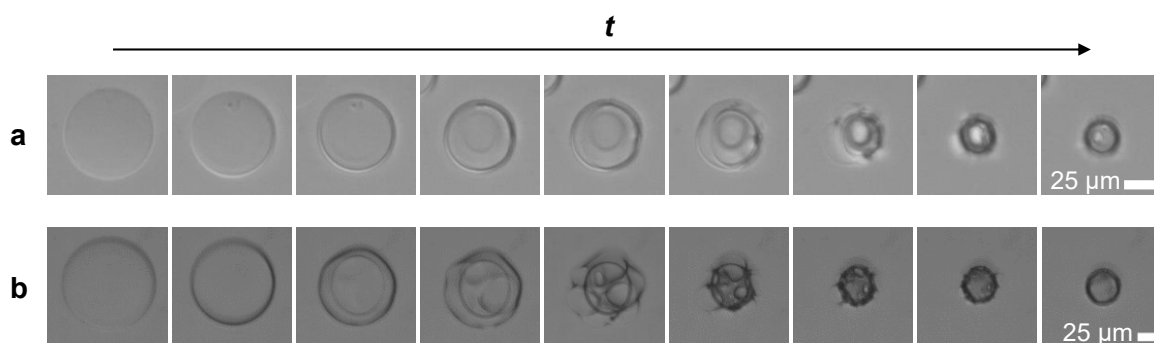


Figure 8.9: Examples for an inhomogeneous collapse with skin layer formation and “bubbles” after a solvent-induced collapse of PNIPAM microgel beads with only 1 mol% BIS and a diameter in water of (a) 67 μm and (b) 120 μm .

8.4 Solvent-jump experiments

Solvent-jump experiments were performed with fluorescent microgel beads with 5 mol% cross-linker and diameters between 20 and 110 μm in their swollen state (for experimental details, see sections 10.3.5 and 10.5.3). In total, six different samples were used. As individual microgel beads were evaluated for the dynamic experiments, the overall polydispersity of the samples played a minor role. The corresponding samples are listed in Table A1 in the Appendix. For each sample, the average diameter in water and in 20 mol%

methanol in water at room temperature was measured. Additionally, the deswelling ratio q_{deswell} in terms of diameter and volume was calculated, i.e. $q_{\text{deswell}}(d) = d(20 \text{ mol\% MeOH})/d(\text{H}_2\text{O})$ or $q_{\text{deswell}}(V) = V(20 \text{ mol\% MeOH})/V(\text{H}_2\text{O})$. The deswelling ratio $q_{\text{deswell}}(d)$ was found to be 0.50 ± 0.02 for all samples and for $q_{\text{deswell}}(V)$ an average value of 0.12 ± 0.013 was calculated. In the following, three microgel bead size ranges are distinguished: microgel beads with a diameter around 25 μm (22 – 29 μm), 60 μm (55 – 65 μm), and 95 μm (89 – 103 μm) in water. Figure 8.10 shows exemplary images of three samples representing the three size ranges.

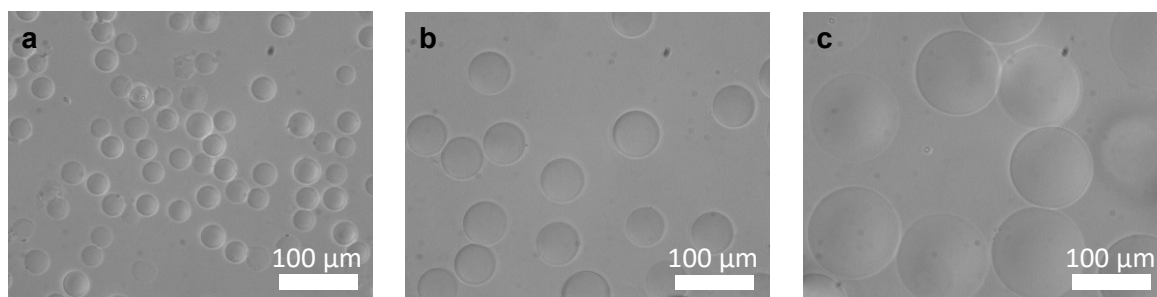


Figure 8.10: Exemplary images of the microgel bead samples of the three size ranges with an average diameter in water of (a) $28 \pm 3 \mu\text{m}$, (b) $54 \pm 4 \mu\text{m}$, and (c) $100 \pm 5 \mu\text{m}$. All images were recorded with the same magnification.

Figure 8.11 displays snapshots of three microgel beads with a diameter of 22, 65, and 101 μm in water and their deswelling with time after a solvent-jump. Comparing the three different size ranges, it becomes obvious that the collapse significantly slows down with increasing microgel size. As mentioned above, no skin layer formation or inhomogeneous collapse behavior was observed for these microgel beads with 5 mol% cross-linker.

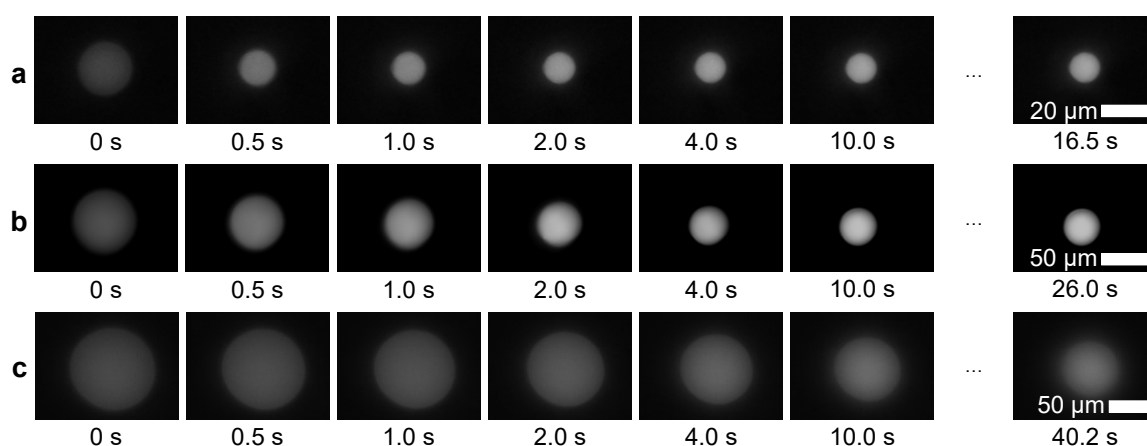


Figure 8.11: Fluorescence images of three different microgel beads with an initial diameter in water (0 s) of (a) 22 μm , (b) 65 μm , and (c) 101 μm at different points in time during the solvent-jump from water to 20 mol% methanol.

8.4.1 Image evaluation

For each video of a solvent-jump experiment, the diameter of the imaged microgel bead in the xy -plane was evaluated as follows: To set up a semi-automatic evaluation by Matlab, the microgel bead size for at least 10 frames, distributed over the full investigation length, was measured by hand (black points, Figure 8.12b). Subsequently, this information was used to manually find the threshold defining when a pixel should be accounted to the microgel bead or to the background. Following, a reference frame that definitely showed a fully swollen microgel bead in water was chosen (e.g. frame 200). In this frame, the pixel with the highest fluorescence intensity was extracted to create a region of interest (ROI, green squares in images, Figure 8.12a). The average intensity in the ROI was evaluated. In each remaining frame of the video, the same position for the ROI was defined and its average intensity was compared to the one of the reference ROI. This value was defined as the intensity ratio (red points, Figure 8.12b). The intensity ratios of the beforehand manually evaluated 10 frames were correlated to the required threshold for a correct size evaluation and interpolated for intensity ratios between 0.5 and 3. Finally, all frames were evaluated using Matlab, and the area of all connected pixels assigned to the microgel bead in each frame was listed. To calculate the corresponding diameter, a perfect circle was assumed. The Matlab script was executed for all frames and the size in each frame was correlated to the corresponding time in the experiment (blue points, Figure 8.12b).

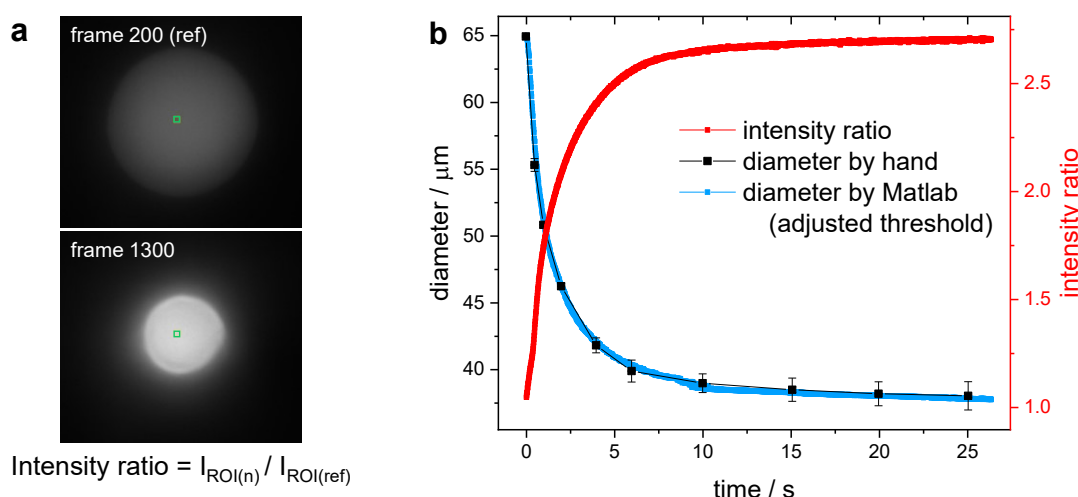


Figure 8.12: Procedure for the image evaluation by Matlab: (a) The ROI (green square) in the reference image, frame 200, is projected to any other frame, e.g. frame 1300. The intensity ratio is defined as the ratio between the average intensity in the ROI of frame n to the reference frame. (b) Comparison of the intensity ratio over time after a solvent-jump and the corresponding diameters by hand or by the optimized Matlab routine.

8.5 Size evolution after a solvent-jump

The deswelling of the microgel beads began shortly after the solvent interface passed across the microgel bead. Being surrounded by the unfavorable mixture the polymer network started to collapse. The first noticeable deviation from the diameter in water was marked as the starting point and was set to $t = 0$ s. The experimental setup and settings allowed the resolution of the whole deswelling process of the microgel beads (Figure 8.13). As already concluded from the visual evaluation of the images (Figure 8.11), the deswelling slows down with increasing size of the microgel beads.

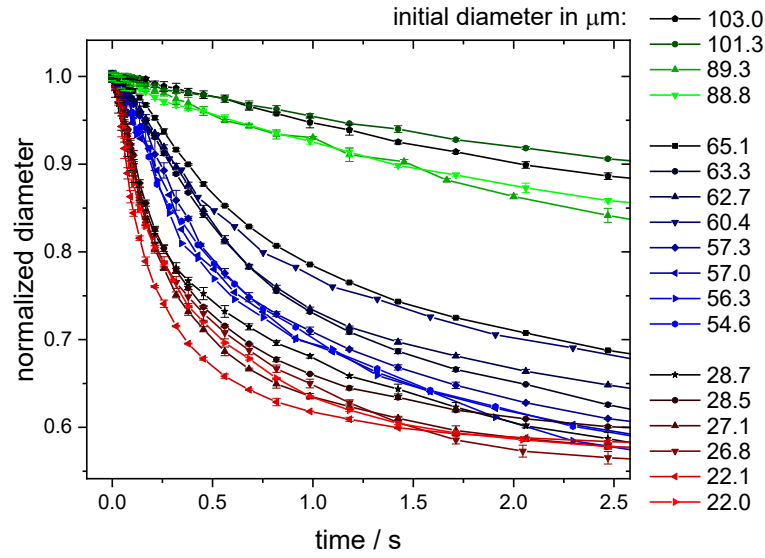


Figure 8.13: Change of the normalized diameter of multiple microgel beads with different initial diameters in water in the first 2.5 s after a solvent-jump from water to 20 mol% methanol. The individual microgel beads of the three size ranges around an average diameter of 25, 60, and 95 μm are indicated with color gradients in red, blue, and green, respectively. Error bars result from the average of the threefold solvent-jumps.

Keidel et al.^[22] proposed a two-step collapse for the cononsolvency-induced deswelling process. To check this statement for the microgel beads investigated in the present study, the measured size evolutions were fitted with both a mono- and a bi-exponential function.

$$d(t) = A_1 e^{-t/\tau_1} + d_0 \quad (9)$$

$$d(t) = A_1 e^{-t/\tau_1} + A_2 e^{-t/\tau_2} + d_0 \quad (10)$$

Before fitting the time-dependent size evolutions, the amount of data points was reduced. After the initial, large size change, the diameter only changes very little. However, depending on the observation length, there is a large amount of data points for the second, slow collapse. If all points are included, the fit optimizes this region to reduce the residual for the largest number of points, although the first size change is more relevant in the physical context. Therefore, the data is increasingly reduced towards long times (Figure A6

in the Appendix). Figure 8.14 shows an exemplary comparison of a mono- and bi-exponential fit for the three different microgel beads already shown in Figure 8.11. The same plots were prepared for all microgel beads and can be found in the Appendix (Figure A7 to Figure A9). The residuals of those fits are plotted below each size evolution and demonstrate that the mono-exponential fits have a higher deviation from the measured data points. Especially, the curvature and final value are not reached using the mono-exponential function. This effect grows with increasing microgel size. A bi-exponential fit properly describes the experimentally observed change of the microgel diameter indicating a two-step process of the collapse of the microgel beads.

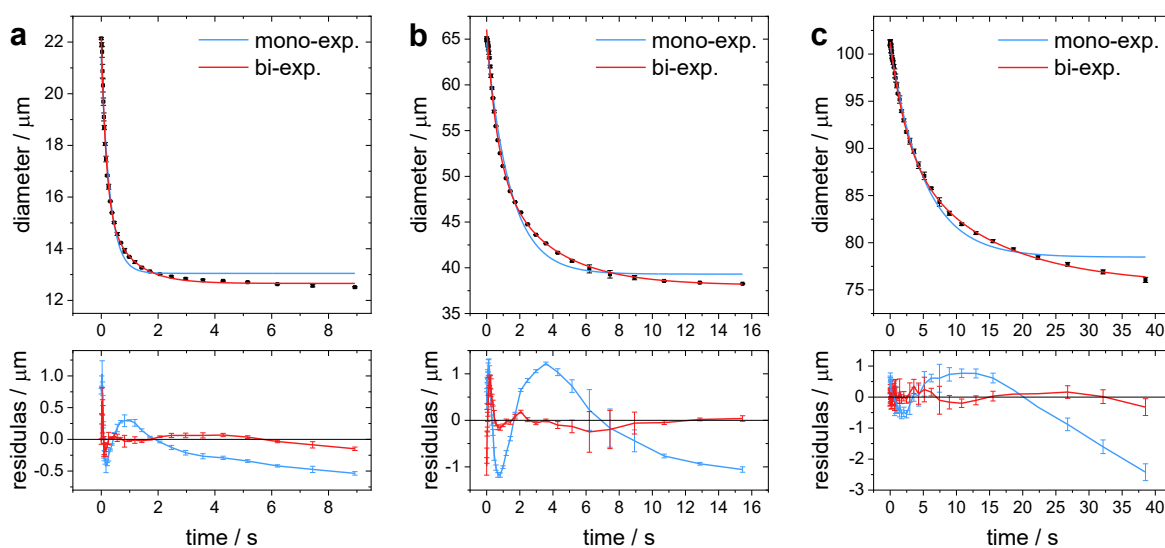


Figure 8.14: Solvent-jump experiments from water to 20 mol% methanol for three different microgel beads with an initial diameter of (a) 22 μm , (b) 65 μm , and (c) 101 μm . The change in diameter was fitted with a mono-exponential (blue) and bi-exponential (red) function. The corresponding residuals of both fits are shown at the bottom of each diagram. For each microgel bead, the solvent-jump was performed three times and the results were averaged.

The existence of a two-step collapse is additionally supported by experiments with varying external osmotic pressure Π (for details, see Chapter 7). Shortly, such osmotic pressure experiments can evaluate the mechanical properties of microgels and the bulk modulus K is given as $K = -V(d\Pi/dV)$ with V the volume of the microgel.^[295] Figure 8.15a shows the correlation between the osmotic pressure and the microgel volume for microgel beads with a diameter of $22 \pm 2 \mu\text{m}$ in water. At low compression, a first linear regime was found indicating a constant bulk modulus K . Here, the polymer network is soft and shows strong deswelling with osmotic pressure down to ~ 0.72 of the diameter in pure water (dashed line). At higher compressions, a second linear regime indicates a change in bulk modulus and the polymer network reveals significantly higher stiffness. For comparison, in the solvent-jump experiment with a similar-sized microgel bead (Figure 8.14a and

Figure 8.15b), ~ 0.714 of the initial diameter was reached when the initial fast collapse was essentially complete (after $2 \times$ the first time constant τ_1 , indicated in Figure 8.15b). Thus, the transition between the first and second kinetic process of the cononsolvency-induced collapse coincides with the transition between the soft network of a swollen microgel bead and the stiffer network of a partially collapsed microgel bead. A change from a soft to a stiffer network occurs due to the expulsion of solvent molecules from the polymer network. Thus, instead of a swollen network with predominant solvent-polymer interactions, a deswollen network with increased polymer-polymer interactions is present. A likely interpretation is that the first kinetic process is influenced by the still porous, solvent-swollen conformation of the network. The porosity allows a fast expulsion of solvent molecules during the solvent-jump experiment. At a specific point, the microgel beads are deswollen so much that the polymer network becomes stiffer and further deswelling is governed by the rearrangement and relaxation of the network chains. Keidel et al.^[22] simulated the initial formation of an intermediate hollowish, core-shell structure which slowly transformed to a globular structure. The transition to a compact globule is significantly slower and was ascribed to the second kinetic process in the solvent-jump experiments presented in this thesis. A two-step process for the deswelling kinetics has also been reported for small microgels after a pressure-jump^[24] and linear chains after a temperature-jump.^[307]

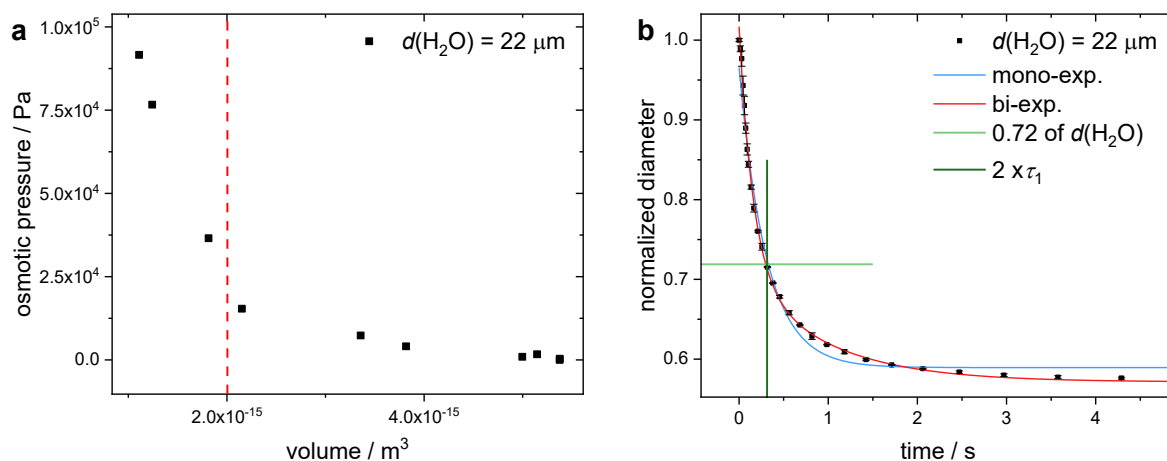


Figure 8.15: (a) Volume of the microgel beads in relation to the osmotic pressure exerted by different amounts of dextran. The dashed line roughly indicates the end of the linear deswelling regime at low compression (~ 0.72 of the diameter in water). (b) Solvent-jump experiment from water to 20 mol% methanol for a microgel bead with an initial diameter of $22 \mu\text{m}$ fitted with a mono-exponential (blue) and bi-exponential (red) function. The horizontal line (light green) marks the deswelling to 0.72 of the initial diameter and the vertical line (dark green) indicates $2 \times \tau_1$.

8.6 Dependence of the deswelling kinetics on the size of the microgel bead

From the bi-exponential fit to the size evolution after a solvent-jump, the first and second time constant, namely τ_1 and τ_2 , were extracted for all investigated microgel beads. Figure 8.16 shows the dependence of both time constants on the diameter of the collapsed microgel beads on a log-log scale. Linear fits exhibited slopes of 1.56 ± 0.05 and 1.77 ± 0.08 for τ_1 and τ_2 , respectively. Hence, the dependence between the time constants and the diameter of the microgel beads in the collapsed state deviates from the square-power law proposed by Tanaka and Fillmore.^[305] Before interpreting this deviation, a closer look at the Tanaka-Fillmore theory and the microgel beads in the present investigation setup was taken.

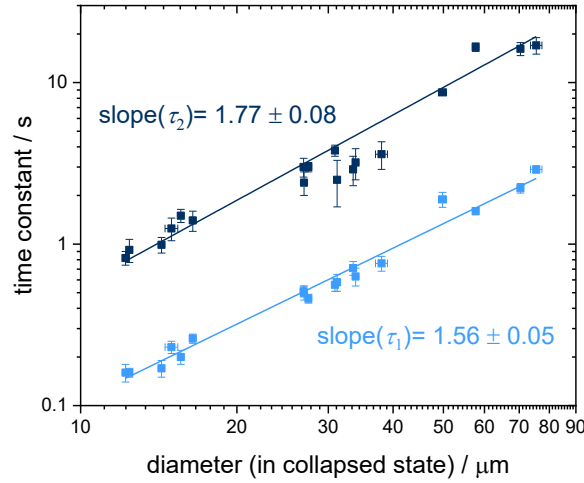


Figure 8.16: Log-log plot of the two time constants, τ_1 (light blue) and τ_2 (dark blue), as a function of the final diameter of the microgel beads in the mixture.

The theoretical description of the swelling kinetics of a spherical gel by Tanaka and Fillmore^[305] in 1979 is based on the collective diffusion of the polymer network relative to the solvent. Within this theory, the kinetic process is described by the displacement of a point in the network from its equilibrium position. The kinetics are related to the elasticity and the friction f between the polymer and the solvent. From an experimental study, they derived that the shear modulus μ of the polymer network can be neglected compared to its bulk modulus K . Therefore, the collective diffusion coefficient D is defined by $D = K/f$. For small isotropic volume changes of a spherical gel with the radius R , Tanaka and Fillmore found a single-exponential decay of the gel radius with time. The characteristic time constant scales with $\tau \sim R(\text{final})^2/D$.^[305,309,310] Later, studies stated that the previous theory by Tanaka and Fillmore is insufficient for non-spherical gels.^[326,327] Thus, they extended the theory by including a non-negligible shear modulus to describe cylindrical and disk-like gels with symmetrical geometries. Additionally, Li and Tanaka^[326] proposed a two-step mechanism

with a network diffusion step and a shear process to reduce the shear energy and re-adjust the shape of the gel. Still, all mechanisms lead to the quadratic dependence of the relaxation time on the radius of the spherical gel. Experimental studies supported the suggested square-power law^[305,313,314,317] and used this correlation to estimate the collective diffusion coefficient.^[24,324,328,329]

However, few studies reported a power-law exponent smaller than 2 and a deviation from the single-exponential function during the initial volume change.^[309,310] For example, Sato Matsuo et al.^[309] defined three processes for the deswelling of larger PNIPAM gels after a temperature-jump imaged with an optical microscope. For gels with a radius between 100 and 1000 μm , the corresponding time constants for the deswelling scale with $R^{1.6}$. A clear explanation for the deviation from the power-law exponent 2 was not found. It was suspected that the experimentally covered size range was insufficient, that the gel structure depended on its size, or that the simple diffusion equation was not valid.^[309,310] Suzuki et al.^[311] investigated the influence of a mechanical constraint on thin PNIPAM films during a temperature-jump. Here, the gels cannot swell and shrink freely along all directions as before; only changes of the thickness of the film are possible. Varying the dimensions of the experimental setup, they found a deviation from the simple square-power law.

8.6.1 Influence of the adhesion

The shape of the microgel beads in the solvent-jump setup of the present work was investigated by confocal fluorescence microscopy (for experimental details, see section 10.5.4). The microgel beads are non-spherical in z -direction due to the adhesion to the glass surface (Figure 8.17).

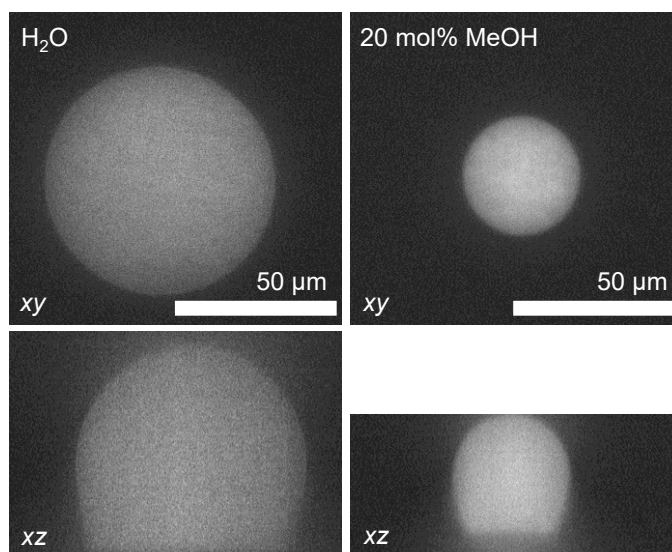


Figure 8.17: Confocal fluorescence microscopy images of the xy - and xz -plane of one microgel bead in water and in 20 mol% methanol.

Thus, the surface area available for a solvent transport is reduced in comparison to a free, spherical gel by the area attached to the glass. This deformation was not considered in the evaluation of the solvent-jump experiments as the temporal resolution of the confocal microscope was insufficient for xzt -scans.

To take into account this reduced surface area, z -scans of several microgel beads of the three different size ranges in the mixture were captured inside the investigation setup using a confocal fluorescence microscope. The surface area (A) of the deformed microgel beads was evaluated as follows (Figure 8.18): An image of the xz -plane of the microgel bead was generated and the central axis (yellow) was inserted. The edge of the microgel bead was first set manually (blue points) and then linearly interpolated along the z -axis (orange dotted line). The microgel bead was sliced across the interpolated edge. Each slice exhibited the shape of a truncated cone. The shell surface of each truncated cone was calculated and added up to receive the surface area of the microgel bead. This procedure was performed for the left and right side of the microgel bead and averaged.

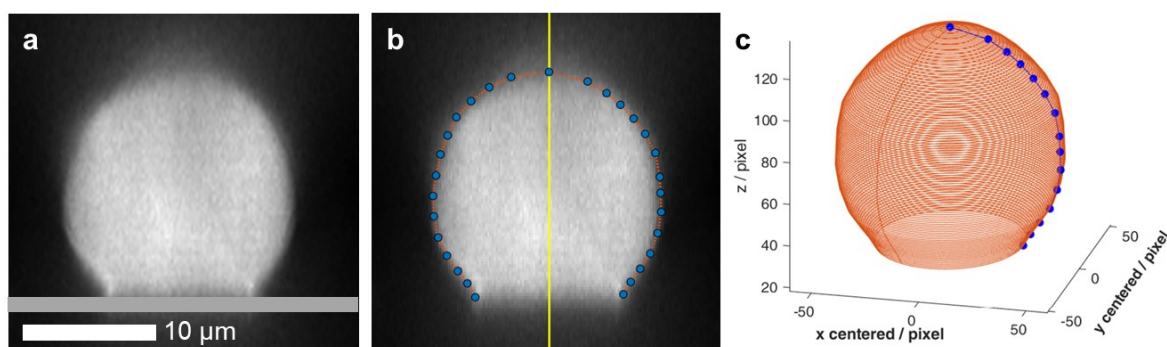


Figure 8.18: (a) Original xz -image of a microgel bead in 20 mol% methanol. The glass surface of the device is on the bottom of the image and indicated by a grey line. (b) xz -image with central axis (yellow), edge points (blue), and interpolation (orange dotted line). (c) 3D-view of the microgel bead.

Then, the effective radius of a theoretical sphere with the same surface area was determined using $R_{\text{eff}} = (A/4\pi)^{1/2}$. The microgel beads imaged in the z -scans are not identical to the ones in the dynamic solvent-jump experiments. Therefore, numerous microgel beads from the same samples were imaged. The ratio of the effective radius (R_{eff}) and the measured radius in xy (R) was calculated and those R_{eff}/R ratios were averaged for the three size ranges (Table 8.1). The R_{eff}/R values decrease with increasing microgel size, though the values for the two smaller microgel sizes are similar. This observation correlates with the trend of the deswelling ratios of the adhered microgel beads during the dynamic experiments: Here, the microgel beads of the two smaller size ranges exhibited a similar deswelling ratio around 0.54. In contrast, the largest size range around 100 μm showed the highest distribution of deswelling ratios and a mean value of 0.66.

Table 8.1: Ratio R_{eff}/R of microgel beads in 20 mol% methanol evaluated from z-scans recorded by a confocal fluorescence microscope. It is distinguished between three microgel size ranges. The number of microgel beads included is listed in the last column.

Size range in water (diameter)	Mean R_{eff}/R (mix)	#microgels
21 – 31 μm	0.93 ± 0.09	16
50 – 71 μm	0.90 ± 0.08	27
89 – 120 μm	0.81 ± 0.04	8

Subsequently, the final, collapsed diameter of the microgel beads in the dynamic experiments was corrected by multiplying the measured diameter with the R_{eff}/R ratio. This correction only affects the slope of the linear fit of the time constants in Figure 8.16 if the adhesion depends on the microgel size leading to different R_{eff}/R ratios. Otherwise, the R_{eff}/R ratio would be identical and every point would have been shifted by the same extent leading to the same slope of the linear fit. Using the R_{eff}/R ratios from Table 8.1 to correct the diameter in Figure 8.16, the slope for τ_1 changes from 1.56 ± 0.05 to 1.76 ± 0.07 and for τ_2 from 1.77 ± 0.08 to 1.96 ± 0.11 (Figure 8.19). As the R_{eff}/R ratio is smaller for the larger microgel beads, the slopes increase and thus also the exponent of the dependence of the time constants on the radius.

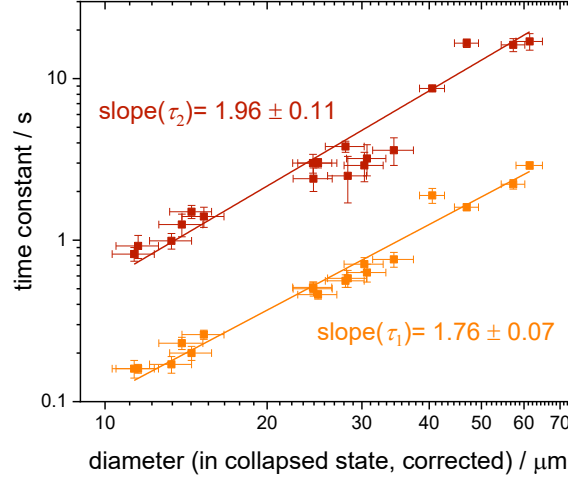


Figure 8.19: Log-log plots of τ (τ_1 in orange and τ_2 in red) vs. the corrected diameter in the mixture considering the reduced surface area of the deformed microgel beads.

Overall, one can state that such an adhesion-induced deformation, which depends on the microgel bead size, can cause an apparent deviation from the scaling law $\tau \sim R(\text{final})^2$ from Tanaka and Fillmore to smaller exponents. The correction due to the reduced surface area reduces this deviation. Still, the exponent of 2 is not reached for the first time constant τ_1 . In case of τ_2 , the corrected, experimentally determined exponent now agrees with the theoretical value of 2 within the range of error. It is proposed that the first process must be

additionally influenced by the inhomogeneity of the polymer network. This explanation is discussed in more detail in the following section.

8.6.2 Discussion of the deviation from the Tanaka and Fillmore scaling law

The deviation from the mono-exponential behavior and the square-power law proposed by Tanaka and Fillmore raises the general question about the physical processes ascribed to the time constants: Microgels do not have a fully homogeneous internal structure. For small microgels synthesized by precipitation polymerization, it is known that the cross-linking density decreases towards the periphery.^[195] This change in cross-linking density is not observed in the case of the sub-millimeter-sized microgel beads produced by microfluidics as they are not polymerized in their collapsed state. However, depending on the experimental conditions, a nano- and micrometer-sized inhomogeneity in the swollen state can occur.^[182,193,194] Seiffert et al.^[182] studied three PNIPAM-based microgel beads with different internal inhomogeneity and compared their size changes during temperature-jump experiments. According to their results, microgel beads bearing a micrometer-sized inhomogeneity exhibit continuous and faster deswelling kinetics than homogeneous gels.

Keidel et al.^[22] investigated small microgels with a low cross-linker content. Here, a very fast initial collapse was found where the first time constant τ_1 was 175 times shorter than the second time constant τ_2 . In the presented measurements, the time constants differ only by a factor between 4 and 10. Keidel et al. rationalized the rapid first process by the cluster formation towards the cross-links and a porous structure of the microgels allowing an easy expulsion of the solvent. It can be assumed that the mesh size of this porous structure is relatively larger in proportion to the overall size for the small, less cross-linked microgels used by Keidel et al. than for the larger, more cross-linked microgel beads in the present study. Therefore, the larger microgel beads could not show such an extreme jump in size as the small microgels in the study by Keidel et al. Still, the larger microgel beads show a rather fast, initial deswelling process. This fast deswelling process could be due to cluster formation and further be accelerated by an internal inhomogeneity. The kinetics of the initial large size reduction is described by the first time constant τ_1 . The proposed mechanism of cluster formation for this first process suggests that the kinetics is related to the size of the porous structure in addition to the surface area of the microgel bead. For this reason, a deviation from the R^2 power-law might be expected even after the correction for the reduced surface area. Within the subsequent slower process, the clusters merge together forming a hollowish structure in case of small microgels.^[22] By rearrangement of the polymers and further deswelling, a compact globular structure is formed. This slow transition is therefore

governed by the diffusion of the solvent through the microgel's surface and the collective diffusion of the polymer network inwards. Here, it is assumed that the microgel beads are already less porous with a rather homogeneous surface. Thus, the dependence of its time constant τ_2 on the available surface area for solvent transport is expected. This explanation is supported by the presented data showing that the R^2 power-law is within the range of the measurement uncertainty for time constant τ_2 .

8.7 Conclusions

In this thesis, a novel microfluidic platform was established to investigate the kinetics of the volume phase transition of adhered PNIPAM microgel beads due to cononsolvency. The setup allows a fast solvent-jump from pure water to an unfavorable mixture of 20 mol% methanol in water and easy imaging of the microgel bead response using microscopy. Various microgel bead sizes, with diameters between 20 and 110 μm in water, were compared. Experimental and theoretical studies on deswelling kinetics of polymer gels in the literature have been inconclusive about the process of the deswelling reporting between one and three relaxation times.

For all microgel beads in the present study, bi-exponential functions, hence two time constants, were required to properly describe the size evolution after the solvent-induced deswelling. Thus, the present measurements support the two-step process proposed by Keidel et al.^[22] for smaller microgels. In contrast to other collapse experiments with PNIPAM gels of comparable size to the microgel beads in this study, no skin layer formation was observed in the present case. Osmotic pressure experiments revealed that the microgel beads collapsed strongly at low compression. However, after this deswelling down to 0.72 of the original size, the polymer network became significantly stiffer. This is in agreement with the interpretation that the two processes of the cononsolvency-induced collapse correlate with this change in mechanical properties of the microgel beads.

The dynamics of the collapse is connected to the size of the microgel beads. As expected, larger microgel beads collapse more slowly than smaller ones. Plotting the two time constants against the final diameter, a dependence of $\tau \sim d(\text{collapsed})^x$ was found with an exponent of 1.56 ± 0.05 and 1.77 ± 0.08 for τ_1 and τ_2 , respectively. Thus, the determined exponents were smaller than 2 as proposed in the theory of Tanaka and Fillmore. Confocal fluorescence microscopy measurements indicate that the microgel beads deform due to the adsorption on the glass bottom of the investigation setup. The deformation of the collapsed microgel beads in the mixture depends on the microgel bead size. This size-dependent deformation of the microgel beads partly explains the deviation from the power-law

$\tau \sim R(\text{final})^2$ to smaller exponents. By correction of the diameter of the collapsed microgel beads considering the reduced surface area, the exponents increased to 1.76 ± 0.07 and 1.96 ± 0.11 for τ_1 and τ_2 , respectively. For τ_2 , the exponent now agrees with the square-power law in the range of error. In case of τ_1 , it is proposed that the process is governed by the inhomogeneous collapse rather than a simple diffusive process.

9. Summary and outlook

Poly-*N*-isopropylacrylamide (PNIPAM)-based systems are of great interest for a variety of applications. Most of them rely on the adaptability of the polymer network to external parameters such as temperature or solvent composition. For the systematic development and optimization of functional materials, a fundamental understanding of the responsiveness and the resulting properties is of crucial importance. In this context, this thesis aimed to gain deeper insight into the cononsolvency effect of PNIPAM gels in water-methanol mixtures. Both pure solvents swell the polymer network, whereas mixtures around 20 mol% methanol cause deswelling of the PNIPAM gels. Additionally, the responsive behavior to temperature and osmotic pressure was included. For this purpose, PNIPAM-based gels over a wide range of sizes – from small microgels of several hundred nanometers to microgel beads in the micrometer range up to macroscopic gels of several millimeters – were investigated. Depending on the scientific question and experimental approach, the PNIPAM gels were functionalized with a fluorescent co-monomer, a solvatochromic dye, or catalytically active moieties. The thesis is divided into equilibrium (Chapter 4 – 7) and dynamic (Chapter 8) investigations.

The largest PNIPAM gels in the range of several millimeters were studied in Chapter 4. These macroscopic gels were equilibrated in various water-methanol mixtures. The large gel size allows to capture spatially resolved Raman spectra distinguishing between the surroundings and the interior of the gel. The spectral analysis by indirect hard modeling (IHM) in combination with mass balancing gives access to the solvent partitioning. Here, an increased methanol fraction is found inside the gel for the unfavorable, cononsolvency-inducing mixtures around 20 mol% methanol. Moreover, the methanol Raman bands are sensitive to the local hydrogen-bonding environment of methanol. In binary water-methanol mixtures, these peaks shift linearly as a function of the composition. In contrast, the peak shifts measured inside the PNIPAM gels clearly deviate from the ones in the respective binary mixtures for the unfavorable water-methanol mixtures. This deviation can be ascribed to the increased methanol fraction inside the gels and different molecular interactions. Regarding the latter, the results point towards donor-type hydrogen bonding of the methanol and the peptide group of PNIPAM in unfavorable water-methanol mixtures.

Similar to the previous chapter, Chapter 5 focuses on the microenvironment inside the PNIPAM gels as a function of the water-methanol composition. This time, microgel beads in the micrometer range were studied. As a mass balance is not feasible for that microgel

size, a fundamentally different experimental approach was taken. PNIPAM microgel beads bearing a primary amine group were covalently labeled with a Nile Red (NR) derivative. NR is a solvatochromic dye and a powerful probe for the local environment. More specifically, NR presents two characteristics that are influenced by the local polarity and hydrogen-bonding ability of the surroundings: the wavelength of the maximum emission and the fluorescence lifetime. Confocal fluorescence spectroscopy methods allow a direct and spatially resolved evaluation of the internal properties of the microgel beads. As before, deviations between the binary mixture and the inside of the microgel beads are found in the cononsolvency-inducing mixtures. The lower polarity inside the microgel beads is ascribed to the polymer collapse and the enrichment of methanol. While the wavelength shift does not allow for differentiation of these overlaying effects, the methanol enrichment can be quantified using fluorescence lifetime imaging (FLIM). First measurements support an increased methanol fraction for the microgel beads initially immersed in a 20 mol% methanol mixture which is in agreement with the findings for the macroscopic gels from Chapter 4. These first experiments demonstrate the high potential of FLIM to gain spatially resolved and quantitative insights into microgel systems. In the future, FLIM experiments can be extended to other water-alcohol mixtures to probe the solvent partitioning between polymer network and surroundings. Furthermore, small NR-labeled microgels from precipitation polymerization could be investigated in next experiments. Although their size is smaller than the diffraction limit, it should be possible to extract an average signal for the entire microgel.

Chapter 6 shows the importance of detailed knowledge of the properties of microgels in different solvent conditions and respective differing swelling states. In this chapter, the catalysis of an aldol reaction using L-proline modified PNIPAM microgels was studied. The hydrophobic environment provided by the polymer network in combination with the general solvent quality for the reagents governs the catalytic activity. The impact of the solvent (water, methanol, and their mixtures) and the temperature were investigated. The characterization of the microgel-catalysts by scattering methods shows the expected temperature-responsive behavior of the microgels in water and basically a non-responsive system in methanol. While the volume phase transition temperature shifts to 35 °C in comparison to pristine PNIPAM microgels, no influence of the incorporated L-proline moieties on the cononsolvency behavior is found. Regarding the catalysis in water, the catalytic activity significantly increases with rising temperature. The course of the temperature-dependent reaction rate resembles the course of the microgel collapse. In contrast, only a small impact of temperature on the apparent reaction rate of the catalysis in the non-responsive methanol system is determined. The collapse of the microgel-catalysts positively influences the

activity. For the catalysis in water-methanol mixtures, overlaying effects were identified. Both, the collapse and the methanol enrichment explain the locally increased reaction rate around the unfavorable, 20 mol% methanol in water mixture.

In the last chapter of the equilibrium part (Chapter 7), the mechanical properties of PNIPAM microgel beads were investigated. In this chapter, the isotropic deswelling of microgels due to an imbalance of internal and external osmotic pressure was evaluated to determine the bulk modulus of the microgel beads. To this end, PNIPAM microgel beads with different sizes and cross-linker contents were immersed and imaged in solutions containing high molecular weight dextran. From the correlation between the volume of the microgel beads and the osmotic pressure exerted by the dextran, the bulk modulus was calculated. Less cross-linked microgel beads show a higher swelling ability and a smaller bulk modulus. For the same amount of cross-linker but different sizes, no distinct impact on the bulk modulus is detected. Interestingly, all samples exhibit a transition between an easily compressible, soft polymer network and a stiffer, partially collapsed network after compression to around 0.72 of the original size. In a future step, the mechanical properties of the microgel beads could be further characterized by atomic force microscopy (AFM). Furthermore, a comparison to small microgels synthesized by precipitation polymerization would be interesting. This synthesis method results in microgels with fundamentally different morphology and cross-linking distribution compared to the microgel beads from microfluidics.

The second part of this thesis focuses on the dynamics of the volume phase transition of microgels. Experimental and theoretical studies are still inconclusive about the processes involved in the deswelling kinetics of polymer gels. While some studies suggest one relaxation time, others propose up to three processes including a plateau region.^[22,308,309,316] To gain new insights, the cononsolvency-induced collapse of fluorescently labeled PNIPAM microgel beads was investigated (Chapter 8). To this end, a custom-made microfluidic platform was developed to realize a rapid solvent-jump from pure water to an unfavorable mixture of 20 mol% methanol in water. The response of microgel beads adhered to the channel surface can easily be imaged by time-resolved fluorescence microscopy. To describe the size evolution of the solvent-induced deswelling, two relaxation times are required. The two-step collapse is found for all investigated microgel beads and is in concordance with previous solvent-jump^[22] and pressure-jump experiments^[24] using small microgels. This indicates that the two-step process of the microgel collapse is a generic feature. The osmotic pressure experiments (Chapter 7) revealed that after compression to 0.72 of the original size, a transition from a soft to a stiffer polymer network occurs. This change in mechanical properties coincides with the transition of the first to the second process of the dynamic

collapse behavior. The first, fast process is responsible for the major part of the volume transition while only a small change in size is observable for the second process. The dynamics of the collapse are connected to the size of the microgels. The presented findings deviate from a prominent theory of Tanaka and Fillmore which suggests a simple scaling law of the relaxation time to the square of the final radius.^[305] Deviations from this power-law have been reported before, but no clear explanation was found.^[309,310] In the present study, smaller exponents are found for both processes. For the second process, this deviation can be ascribed to the adhesion-induced deformation and the resulting reduction of the surface area of the microgel beads. For the first process, an additional influence of an inhomogeneous collapse with cluster formation is assumed. In the future, the presented approach can be extended to study microgel beads with different cross-linker contents or to examine the inverse process, i.e. the swelling of the microgel beads. Furthermore, the investigation platform can be applied to study microgel beads with other architectures such as anisometric microgel beads or microgel capsules. Finally, it would be interesting to compare the obtained results to free-flowing microgel beads to verify the proposed influence of the adhesion.

To conclude, this thesis addresses several fundamental aspects of the influence of external stimuli, especially the cononsolvency effect, on the properties and response of microgels under equilibrium and dynamic conditions. The first part revealed local properties and differences between microgel and surroundings depending on the solvent composition, such as solvent partitioning, hydrogen bonding, or polarity: Methanol is enriched inside the gels in the cononsolvency-inducing mixtures. The collapse of the gels in unfavorable mixtures and the higher internal methanol fraction result in a less polar polymer network. This higher hydrophobicity can be favorable for applications with hydrophobic components, as demonstrated by an example from the field of catalysis. In the second part, the kinetics of the deswelling of PNIPAM microgel beads after a sudden change in solvent quality were examined. The dynamic collapse proceeds in two steps which could be aligned with changes in the mechanical properties. The dynamics as a function of the microgel bead size suggest the influence of the adhesion-induced deformation and an inhomogeneous initial collapse. Overall, the presented findings provide further understanding of the cononsolvency effect. In the future, the experimental approaches can be extended to other and more complex systems. Finally, a theoretical model that can capture the presented unique details of PNIPAM gels in cononsolvency mixtures would be helpful to reproduce and predict the performance of functional materials.

10. Experimental section

In the following part, materials and experimental details are presented. Microfluidics and Raman measurements are described in a general manner before details and variations are highlighted for the specific investigated systems. An overview of all PNIPAM gels used in this thesis is given in Table A2 – Table A6 in the Appendix.

10.1 Materials

Table 10.1: Chemicals, solvents, and materials used and their supplier.

Name	Supplier
Ammonium persulfate (APS)	GE Healthcare Bio-Sciences
Aquapel	PPG
Dextran ($M_w = 150\,000$ g/mol)	Alfa Aesar
<i>N,N'</i> -Dicyclohexylcarbodiimide (DCC)	Sigma-Aldrich
4-Dimethylaminopyridine (DMAP)	Acros Organics
Krytox	Chemours
Methacryloxyethyl thiocarbamoyl rhodamine B (MTRB)	Polysciences
<i>N</i> -(3-Aminopropyl)methacrylamide hydrochloride (APMA)	Sigma-Aldrich
<i>N</i> -Isopropylacrylamide (NIPAM)	Acros Organics
<i>N,N'</i> -Methylenebis(acrylamide) (BIS)	Sigma-Aldrich
<i>N</i> -Hydroxysuccinimide (NHS)	Sigma-Aldrich
<i>N,N,N',N'</i> -Tetramethylethylenediamine (TEMED)	Merck
Novec 7500	3M
Paraffin oil	Sigma-Aldrich
Polyethylene glycol (PEG, $M_w = 8000$ g/mol, BioUltra)	Sigma-Aldrich
Polydimethylsiloxane (Sylgard 184)	Dow Corning
Span 80	Sigma-Aldrich
Acetone	Sigma-Aldrich
Dimethylformamide (DMF)	VWR
1,4-Dioxane	Sigma-Aldrich
n-Hexane	Sigma-Aldrich
Methanol (MeOH, Uvasol)	Merck
2-Propanol	Sigma-Aldrich
Water (deionized, for Raman measurements only)	Bernd Kraft
96 or 48 flat bottom Cellstar well plates	Greiner Bio-One
Fine Bore Polythene Tubing (800/100/120)	Portex

10.2 Macroscopic PNIPAM gels

Macroscopic PNIPAM gels were prepared using a cooled molding approach. Here, 48 and 96 well plates served as molds (height 17.4 mm, diameter 11.05 – 11.56 mm and height 10.9 mm, diameter 6.39 – 6.96 mm, respectively). A solution of NIPAM, BIS (5 mol%, if not stated otherwise), and TEMED (0.5 vol%) was prepared. Separately, APS was dissolved in water. Both solutions were degassed for 10 minutes. Then, APS was added (1 mol%) to the monomer solution and mixed. Immediately afterwards, the solution was casted into a 96 and/or 48 well plate, sealed with a coverslip, and kept in the fridge overnight to complete the polymerization. During the synthesis procedure, all solutions, well plates, and coverslips were cooled with ice. Finally, the gels were removed from the well plate and washed in MilliQ water for 2 weeks.

10.2.1 Mass balance experiments

The macroscopic PNIPAM gels were dried for one week at atmospheric pressure and one week under vacuum. The weight of the individual, dried gels was determined with a microbalance. Then, a certain water-methanol mixture of known composition was added. The sample vials were closed and kept at 23 °C for about 7 days to achieve equilibrium. Subsequently, Raman microspectroscopy measurements were performed at two measurement points, one for the surrounding solution and a second one for the gel itself. Afterwards, the gels were removed from their vial and weighed. The solvent composition of the surrounding solution was evaluated by spectral analysis of the component areas using indirect hard modeling (IHM) as described below (section 10.4), whereas the methanol concentration inside the gel was calculated by mass balancing. Previous to the removal of the gel, Raman spectra were captured inside the equilibrated PNIPAM gel to perform a peak shift analysis.

10.3 Microfluidics

Microfluidics was used for the synthesis of PNIPAM microgel beads with different cross-linker contents (Chapter 7), of rhodamine-labeled PNIPAM microgel beads (Chapter 8) as well as of solvatochromic PNIPAM microgel beads (Chapter 5). Additionally, a microfluidic investigation setup was used for solvent-mediated collapse experiments (Chapter 8).

10.3.1 Preparation of microfluidic devices

For the synthesis of PNIPAM microgels and the dynamic investigations, PDMS-based microfluidic chips were used. Both devices were produced by soft lithography using the following procedure (Figure 10.1):

The desired microfluidic design was sketched in a computer-aided design (CAD) software. Subsequently, a photomask was prepared (a, b). A silicon wafer spin-coated with a photoresist was covered with the photomask and exposed to UV light (c). During the baking and development step (d), only the photoresist exposed to UV remained, leaving a patterned surface profile. In the case of the flow-focusing devices, silicon wafers of the designs were available, whereas the master of the Y-inlet microfluidic device was custom-made and printed onto a glass slide using a multiphoton 3D printer (Nanoscribe, Photonic Professional GT). For the preparation of each microfluidic device, polydimethylsiloxane (PDMS) was poured onto the patterned master slide (e). The PDMS was cured for 2 days at room temperature or at 60 °C for 4 h after vacuum treatment. The PDMS replica was peeled off the wafer (f) and holes of 0.75 mm in diameter for the inlet and outlet tubing were punched into the PDMS (g). Subsequently, the PDMS replicas were cleaned by sonication in isopropanol for 15 minutes. After sonication, the PDMS was washed with isopropanol and dried using a nitrogen stream. This procedure was repeated three times with isopropanol and another three times with deionized water. In parallel, the corresponding microscope slides for the synthesis (Marienfeld Superior, 76 x 52 x 1 mm) or the dynamic investigations (Marienfeld Superior, 1.5 H, 50 x 24 mm, 170 μ m thickness) were sonicated in acetone and washed in an identical procedure with acetone (2x), isopropanol (2x) and deionized water (2x). Afterwards, all cleaned parts were dried in the oven at 60 °C for 1 h. Finally, the devices were fabricated by O₂-plasma bonding (PVA TePla 100 Plasma System) of the PDMS replicas onto the glass slide (h, i). The bonded devices were stored in the oven at 60 °C for 1 h.

10.3.2 Microfluidic synthesis

Spherical PNIPAM microgels were prepared using PDMS-based flow-focusing microfluidic devices. Here, three devices with different dimensions of the cross-section were used to achieve a wide range of droplet sizes. More specifically, channel widths of 20, 30, or 50 μ m were available (Figure 10.2).

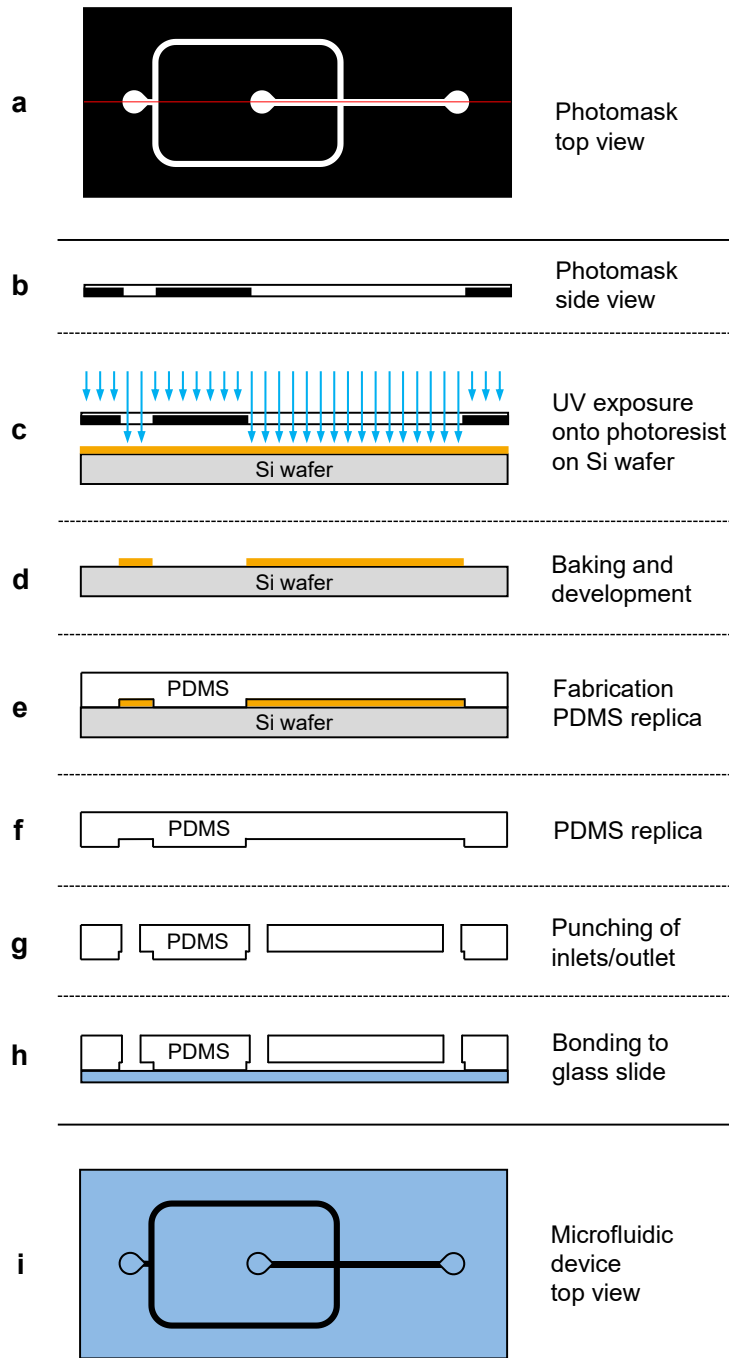


Figure 10.1: Scheme of the preparation of a microfluidic device using soft lithography. (a, i) show a top view of the photomask and the final device, respectively. (b - h) depict the side view of the preparation process along the red line marked in (a). Adapted from ref. [140].

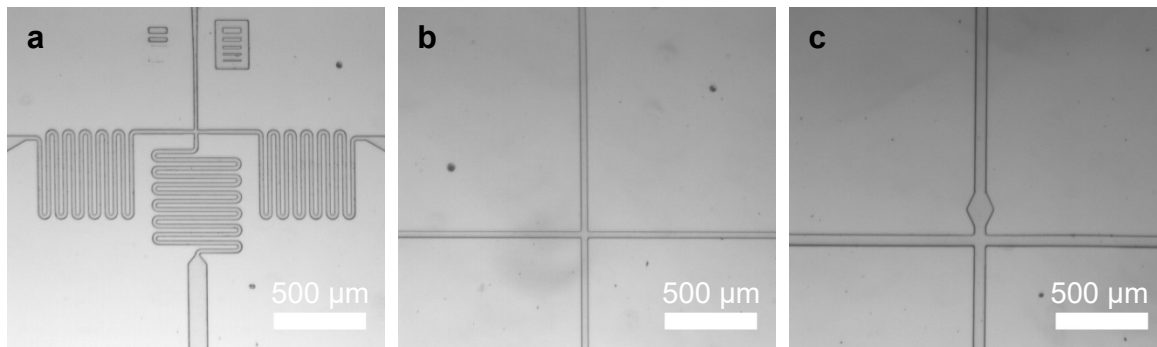


Figure 10.2: Cross-sections of the flow-focusing microfluidic devices with different channel widths: (a) 20 μm , (b) 30 μm , and (c) 50 μm .

Prior to the synthesis, a surface modification of the channels was carried out to render the devices suitable for water-in-oil emulsification. To this end, a filtered solution of Aquapel was injected into the channels to apply a hydrophobic monolayer. After a few minutes, the solution was removed by air and the devices were stored for 1 h at 60 °C.

The synthesis procedure is based on findings of Di Lorenzo and Seiffert.^[169] NIPAM was recrystallized in n-hexane for all microfluidic syntheses. All other chemicals were used as received. The general composition of the aqueous phase includes the monomer NIPAM, a co-monomer (if desired), the cross-linker BIS, and the initiator APS. In total, a mass fraction of 100 mg/mL (without APS) was reached. The oil phase comprises a hydrofluorether (Novec 7500) and 1.8 wt% of a fluorinated surfactant (Krytox). Additionally, 2 vol% of TEMED was added. Before transferring the solutions into Hamilton glass syringes, they were degassed with N₂ for 15 minutes. The syringes were put into syringe pumps (Harvard Apparatus) and the syringe with the aqueous phase was protected from light with aluminum foil. The syringes were connected to the PDMS devices with PE tubing. Depending on the channel width and desired droplet size, different flow rates were set. The droplet formation and size were observed and imaged with an inverted optical microscope (Motic AE2000) connected to a camera (0.65x, Point Grey Flea 3) controlled by FlyCapture Software. The generated droplets were collected in a vial containing 1 mL of the oil phase which was covered with a paraffin oil layer to prevent oxygen diffusion. Due to the different densities, the microgels accumulated between these two oils. Finally, the synthesized microgels were allowed to polymerize at room temperature overnight (> 12 h) before testing their stability.

The purification process of the microgels in the oil phase consisted of several washing steps with solvents of increasing polarity until water was reached. The respective solvent was added and the mixture was carefully shaken. The washing phase was removed after phase separation. The following sequence of solvents was used: Novec 7500 (1x), hexane with 1 wt% Span 80 (1x), hexane (3x), isopropanol (3x), dioxane (3x), and water (> 3x). When transferring from dioxane to water, the microgels in dioxane and the water were pre-cooled at 4 °C for several hours before mixing. After successful purification, the microgels were stored at room temperature in water.

10.3.3 PNIPAM microgel beads with varying size and cross-linker content

PNIPAM microgel beads with different sizes and cross-linker contents were synthesized for osmotic pressure experiments (Chapter 7). An aqueous phase containing NIPAM, BIS (5 or 1.2 mol%), and APS (8 or 9.5 mg/mL, respectively) was prepared. The oil phase comprised

Novec 7500, Krytox (1.8 wt%) as a surfactant, and TEMED (2 vol%) as the accelerator. Droplet generation, collection, and purification were performed as described in section 10.3.2. Flow-focusing PDMS chips with a diameter of 20, 30, or 50 μm at the cross-section were used. The microgel beads were stored in water after purification.

10.3.4 Nile Red-labeled microgel beads

Solvatochromic microgel beads are investigated in Chapter 5. PNIPAM microgel beads labeled with an O-carboxylic derivative of Nile Red (NR) were synthesized in several steps. The composition of the aqueous phase of the microfluidic synthesis included the monomer NIPAM, the co-monomer APMA, the cross-linker BIS (5 mol%), and the initiator APS (7 mg/mL). Either 1 or 3 mol% APMA was used (sample codes: MG-PNIPAM-APMA-1 and MG-PNIPAM-APMA-3, respectively). The oil phase comprised a hydrofluorether (Novec 7500, 3M) and 1.8 wt% of a fluorinated surfactant (Krytox). Additionally, 2 vol% of TEMED was added. Droplets were fabricated using a PDMS chip with a diameter of 20 μm at the cross-section. Droplet generation, collection, and purification were performed as described in section 10.3.2. For the subsequent labeling step, the microgel beads were transferred to a buffer solution or methanol after purification. A functionalized NR-label bearing a carboxylic acid group was synthesized by the group of Dr. Andrey Klymchenko at the Laboratoire de Biophotonique et Pharmacologie at the University of Strasbourg (France). By a DCC coupling reaction, the NR-O-C-COOH was then transformed to NR-O-C-COO-NHS. To this end, NR-O-C-COOH (0.0082 g) and NHS (0.0111 g) were dissolved in 15 mL DMF and kept in an ice bath for 10 minutes under nitrogen. Subsequently, DMAP (0.0048 g in 2 mL DMF) and DCC (0.011 g in 3 mL DMF) were added to the solution. At room temperature, the reaction took place for 3 h under N_2 . The crude reaction mixture containing the new NR derivative was stored in the fridge under inert gas. To label the microgel beads, the NR derivative (~ 0.1 vol% of microgel dispersion) was added to 1 mg/mL microgel beads in methanol or phosphate buffer solution (pH 8). After vigorous shaking, the vial was mixed on the roller mixer overnight. Finally, excess dye was removed by several washing and phase separation steps ($> 10\times$) with the respective solvent.

10.3.5 Rhodamine-labeled microgel beads

Fluorescently labeled PNIPAM microgels in the size range of 20 – 110 μm in diameter were synthesized via droplet microfluidics for dynamic investigations of the cononsolvency-induced collapse (Chapter 8). The water phase contained NIPAM, BIS (5 mol%), and APS (9 mg/mL) as the initiator. To obtain fluorescently labeled microgels, MTRB (< 0.1 mol%) was added to the aqueous phase. A fluorinated oil phase (Novec 7500 and 1.8 wt% of the

fluorinated surfactant Krytox) in combination with TEMED (2 vol%) was used as continuous phase. The droplet generation was achieved using flow-focusing PDMS chips with a diameter of 20, 30, or 50 μm at the cross-section. Additionally, the flow rates were varied to obtain different microgel bead sizes. Purification was performed as described in section 10.3.2. It was carefully observed that the isopropanol washing steps were sufficient to remove all excess dye. The microgel beads were stored in water after purification. In order to determine the diameter of the microgels in the samples, they were imaged in water and in the most unfavorable cononsolvency mixture of 20 mol% methanol in water under equilibrium conditions. To this end, a part of the microgels in water was repetitively washed with the mixture and transferred to a closed chamber consisting of a spacer of 120 μm in height (Secure Seal imaging spacer) to prevent evaporation of methanol during imaging. Subsequently, the microgel sizes of at least 300 microgels in water and 150 microgels in the mixture were measured by hand (Table A1 in the Appendix).

10.4 Raman microspectroscopy measurements

All Raman microspectroscopy measurements were performed on an inverse confocal Raman microscope (inVia, Renishaw, Leica microscope) equipped with a frequency-doubled Nd:YAG-laser of 100 mW at 532 nm excitation wavelength. The attached multichannel analyzer consists of a spectrometer with a grating of 1800 l/mm and a cooled CCD camera. All measurements were performed at room temperature (23 °C) with an air objective (20x). Depending on the experimental setup (investigation platform, gel size, solvent composition) and purpose of the measurement, different exposure times, numbers of acquisitions, and spectral regions were chosen.

10.4.1 Indirect hard modeling (IHM)

Spectral analysis was conducted using indirect hard modeling (IHM)^[128,210,218,221] (also see section 3.2.2). To this end, spectra of pure water and pure methanol were measured to create pure component models. These spectra were modeled with peak-shaped pseudo-Voigt functions. Figure 10.3 shows the pure component models of water and methanol for the high wavenumber region (2700 – 3800 cm^{-1}). The OH stretching of water was modeled with five peak functions. The CH symmetric and asymmetric stretching and the OH stretching band of methanol required six peak functions. A spectral model for the glass signal of either the vial, cuvette (Chapter 4), or the microfluidic glass chip (Chapter 8) was modeled by another pure component model and used to describe the background. The pure component model for PNIPAM was created by complementary hard modeling (CHM)^[220] of a spectrum of slightly

hydrated PNIPAM microgels. The pure component model of PNIPAM was only included for the evaluation of measurements inside the gels.

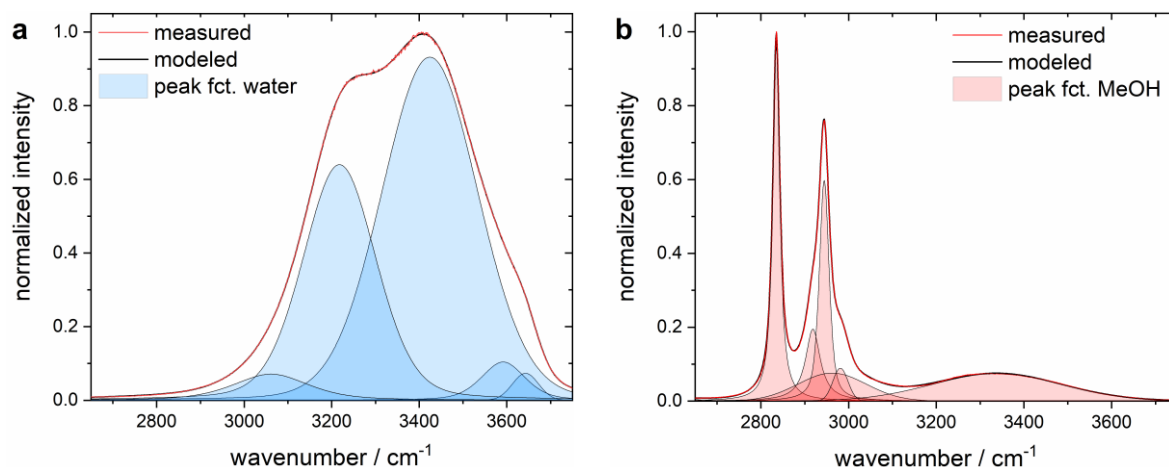


Figure 10.3: Pure component spectrum (red) and model (black) with individual peak functions for (a) water (light blue) and (b) methanol (light red) used in IHM.

All pure component models were combined into a mixture model. For each peak function in the mixture model, several parameters are available, namely peak position, full width at half maximum (FWHM), and Gaussian part of the pseudo-Voigt peak shape. For each peak function, parameters were assigned as fixed or flexible based on calibration data of binary water-methanol mixtures. Flexible parameters can be adjusted – as an additional degree of freedom – during optimization in the following spectral fitting step to account for nonlinear effects. Spectral fitting minimizes the residuals between the measured spectrum and the spectral mixture model in a least-squares procedure. For each pure component in the mixture model, the intensities were integrated and weighted. Calibration spectra of binary mixtures of known composition were analyzed to determine the calibration factors for converting the weight into the corresponding mole fraction. To extract peak positions, only the spectral range of the relevant peak was evaluated. The remaining spectrum was excluded from the evaluation and the mixture model was reduced accordingly.

10.4.2 Raman measurements of macroscopic PNIPAM gels

For the mass balance experiment and peak shift analysis in Chapter 4, two separate spectral regions ($619 - 2287 \text{ cm}^{-1}$ and $2505 - 3825 \text{ cm}^{-1}$) were recorded. The fingerprint region around 1500 cm^{-1} was solely used to determine the position of the methanol-CO peak (1035.3 cm^{-1} in pure methanol). Here, the exposure time was set to 5 s but lowered to 2 s for $> 50 \text{ mol\%}$ methanol. The higher wavenumber region was evaluated for the mass balancing experiment as well as for the determination of the position of the methanol-CH peak (2836.5 cm^{-1} in pure methanol). The exposure time was set to 1 s but lowered to 0.5 s for the

measurement of the pure methanol. In all cases, full laser power was used and 10 accumulations were averaged to improve the signal-to-noise ratio. Measurements were conducted for multiple reference solutions, inside the equilibrated PNIPAM gels, and for their surrounding solution. Spectral analysis was conducted using IHM which is described in detail in section 10.4.1. For the methanol-CO peak and the methanol-CH peak, the spectral ranges of $975 - 1075 \text{ cm}^{-1}$ and $2800 - 2860 \text{ cm}^{-1}$ were considered, respectively.

10.4.3 Characterization of the solvent-jump setup

To characterize the investigation setup for the solvent-jump experiments (section 8.3), Raman microspectroscopy was applied. To circumvent a PDMS signal in the spectra, a glass device of comparable dimensions and shape as the Y-inlet PDMS-device (channel width $1000 \text{ }\mu\text{m}$, height $100 \text{ }\mu\text{m}$) was purchased from Micronit. The width of the interface between water and the water-methanol mixture at different flow rates and positions in the channel was determined. To this end, Raman spectra were taken across the channel perpendicular to the flow direction every $5 \text{ }\mu\text{m}$. These measurements were conducted at different channel heights (10 , 20 , or $50 \text{ }\mu\text{m}$ above the glass surface) and at various distances from the inlets (200 , 400 , 600 , 1000 , or $1500 \text{ }\mu\text{m}$) as illustrated in Figure 8.3. Spectra of the wavenumber region $2505 - 3825 \text{ cm}^{-1}$ were recorded with an exposure time of 1 s and 100% laser power. Three accumulations were measured to improve the signal-to-noise ratio.

Moreover, the time required for the exchange of the solvent at a distinct position in the channel during the solvent-jump experiment was investigated. To this end, the aforementioned solvent-jump procedure was also performed with and without a microgel present at the measuring point. Here, time-resolved spectra of the wavenumber region $2505 - 3825 \text{ cm}^{-1}$ were captured. The exposure time was set to 0.2 s and 100% laser power was used. Due to data processing, a time resolution of around 0.37 s could be realized. Consequently, the time-resolved Raman measurements cannot provide an exact velocity of the solvent-jump, but give a rough indication. IHM was used for the spectral analysis (see section 10.4.1 for details): Spectra of pure water and pure methanol were measured and modeled with peak-shaped pseudo-Voigt functions to create pure component models. The pure component model for PNIPAM was created by CHM^[220] of a spectrum of a slightly hydrated PNIPAM microgel. Only for the measurement inside the PNIPAM microgel, the respective pure component model was included in the spectral fitting step. In general, the high overlap of PNIPAM and methanol in the spectra in combination with nonlinear effects in water-methanol mixtures limit the accuracy of the quantitative results. Thus, the results were solely interpreted qualitatively.

10.5 Fluorescence measurements

10.5.1 Fluorescence spectroscopy

Fluorescence spectroscopy measurements of solvatochromic microgel beads were performed by Dr. Silvia Centeno Benigno (Chapter 5). Fluorescence spectra were measured using a home-made fluorescence confocal microscope consisting of an Olympus IX81 inverted microscope equipped with a 100x 1.3NA oil immersion objective. A 150 μm pinhole was placed in the focal detection plane followed by a Shamrock 300i spectrometer equipped with a 300 lines/mm diffraction grating with blaze at 760 nm. As excitation source, 3 mW of the 514.5 nm line of an Ar⁺ laser was coupled into the microscope with the appropriate optics. Fluorescence spectra were collected by the objective and transmitted through an HCBSR514 dichroic filter and a long pass 514 filter. After spatial filtering at the pinhole, the signal was focused on the spectrometer entrance slit. The excitation light was focused on the approximate center of each microgel bead and 10 accumulated spectra with an acquisition time of 1 s in the conventional mode were recorded.

For the sample preparation (MG-PNIPAM-APMA-3-NR), $\sim 12 \mu\text{L}$ of a microgel bead dispersion in methanol were spin-coated on a Hellmanex and plasma cleaned microscope slide of 170 μm thickness. Subsequently, a chamber was created by gluing a 4 mL vial with cut-off bottom onto the prepared glass slide. Finally, the desired solvent was added into the chamber which was then closed with a cap. Multiple microgel beads were investigated in each solvent. For each, spectra were captured at the center of the microgel bead (xy plane) and at 5 different heights (\sim center and $\pm 7 \mu\text{m}$, $\pm 14 \mu\text{m}$). For the reference measurements, only NR-O-C-COOH in various solvents was measured. Besides the pure solvents water and methanol, various mixtures were investigated. For the wavelength calibration of the grating position, the Raman lines of pure, liquid toluene were used. In addition to this, the intensity of the spectra was corrected as follows: The spectra of the NR-O-C-COOH in the different water-methanol mixtures were corrected by applying wavelength-dependent intensity correction factors evaluated by comparing the recorded spectrum of NR in methanol and the previously recorded and corrected spectrum in a fluorescence spectrometer (FP-6500, Jasco). From the corrected and uncorrected NR-O-C-COOH spectra in the water-methanol mixtures, a linear calibration was obtained for estimating the position of the emission maximum without the need to correct for the whole spectrum. This correction was applied for estimating the emission maximum position (λ_{max}) of the spectra recorded in the microgel beads.

10.5.2 Fluorescence lifetime imaging (FLIM)

Fluorescence lifetime measurements of solvatochromic microgel beads were performed by Dr. Silvia Centeno Benigno (Chapter 5). The measurements were conducted using a time-resolved confocal fluorescence microscope (MicroTime200, PicoQuant) comprising an Olympus IX81 inverted microscope. The setup is equipped with a FLIMbee galvo scanner, two single-photon avalanche diodes (SPADs, Excelitas) as detectors, and a time-correlated single photon counting (TCSPC) module (HydraHarp400). Fluorescence lifetime imaging (FLIM) was realized with a 532 nm excitation laser and a 60x 1.2NA water immersion objective. Images were recorded by galvo scanning at a fixed height ($\sim 2 \mu\text{m}$) above the coverslip. Sample areas ranging from approximately 115×115 to $140 \times 140 \mu\text{m}^2$ were imaged with a pixel size between 150 and 179 nm and a dwell time of $1.3 \mu\text{s}/\text{pixel}$. Each image is the accumulation of 200 frames. For data handling and analysis, the system software SymPhoTime 64 was used. On the one hand, reference measurements using the NR-O-C-COOH in various water-methanol mixtures ($x(\text{MeOH}) = 0.15, 0.25, 0.35, 0.5, \text{ or } 1$) were conducted. On the other hand, NR-labeled microgel beads (MG-PNIPAM-APMA-3-NR) were measured under three different conditions. The procedure of the sample and measurement chamber preparation was done as described in the previous section 10.5.1. Microgel beads were imaged in their partly dried state after spin-coating a dispersion in methanol, immersed in pure methanol, or in a water-methanol mixture containing 20 mol% methanol. For each condition, several microgel beads were investigated. In the resulting images, each microgel bead was defined as a single region of interest (ROI), and the fluorescence decay was analyzed for each ROI. The decay was fitted with a multi-exponential function to obtain the lifetime components. These components were used to analyze the fluorescence decay of each pixel and create the final FLIM image.

10.5.3 Time-resolved fluorescence microscopy

The response of rhodamine-labeled microgel beads after a solvent-jump was imaged by time-resolved fluorescence microscopy (Chapter 8, section 8.4). The fast change in solvent composition from pure water to a mixture of 20 mol% methanol in water was realized using a PDMS-based microfluidic setup with Y-shaped inlets (see section 8.2). The change in size of a microgel bead was captured using a Nikon Eclipse TE3000 inverted fluorescence microscope (Nikon Intensilight C-HGFI) connected to a camera (Blackfly S BFS-U3-16S2M). The framerate varied between 49 and 66 Hz. For most investigated microgel beads, three repetitions of the cononsolvency-induced collapse were imaged. The three repetitive experiments confirmed the reproducibility of the solvent-jump and the results were

averaged. For a few microgel beads, the size change after a solvent-jump was captured for a longer time. As long exposure times led to bleaching of the fluorescent dye, no threefold experiments were possible.

10.5.4 Spinning-disk confocal fluorescence microscopy

The shape of microgel beads adhered to the dynamic investigation setup was investigated by confocal fluorescence microscopy (see section 8.6.1). A commercial VisiScope Spinning Disk DC Confocal system (Visitron Systems GmbH) equipped with a spinning disc unit CSI-X1 (Yokogawa) was used to image the fluorescent microgel beads. Z-scans of the microgel beads in water or in a 20 mol% methanol-water mixture were performed. To this end, the microfluidic device was placed onto a *xy*-piezo table (SmarAct GmbH) of a commercial inverted microscope Eclipse Ti-E (Nikon). The samples were illuminated with a 561 nm laser (500 mW). The fluorescence of the copolymerized rhodamine B derivative was collected with an adapted 60x/1.20 NA water objective (U Plan S Apo, Olympus) and afterwards separated from the excitation laser using a quad-line beam splitter Di01-T405/488/568/647 (Semrock). Background light remaining from the excitation light was suppressed using a bandpass filter ET605/70m (Chroma) in the emission path. Emission was detected by an EMCCD camera (Andor iXON Ultra 888). All measurements were performed at room temperature.

10.6 Synthesis and characterization of L-proline modified PNIPAM microgels

The L-proline modified PNIPAM microgels (Chapter 6) were synthesized by precipitation polymerization (sample code: SFB985_C6_DK_P000323). To this end, NIPAM (90 mol%), a polymerizable form of L-proline (10 mol%), and BIS (~ 2 mol%) were polymerized in water at 70 °C with AMPA as initiator. The microgel-catalysts were freeze-dried previous to catalytic testing. The content of remaining water was analyzed by thermogravimetric analysis (TGA). The amount of L-proline incorporated in the polymer network was determined by attenuated total reflection Fourier transform infrared (ATR-FTIR). The swelling behavior was investigated by light scattering. The catalytic testing was performed at room temperature (25 °C) in water, methanol, and various water-methanol mixtures. The microgel-catalysts (0.1 eq L-proline groups) were mixed with 4-nitrobenzaldehyde (1 eq) and cyclohexanone (5 eq). For the reference experiments with unbound L-proline, the same equivalents were chosen. After each run, the reaction was terminated by the separation of the catalysts. Subsequently, the solvent was removed and the conversion was determined by

^1H nuclear magnetic resonance (^1H -NMR) spectroscopy. In addition to experiments, dissipative particle dynamics (DPD) simulations were performed. Here, the microgel-catalysts and the reagents were studied at various temperatures in water or methanol.

For more experimental and simulation details, refer to Kleinschmidt et al.^[72]

10.6.1 Dynamic light scattering (DLS)

The size of the microgel-catalysts in various solvents was measured using dynamic light scattering experiments. For performing the measurements an ALV setup connected to a goniometer equipped with a HeNe laser ($\lambda = 633 \text{ nm}$) was used. The temperature of the index-match-bath filled with toluene was controlled by a programmable thermostat (Julabo F32). Highly diluted samples of the freeze-dried microgel-catalysts were investigated to avoid multiple scattering. The solutions were filtered using cellulose acetate (CA) filters (Minisart®, pore size $0.8 \mu\text{m}$). For temperature-resolved measurements in water and methanol, the value of the temperature was adjusted between $20 - 50 \text{ }^\circ\text{C}$ in steps of $2 \text{ }^\circ\text{C}$. In the case of the sample in 20 mol% methanol, the temperature was varied between $10 - 40 \text{ }^\circ\text{C}$. According to literature scattering angles between 40° and 110° in steps of 10° were evaluated for each temperature. Additionally, individual q -dependent measurements were performed at $25 \text{ }^\circ\text{C}$ in all solvents and in water at 60, 70, and $75 \text{ }^\circ\text{C}$. Here, the scattering angle was varied in steps of 5° . For measurements in various water-methanol mixtures, solely q -dependent measurements at $25 \text{ }^\circ\text{C}$ between 40° and 110° in steps of 5° were performed. Corresponding values of refractive indices and viscosities of the water-methanol mixtures were taken from the literature (Table 10.2). The average diffusion coefficient was determined from the second-order cumulant. The Stokes-Einstein equation was applied to determine the corresponding hydrodynamic radius (R_h). Samples were prepared several times. The error bars were then obtained by averaging over several q -dependent measurements and the deviation within the results of the q -dependence.

Table 10.2: Refractive indices and viscosities of the binary water-methanol mixtures used for DLS measurements.^[330,331]

$x(\text{MeOH})$	Refractive index	Viscosity / mP
0.11	1.3365	13.45
0.15	1.3375	14.40
0.20	1.3388	15.50
0.35	1.3396	15.49
0.50	1.3389	13.30
0.60	1.3380	10.69
0.80	1.3334	8.30

10.6.2 Static light scattering (SLS)

Highly diluted samples of the microgel-catalysts were investigated to prevent multiple scattering and an influence of the structure factor. After redispersion, all samples were filtered with CA filters (Minisart®, pore size 0.8 µm). All experiments were performed on a closed goniometer from SLS-Systemtechnik GmbH with two laser wavelengths of 407 and 640 nm. In total, a q -range between 0.003 and 0.04 nm⁻¹ was covered. The temperature of the toluene bath was controlled by a thermostat (Julabo CF40). Before each measurement, the temperature was equilibrated for at least 10 min. The scattering intensity was corrected by subtraction of the respective solvent scattering. Due to an increase in scattering intensity of the solvent background at low q , q -values below 0.0056 nm⁻¹ were excluded for the evaluation of the radius of gyration (R_g). R_g was determined from the Guinier plot at small q -values for the microgel-catalysts in water (25, 45 °C), methanol (25 °C), and 20 mol% methanol (10, 25 °C).

10.7 Osmotic pressure experiments

Osmotic pressure experiments are discussed in Chapter 7. Dextran ($M_w = 150\,000$ g/mol) was mixed with bidistilled, filtered MiliQ water to reach concentrations between 1 and 30 wt%. For dissolution, the vials were rolled overnight. Subsequently, a certain volume of dextran solution was mixed with a certain volume of the microgel bead dispersion. The respective weights were noted to calculate the exact amount of dextran in the final solution. The following empirical relation between the osmotic pressure (in Pa) and the weight fraction of dextran (ω) was applied: $\Pi = 286\omega + 87\omega^2 + 5\omega^3$.^[332] In order to determine the diameter of the microgel beads in the samples of different osmotic pressure, ~ 8.5 µL were transferred to a closed chamber using a spacer of 120 µm in height (Secure Seal imaging spacer). Subsequently, bright field images were captured using a 20x objective of a microscope (Nikon Intensilight C-HGFI) connected to a camera (Blackfly S BFS-U3-16S2M). Finally, the sizes of numerous microgel beads in each surrounding was measured by hand and averaged. In total, five microgel samples with different sizes in water and cross-linker content were investigated (see section 10.3.3). For one sample (MG-5-S), the same experiment was conducted using PEG ($M_w = 8000$ g/mol, 1 – 30 wt%) instead of dextran.

References

- [1] Jenkins, A. D.; Kratochvíl, P.; Stepto, R. F. T.; Suter, U. W., Glossary of basic terms in polymer science (IUPAC Recommendations 1996). *Pure Appl. Chem.* **1996**, *68*, 2287-2311.
- [2] Aguilar, M. R.; San Román, J., Introduction to Smart Polymers and Their Applications. In *Smart Polymers and their Applications (Second Edition)*, Aguilar, M. R.; San Román, J., Eds. Woodhead Publishing: 2019; pp 1-11.
- [3] Pelton, R., Temperature-sensitive aqueous microgels. *Adv. Colloid Interface Sci.* **2000**, *85*, 1-33.
- [4] Pich, A.; Richtering, W., Microgels by Precipitation Polymerization: Synthesis, Characterization, and Functionalization. In *Chemical Design of Responsive Microgels*, Pich, A.; Richtering, W., Eds. Springer Berlin Heidelberg: 2011; Vol. 234, pp 1-37.
- [5] Plamper, F. A.; Richtering, W., Functional Microgels and Microgel Systems. *Acc. Chem. Res.* **2017**, *50*, 131-140.
- [6] Heskins, M.; Guillet, J. E., Solution Properties of Poly(*N*-isopropylacrylamide). *J. Macromol. Sci., Part A: Chem.* **1968**, *2*, 1441-1455.
- [7] Schild, H. G., Poly(*N*-isopropylacrylamide): experiment, theory and application. *Prog. Polym. Sci.* **1992**, *17*, 163-249.
- [8] Plummer, R.; Hill, D. J. T.; Whittaker, A. K., Solution Properties of Star and Linear Poly(*N*-isopropylacrylamide). *Macromolecules* **2006**, *39*, 8379-8388.
- [9] Yu, Y.; Lopez de la Cruz, R. A.; Kieviet, B. D.; Gojzewski, H.; Pons, A.; Julius Vancso, G.; de Beer, S., Pick up, move and release of nanoparticles utilizing co-non-solvency of PNIPAM brushes. *Nanoscale* **2017**, *9*, 1670-1675.
- [10] Pelton, R.; Hoare, T., Microgels and Their Synthesis: An Introduction. In *Microgel Suspensions*, Wiley-VCH Verlag GmbH & Co. KGaA: 2011; pp 1-32.
- [11] Seiffert, S.; Kummerlöwe, C.; Vennemann, N., *Lechner, Gehrke, Nordmeier - Makromolekulare Chemie*. Springer-Verlag GmbH: Berlin, Heidelberg, 2020; p 869.
- [12] Nayak, A. K.; Das, B., Introduction to polymeric gels. In *Polymeric Gels*, Pal, K.; Banerjee, I., Eds. Woodhead Publishing: 2018; pp 3-27.
- [13] Braun, D.; Cherdron, H.; Rehahn, M.; Ritter, H.; Voit, B., *Polymer Synthesis: Theory and Practice: Fundamentals, Methods, Experiments*. 4th ed.; Springer-Verlag Berlin Heidelberg: 2006.
- [14] Alemán, J. V.; Chadwick, A. V.; He, J.; Hess, M.; Horie, K.; Jones, R. G.; Kratochvíl, P.; Meisel, I.; Mita, I.; Moad, G.; Penczek, S.; Stepto, R. F. T., Definitions of terms relating to the structure and processing of sols, gels, networks, and inorganic-organic hybrid materials (IUPAC Recommendations 2007). *Pure Appl. Chem.* **2007**, *79*, 1801-1829.

- [15] Karg, M.; Pich, A.; Hellweg, T.; Hoare, T.; Lyon, L. A.; Crassous, J. J.; Suzuki, D.; Gumerov, R. A.; Schneider, S.; Potemkin, I. I.; Richtering, W., Nanogels and Microgels: From Model Colloids to Applications, Recent Developments, and Future Trends. *Langmuir* **2019**, *35*, 6231-6255.
- [16] Hofzumahaus, C.; Hebbeker, P.; Schneider, S., Monte Carlo simulations of weak polyelectrolyte microgels: pH-dependence of conformation and ionization. *Soft Matter* **2018**, *14*, 4087-4100.
- [17] Hoare, T.; Pelton, R., Highly pH and Temperature Responsive Microgels Functionalized with Vinylacetic Acid. *Macromolecules* **2004**, *37*, 2544-2550.
- [18] Kojima, H.; Tanaka, F.; Scherzinger, C.; Richtering, W., Temperature dependent phase behavior of PNIPAM microgels in mixed water/methanol solvents. *J. Polym. Sci., Part B: Polym. Phys.* **2013**, *51*, 1100-1111.
- [19] Scherzinger, C.; Schwarz, A.; Bardow, A.; Leonhard, K.; Richtering, W., Cononsolvency of poly-*N*-isopropyl acrylamide (PNIPAM): Microgels versus linear chains and macrogels. *Curr. Opin. Colloid Interface Sci.* **2014**, *19*, 84-94.
- [20] Zhu, P. W.; Napper, D. H., Light scattering studies of poly(*N*-isopropylacrylamide) microgel particles in mixed water-acetic acid solvents. *Macromol. Chem. Phys.* **1999**, *200*, 1950-1955.
- [21] Crowther, H. M.; Vincent, B., Swelling behavior of poly-*N*-isopropylacrylamide microgel particles in alcoholic solutions. *Colloid. Polym. Sci.* **1998**, *276*, 46-51.
- [22] Keidel, R.; Ghavami, A.; Lugo, D. M.; Lotze, G.; Virtanen, O.; Beumers, P.; Pedersen, J. S.; Bardow, A.; Winkler, R. G.; Richtering, W., Time-resolved structural evolution during the collapse of responsive hydrogels: The microgel-to-particle transition. *Sci. Adv.* **2018**, *4*, eaao7086.
- [23] Daly, E.; Saunders, B. R., A Study of the Effect of Electrolyte on the Swelling and Stability of Poly(*N*-isopropylacrylamide) Microgel Dispersions. *Langmuir* **2000**, *16*, 5546-5552.
- [24] Wrede, O.; Reimann, Y.; Lülldorf, S.; Emmrich, D.; Schneider, K.; Schmid, A. J.; Zauser, D.; Hannappel, Y.; Beyer, A.; Schweins, R.; Gölzhäuser, A.; Hellweg, T.; Sottmann, T., Volume phase transition kinetics of smart *N*-*n*-propylacrylamide microgels studied by time-resolved pressure jump small angle neutron scattering. *Sci. Rep.* **2018**, *8*, 13781.
- [25] Lietor-Santos, J.-J.; Sierra-Martin, B.; Vavrin, R.; Hu, Z.; Gasser, U.; Fernandez-Nieves, A., Deswelling Microgel Particles Using Hydrostatic Pressure. *Macromolecules* **2009**, *42*, 6225-6230.
- [26] Grobelny, S.; Hofmann, C. H.; Erbkamp, M.; Plamper, F. A.; Richtering, W.; Winter, R., Conformational changes upon high pressure induced hydration of poly(*N*-isopropylacrylamide) microgels. *Soft Matter* **2013**, *9*, 5862-5866.
- [27] Zhang, H.; Koens, L.; Lauga, E.; Mourran, A.; Möller, M., A Light-Driven Microgel Rotor. *Small* **2019**, *15*, 1903379.
- [28] Garcia, A.; Marquez, M.; Cai, T.; Rosario, R.; Hu, Z.; Gust, D.; Hayes, M.; Vail, S. A.; Park, C.-D., Photo-, Thermally, and pH-Responsive Microgels. *Langmuir* **2007**, *23*, 224-229.

- [29] Gorelikov, I.; Field, L. M.; Kumacheva, E., Hybrid Microgels Photoresponsive in the Near-Infrared Spectral Range. *J. Am. Chem. Soc.* **2004**, *126*, 15938-15939.
- [30] Backes, S.; Witt, M. U.; Roeben, E.; Kuhrt, L.; Aleed, S.; Schmidt, A. M.; von Klitzing, R., Loading of PNIPAM Based Microgels with CoFe₂O₄ Nanoparticles and Their Magnetic Response in Bulk and at Surfaces. *J. Phys. Chem. B* **2015**, *119*, 12129-12137.
- [31] Bhattacharya, S.; Eckert, F.; Boyko, V.; Pich, A., Temperature-, pH-, and Magnetic-Field-Sensitive Hybrid Microgels. *Small* **2007**, *3*, 650-657.
- [32] Mergel, O.; Wünnemann, P.; Simon, U.; Böker, A.; Plamper, F. A., Microgel Size Modulation by Electrochemical Switching. *Chem. Mater.* **2015**, *27*, 7306-7312.
- [33] Dubbert, J.; Honold, T.; Pedersen, J. S.; Radulescu, A.; Drechsler, M.; Karg, M.; Richtering, W., How Hollow Are Thermoresponsive Hollow Nanogels? *Macromolecules* **2014**, *47*, 8700-8708.
- [34] Wypysek, S. K.; Scotti, A.; Alziyadi, M. O.; Potemkin, I. I.; Denton, A. R.; Richtering, W., Tailoring the Cavity of Hollow Polyelectrolyte Microgels. *Macromol. Rapid Commun.* **2020**, *41*, 1900422.
- [35] Seiffert, S.; Thiele, J.; Abate, A. R.; Weitz, D. A., Smart Microgel Capsules from Macromolecular Precursors. *J. Am. Chem. Soc.* **2010**, *132*, 6606-6609.
- [36] Dubbert, J.; Nothdurft, K.; Karg, M.; Richtering, W., Core-Shell-Shell and Hollow Double-Shell Microgels with Advanced Temperature Responsiveness. *Macromol. Rapid Commun.* **2015**, *36*, 159-164.
- [37] Nickel, A. C.; Scotti, A.; Houston, J. E.; Ito, T.; Crassous, J.; Pedersen, J. S.; Richtering, W., Anisotropic Hollow Microgels That Can Adapt Their Size, Shape, and Softness. *Nano Lett.* **2019**, *19*, 8161-8170.
- [38] Krüger, A. J. D.; Bakirman, O.; Guerzoni, L. P. B.; Jans, A.; Gehlen, D. B.; Rommel, D.; Haraszti, T.; Kuehne, A. J. C.; De Laporte, L., Compartmentalized Jet Polymerization as a High-Resolution Process to Continuously Produce Anisometric Microgel Rods with Adjustable Size and Stiffness. *Adv. Mater.* **2019**, *31*, 1903668.
- [39] Xu, S.; Nie, Z.; Seo, M.; Lewis, P.; Kumacheva, E.; Stone, H. A.; Garstecki, P.; Weibel, D. B.; Gitlin, I.; Whitesides, G. M., Generation of Monodisperse Particles by Using Microfluidics: Control over Size, Shape, and Composition. *Angew. Chem. Int. Ed.* **2005**, *44*, 724-728.
- [40] Wolff, H. J. M.; Linkhorst, J.; Göttlich, T.; Savinsky, J.; Krüger, A. J. D.; de Laporte, L.; Wessling, M., Soft temperature-responsive microgels of complex shape in stop-flow lithography. *Lab Chip* **2020**, *20*, 285-295.
- [41] Saunders, B. R.; Laajam, N.; Daly, E.; Teow, S.; Hu, X.; Stepto, R., Microgels: From responsive polymer colloids to biomaterials. *Adv. Colloid Interface Sci.* **2009**, *147-148*, 251-262.
- [42] Pelton, R. H.; Chibante, P., Preparation of aqueous latices with *N*-isopropylacrylamide. *Colloids and Surfaces* **1986**, *20*, 247-256.
- [43] Landfester, K.; Musyanovych, A., Hydrogels in Miniemulsions. In *Chemical Design of Responsive Microgels*, Pich, A.; Richtering, W., Eds. Springer Berlin Heidelberg: Berlin, Heidelberg, 2011; pp 39-63.

- [44] Tobita, H.; Kumagai, M.; Aoyagi, N., Microgel formation in emulsion polymerization. *Polymer* **2000**, *41*, 481-487.
- [45] Kim, J.-W.; Chu, L.-Y., New Functional Microgels from Microfluidics. In *Microgel Suspensions*, Wiley-VCH Verlag GmbH & Co. KGaA: 2011; pp 53-70.
- [46] Tumarkin, E.; Kumacheva, E., Microfluidic generation of microgels from synthetic and natural polymers. *Chem. Soc. Rev.* **2009**, *38*, 2161-2168.
- [47] Utada, A. S.; Lorenceau, E.; Link, D. R.; Kaplan, P. D.; Stone, H. A.; Weitz, D. A., Monodisperse Double Emulsions Generated from a Microcapillary Device. *Science* **2005**, *308*, 537-541.
- [48] Sugiura, S.; Nakajima, M.; Tong, J.; Nabetani, H.; Seki, M., Preparation of Monodispersed Solid Lipid Microspheres Using a Microchannel Emulsification Technique. *J. Colloid Interface Sci.* **2000**, *227*, 95-103.
- [49] Dendukuri, D.; Tsoi, K.; Hatton, T. A.; Doyle, P. S., Controlled Synthesis of Nonspherical Microparticles Using Microfluidics. *Langmuir* **2005**, *21*, 2113-2116.
- [50] Nie, Z.; Xu, S.; Seo, M.; Lewis, P. C.; Kumacheva, E., Polymer Particles with Various Shapes and Morphologies Produced in Continuous Microfluidic Reactors. *J. Am. Chem. Soc.* **2005**, *127*, 8058-8063.
- [51] Karg, M.; Prévost, S.; Brandt, A.; Wallacher, D.; von Klitzing, R.; Hellweg, T., Poly-NIPAM Microgels with Different Cross-Linker Densities. In *Intelligent Hydrogels*, Sadowski, G.; Richtering, W., Eds. Springer International Publishing: Cham, 2013; pp 63-76.
- [52] McPhee, W.; Tam, K. C.; Pelton, R., Poly(*N*-isopropylacrylamide) Latices Prepared with Sodium Dodecyl Sulfate. *J. Colloid Interface Sci.* **1993**, *156*, 24-30.
- [53] Varga, I.; Gilányi, T.; Mészáros, R.; Filipcsei, G.; Zrínyi, M., Effect of Cross-Link Density on the Internal Structure of Poly(*N*-isopropylacrylamide) Microgels. *J. Phys. Chem. B* **2001**, *105*, 9071-9076.
- [54] Brugnoli, M.; Nickel, A. C.; Kröger, L. C.; Scotti, A.; Pich, A.; Leonhard, K.; Richtering, W., Synthesis and structure of deuterated ultra-low cross-linked poly(*N*-isopropylacrylamide) microgels. *Polym. Chem.* **2019**, *10*, 2397-2405.
- [55] Gao, J.; Frisken, B. J., Cross-Linker-Free *N*-Isopropylacrylamide Gel Nanospheres. *Langmuir* **2003**, *19*, 5212-5216.
- [56] Bachman, H.; Brown, A. C.; Clarke, K. C.; Dhada, K. S.; Douglas, A.; Hansen, C. E.; Herman, E.; Hyatt, J. S.; Kodlekere, P.; Meng, Z.; Saxena, S.; Spears Jr, M. W.; Welsch, N.; Lyon, L. A., Ultrasoft, highly deformable microgels. *Soft Matter* **2015**, *11*, 2018-2028.
- [57] Wu, C.; Zhou, S.; Au-yeung, S. C. F.; Jiang, S., Volume phase transition of spherical microgel particles. *Die Angewandte Makromolekulare Chemie* **1996**, *240*, 123-136.
- [58] Hertle, Y.; Zeiser, M.; Hasenöhl, C.; Busch, P.; Hellweg, T., Responsive P(NIPAM-co-NtBAM) microgels: Flory–Rehner description of the swelling behaviour. *Colloid. Polym. Sci.* **2010**, *288*, 1047-1059.
- [59] Stuart, M. A. C.; Huck, W. T. S.; Genzer, J.; Müller, M.; Ober, C.; Stamm, M.; Sukhorukov, G. B.; Szleifer, I.; Tsukruk, V. V.; Urban, M.; Winnik, F.; Zauscher, S.;

- Luzinov, I.; Minko, S., Emerging applications of stimuli-responsive polymer materials. *Nat. Mater.* **2010**, *9*, 101-113.
- [60] Agrawal, G.; Agrawal, R., Functional Microgels: Recent Advances in Their Biomedical Applications. *Small* **2018**, *14*, 1801724.
- [61] Daly, A. C.; Riley, L.; Segura, T.; Burdick, J. A., Hydrogel microparticles for biomedical applications. *Nature Reviews Materials* **2020**, *5*, 20-43.
- [62] Ward, M. A.; Georgiou, T. K., Thermoresponsive Polymers for Biomedical Applications. *Polymers* **2011**, *3*, 1215-1242.
- [63] Mura, S.; Nicolas, J.; Couvreur, P., Stimuli-responsive nanocarriers for drug delivery. *Nat. Mater.* **2013**, *12*, 991-1003.
- [64] Guerzoni, L. P. B.; Bohl, J.; Jans, A.; Rose, J. C.; Koehler, J.; Kuehne, A. J. C.; De Laporte, L., Microfluidic fabrication of polyethylene glycol microgel capsules with tailored properties for the delivery of biomolecules. *Biomater. Sci.* **2017**, *5*, 1549-1557.
- [65] Al-Tikriti, Y.; Hansson, P., Drug-Eluting Polyacrylate Microgels: Loading and Release of Amitriptyline. *J. Phys. Chem. B* **2020**, *124*, 2289-2304.
- [66] Hoare, T.; Pelton, R., Impact of Microgel Morphology on Functionalized Microgel–Drug Interactions. *Langmuir* **2008**, *24*, 1005-1012.
- [67] Schmid, A. J.; Dubbert, J.; Rudov, A. A.; Pedersen, J. S.; Lindner, P.; Karg, M.; Potemkin, I. I.; Richtering, W., Multi-Shell Hollow Nanogels with Responsive Shell Permeability. *Sci. Rep.* **2016**, *6*, 22736.
- [68] Chen, J.; Wu, M.; Veroniaina, H.; Mukhopadhyay, S.; Li, J.; Wu, Z.; Wu, Z.; Qi, X., Poly(*N*-isopropylacrylamide) derived nanogels demonstrated thermosensitive self-assembly and GSH-triggered drug release for efficient tumor Therapy. *Polym. Chem.* **2019**, *10*, 4031-4041.
- [69] Peng, H.; Huang, X.; Oppermann, A.; Melle, A.; Weger, L.; Karperien, M.; Wöll, D.; Pich, A., A facile approach for thermal and reduction dual-responsive prodrug nanogels for intracellular doxorubicin delivery. *J. Mater. Chem. B* **2016**, *4*, 7572-7583.
- [70] Wiese, S.; Spiess, A. C.; Richtering, W., Microgel-Stabilized Smart Emulsions for Biocatalysis. *Angew. Chem. Int. Ed.* **2013**, *52*, 576-579.
- [71] Wu, S.; Dzubiella, J.; Kaiser, J.; Drechsler, M.; Guo, X.; Ballauff, M.; Lu, Y., Thermosensitive Au-PNIPA Yolk–Shell Nanoparticles with Tunable Selectivity for Catalysis. *Angew. Chem. Int. Ed.* **2012**, *51*, 2229-2233.
- [72] Kleinschmidt, D.; Nothdurft, K.; Anakhov, M. V.; Meyer, A. A.; Mork, M.; Gumerov, R. A.; Potemkin, I. I.; Richtering, W.; Pich, A., Microgel organocatalysts: modulation of reaction rates at liquid–liquid interfaces. *Mater. Adv.* **2020**, *1*, 2983-2993.
- [73] Welsch, N.; Ballauff, M.; Lu, Y., Microgels as Nanoreactors: Applications in Catalysis. In *Chemical Design of Responsive Microgels*, Pich, A.; Richtering, W., Eds. Springer Berlin Heidelberg: Berlin, Heidelberg, 2011; pp 129-163.
- [74] Ferguson, C. T. J.; Huber, N.; Landfester, K.; Zhang, K. A. I., Dual-Responsive Photocatalytic Polymer Nanogels. *Angew. Chem. Int. Ed.* **2019**, *58*, 10567-10571.

- [75] Kleinschmidt, D.; Fernandes, M. S.; Mork, M.; Meyer, A. A.; Krischel, J.; Anakhov, M. V.; Gumerov, R. A.; Potemkin, I. I.; Rueping, M.; Pich, A., Enhanced catalyst performance through compartmentalization exemplified by colloidal L-proline modified microgel catalysts. *J. Colloid Interface Sci.* **2020**, *559*, 76-87.
- [76] Borrmann, R.; Palchyk, V.; Pich, A.; Rueping, M., Reversible Switching and Recycling of Adaptable Organic Microgel Catalysts (Microgelzymes) for Asymmetric Organocatalytic Desymmetrization. *ACS Catal.* **2018**, *8*, 7991-7996.
- [77] Terashima, T.; Ouchi, M.; Ando, T.; Sawamoto, M., Oxidation of sec-alcohols with Ru(II)-bearing microgel star polymer catalysts via hydrogen transfer reaction: Unique microgel-core catalysis. *J. Polym. Sci., Part A: Polym. Chem.* **2011**, *49*, 1061-1069.
- [78] Wang, J.; Liu, Y.; Li, X.; Luo, Y.; Zheng, L.; Hu, J.; Chen, G.; Chen, H., Ultralow Crosslinked Microgel Brings Ultrahigh Catalytic Efficiency. *Macromol. Rapid Commun.* **2020**, *41*, 2000135.
- [79] Wiese, S.; Tsvetkova, Y.; Daleiden, N. J. E.; Spieß, A. C.; Richtering, W., Microgel stabilized emulsions: Breaking on demand. *Colloids and Surfaces A: Physicochemical and Engineering Aspects* **2016**, *495*, 193-199.
- [80] Destribats, M.; Lapeyre, V.; Wolfs, M.; Sellier, E.; Leal-Calderon, F.; Ravaine, V.; Schmitt, V., Soft microgels as Pickering emulsion stabilisers: role of particle deformability. *Soft Matter* **2011**, *7*, 7689-7698.
- [81] Gao, Y.; Li, X.; Serpe, M. J., Stimuli-responsive microgel-based etalons for optical sensing. *RSC Adv.* **2015**, *5*, 44074-44087.
- [82] Yetisen, A. K.; Butt, H.; Volpatti, L. R.; Pavlichenko, I.; Humar, M.; Kwok, S. J. J.; Koo, H.; Kim, K. S.; Naydenova, I.; Khademhosseini, A.; Hahn, S. K.; Yun, S. H., Photonic hydrogel sensors. *Biotechnol. Adv.* **2016**, *34*, 250-271.
- [83] Aliberti, A.; Ricciardi, A.; Giaquinto, M.; Micco, A.; Bobeico, E.; La Ferrara, V.; Ruvo, M.; Cutolo, A.; Cusano, A., Microgel assisted Lab-on-Fiber Optrode. *Sci. Rep.* **2017**, *7*, 14459.
- [84] Sigolaeva, L. V.; Gladyr, S. Y.; Mergel, O.; Gelissen, A. P. H.; Noyong, M.; Simon, U.; Pergushov, D. V.; Kurochkin, I. N.; Plamper, F. A.; Richtering, W., Easy-Preparable Butyrylcholinesterase/Microgel Construct for Facilitated Organophosphate Biosensing. *Anal. Chem.* **2017**, *89*, 6091-6098.
- [85] Mourran, A.; Zhang, H.; Vinokur, R.; Möller, M., Soft Microrobots Employing Nonequilibrium Actuation via Plasmonic Heating. *Adv. Mater.* **2017**, *29*, 1604825.
- [86] Lohaus, T.; de Wit, P.; Kather, M.; Menne, D.; Benes, N. E.; Pich, A.; Wessling, M., Tunable permeability and selectivity: Heatable inorganic porous hollow fiber membrane with a thermo-responsive microgel coating. *J. Membr. Sci.* **2017**, *539*, 451-457.
- [87] Winnik, F. M.; Ringsdorf, H.; Venzmer, J., Methanol-water as a co-nonsolvent system for poly(*N*-isopropylacrylamide). *Macromolecules* **1990**, *23*, 2415-2416.
- [88] Schild, H. G.; Muthukumar, M.; Tirrell, D. A., Cononsolvency in mixed aqueous solutions of poly(*N*-isopropylacrylamide). *Macromolecules* **1991**, *24*, 948-952.

- [89] H  ther, A.; Xu, X.; Maurer, G., Swelling of *N*-isopropyl acrylamide hydrogels in water and aqueous solutions of ethanol and acetone. *Fluid Phase Equilib.* **2004**, *219*, 231-244.
- [90] Mukae, K.; Sakurai, M.; Sawamura, S.; Makino, K.; Kim, S. W.; Ueda, I.; Shirahama, K., Swelling of poly(*N*-isopropylacrylamide) gels in water-alcohol (C1-C4) mixed solvents. *J. Phys. Chem.* **1993**, *97*, 737-741.
- [91] Yamauchi, H.; Maeda, Y., LCST and UCST Behavior of Poly(*N*-isopropylacrylamide) in DMSO/Water Mixed Solvents Studied by IR and Micro-Raman Spectroscopy. *J. Phys. Chem. B* **2007**, *111*, 12964-12968.
- [92] Winnik, F. M.; Ottaviani, M. F.; Bossmann, S. H.; Pan, W.; Garcia-Garibay, M.; Turro, N. J., Cononsolvency of poly(*N*-isopropylacrylamide): a look at spin-labeled polymers in mixtures of water and tetrahydrofuran. *Macromolecules* **1993**, *26*, 4577-4585.
- [93] Dalkas, G.; Pagonis, K.; Bokias, G., Control of the lower critical solution temperature—type cononsolvency properties of poly(*N*-isopropylacrylamide) in water—dioxane mixtures through copolymerisation with acrylamide. *Polymer* **2006**, *47*, 243-248.
- [94] Zhu, P.-w.; Chen, L., Effects of cosolvent partitioning on conformational transitions and chain flexibility of thermoresponsive microgels. *Phys. Rev. E* **2019**, *99*, 022501.
- [95] Thivaos, I.; Bokias, G., Adsorption of nile red by poly(*N*-isopropylacrylamide) gels in binary water/tetrahydrofuran mixtures. *J. Appl. Polym. Sci.* **2010**, *116*, 1509-1514.
- [96] Mahdavi, H.; Mahdi Sadeghzadeh, B. O.; Qazvini, N. T., Phase behavior study of poly(*N*-tertbutylacrylamide-*co*-acrylamide) in the mixture of water–methanol: The role of polymer–nonsolvent second-order interactions. *J. Polym. Sci., Part B: Polym. Phys.* **2009**, *47*, 455-462.
- [97] Orakdogan, N.; Okay, O., Reentrant conformation transition in poly(*N,N*-dimethylacrylamide) hydrogels in water–organic solvent mixtures. *Polymer* **2006**, *47*, 561-568.
- [98] Wolf, B. A.; Willms, M. M., Measured and calculated solubility of polymers in mixed solvents: Co-nonsolvency. *Die Makromolekulare Chemie* **1978**, *179*, 2265-2277.
- [99] Guettari, M.; Gomati, R.; Gharbi, A., Effect of Temperature on Cononsolvency of Polyvinylpyrrolidone in Water/Methanol Mixture. *J. Macromol. Sci., Part B: Phys.* **2010**, *49*, 552-562.
- [100] Takahashi, N.; Kanaya, T.; Nishida, K.; Kaji, K., Effects of cononsolvency on gelation of poly(vinyl alcohol) in mixed solvents of dimethyl sulfoxide and water. *Polymer* **2003**, *44*, 4075-4078.
- [101] Maeda, Y.; Nakamura, T.; Ikeda, I., Change in Solvation of Poly(*N,N*-diethylacrylamide) during Phase Transition in Aqueous Solutions As Observed by IR Spectroscopy. *Macromolecules* **2002**, *35*, 10172-10177.
- [102] Scherzinger, C.; Balaceanu, A.; Hofmann, C. H.; Schwarz, A.; Leonhard, K.; Pich, A.; Richtering, W., Cononsolvency of mono- and di-alkyl *N*-substituted poly(acrylamide)s and poly(vinyl caprolactam). *Polymer* **2015**, *62*, 50-59.

- [103] Maeda, Y.; Yamabe, M., A unique phase behavior of random copolymer of *N*-isopropylacrylamide and *N,N*-diethylacrylamide in water. *Polymer* **2009**, *50*, 519-523.
- [104] Scherzinger, C.; Lindner, P.; Keerl, M.; Richtering, W., Cononsolvency of Poly(*N,N*-diethylacrylamide) (PDEAAM) and Poly(*N*-isopropylacrylamide) (PNIPAM) Based Microgels in Water/Methanol Mixtures: Copolymer vs Core–Shell Microgel. *Macromolecules* **2010**, *43*, 6829-6833.
- [105] Tanaka, F.; Koga, T.; Winnik, F. M., Temperature-Responsive Polymers in Mixed Solvents: Competitive Hydrogen Bonds Cause Cononsolvency. *Phys. Rev. Lett.* **2008**, *101*, 028302.
- [106] Dudowicz, J.; Freed, K. F.; Douglas, J. F., Relation Between Solvent Quality and Phase Behavior of Ternary Mixtures of Polymers and Two Solvents that Exhibit Cononsolvency. *J. Phys. Chem. B* **2016**, *120*, 5753-5758.
- [107] Tanaka, F.; Koga, T.; Kojima, H.; Xue, N.; Winnik, F. M., Preferential Adsorption and Co-nonsolvency of Thermoresponsive Polymers in Mixed Solvents of Water/Methanol. *Macromolecules* **2011**, *44*, 2978-2989.
- [108] Pérez-Ramírez, H. A.; Haro-Pérez, C.; Vázquez-Contreras, E.; Klapp, J.; Bautista-Carbajal, G.; Odriozola, G., P-NIPAM in water–acetone mixtures: experiments and simulations. *Phys. Chem. Chem. Phys.* **2019**, *21*, 5106-5116.
- [109] Bharadwaj, S.; van der Vegt, N. F. A., Does Preferential Adsorption Drive Cononsolvency? *Macromolecules* **2019**, *52*, 4131-4138.
- [110] Wang, N.; Ru, G.; Wang, L.; Feng, J., ¹H MAS NMR Studies of the Phase Separation of Poly(*N*-isopropylacrylamide) Gel in Binary Solvents. *Langmuir* **2009**, *25*, 5898-5902.
- [111] Mukherji, D.; Marques, C. M.; Kremer, K., Polymer collapse in miscible good solvents is a generic phenomenon driven by preferential adsorption. *Nat. Commun.* **2014**, *5*, 4882.
- [112] Liu, B.; Wang, J.; Ru, G.; Liu, C.; Feng, J., Phase Transition and Preferential Alcohol Adsorption of Poly(*N,N*-diethylacrylamide) Gel in Water/Alcohol Mixtures. *Macromolecules* **2015**, *48*, 1126-1133.
- [113] Rodríguez-Ropero, F.; Hajari, T.; van der Vegt, N. F. A., Mechanism of Polymer Collapse in Miscible Good Solvents. *J. Phys. Chem. B* **2015**, *119*, 15780-15788.
- [114] Michailova, V. I.; Momekova, D. B.; Velichkova, H. A.; Ivanov, E. H.; Kotsilkova, R. K.; Karashanova, D. B.; Mileva, E. D.; Dimitrov, I. V.; Rangelov, S. M., Self-Assembly of a Thermally Responsive Double-Hydrophilic Copolymer in Ethanol–Water Mixtures: The Effect of Preferential Adsorption and Co-Nonsolvency. *J. Phys. Chem. B* **2018**, *122*, 6072-6078.
- [115] Winnik, F. M.; Ottaviani, M. F.; Bossmann, S. H.; Garcia-Garibay, M.; Turro, N. J., Consolvency of poly(*N*-isopropylacrylamide) in mixed water-methanol solutions: a look at spin-labeled polymers. *Macromolecules* **1992**, *25*, 6007-6017.
- [116] Pica, A.; Graziano, G., An alternative explanation of the cononsolvency of poly(*N*-isopropylacrylamide) in water-methanol solutions. *Phys. Chem. Chem. Phys.* **2016**, *18*, 25601-25608.

- [117] Dalgicdir, C.; Rodríguez-Ropero, F.; van der Vegt, N. F. A., Computational Calorimetry of PNIPAM Cononsolvency in Water/Methanol Mixtures. *J. Phys. Chem. B* **2017**, *121*, 7741-7748.
- [118] Zuo, T.; Ma, C.; Jiao, G.; Han, Z.; Xiao, S.; Liang, H.; Hong, L.; Bowron, D.; Soper, A.; Han, C. C.; Cheng, H., Water/Cosolvent Attraction Induced Phase Separation: A Molecular Picture of Cononsolvency. *Macromolecules* **2019**, *52*, 457-464.
- [119] Zhang, G.; Wu, C., The Water/Methanol Complexation Induced Reentrant Coil-to-Globule-to-Coil Transition of Individual Homopolymer Chains in Extremely Dilute Solution. *J. Am. Chem. Soc.* **2001**, *123*, 1376-1380.
- [120] Hofmann, C. H.; Plamper, F. A.; Scherzinger, C.; Hietala, S.; Richtering, W., Cononsolvency Revisited: Solvent Entrapment by *N*-Isopropylacrylamide and *N,N*-Diethylacrylamide Microgels in Different Water/Methanol Mixtures. *Macromolecules* **2013**, *46*, 523-532.
- [121] Walter, J.; Sehart, J.; Vrabec, J.; Hasse, H., Molecular Dynamics and Experimental Study of Conformation Change of Poly(*N*-isopropylacrylamide) Hydrogels in Mixtures of Water and Methanol. *J. Phys. Chem. B* **2012**, *116*, 5251-5259.
- [122] Mukherji, D.; Wagner, M.; Watson, M. D.; Winzen, S.; de Oliveira, T. E.; Marques, C. M.; Kremer, K., Relating side chain organization of PNIPAm with its conformation in aqueous methanol. *Soft Matter* **2016**, *12*, 7995-8003.
- [123] Bischofberger, I.; Calzolari, D. C. E.; De Los Rios, P.; Jelezarov, I.; Trappe, V., Hydrophobic hydration of poly-*N*-isopropyl acrylamide: a matter of the mean energetic state of water. *Sci. Rep.* **2014**, *4*, 4377.
- [124] Hofmann, C. H.; Grobelny, S.; Erlkamp, M.; Winter, R.; Richtering, W., Influence of high-pressure on cononsolvency of poly(*N*-isopropylacrylamide) nanogels in water/methanol mixtures. *Polymer* **2014**, *55*, 2000-2007.
- [125] Backes, S.; Krause, P.; Tabaka, W.; Witt, M. U.; von Klitzing, R., Combined Cononsolvency and Temperature Effects on Adsorbed PNIPAM Microgels. *Langmuir* **2017**, *33*, 14269-14277.
- [126] Niebuur, B.-J.; Ko, C.-H.; Zhang, X.; Claude, K.-L.; Chiappisi, L.; Schulte, A.; Papadakis, C. M., Pressure Dependence of the Cononsolvency Effect in Aqueous Poly(*N*-isopropylacrylamide) Solutions: A SANS Study. *Macromolecules* **2020**, *53*, 3946-3955.
- [127] Pica, A.; Graziano, G., Hydrostatic pressure effect on PNIPAM cononsolvency in water-methanol solutions. *Biophys. Chem.* **2017**, *231*, 34-38.
- [128] Nothdurft, K.; Müller, D. H.; Brands, T.; Bardow, A.; Richtering, W., Enrichment of methanol inside pNIPAM gels in the cononsolvency-induced collapse. *Phys. Chem. Chem. Phys.* **2019**, *21*, 22811-22818.
- [129] Maeda, Y.; Yamamoto, H.; Ikeda, I., Phase Separation of Aqueous Solutions of Poly(*N*-isopropylacrylamide) Investigated by Confocal Raman Microscopy. *Macromolecules* **2003**, *36*, 5055-5057.
- [130] Yang, M.; Zhao, K., Cononsolvency of poly(*N*-isopropylacrylamide) in methanol aqueous solution—insight by dielectric spectroscopy. *J. Polym. Sci., Part B: Polym. Phys.* **2017**, *55*, 1227-1234.

- [131] Ottaviani, M. F.; Winnik, F. M.; Bossmann, S. H.; Turro, N. J., Phase Separation of Poly(*N*-isopropylacrylamide) in Mixtures of Water and Methanol: A Spectroscopic Study of the Phase-Transition Process with a Polymer Tagged with a Fluorescent Dye and a Spin Label. *Helv. Chim. Acta* **2001**, *84*, 2476-2492.
- [132] Geiger, C.; Reitenbach, J.; Kreuzer, L. P.; Widmann, T.; Wang, P.; Cubitt, R.; Henschel, C.; Laschewsky, A.; Papadakis, C. M.; Müller-Buschbaum, P., PMMA-*b*-PNIPAM Thin Films Display Cononsolvency-Driven Response in Mixed Water/Methanol Vapors. *Macromolecules* **2021**, *54*, 3517-3530.
- [133] Kreuzer, L. P.; Lindenmeir, C.; Geiger, C.; Widmann, T.; Hildebrand, V.; Laschewsky, A.; Papadakis, C. M.; Müller-Buschbaum, P., Poly(sulfobetaine) versus Poly(*N*-isopropylmethacrylamide): Co-Nonsolvency-Type Behavior of Thin Films in a Water/Methanol Atmosphere. *Macromolecules* **2021**, *54*, 1548-1556.
- [134] Xu, J.; Zhu, Z.; Luo, S.; Wu, C.; Liu, S., First Observation of Two-Stage Collapsing Kinetics of a Single Synthetic Polymer Chain. *Phys. Rev. Lett.* **2006**, *96*, 027802.
- [135] Whitesides, G. M., The origins and the future of microfluidics. *Nature* **2006**, *442*, 368-373.
- [136] Shang, L.; Cheng, Y.; Zhao, Y., Emerging Droplet Microfluidics. *Chem. Rev.* **2017**, *117*, 7964-8040.
- [137] Mark, D.; Haeberle, S.; Roth, G.; von Stetten, F.; Zengerle, R., Microfluidic lab-on-a-chip platforms: requirements, characteristics and applications. *Chem. Soc. Rev.* **2010**, *39*, 1153-1182.
- [138] Zhong, Q.; Ding, H.; Gao, B.; He, Z.; Gu, Z., Advances of Microfluidics in Biomedical Engineering. *Advanced Materials Technologies* **2019**, *4*, 1800663.
- [139] Yeo, L. Y.; Chang, H.-C.; Chan, P. P. Y.; Friend, J. R., Microfluidic Devices for Bioapplications. *Small* **2011**, *7*, 12-48.
- [140] Mazutis, L.; Gilbert, J.; Ung, W. L.; Weitz, D. A.; Griffiths, A. D.; Heyman, J. A., Single-cell analysis and sorting using droplet-based microfluidics. *Nature Protocols* **2013**, *8*, 870-891.
- [141] Zheng, B.; Tice, J. D.; Roach, L. S.; Ismagilov, R. F., A Droplet-Based, Composite PDMS/Glass Capillary Microfluidic System for Evaluating Protein Crystallization Conditions by Microbatch and Vapor-Diffusion Methods with On-Chip X-Ray Diffraction. *Angew. Chem. Int. Ed.* **2004**, *43*, 2508-2511.
- [142] Feng, H.; Zheng, T.; Li, M.; Wu, J.; Ji, H.; Zhang, J.; Zhao, W.; Guo, J., Droplet-based microfluidics systems in biomedical applications. *ELECTROPHORESIS* **2019**, *40*, 1580-1590.
- [143] Marre, S.; Jensen, K. F., Synthesis of micro and nanostructures in microfluidic systems. *Chem. Soc. Rev.* **2010**, *39*, 1183-1202.
- [144] Nge, P. N.; Rogers, C. I.; Woolley, A. T., Advances in Microfluidic Materials, Functions, Integration, and Applications. *Chem. Rev.* **2013**, *113*, 2550-2583.
- [145] Stone, H. A.; Stroock, A. D.; Ajdari, A., Engineering Flows in Small Devices: Microfluidics Toward a Lab-on-a-Chip. *Annual Review of Fluid Mechanics* **2004**, *36*, 381-411.

- [146] Fallahi, H.; Zhang, J.; Phan, H.-P.; Nguyen, N.-T., Flexible Microfluidics: Fundamentals, Recent Developments, and Applications. *Micromachines* **2019**, *10*, 830.
- [147] Squires, T. M.; Quake, S. R., Microfluidics: Fluid physics at the nanoliter scale. *Rev. Mod. Phys.* **2005**, *77*, 977-1026.
- [148] Nunes, J. K.; Tsai, S. S. H.; Wan, J.; Stone, H. A., Dripping and jetting in microfluidic multiphase flows applied to particle and fiber synthesis. *J. Phys. D: Appl. Phys.* **2013**, *46*, 114002.
- [149] Shah, R. K.; Kim, J.-W.; Agresti, J. J.; Weitz, D. A.; Chu, L.-Y., Fabrication of monodisperse thermosensitive microgels and gel capsules in microfluidic devices. *Soft Matter* **2008**, *4*, 2303-2309.
- [150] Teh, S.-Y.; Lin, R.; Hung, L.-H.; Lee, A. P., Droplet microfluidics. *Lab Chip* **2008**, *8*, 198-220.
- [151] McDonald, J. C.; Duffy, D. C.; Anderson, J. R.; Chiu, D. T.; Wu, H.; Schueller, O. J. A.; Whitesides, G. M., Fabrication of microfluidic systems in poly(dimethylsiloxane). *ELECTROPHORESIS* **2000**, *21*, 27-40.
- [152] Chu, L.-Y.; Utada, A. S.; Shah, R. K.; Kim, J.-W.; Weitz, D. A., Controllable Monodisperse Multiple Emulsions. *Angew. Chem. Int. Ed.* **2007**, *46*, 8970-8974.
- [153] Abate, A. R.; Weitz, D. A., High-Order Multiple Emulsions Formed in Poly(dimethylsiloxane) Microfluidics. *Small* **2009**, *5*, 2030-2032.
- [154] Zhou, J.; Ellis, A. V.; Voelcker, N. H., Recent developments in PDMS surface modification for microfluidic devices. *ELECTROPHORESIS* **2010**, *31*, 2-16.
- [155] Lee, J. N.; Park, C.; Whitesides, G. M., Solvent Compatibility of Poly(dimethylsiloxane)-Based Microfluidic Devices. *Anal. Chem.* **2003**, *75*, 6544-6554.
- [156] Debon, A. P.; Wootton, R. C. R.; Elvira, K. S., Droplet confinement and leakage: Causes, underlying effects, and amelioration strategies. *Biomicrofluidics* **2015**, *9*, 024119.
- [157] Berdichevsky, Y.; Khandurina, J.; Guttman, A.; Lo, Y. H., UV/ozone modification of poly(dimethylsiloxane) microfluidic channels. *Sensors and Actuators B: Chemical* **2004**, *97*, 402-408.
- [158] Subramanian, B.; Kim, N.; Lee, W.; Spivak, D. A.; Nikitopoulos, D. E.; McCarley, R. L.; Soper, S. A., Surface Modification of Droplet Polymeric Microfluidic Devices for the Stable and Continuous Generation of Aqueous Droplets. *Langmuir* **2011**, *27*, 7949-7957.
- [159] Sui, G.; Wang, J.; Lee, C.-C.; Lu, W.; Lee, S. P.; Leyton, J. V.; Wu, A. M.; Tseng, H.-R., Solution-Phase Surface Modification in Intact Poly(dimethylsiloxane) Microfluidic Channels. *Anal. Chem.* **2006**, *78*, 5543-5551.
- [160] Wang, D.; Goel, V.; Oleschuk, R. D.; Horton, J. H., Surface Modification of Poly(dimethylsiloxane) with a Perfluorinated Alkoxysilane for Selectivity toward Fluorous Tagged Peptides. *Langmuir* **2008**, *24*, 1080-1086.
- [161] Cretich, M.; Sadini, V.; Damin, F.; Di Carlo, G.; Oldani, C.; Chiari, M., Functionalization of poly(dimethylsiloxane) by chemisorption of copolymers: DNA

- microarrays for pathogen detection. *Sensors and Actuators B: Chemical* **2008**, *132*, 258-264.
- [162] Fortin, J. B.; Lu, T. M., A Model for the Chemical Vapor Deposition of Poly(*para*-xylylene) (Parylene) Thin Films. *Chem. Mater.* **2002**, *14*, 1945-1949.
- [163] Hu, S.; Ren, X.; Bachman, M.; Sims, C. E.; Li, G. P.; Allbritton, N., Surface Modification of Poly(dimethylsiloxane) Microfluidic Devices by Ultraviolet Polymer Grafting. *Anal. Chem.* **2002**, *74*, 4117-4123.
- [164] Wu, D.; Zhao, B.; Dai, Z.; Qin, J.; Lin, B., Grafting epoxy-modified hydrophilic polymers onto poly(dimethylsiloxane) microfluidic chip to resist nonspecific protein adsorption. *Lab Chip* **2006**, *6*, 942-947.
- [165] Akamatsu, Y.; Makita, K.; Inaba, H.; Minami, T., Water-repellent coating films on glass prepared from hydrolysis and polycondensation reactions of fluoroalkyltrialkoxysilane. *Thin Solid Films* **2001**, *389*, 138-145.
- [166] Kuehne, A. J. C.; Weitz, D. A., Highly monodisperse conjugated polymer particles synthesized with drop-based microfluidics. *Chem. Commun.* **2011**, *47*, 12379-12381.
- [167] Tan, C. P.; Craighead, H. G., Surface Engineering and Patterning Using Parylene for Biological Applications. *Materials* **2010**, *3*, 1803-1832.
- [168] Kim, J.-W.; Utada, A. S.; Fernández-Nieves, A.; Hu, Z.; Weitz, D. A., Fabrication of Monodisperse Gel Shells and Functional Microgels in Microfluidic Devices. *Angew. Chem.* **2007**, *119*, 1851-1854.
- [169] Di Lorenzo, F.; Seiffert, S., Effect of Droplet Size in Acrylamide-Based Microgel Formation by Microfluidics. *Macromol. React. Eng.* **2016**, *10*, 201-205.
- [170] Seiffert, S.; Weitz, D. A., Controlled fabrication of polymer microgels by polymer-analogous gelation in droplet microfluidics. *Soft Matter* **2010**, *6*, 3184-3190.
- [171] Jeong, W. J.; Kim, J. Y.; Choo, J.; Lee, E. K.; Han, C. S.; Beebe, D. J.; Seong, G. H.; Lee, S. H., Continuous Fabrication of Biocatalyst Immobilized Microparticles Using Photopolymerization and Immiscible Liquids in Microfluidic Systems. *Langmuir* **2005**, *21*, 3738-3741.
- [172] Seiffert, S.; Weitz, D. A., Microfluidic fabrication of smart microgels from macromolecular precursors. *Polymer* **2010**, *51*, 5883-5889.
- [173] Shepherd, R. F.; Conrad, J. C.; Rhodes, S. K.; Link, D. R.; Marquez, M.; Weitz, D. A.; Lewis, J. A., Microfluidic Assembly of Homogeneous and Janus Colloid-Filled Hydrogel Granules. *Langmuir* **2006**, *22*, 8618-8622.
- [174] Prasad, N.; Perumal, J.; Choi, C.-H.; Lee, C.-S.; Kim, D.-P., Generation of Monodisperse Inorganic–Organic Janus Microspheres in a Microfluidic Device. *Adv. Funct. Mater.* **2009**, *19*, 1656-1662.
- [175] Seo, K. D.; Choi, A.; Doh, J.; Kim, D. S., Synthesis of Poly(*N*-isopropylacrylamide) Janus Microhydrogels for Anisotropic Thermo-responsiveness and Organophilic/Hydrophilic Loading Capability. *J Vis Exp.* **2016**, 52813.
- [176] Wan, J.; Bick, A.; Sullivan, M.; Stone, H. A., Controllable Microfluidic Production of Microbubbles in Water-in-Oil Emulsions and the Formation of Porous Microparticles. *Adv. Mater.* **2008**, *20*, 3314-3318.

- [177] Xu, J. H.; Li, S. W.; Wang, Y. J.; Luo, G. S., Controllable gas-liquid phase flow patterns and monodisperse microbubbles in a microfluidic T-junction device. *Appl. Phys. Lett.* **2006**, *88*, 133506.
- [178] Kanai, T.; Ohtani, K.; Fukuyama, M.; Katakura, T.; Hayakawa, M., Preparation of monodisperse PNIPAM gel particles in a microfluidic device fabricated by stereolithography. *Polym. J.* **2011**, *43*, 987-990.
- [179] Habicht, A.; Schmolke, W.; Lange, F.; Saalwächter, K.; Seiffert, S., The Non-effect of Polymer-Network Inhomogeneities in Microgel Volume Phase Transitions: Support for the Mean-Field Perspective. *Macromol. Chem. Phys.* **2014**, *215*, 1116-1133.
- [180] Choi, C.-H.; Jung, J.-H.; Kim, D.-W.; Chung, Y.-M.; Lee, C.-S., Novel one-pot route to monodisperse thermosensitive hollow microcapsules in a microfluidic system. *Lab Chip* **2008**, *8*, 1544-1551.
- [181] Kim, B. I.; Jeong, S. W.; Lee, K. G.; Park, T. J.; Park, J. Y.; Song, J. J.; Lee, S. J.; Lee, C.-S., Synthesis of Bioactive Microcapsules Using a Microfluidic Device. *Sensors (Basel, Switzerland)* **2012**, *12*, 10136-10147.
- [182] Seiffert, S., Impact of Polymer Network Inhomogeneities on the Volume Phase Transition of Thermoresponsive Microgels. *Macromol. Rapid Commun.* **2012**, *33*, 1135-1142.
- [183] Seiffert, S.; Oppermann, W.; Saalwächter, K., Hydrogel formation by photocrosslinking of dimethylmaleimide functionalized polyacrylamide. *Polymer* **2007**, *48*, 5599-5611.
- [184] Sugiura, S.; Oda, T.; Izumida, Y.; Aoyagi, Y.; Satake, M.; Ochiai, A.; Ohkohchi, N.; Nakajima, M., Size control of calcium alginate beads containing living cells using micro-nozzle array. *Biomaterials* **2005**, *26*, 3327-3331.
- [185] Zhang, H.; Tumarkin, E.; Sullan, R. M. A.; Walker, G. C.; Kumacheva, E., Exploring Microfluidic Routes to Microgels of Biological Polymers. *Macromol. Rapid Commun.* **2007**, *28*, 527-538.
- [186] Yeh, C.-H.; Chen, K.-R.; Lin, Y.-C., Developing heatable microfluidic chip to generate gelatin emulsions and microcapsules. *Microfluidics and Nanofluidics* **2013**, *15*, 775-784.
- [187] Huang, S.; Lin, B.; Qin, J., Microfluidic synthesis of tunable poly-(N-isopropylacrylamide) microparticles via PEG adjustment. *ELECTROPHORESIS* **2011**, *32*, 3364-3370.
- [188] Virtanen, O. L. J.; Ala-Mutka, H. M.; Richtering, W., Can the Reaction Mechanism of Radical Solution Polymerization Explain the Microgel Final Particle Volume in Precipitation Polymerization of N-Isopropylacrylamide? *Macromol. Chem. Phys.* **2015**, *216*, 1431-1440.
- [189] Virtanen, O. L. J.; Kather, M.; Meyer-Kirschner, J.; Melle, A.; Radulescu, A.; Viell, J.; Mitsos, A.; Pich, A.; Richtering, W., Direct Monitoring of Microgel Formation during Precipitation Polymerization of N-Isopropylacrylamide Using in Situ SANS. *ACS Omega* **2019**, *4*, 3690-3699.

- [190] Gao, J.; Frisken, B. J., Influence of Reaction Conditions on the Synthesis of Self-Cross-Linked *N*-Isopropylacrylamide Microgels. *Langmuir* **2003**, *19*, 5217-5222.
- [191] Ksiazkiewicz, A. N.; Bering, L.; Jung, F.; Wolter, N. A.; Viell, J.; Mitsos, A.; Pich, A., Closing the 1–5 μm size gap: Temperature-programmed, fed-batch synthesis of μm -sized microgels. *Chem. Eng. J.* **2020**, *379*, 122293.
- [192] Meng, Z.; Smith, M. H.; Lyon, L. A., Temperature-programmed synthesis of micron-sized multi-responsive microgels. *Colloid. Polym. Sci.* **2009**, *287*, 277-285.
- [193] Seiffert, S., Origin of nanostructural inhomogeneity in polymer-network gels. *Polym. Chem.* **2017**, *8*, 4472-4487.
- [194] Shibayama, M., Spatial inhomogeneity and dynamic fluctuations of polymer gels. *Macromol. Chem. Phys.* **1998**, *199*, 1-30.
- [195] Stieger, M.; Richtering, W.; Pedersen, J. S.; Lindner, P., Small-angle neutron scattering study of structural changes in temperature sensitive microgel colloids. *J. Chem. Phys.* **2004**, *120*, 6197-6206.
- [196] Boon, N.; Schurtenberger, P., Swelling of micro-hydrogels with a crosslinker gradient. *Phys. Chem. Chem. Phys.* **2017**, *19*, 23740-23746.
- [197] Siemes, E.; Nevskiy, O.; Sysoiev, D.; Turnhoff, S. K.; Oppermann, A.; Huhn, T.; Richtering, W.; Wöll, D., Nanoscopic Visualization of Cross-Linking Density in Polymer Networks with Diarylethene Photoswitches. *Angew. Chem. Int. Ed.* **2018**, *57*, 12280-12284.
- [198] Kröger, L. C.; Kopp, W. A.; Leonhard, K., Prediction of Chain Propagation Rate Constants of Polymerization Reactions in Aqueous NIPAM/BIS and VCL/BIS Systems. *J. Phys. Chem. B* **2017**, *121*, 2887-2895.
- [199] Wu, X.; Pelton, R. H.; Hamielec, A. E.; Woods, D. R.; McPhee, W., The kinetics of poly(*N*-isopropylacrylamide) microgel latex formation. *Colloid. Polym. Sci.* **1994**, *272*, 467-477.
- [200] Scotti, A.; Bochenek, S.; Brugnoli, M.; Fernandez-Rodriguez, M. A.; Schulte, M. F.; Houston, J. E.; Gelissen, A. P. H.; Potemkin, I. I.; Isa, L.; Richtering, W., Exploring the colloid-to-polymer transition for ultra-low crosslinked microgels from three to two dimensions. *Nat. Commun.* **2019**, *10*, 1418.
- [201] Koizumi, S.; Monkenbusch, M.; Richter, D.; Schwahn, D.; Farago, B., Concentration fluctuations in polymer gel investigated by neutron scattering: Static inhomogeneity in swollen gel. *J. Chem. Phys.* **2004**, *121*, 12721-12731.
- [202] Smith, E.; Dent, G., *Modern Raman Spectroscopy: A Practical Approach*. 2nd ed.; John Wiley & Sons Ltd: Hoboken, New Jersey, 2019.
- [203] Schrader, B., *Infrared and Raman Spectroscopy: Methods and Applications*. VCH Verlagsgesellschaft GmbH: Weinheim, 2008.
- [204] Vandenabeele, P., *Practical Raman Spectroscopy: An Introduction*. John Wiley & Sons, Ltd: 2013.
- [205] Pelletier, M. J., Quantitative Analysis Using Raman Spectrometry. *Appl. Spectrosc.* **2003**, *57*, 20A-42A.

- [206] Li, F.; Men, Z.; Li, S.; Wang, S.; Li, Z.; Sun, C., Study of hydrogen bonding in ethanol-water binary solutions by Raman spectroscopy. *Spectrochim. Acta, Part A* **2018**, *189*, 621-624.
- [207] Dixit, S.; Poon, W. C. K.; Crain, J.; Dixit, S.; Poon, W. C. K., Hydration of methanol in aqueous solutions: a Raman spectroscopic study. *J. Phys.: Condens. Matter* **2000**, *12*, L323.
- [208] Burikov, S.; Dolenko, T.; Patsaeva, S.; Starokurov, Y.; Yuzhakov, V., Raman and IR spectroscopy research on hydrogen bonding in water-ethanol systems. *Mol. Phys.* **2010**, *108*, 2427-2436.
- [209] Hu, Q.; Ouyang, S.; Li, J.; Cao, Z., Raman spectroscopic investigation on pure D₂O/H₂O from 303 to 573 K: interpretation and implications for water structure. *J. Raman Spectrosc.* **2017**, *48*, 610-617.
- [210] Peters, C.; Wolff, L.; Haase, S.; Thien, J.; Brands, T.; Koß, H.-J.; Bardow, A., Multicomponent diffusion coefficients from microfluidics using Raman microspectroscopy. *Lab Chip* **2017**, *17*, 2768-2776.
- [211] Peters, C.; Thien, J.; Wolff, L.; Koß, H.-J.; Bardow, A., Quaternary Diffusion Coefficients in Liquids from Microfluidics and Raman Microspectroscopy: Cyclohexane + Toluene + Acetone + Methanol. *J. Chem. Eng. Data* **2020**, *65*, 1273-1288.
- [212] Amer, M., *Raman Spectroscopy for Soft Matter Applications*. John Wiley & Sons, Inc.: Hoboken, New Jersey, 2009.
- [213] Meyer-Kirschner, J.; Kather, M.; Pich, A.; Engel, D.; Marquardt, W.; Viell, J.; Mitsos, A., In-line Monitoring of Monomer and Polymer Content During Microgel Synthesis Using Precipitation Polymerization via Raman Spectroscopy and Indirect Hard Modeling. *Appl. Spectrosc.* **2016**, *70*, 416-426.
- [214] Tsuboi, Y.; Nishino, M.; Kitamura, N., Laser-Induced Reversible Volume Phase Transition of a Poly(*N*-isopropylacrylamide) Gel Explored by Raman Microspectroscopy. *Polym. J.* **2008**, *40*, 367-374.
- [215] Ferraro, J. R.; Nakamoto, K.; Brown, C. W., *Introductory Raman Spectroscopy (Second Edition)*. Elsevier: 2003.
- [216] Raman, C. V.; Krishnan, K. S., A New Type of Secondary Radiation. *Nature* **1928**, *121*, 501-502.
- [217] Ferraro, J. R.; Nakamoto, K.; Brown, C. W., Basic Theory. In *Introductory Raman Spectroscopy (Second Edition)*, Ferraro, J. R.; Nakamoto, K.; Brown, C. W., Eds. Elsevier: 2003; pp 1-94.
- [218] Alsmeyer, F.; Koß, H.-J.; Marquardt, W., Indirect Spectral Hard Modeling for the Analysis of Reactive and Interacting Mixtures. *Appl. Spectrosc.* **2004**, *58*, 975-985.
- [219] Bardow, A.; Marquardt, W.; Göke, V.; Koss, H.-J.; Lucas, K., Model-based measurement of diffusion using Raman spectroscopy. *AIChE J.* **2003**, *49*, 323-334.
- [220] Kriesten, E.; Mayer, D.; Alsmeyer, F.; Minnich, C. B.; Greiner, L.; Marquardt, W., Identification of unknown pure component spectra by indirect hard modeling. *Chemom. Intell. Lab. Syst.* **2008**, *93*, 108-119.

- [221] Alsmeyer, F.; Marquardt, W., Automatic Generation of Peak-Shaped Models. *Appl. Spectrosc.* **2004**, *58*, 986-994.
- [222] Beumers, P.; Engel, D.; Brands, T.; Koß, H. J.; Bardow, A., Robust analysis of spectra with strong background signals by First-Derivative Indirect Hard Modeling (FD-IHM). *Chemom. Intell. Lab. Syst.* **2018**, *172*, 1-9.
- [223] Kriesten, E.; Alsmeyer, F.; Bardow, A.; Marquardt, W., Fully automated indirect hard modeling of mixture spectra. *Chemom. Intell. Lab. Syst.* **2008**, *91*, 181-193.
- [224] Maeda, Y.; Kitano, H., The structure of water in polymer systems as revealed by Raman spectroscopy. *Spectrochim. Acta, Part A* **1995**, *51*, 2433-2446.
- [225] Holden, C. A.; Hunnicutt, S. S.; Sánchez-Ponce, R.; Craig, J. M.; Rutan, S. C., Study of Complexation in Methanol/Water Mixtures by Infrared and Raman Spectroscopy and Multivariate Curve Resolution—Alternating Least-Squares Analysis. *Appl. Spectrosc.* **2003**, *57*, 483-490.
- [226] Gruenloh, C. J.; Florio, G. M.; Carney, J. R.; Hagemeister, F. C.; Zwier, T. S., C–H Stretch Modes as a Probe of H-Bonding in Methanol-Containing Clusters. *J. Phys. Chem. A* **1999**, *103*, 496-502.
- [227] Pepperkok, R.; Ellenberg, J., High-throughput fluorescence microscopy for systems biology. *Nature Reviews Molecular Cell Biology* **2006**, *7*, 690-696.
- [228] Wöll, D.; Flors, C., Super-resolution Fluorescence Imaging for Materials Science. *Small Methods* **2017**, *1*, 1700191.
- [229] Lakowicz, J. R., *Principles of Fluorescence Spectroscopy*. 3rd ed.; Springer Science+Business Media: New York, 2007.
- [230] Kubitscheck, U., *Fluorescence Microscopy: From Principles to Biological Applications*. 2nd ed.; Wiley-VCH Verlag GmbH & Co. KGaA: Weinheim, 2017.
- [231] John Frederick William, H., On a Case of Superficial Colour Presented by a Homogeneous Liquid Internally Colourless. *Philos. Trans. R. Soc. London* **1845**, *135*, 143-145.
- [232] M. Sauer; J. Hofkens; Enderlein, J., Basic Principles of Fluorescence Spectroscopy. In *Handbook of Fluorescence Spectroscopy and Imaging*, 2011; pp 1-30.
- [233] Murphy, D. B.; Davidson, M. W., *Fundamentals of Light Microscopy and Electronic Imaging*. 2nd ed.; Wiley-Blackwell: Hoboken, New Jersey, 2013.
- [234] Klymchenko, A. S., Solvatochromic and Fluorogenic Dyes as Environment-Sensitive Probes: Design and Biological Applications. *Acc. Chem. Res.* **2017**, *50*, 366-375.
- [235] Reichardt, C.; Welton, T., Solvent Effects on the Absorption Spectra of Organic Compounds. In *Solvents and Solvent Effects in Organic Chemistry*, 2010; pp 359-424.
- [236] Pietsch, C.; Schubert, U. S.; Hoogenboom, R., Aqueous polymeric sensors based on temperature-induced polymer phase transitions and solvatochromic dyes. *Chem. Commun.* **2011**, *47*, 8750-8765.
- [237] Sutter, M.; Oliveira, S.; Sanders, N. N.; Lucas, B.; van Hoek, A.; Hink, M. A.; Visser, A. J. W. G.; De Smedt, S. C.; Hennink, W. E.; Jiskoot, W., Sensitive Spectroscopic

- Detection of Large and Denatured Protein Aggregates in Solution by Use of the Fluorescent Dye Nile Red. *J. Fluoresc.* **2007**, *17*, 181-192.
- [238] Cser, A.; Nagy, K.; Biczók, L., Fluorescence lifetime of Nile Red as a probe for the hydrogen bonding strength with its microenvironment. *Chem. Phys. Lett.* **2002**, *360*, 473-478.
- [239] Rai, V.; Dey, N., The Basics of Confocal Microscopy. In *Laser Scanning, Theory and Applications*, Wang, P. C.-C., Ed. InTech: 2011.
- [240] Minsky, M., Memoir on inventing the confocal scanning microscope. *Scanning* **1988**, *10*, 128-138.
- [241] Gräf, R.; Rietdorf, J.; Zimmermann, T., Live Cell Spinning Disk Microscopy. In *Microscopy Techniques*, Rietdorf, J., Ed. Springer Berlin Heidelberg: Berlin, Heidelberg, 2005; pp 57-75.
- [242] Petráň, M.; Hadravský, M.; Egger, M. D.; Galambos, R., Tandem-Scanning Reflected-Light Microscope. *J. Opt. Soc. Am.* **1968**, *58*, 661-664.
- [243] Al-Kofahi, O.; Can, A.; Lasek, S.; Szarowski, D. H.; Turner, J. N.; Roysam, B., Algorithms for accurate 3D registration of neuronal images acquired by confocal scanning laser microscopy. *J. Microsc.* **2003**, *211*, 8-18.
- [244] Amiya, T.; Hirokawa, Y.; Hirose, Y.; Li, Y.; Tanaka, T., Reentrant phase transition of *N*-isopropylacrylamide gels in mixed solvents. *J. Chem. Phys.* **1987**, *86*, 2375-2379.
- [245] Hirotsu, S., Phase Transition of a Polymer Gel in Pure and Mixed Solvent Media. *J. Phys. Soc. Jpn.* **1987**, *56*, 233-242.
- [246] Chee, C. K.; Hunt, B. J.; Rimmer, S.; Soutar, I.; Swanson, L., Time-resolved fluorescence anisotropy studies of the cononsolvency of poly(*N*-isopropylacrylamide) in mixtures of methanol and water. *Soft Matter* **2011**, *7*, 1176-1184.
- [247] Arndt, M. C.; Sadowski, G., Modeling Poly(*N*-isopropylacrylamide) Hydrogels in Water/Alcohol Mixtures with PC-SAFT. *Macromolecules* **2012**, *45*, 6686-6696.
- [248] Costa, R. O. R.; Freitas, R. F. S., Phase behavior of poly(*N*-isopropylacrylamide) in binary aqueous solutions. *Polymer* **2002**, *43*, 5879-5885.
- [249] Zhu, P. W.; Napper, D. H., Light scattering studies of poly(*N*-isopropylacrylamide) microgel particles in mixed water-acetic acid solvents. *Macromolecular Chemistry and Physics* **1999**, *200*, 1950-1955.
- [250] Wang, J.; Wang, N.; Liu, B.; Bai, J.; Gong, P.; Ru, G.; Feng, J., Preferential adsorption of the additive is not a prerequisite for cononsolvency in water-rich mixtures. *Phys. Chem. Chem. Phys.* **2017**, *19*, 30097-30106.
- [251] Mukherji, D.; Watson, M. D.; Morsbach, S.; Schmutz, M.; Wagner, M.; Marques, C. M.; Kremer, K., Soft and Smart: Co-nonsolvency-Based Design of Multiresponsive Copolymers. *Macromolecules* **2019**, *52*, 3471-3478.
- [252] Wang, X.; Huang, H.; Liu, H.; Rehfeldt, F.; Wang, X.; Zhang, K., Multi-Responsive Bilayer Hydrogel Actuators with Programmable and Precisely Tunable Motions. *Macromol. Chem. Phys.* **2019**, *220*, 1800562.

- [253] Nian, S.; Pu, L., Racemic Fluorescence Probe for Enantiomeric Excess Determination: Application of Cononsolvency of a Polymer in Sensing. *J. Org. Chem.* **2019**, *84*, 909-913.
- [254] Li, C.-W.; Merlitz, H.; Wu, C.-X.; Sommer, J.-U., Nanopores as Switchable Gates for Nanoparticles: A Molecular Dynamics Study. *Macromolecules* **2018**, *51*, 6238-6247.
- [255] Ge, Z.; Xie, D.; Chen, D.; Jiang, X.; Zhang, Y.; Liu, H.; Liu, S., Stimuli-Responsive Double Hydrophilic Block Copolymer Micelles with Switchable Catalytic Activity. *Macromolecules* **2007**, *40*, 3538-3546.
- [256] Hüther, A. Experimentelle und theoretische Untersuchungen zum Quellungsgleichgewicht von Hydrogelen in wässrigen Lösungen. Dissertation, TU Kaiserslautern, VDI-Verl. Düsseldorf :, 2001.
- [257] Numata, Y.; Iida, Y.; Tanaka, H., Quantitative analysis of alcohol–water binary solutions using Raman spectroscopy. *J. Quant. Spectrosc. Radiat. Transfer* **2011**, *112*, 1043-1049.
- [258] Purohit, A.; Centeno, S. P.; Wypysek, S. K.; Richtering, W.; Wöll, D., Microgel PAINT – nanoscopic polarity imaging of adaptive microgels without covalent labelling. *Chem. Sci.* **2019**, *10*, 10336-10342.
- [259] Parasuraman, D.; Serpe, M. J., Poly (*N*-Isopropylacrylamide) Microgel-Based Assemblies for Organic Dye Removal from Water. *ACS Appl. Mater. Interfaces* **2011**, *3*, 4714-4721.
- [260] Mase, N.; Nakai, Y.; Ohara, N.; Yoda, H.; Takabe, K.; Tanaka, F.; Barbas, C. F., Organocatalytic Direct Asymmetric Aldol Reactions in Water. *J. Am. Chem. Soc.* **2006**, *128*, 734-735.
- [261] Scherzinger, C.; Holderer, O.; Richter, D.; Richtering, W., Polymer dynamics in responsive microgels: influence of cononsolvency and microgel architecture. *Phys. Chem. Chem. Phys.* **2012**, *14*, 2762-2768.
- [262] Nothdurft, K.; Müller, D. H.; Mürtz, S. D.; Meyer, A. A.; Guerzoni, L. P. B.; Jans, A.; Kühne, A. J. C.; De Laporte, L.; Brands, T.; Bardow, A.; Richtering, W., Is the Microgel Collapse a Two-Step Process? Exploiting Cononsolvency to Probe the Collapse Dynamics of Poly-*N*-isopropylacrylamide (pNIPAM). *J. Phys. Chem. B* **2021**, *125*, 1503-1512.
- [263] Stuart, M. C. A.; van de Pas, J. C.; Engberts, J. B. F. N., The use of Nile Red to monitor the aggregation behavior in ternary surfactant–water–organic solvent systems. *J. Phys. Org. Chem.* **2005**, *18*, 929-934.
- [264] Yang, Z.; Cao, J.; He, Y.; Yang, J. H.; Kim, T.; Peng, X.; Kim, J. S., Macro-/micro-environment-sensitive chemosensing and biological imaging. *Chem. Soc. Rev.* **2014**, *43*, 4563-4601.
- [265] Bongiovanni, M. N.; Godet, J.; Horrocks, M. H.; Tosatto, L.; Carr, A. R.; Wirthensohn, D. C.; Ranasinghe, R. T.; Lee, J.-E.; Ponjavic, A.; Fritz, J. V.; Dobson, C. M.; Klenerman, D.; Lee, S. F., Multi-dimensional super-resolution imaging enables surface hydrophobicity mapping. *Nat. Commun.* **2016**, *7*, 13544.

- [266] Moon, S.; Yan, R.; Kenny, S. J.; Shyu, Y.; Xiang, L.; Li, W.; Xu, K., Spectrally Resolved, Functional Super-Resolution Microscopy Reveals Nanoscale Compositional Heterogeneity in Live-Cell Membranes. *J. Am. Chem. Soc.* **2017**, *139*, 10944-10947.
- [267] Jagadeesan, D.; Nasimova, I.; Gourevich, I.; Starodubtsev, S.; Kumacheva, E., Microgels for the Encapsulation and Stimulus-Responsive Release of Molecules with Distinct Polarities. *Macromol. Biosci.* **2011**, *11*, 889-896.
- [268] Plenderleith, R.; Swift, T.; Rimmer, S., Highly-branched poly(*N*-isopropyl acrylamide)s with core-shell morphology below the lower critical solution temperature. *RSC Adv.* **2014**, *4*, 50932-50937.
- [269] Locatelli-Champagne, C.; Cloitre, M., Monitoring mesoglobules formation in PNIPAm solutions using Nile Red solvatochromism. *Colloid. Polym. Sci.* **2013**, *291*, 2911-2916.
- [270] Pich, A.; Karak, A.; Lu, Y.; Ghosh, A. K.; Adler, H.-J. P., Tuneable Catalytic Properties of Hybrid Microgels Containing Gold Nanoparticles. *J. Nanosci. Nanotechnol.* **2006**, *6*, 3763-3769.
- [271] Brändel, T.; Sabadasch, V.; Hannappel, Y.; Hellweg, T., Improved Smart Microgel Carriers for Catalytic Silver Nanoparticles. *ACS Omega* **2019**, *4*, 4636-4649.
- [272] Lu, Y.; Proch, S.; Schrinner, M.; Drechsler, M.; Kempe, R.; Ballauff, M., Thermosensitive core-shell microgel as a “nanoreactor” for catalytic active metal nanoparticles. *J. Mater. Chem.* **2009**, *19*, 3955-3961.
- [273] Zayas, H. A.; Lu, A.; Valade, D.; Amir, F.; Jia, Z.; O'Reilly, R. K.; Monteiro, M. J., Thermoresponsive Polymer-Supported L-Proline Micelle Catalysts for the Direct Asymmetric Aldol Reaction in Water. *ACS Macro Lett.* **2013**, *2*, 327-331.
- [274] Neumann, L. N.; Baker, M. B.; Leenders, C. M. A.; Voets, I. K.; Lafleur, R. P. M.; Palmans, A. R. A.; Meijer, E. W., Supramolecular polymers for organocatalysis in water. *Org. Biomol. Chem.* **2015**, *13*, 7711-7719.
- [275] Font, D.; Jimeno, C.; Pericàs, M. A., Polystyrene-Supported Hydroxyproline: An Insoluble, Recyclable Organocatalyst for the Asymmetric Aldol Reaction in Water. *Org. Lett.* **2006**, *8*, 4653-4655.
- [276] Benaglia, M.; Cinquini, M.; Cozzi, F.; Puglisi, A.; Celentano, G., Poly(Ethylene Glycol)-Supported Proline: A Versatile Catalyst for the Enantioselective Aldol and Iminoaldol Reactions. *Adv. Synth. Catal.* **2002**, *344*, 533-542.
- [277] Lu, A.; Moatsou, D.; Hands-Portman, I.; Longbottom, D. A.; O'Reilly, R. K., Recyclable L-Proline Functional Nanoreactors with Temperature-Tuned Activity Based on Core-Shell Nanogels. *ACS Macro Lett.* **2014**, *3*, 1235-1239.
- [278] Lindner, P.; Zemb, T., *Neutrons, X-rays and Light: Scattering Methods Applied to Soft Condensed Matter*. 1st ed.; Elsevier Science B.V. : Amsterdam, 2002.
- [279] Senff, H.; Richtering, W., Influence of cross-link density on rheological properties of temperature-sensitive microgel suspensions. *Colloid. Polym. Sci.* **2000**, *278*, 830-840.

- [280] Kristensen, T. E.; Vestli, K.; Fredriksen, K. A.; Hansen, F. K.; Hansen, T., Synthesis of Acrylic Polymer Beads for Solid-Supported Proline-Derived Organocatalysts. *Org. Lett.* **2009**, *11*, 2968-2971.
- [281] Zotova, N.; Franzke, A.; Armstrong, A.; Blackmond, D. G., Clarification of the Role of Water in Proline-Mediated Aldol Reactions. *J. Am. Chem. Soc.* **2007**, *129*, 15100-15101.
- [282] Saxena, S.; Hansen, C. E.; Lyon, L. A., Microgel mechanics in biomaterial design. *Acc. Chem. Res.* **2014**, *47*, 2426-2434.
- [283] Mitragotri, S.; Lahann, J., Physical approaches to biomaterial design. *Nat. Mater.* **2009**, *8*, 15-23.
- [284] Wyss, H. M.; Mattsson, J.; Franke, T.; Fernandez-Nieves, A.; Weitz, D. A., Mechanics of Single Microgel Particles. In *Microgel Suspensions*, Fernandez-Nieves, A.; Wyss, H. M.; Mattsson, J.; Weitz, D. A., Eds. 2011; pp 311-325.
- [285] Liétor-Santos, J. J.; Sierra-Martín, B.; Fernández-Nieves, A., Bulk and shear moduli of compressed microgel suspensions. *Phys. Rev. E* **2011**, *84*, 060402.
- [286] Kumachev, A.; Tumarkin, E.; Walker, G. C.; Kumacheva, E., Characterization of the mechanical properties of microgels acting as cellular microenvironments. *Soft Matter* **2013**, *9*, 2959-2965.
- [287] Schmidt, S.; Zeiser, M.; Hellweg, T.; Duschl, C.; Fery, A.; Möhwald, H., Adhesion and Mechanical Properties of PNIPAM Microgel Films and Their Potential Use as Switchable Cell Culture Substrates. *Adv. Funct. Mater.* **2010**, *20*, 3235-3243.
- [288] Hashmi, S. M.; Dufresne, E. R., Mechanical properties of individual microgel particles through the deswelling transition. *Soft Matter* **2009**, *5*, 3682-3688.
- [289] Huth, S.; Sindt, S.; Selhuber-Unkel, C., Automated analysis of soft hydrogel microindentation: Impact of various indentation parameters on the measurement of Young's modulus. *PLoS ONE* **2019**, *14*, e0220281.
- [290] Abate, A. R.; Han, L.; Jin, L.; Suo, Z.; Weitz, D. A., Measuring the elastic modulus of microgels using microdrops. *Soft Matter* **2012**, *8*, 10032-10035.
- [291] Yuan, M.; Ju, X.; Xie, R.; Wang, W.; Chu, L., Micromechanical properties of poly(*N*-isopropylacrylamide) hydrogel microspheres determined using a simple method. *Particuology* **2015**, *19*, 164-172.
- [292] Voudouris, P.; Florea, D.; van der Schoot, P.; Wyss, H. M., Micromechanics of temperature sensitive microgels: dip in the Poisson ratio near the LCST. *Soft Matter* **2013**, *9*, 7158-7166.
- [293] Wyss, H. M.; Franke, T.; Mele, E.; Weitz, D. A., Capillary micromechanics: Measuring the elasticity of microscopic soft objects. *Soft Matter* **2010**, *6*, 4550-4555.
- [294] Sleetboom, J. J. F.; Voudouris, P.; Punter, M. T. J. J. M.; Aangenendt, F. J.; Florea, D.; van der Schoot, P.; Wyss, H. M., Compression and Reswelling of Microgel Particles after an Osmotic Shock. *Phys. Rev. Lett.* **2017**, *119*, 098001.
- [295] Sierra-Martin, B.; Frederick, J. A.; Laporte, Y.; Markou, G.; Liétor-Santos, J. J.; Fernandez-Nieves, A., Determination of the bulk modulus of microgel particles. *Colloid. Polym. Sci.* **2011**, *289*, 721-728.

- [296] Sierra-Martín, B.; Laporte, Y.; South, A. B.; Lyon, L. A.; Fernández-Nieves, A., Bulk modulus of poly(*N*-isopropylacrylamide) microgels through the swelling transition. *Phys. Rev. E* **2011**, *84*, 011406.
- [297] Ruscito, A.; Chiessi, E.; Toumia, Y.; Oddo, L.; Domenici, F.; Paradossi, G., Microgel Particles with Distinct Morphologies and Common Chemical Compositions: A Unified Description of the Responsivity to Temperature and Osmotic Stress. *Gels* **2020**, *6*, 34.
- [298] Guo, M.; Wyss, H. M., Micromechanics of Soft Particles. *Macromol. Mater. Eng.* **2011**, *296*, 223-229.
- [299] Saunders, B. R.; Vincent, B., Thermal and osmotic deswelling of poly(NIPAM) microgel particles. *J. Chem. Soc., Faraday Trans.* **1996**, *92*, 3385-3389.
- [300] Nolan, C. M.; Reyes, C. D.; Debord, J. D.; García, A. J.; Lyon, L. A., Phase Transition Behavior, Protein Adsorption, and Cell Adhesion Resistance of Poly(ethylene glycol) Cross-Linked Microgel Particles. *Biomacromolecules* **2005**, *6*, 2032-2039.
- [301] Stanley, C. B.; Strey, H. H., Measuring Osmotic Pressure of Poly(ethylene glycol) Solutions by Sedimentation Equilibrium Ultracentrifugation. *Macromolecules* **2003**, *36*, 6888-6893.
- [302] Ishida, T.; Akagi, M.; Sugimoto, H.; Onoue, Y.; Iwai, Y.; Arai, Y., Swelling equilibria of poly(*N*-isopropylacrylamide) gel in aqueous polymer solutions. *Fluid Phase Equilib.* **1995**, *104*, 119-129.
- [303] Ishida, T.; Akagi, M.; Sugimoto, H.; Iwai, Y.; Arai, Y., Swelling behaviors of poly(*N*-isopropylacrylamide) gel in poly(ethylene glycol)-water mixtures. *Macromolecules* **1993**, *26*, 7361-7362.
- [304] Gelissen, A. P. H.; Scotti, A.; Turnhoff, S. K.; Janssen, C.; Radulescu, A.; Pich, A.; Rudov, A. A.; Potemkin, I. I.; Richtering, W., An anionic shell shields a cationic core allowing for uptake and release of polyelectrolytes within core-shell responsive microgels. *Soft Matter* **2018**, *14*, 4287-4299.
- [305] Tanaka, T.; Fillmore, D. J., Kinetics of swelling of gels. *J. Chem. Phys.* **1979**, *70*, 1214-1218.
- [306] Appavoo, D.; Park, S. Y.; Zhai, L., Responsive polymers for medical diagnostics. *J. Mater. Chem. B* **2020**, *8*, 6217-6232.
- [307] Tang, Y.; Liu, X., Collapse kinetics for individual poly(*N*-isopropylmethacrylamide) chains. *Polymer* **2010**, *51*, 897-901.
- [308] Wang, J.; Gan, D.; Lyon, L. A.; El-Sayed, M. A., Temperature-Jump Investigations of the Kinetics of Hydrogel Nanoparticle Volume Phase Transitions. *J. Am. Chem. Soc.* **2001**, *123*, 11284-11289.
- [309] Sato Matsuo, E.; Tanaka, T., Kinetics of discontinuous volume-phase transition of gels. *J. Chem. Phys.* **1988**, *89*, 1695-1703.
- [310] Tanaka, T.; Sato, E.; Hirokawa, Y.; Hirotsu, S.; Peetermans, J., Critical Kinetics of Volume Phase Transition of Gels. *Phys. Rev. Lett.* **1985**, *55*, 2455-2458.
- [311] Suzuki, A.; Hara, T., Kinetics of one-dimensional swelling and shrinking of polymer gels under mechanical constraint. *J. Chem. Phys.* **2001**, *114*, 5012-5015.

- [312] Andersson, M.; Axelsson, A.; Zacchi, G., Swelling kinetics of poly(*N*-isopropylacrylamide) gel. *J. Controlled Release* **1998**, *50*, 273-281.
- [313] Dupin, D.; Rosselgong, J.; Armes, S. P.; Routh, A. F., Swelling Kinetics for a pH-Induced Latex-to-Microgel Transition. *Langmuir* **2007**, *23*, 4035-4041.
- [314] Yin, J.; Dupin, D.; Li, J.; Armes, S. P.; Liu, S., pH-Induced Deswelling Kinetics of Sterically Stabilized Poly(2-vinylpyridine) Microgels Probed by Stopped-Flow Light Scattering. *Langmuir* **2008**, *24*, 9334-9340.
- [315] Huang, N.; Guan, Y.; Zhu, X. X.; Zhang, Y., Swelling Kinetics of Microgels Embedded in a Polyacrylamide Hydrogel Matrix. *ChemPhysChem* **2014**, *15*, 1785-1792.
- [316] Nikolov, S.; Fernandez-Nieves, A.; Alexeev, A., Mesoscale modeling of microgel mechanics and kinetics through the swelling transition. *Appl. Math. Mech.* **2018**, *39*, 47-62.
- [317] Suárez, I. J.; Fernández-Nieves, A.; Márquez, M., Swelling Kinetics of Poly(*N*-isopropylacrylamide) Minigels. *J. Phys. Chem. B* **2006**, *110*, 25729-25733.
- [318] Mochizuki, K., On–Off of Co-non-solvency for Poly(*N*-vinylcaprolactam) in Alcohol–Water Mixtures: A Molecular Dynamics Study. *J. Phys. Chem. B* **2020**, *124*, 9951-9957.
- [319] Tavagnacco, L.; Zaccarelli, E.; Chiessi, E., Molecular description of the coil-to-globule transition of Poly(*N*-isopropylacrylamide) in water/ethanol mixture at low alcohol concentration. *J. Mol. Liq.* **2020**, *297*, 111928.
- [320] Smiley-Wiens, J. B.; Serpe, M. J., Solvent exchange kinetics in poly(*N*-isopropylacrylamide) microgel-based etalons. *Colloid. Polym. Sci.* **2013**, *291*, 971-979.
- [321] Brewer, L. R.; Bianco, P. R., Laminar flow cells for single-molecule studies of DNA-protein interactions. *Nature Methods* **2008**, *5*, 517-525.
- [322] Kamholz, A. E.; Schilling, E. A.; Yager, P., Optical measurement of transverse molecular diffusion in a microchannel. *Biophys. J.* **2001**, *80*, 1967-1972.
- [323] Madariaga-Marcos, J.; Corti, R.; Hormeño, S.; Moreno-Herrero, F., Characterizing microfluidic approaches for a fast and efficient reagent exchange in single-molecule studies. *Sci. Rep.* **2020**, *10*, 18069.
- [324] Shibayama, M.; Nagai, K., Shrinking Kinetics of Poly(*N*-isopropylacrylamide) Gels T-Jumped across Their Volume Phase Transition Temperatures. *Macromolecules* **1999**, *32*, 7461-7468.
- [325] Okajima, T.; Harada, I.; Nishio, K.; Hirotsu, S., Kinetics of volume phase transition in poly(*N*-isopropylacrylamide) gels. *J. Chem. Phys.* **2002**, *116*, 9068-9077.
- [326] Li, Y.; Tanaka, T., Kinetics of swelling and shrinking of gels. *J. Chem. Phys.* **1990**, *92*, 1365-1371.
- [327] Peters, A.; Candau, S. J., Kinetics of swelling of spherical and cylindrical gels. *Macromolecules* **1988**, *21*, 2278-2282.
- [328] Maeda, S.; Kato, T.; Kogure, H.; Hosoya, N., Rapid response of thermo-sensitive hydrogels with porous structures. *Appl. Phys. Lett.* **2015**, *106*, 171909.

-
- [329] Takigawa, T.; Yamawaki, T.; Takahashi, K.; Masuda, T., Deswelling Kinetics of Poly(*N*-isopropylacrylamide) Gels at Volume-Phase Transition. *Polym. J.* **1999**, *31*, 595-598.
- [330] Mikhail, S. Z.; Kimel, W. R., Densities and Viscosities of Methanol-Water Mixtures. *J. Chem. Eng. Data* **1961**, *6*, 533-537.
- [331] Wohlfarth, C., Refractive index of the mixture (1) water; (2) methanol: Datasheet from Landolt-Börnstein - Group III Condensed Matter in SpringerMaterials In *Refractive Indices of Pure Liquids and Binary Liquid Mixtures (Supplement to III/38)*, Lechner, M. D., Ed. Springer-Verlag Berlin Heidelberg: 2008; Vol. 47.
- [332] Bonnet-Gonnet, C.; Belloni, L.; Cabane, B., Osmotic Pressure of Latex Dispersions. *Langmuir* **1994**, *10*, 4012-4021.
- [333] Nothdurft, K. Synthesis and Characterization of Responsive and Anisotropic PNIPAM-based Microgels. Master thesis, RWTH Aachen University, 2017.

List of symbols and abbreviations

A	Area
\mathcal{A}	Mixture model
\mathcal{A}_i^*	Pure component model
AFM	Atomic force microscopy
APMA	<i>N</i> -(3-Aminopropyl)methacrylamide hydrochloride
APS	Ammonium persulfate
ATR	Attenuated total reflection
\mathcal{B}	Background model
BIS	<i>N,N'</i> -Methylenebis(acrylamide)
CA	Cellulose acetate
CAD	Computer-aided design
CCD	Charge-coupled device
CHM	Complemental hard modeling
CLS	Classical least squares
D	Diffusion coefficient
d	Diameter
DCC	<i>N,N'</i> -Dicyclohexylcarbodiimide
DEAAM	<i>N,N</i> -Diethylacrylamide
DLS	Dynamic light scattering
DMAP	4-Dimethylaminopyridine
DMF	Dimethylformamide
DMMI	Dimethylmaleimide
DMSO	Dimethyl sulfoxide
DPD	Dissipative particle dynamics
η	Viscosity
f	Friction coefficient
FLIM	Fluorescence lifetime imaging
FTIR	Fourier transform infrared
FWHM	Full width at half maximum
MAS NMR	Magic-angle spinning nuclear magnetic resonance
I	Intensity
IHM	Indirect hard modeling

K	Bulk modulus
k_{app}	Apparent reaction rate constant
$k_{i,j}$	Calibration factor
λ	Wavelength
l	Characteristic length
LCST	Lower critical solution temperature
LED	Light-emitting diode
M_w	Weight average molecular weight
m_i	Mass of i
μ	Shear modulus
MeOH	Methanol
MTRB	Methacryloxyethyl thiocarbamoyl rhodamine B
n_i	Number of i
NHS	<i>N</i> -Hydroxysuccinimide
NIPAM	<i>N</i> -Isopropylacrylamide
NMR	Nuclear magnetic resonance
NR	Nile red
Π	Osmotic pressure
PE	Polyethylene
PEG	Polyethylene glycol
PDEAAM	Poly- <i>N,N</i> -diethylacrylamide
PDMS	Polydimethylsiloxane
PMMA	Polymethyl methacrylate
PMT	Photomultiplier tube
PNIPAM	Poly- <i>N</i> -isopropylacrylamide
PVA	Polyvinyl alcohol
PVP	Polyvinylpyrrolidone
q_{swell}	Swelling ratio
q_{deswell}	Deswelling ratio
q	Scattering vector
ρ	Density
R	Radius
R_{eff}	Effective radius
R_g	Radius of gyration
R_h	Hydrodynamic radius

Re	Reynolds number
RMSE	Root-mean-square error
ROI	Region of interest
SANS	Small-angle neutron scattering
SAXS	Small-angle X-ray scattering
SDS	Sodium dodecyl sulfate
SLS	Static Light Scattering
SPAD	Single-photon avalanche diode
T	Temperature
t	Time
τ	Time constant/fluorescence lifetime
τ	Time constant/relaxation time
TCSPC	Time-correlated single photon counting
TGA	Thermogravimetric analysis
THF	Tetrahydrofuran
TEMED	N,N,N',N' -Tetramethylethylenediamine
TR-SAXS	Time-resolved small-angle X-ray scattering
ULC	Ultra-low cross-linked
UV	Ultraviolet
u	Fluid velocity
ν	Frequency
$\tilde{\nu}$	Wavenumber
V	Volume
VCL	N -Vinylcaprolactam
VPT	Volume phase transition
VPTT	Volume phase transition temperature
ω_i	Weight fraction of i
x_i	Mole fraction of i
ζ_i	Weighting factor

Appendix

Chapter 4 – macroscopic PNIPAM gels

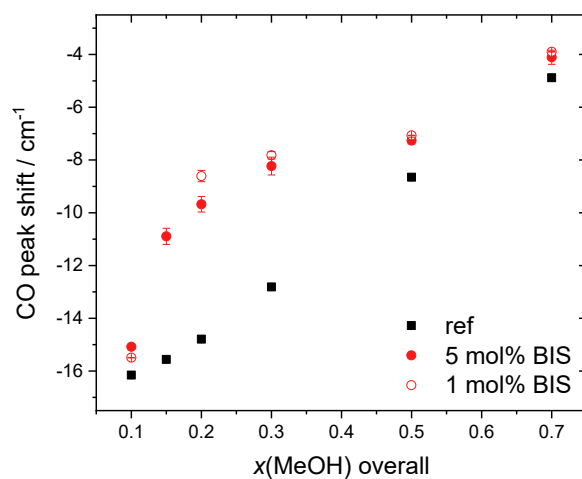


Figure A1: Comparison of the methanol CO-peak shift extracted from spectra measured in a binary reference solution of solely water and methanol (black) and inside PNIPAM macrogels with 5 mol% (red, full) or 1 mol% (red, open) cross-linker.

Chapter 5 – solvatochromic microgels

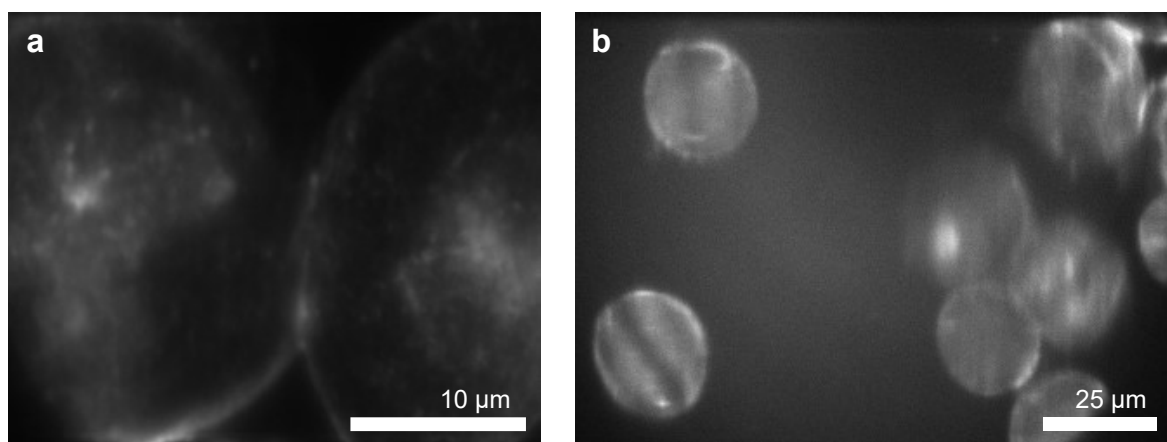


Figure A2: NR-labeled PNIPAM microgels in methanol. The PNIPAM microgels with 1 mol% APMA were labeled in buffer solution. Images were captured using a confocal fluorescence microscope.

Chapter 7 – osmotic pressure experiments

In the case of the microgel beads cross-linked with only 1.2 mol% BIS, no clear second linear regime was found in the Π - V plots (Figure 7.4). Therefore, the local slope and volume at each point were used to calculate the corresponding bulk modulus as exemplarily shown for MG-1.2-L in Figure A3a. The resulting bulk moduli as a function of the normalized diameter are displayed in Figure A3b. For the deswelling at low osmotic pressures, the bulk moduli are similar to each other and close to the average value of 8 ± 1 kPa (black line). However, further deswelling to below ~ 0.7 of the diameter in water is accompanied by a significant increase of the bulk modulus.

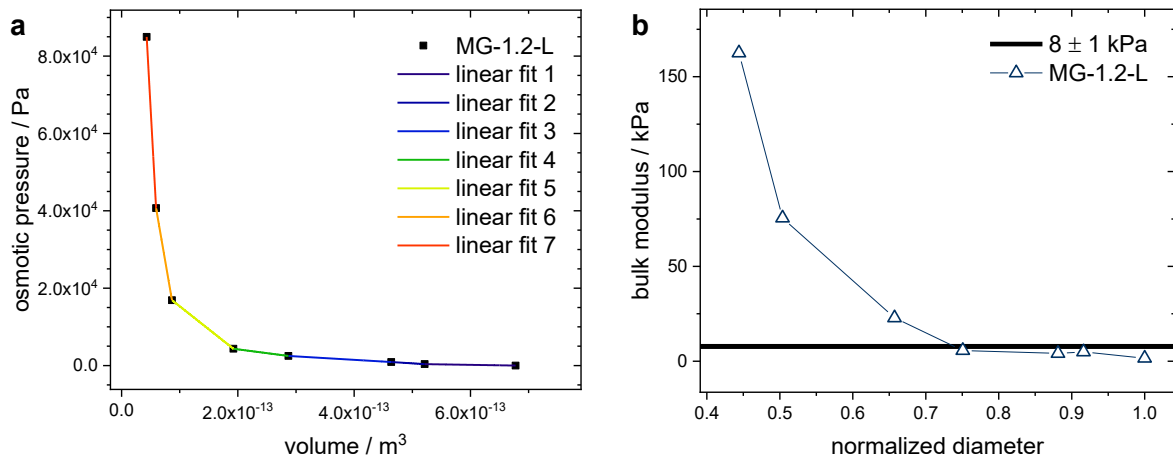


Figure A3: (a) External osmotic pressure in relation to the volume of the microgel beads with 1.2 mol% cross-linker (MG-1.2-L). For each point, the local slope and volume were evaluated to calculate the bulk modulus. (b) Bulk modulus of MG-1.2-L in different swelling states. The diameter was normalized to the size in water. The bulk modulus extracted from a linear fit at low osmotic pressures (8 ± 1 kPa, Figure 7.4) is indicated by a black line.

Chapter 8 – dynamics of the cononsolvency-induced collapse

For the solvent-jump experiments in Chapter 8, fluorescent microgel beads with 5 mol% cross-linker and different sizes were synthesized by microfluidics (see experimental section 10.3.5). Table A1 lists the average diameter of the microgel beads in water and in 20 mol% methanol (MeOH) as well as the corresponding deswelling ratios.

Table A1: Fluorescent microgel samples synthesized by microfluidics. The diameter in water was averaged for > 300 microgels and the diameter in 20 mol% methanol for > 150 microgels. The deswelling ratio q_{deswell} is defined as the ratio $q_{\text{deswell}}(d) = d(20 \text{ mol\% MeOH})/d(\text{H}_2\text{O})$ or $q_{\text{deswell}}(V) = V(20 \text{ mol\% MeOH})/V(\text{H}_2\text{O})$.

Sample code	$d(\text{H}_2\text{O})$ in μm	$d(\text{mix})$ in μm	$q_{\text{deswell}}(d)$	$q_{\text{deswell}}(V)$
SFB985_B3_KN_M000262	28 ± 3	14 ± 2	0.50	0.13
SFB985_B3_KN_M000589	52 ± 2	24 ± 3	0.46	0.10
SFB985_B3_KN_M000499	53 ± 2	27 ± 2	0.51	0.13
SFB985_B3_KN_M000498	54 ± 4	27 ± 2	0.50	0.13
SFB985_B3_KN_M000502	70 ± 4	36 ± 2	0.51	0.14
SFB985_B3_KN_M000497	100 ± 5	49 ± 2	0.49	0.12

The evaluation of the width of the interface between water and the unfavorable 20 mol% methanol in water mixture is discussed in section 8.3.1 for a 50/50 flow rate ratio. Figure A4 displays the results for other flow rate ratios between water and mixture for different heights (z) and distances from the inlets (y).

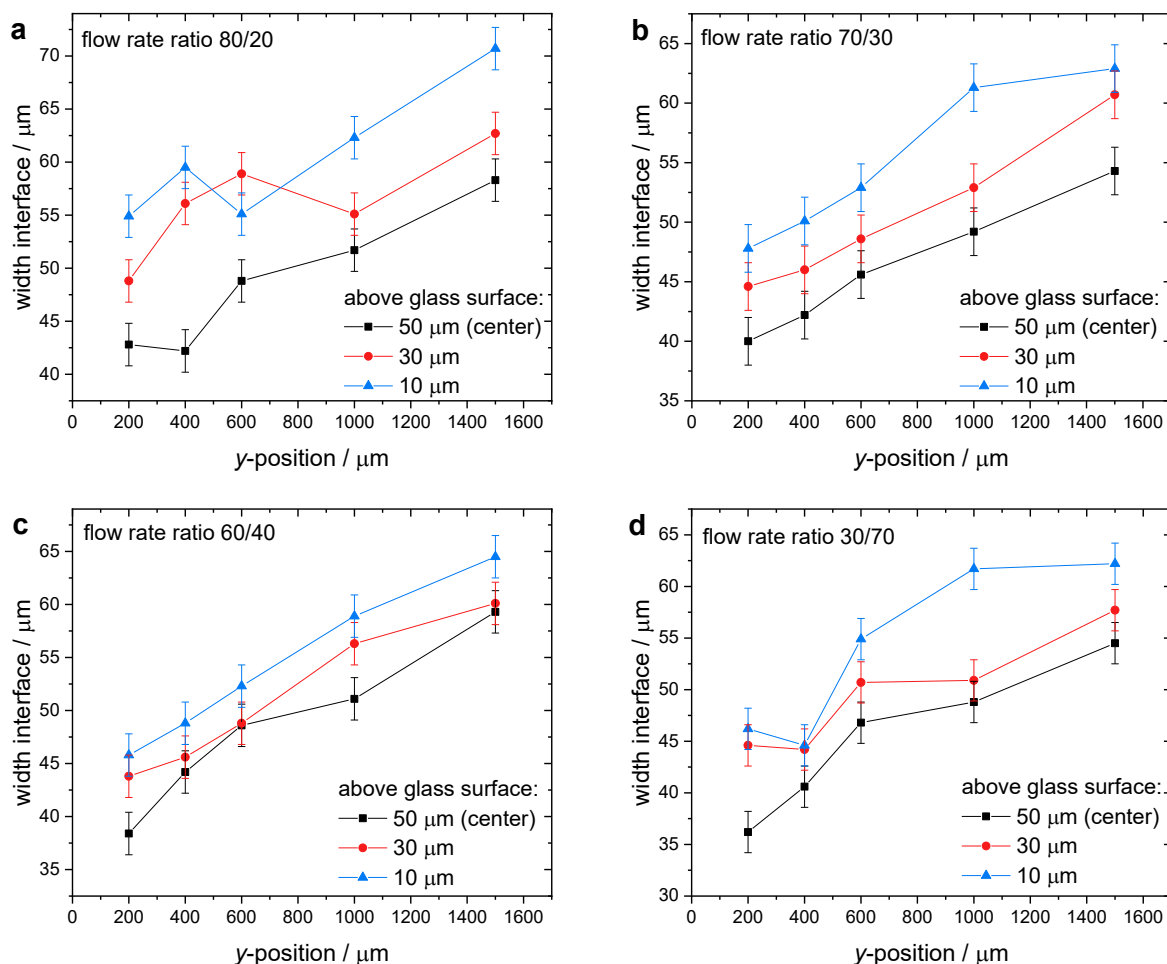


Figure A4: Evaluation of the width of the interface between pure water and 20 mol% methanol in water using Raman microspectroscopy as a function of the distance from the inlets (y) and the height (z). Various flow rate ratios between the water and mixture phase were investigated: (a) 80/20, (b) 70/30, (c) 60/40, and (d) 30/70. Measurements were performed 10, 30, or 50 μm above the glass surface of the channel. 50 μm corresponds to the center of the channel height.

The width and shape of the solvent interface can be affected by the microgel beads. Microgel beads can strongly bend the interface. In the example shown in Figure A5, several microgel beads are attached next to each other across the channel width and in contact with each other. Only the one furthest to the right had an individual spot. The flow rate ratio of the co-flow coming from the bottom left corner was adjusted to cause a solvent-jump from water to the mixture. The interface (darkish stream) started to move across the channel (from the bottom right to the upper left corner of the images). Reaching the first, individual microgel bead, the interface already started to slightly bend. While the interface crossed over

the individual microgel bead with no problem, it did not proceed completely to the other side of the channel. The remaining microgels on the aqueous side prevented the full solvent-jump by strongly bending the solvent interface. Although the interface should be to the left of the second microgel bead, the bead did not collapse with time. Only the individual microgel bead collapsed as expected in the water-methanol mixture. Additionally, the solvent interface appears less sharp due to the bending, i.e. behind the microgel beads.

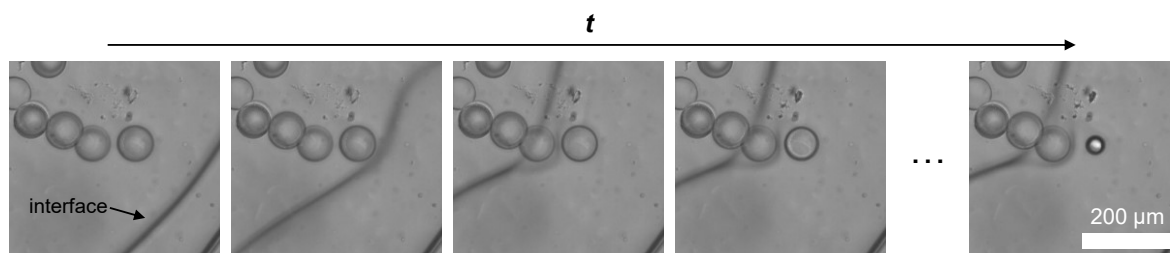


Figure A5: Example for the influence of a microgel bead on the interface between the co-flow of water and mixture.

The size evolutions of the microgel beads after a solvent-jump from water to 20 mol% methanol are discussed in section 8.5. The diameter of the microgel beads was extracted for every frame of the video of the solvent-jump experiment. Before fitting the size evolutions, the data points were reduced in order to give more weight to the first collapse with the major volume change. Thus, the data points are increasingly reduced with time and only every 1.2^n -th frame remained (Figure A6).

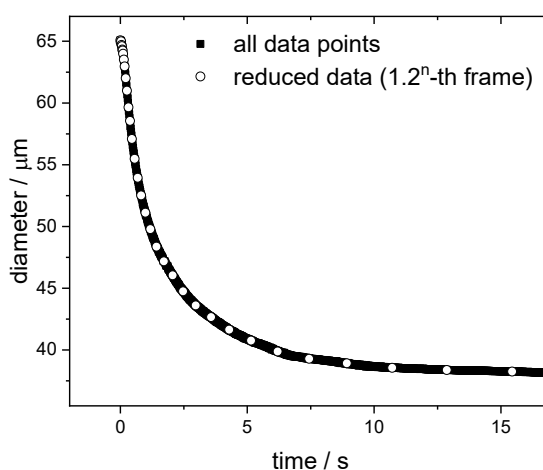


Figure A6: The data points obtained from the video image analysis (full symbols) were reduced to every 1.2^n -th frame (open symbols).

All size evolutions were evaluated with a mono- and bi-exponential function for all investigated microgel beads. The results for the microgel beads of the smallest size range (around 25 μm) are shown in Figure A7, of the medium size range (around 60 μm) in Figure A8 and of the largest size range (around 95 μm) in Figure A9. For all, the mono-

exponential fit (blue) is not sufficient to properly describe the change in diameter with time. A bi-exponential fit is required indicating a two-step process for the volume phase transition.

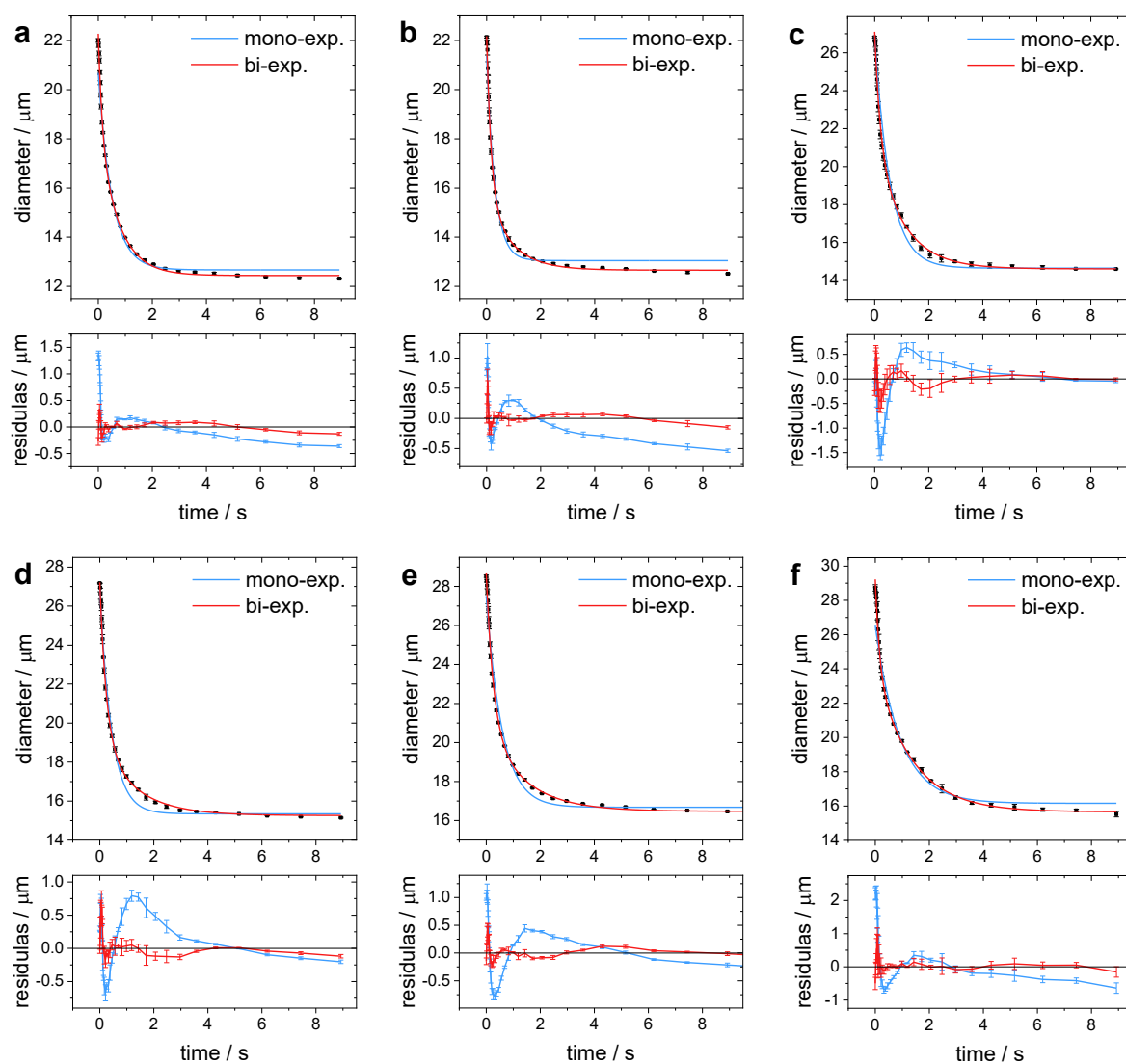


Figure A7: Solvent-jump experiments from water to 20 mol% methanol for the microgels of the smallest size range around $25 \mu\text{m}$. The change in diameter was fitted with a mono-exponential (blue) and bi-exponential (red) function. The corresponding residuals of both fits are shown at the bottom of each diagram. For each microgel, the solvent-jump was performed three times and the results were averaged.

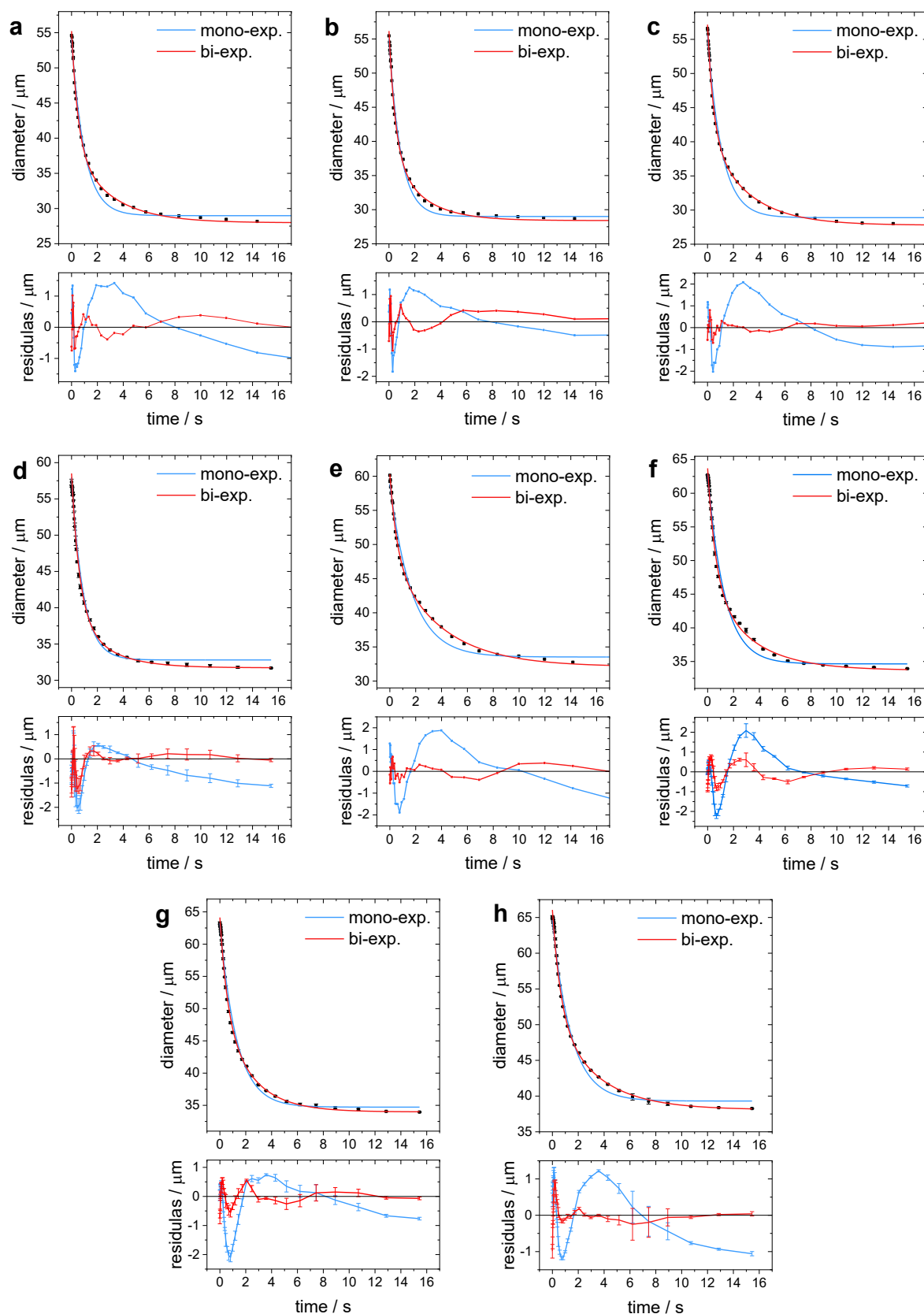


Figure A8: Solvent-jump experiments from water to 20 mol% methanol for the microgels of the medium size range around 60 μm . The change in diameter was fitted with a mono-exponential (blue) and bi-exponential (red) function. The corresponding residuals of both fits are shown at the bottom of each diagram. For each microgel, the solvent-jump was performed three times and the results were averaged (except for a-c and e).

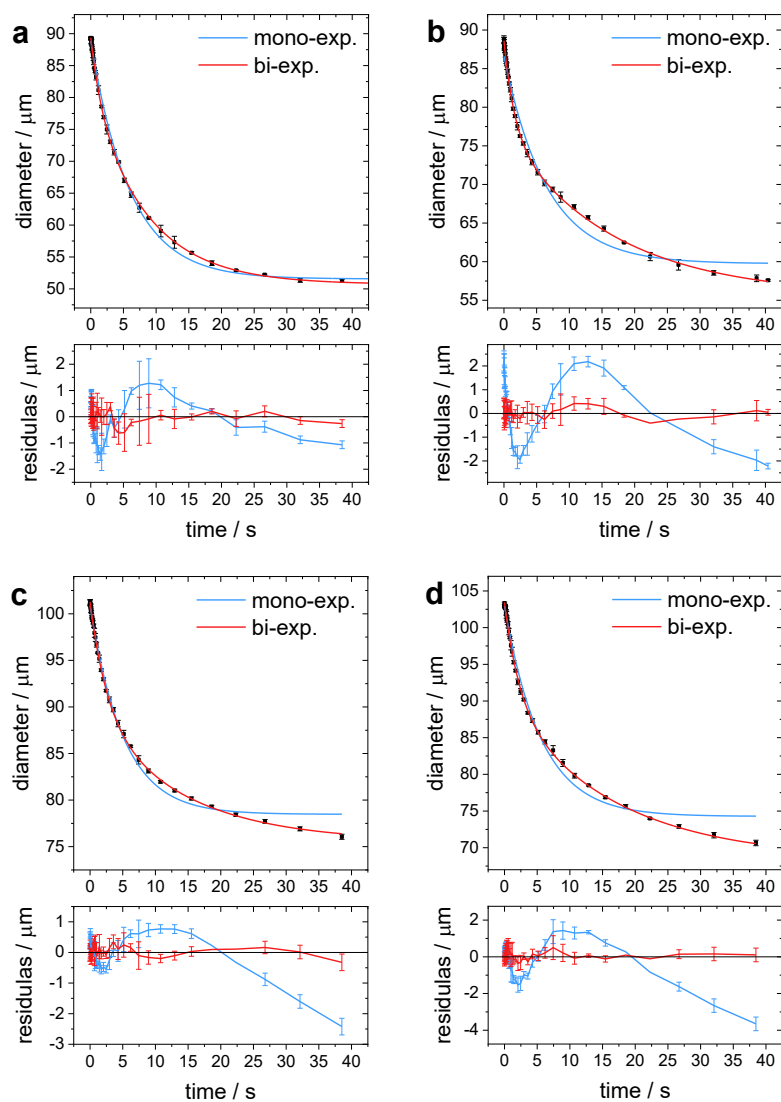


Figure A9: Solvent-jump experiments from water to 20 mol% methanol for the microgels of the largest size range around 95 μm . The change in diameter was fitted with a mono-exponential (blue) and bi-exponential (red) function. The corresponding residuals of both fits are shown at the bottom of each diagram. For each microgel, the solvent-jump was performed three times and the results were averaged.

Overview samples

Overview of samples investigated within this thesis. For each, the sample codes, composition, and size are listed and an exemplary image (if available) is shown.

Table A2: Overview of macroscopic PNIPAM gels investigated in Chapter 4.

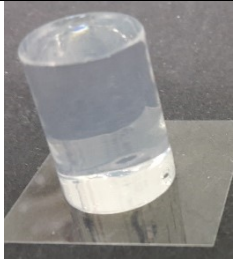
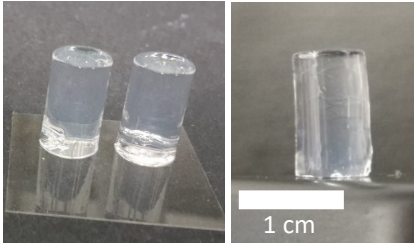
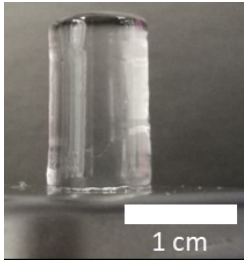
Lab book code	Composition Diameter in water	Photograph (cover slip: 22 x 22 mm)
KN-H64 to -H70 KN-H91 to -H100	NIPAM BIS (5 mol%) Macrogels from 48 well plate	
KN-H32 to -H38	NIPAM BIS (5 mol%) Macrogels from 96 well plate	
KN-H125 and -H126	NIPAM BIS (1 mol%) Macrogels from 48 well plate	
KN-H131 and -H135	NIPAM BIS (1 mol%) Macrogels from 96 well plate	

Table A3: PNIPAM-based microgel beads investigated in Chapter 5.

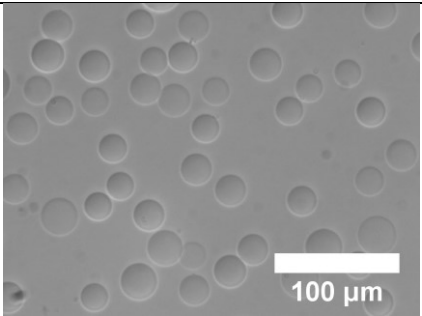
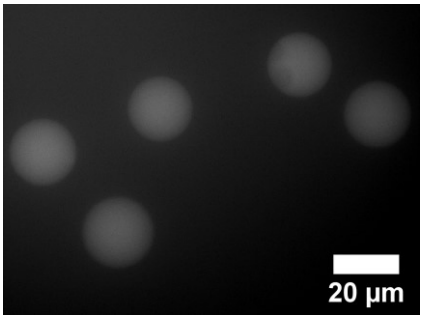
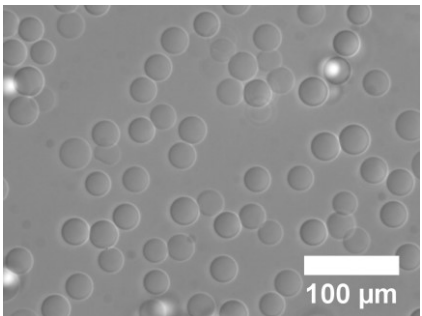
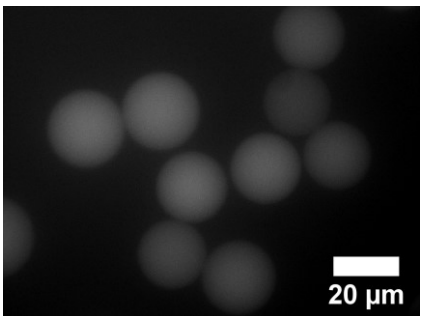
Lab book code SFB Sample Management Thesis code	Composition Diameter	Image
KN-MF33 SFB985_B3_KN_M000263 MG-PNIPAM-APMA-3	NIPAM BIS (5 mol%) APMA (3 mol%) $25 \pm 3 \mu\text{m}$ (water)	
KN-MF33-NR SFB985_B3_KN_M000296 MG-PNIPAM-APMA-3-NR	NIPAM BIS (5 mol%) APMA (3 mol%) Nile Red labeled $23 \pm 3 \mu\text{m}$ (MeOH)	
KN-MF34 SFB985_B3_KN_M000264 MG-PNIPAM-APMA-1	NIPAM BIS (5 mol%) APMA (1 mol%) $26 \pm 2 \mu\text{m}$ (water)	
KN-MF34-NR2 SFB985_B3_KN_M000297 MG-PNIPAM-APMA-1-NR	NIPAM BIS (5 mol%) APMA (1 mol%) Nile Red labeled $22 \pm 2 \mu\text{m}$ (MeOH)	

Table A4: PNIPAM microgel beads investigated in Chapter 7.

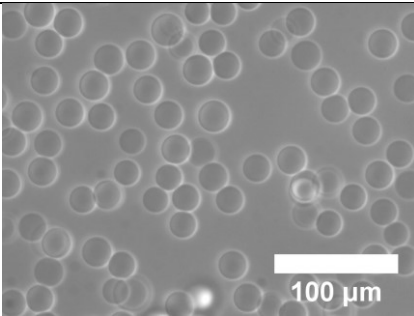
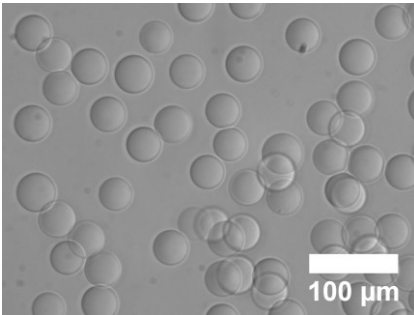
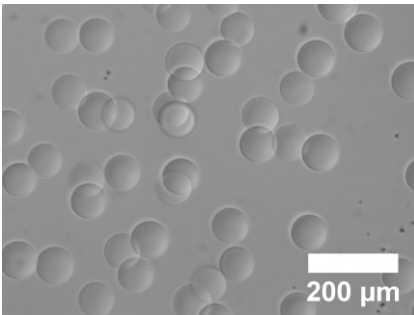
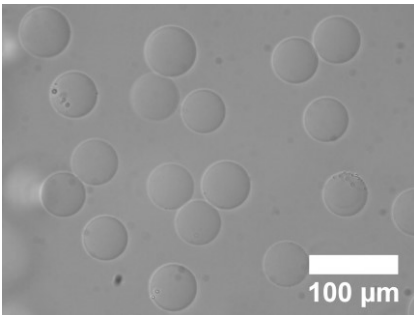
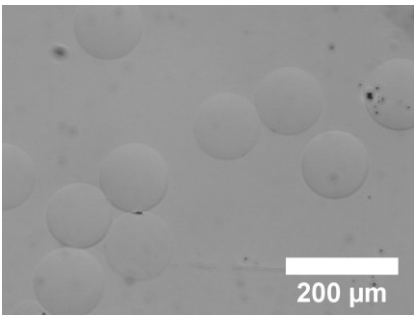
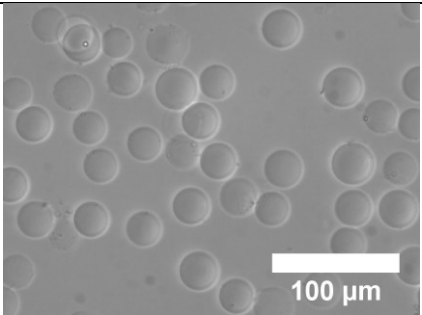
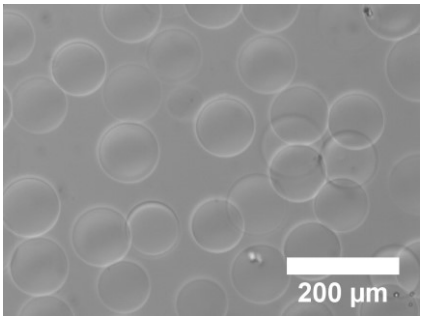
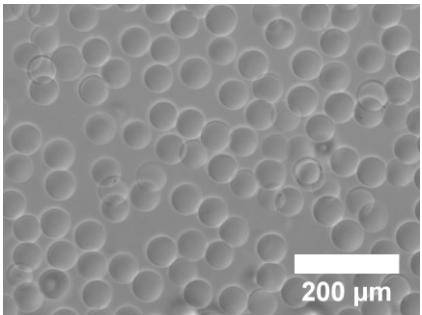
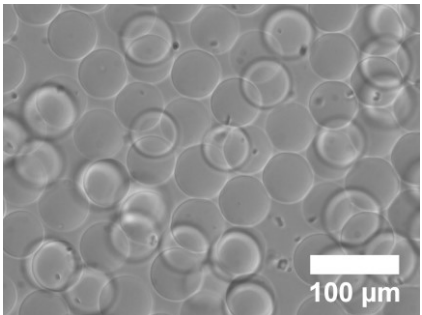
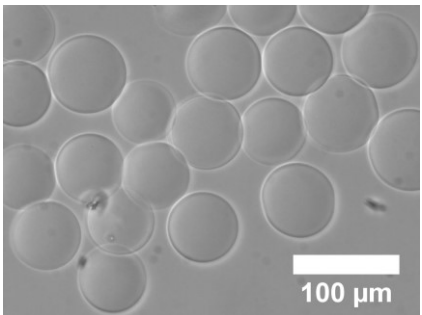
Lab book code SFB Sample Management Thesis code	Composition Diameter in water	Image
KN-MF30 SFB985_B3_KN_M000504 MG-5-S	NIPAM BIS (5 mol%) $22 \pm 2 \mu\text{m}$	
KN-MF39 SFB985_B3_KN_M000605 MG-5-M	NIPAM BIS (5 mol%) $39 \pm 2 \mu\text{m}$	
KN-MF40b SFB985_B3_KN_M000606 MG-5-L	NIPAM BIS (5 mol%) $79 \pm 4 \mu\text{m}$	
KN-MF41 SFB985_B3_KN_M000607 MG-1.2-M	NIPAM BIS (1.2 mol%) $49 \pm 2 \mu\text{m}$	
KN-MF42 SFB985_B3_KN_M000608 MG-1.2-L	NIPAM BIS (1.2 mol%) $109 \pm 6 \mu\text{m}$	

Table A5: PNIPAM-based microgel beads investigated in Chapter 8.

Lab book code SFB Sample Management	Composition Diameter in water	Image
KN-MF23 SFB985_B3_KN_M000262	NIPAM BIS (5 mol%) MTRB (< 0.1 mol%) $28 \pm 3 \mu\text{m}$	 Micrograph showing numerous small, spherical microgel beads. A scale bar in the bottom right corner indicates 100 μm.
KN-SM5 SFB985_B3_KN_M000497	NIPAM BIS (5 mol%) MTRB (< 0.1 mol%) $100 \pm 5 \mu\text{m}$	 Micrograph showing numerous medium-sized, spherical microgel beads. A scale bar in the bottom right corner indicates 200 μm.
KN-SM7 SFB985_B3_KN_M000498	NIPAM BIS (5 mol%) MTRB (< 0.1 mol%) $54 \pm 4 \mu\text{m}$	 Micrograph showing numerous medium-sized, spherical microgel beads. A scale bar in the bottom right corner indicates 200 μm.
KN-SM9 SFB985_B3_KN_M000499	NIPAM BIS (5 mol%) MTRB (< 0.1 mol%) $53 \pm 2 \mu\text{m}$	 Micrograph showing numerous medium-sized, spherical microgel beads. A scale bar in the bottom right corner indicates 100 μm.
KN-SM13 SFB985_B3_KN_M000502	NIPAM BIS (5 mol%) MTRB (< 0.1 mol%) $70 \pm 4 \mu\text{m}$	 Micrograph showing numerous medium-sized, spherical microgel beads. A scale bar in the bottom right corner indicates 100 μm.

Continuation Table A5.

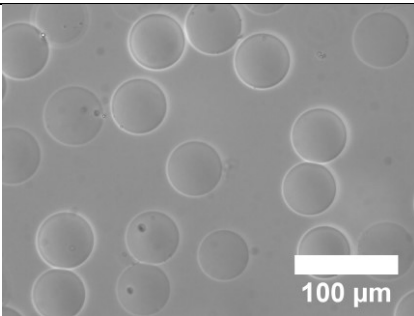
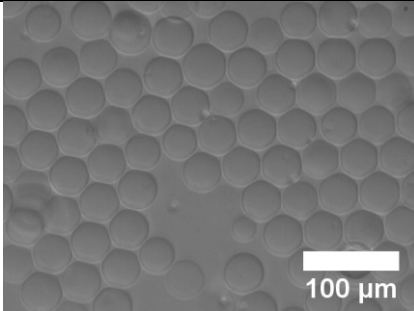
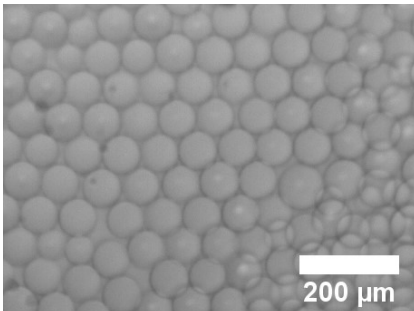
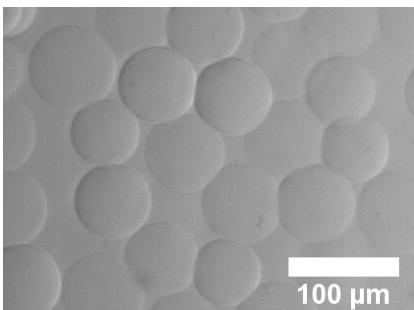
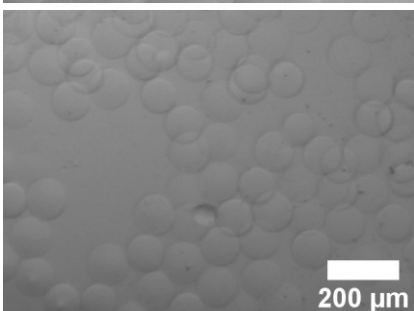
Sample Codes: Lab book SFB Sample Management	Composition Diameter in water	Image
KN-AM14 SFB985_B3_KN_M000589	NIPAM BIS (5 mol%) MTRB (< 0.1 mol%) $55 \pm 3 \mu\text{m}$	

Table A6: PNIPAM microgel beads used for single, complementary measurements. These samples were already synthesized during my master thesis.^[333]

Lab book code SFB Sample Management In this thesis	Composition Diameter in water	Image
KN-MF17 SFB985_B3_KN_M000260 Thesis: Figure 8.2	NIPAM BIS (5 mol%) $45 \pm 2 \mu\text{m}$	 Micrograph showing a dense packing of spherical PNIPAM microgel beads. A white scale bar in the bottom right corner indicates 100 μm.
KN-MF17b SFB985_B3_KN_M000261 Thesis: Figure 1.3, Figure 8.6d and Figure A5	NIPAM BIS (5 mol%) $78 \pm 2 \mu\text{m}$	 Micrograph showing spherical PNIPAM microgel beads. A white scale bar in the bottom right corner indicates 200 μm.
KN-MF20 SFB985_B3_KN_M000620 Thesis: Figure 8.9a	NIPAM BIS (1 mol%) $67 \pm 3 \mu\text{m}$	 Micrograph showing spherical PNIPAM microgel beads. A white scale bar in the bottom right corner indicates 100 μm.
KN-MF21 SFB985_B3_KN_M000621 Thesis: Figure 8.9b	NIPAM BIS (1 mol%) $113 \pm 4 \mu\text{m}$	 Micrograph showing spherical PNIPAM microgel beads. A white scale bar in the bottom right corner indicates 200 μm.

Acknowledgements

Here, I would like to thank the many people who have helped me, in so many different ways, during this thesis.

First and foremost, I want to thank Walter for the opportunity to do my thesis in his group. I am very grateful for the guidance and great scientific and personal support within the last years, but also the freedom I had in my work. Furthermore, I thank him for the many constructive discussions and the opportunity to attend conferences and courses.

Special thanks go to André Bardow for agreeing to be the second referee of my thesis and for his fruitful insights regarding my work. Additionally, I would like to thank Thorsten Brands, David Müller, and Rico Keidel for many helpful discussions of our joint SFB B3 project.

I greatly enjoyed my time at the IPC (Institute of Physical Chemistry) and would like to thank all my colleagues and former colleagues from the institute and the SFB 985 for the good working atmosphere. I want to thank Denise Kleinschmidt and Andrea Scotti for the good cooperation and feedback on joint projects. I would like to thank Silvia Centeno Benigno and Dominik Wöll for our joint work on solvatochromic microgels and for performing the fluorescence spectroscopy measurements. Moreover, I want to express my gratitude to the people from DWI (Leibniz-Institute for Interactive Materials), particularly Alex Jans and Luis Busca Guerzoni, as well as Arne Lüken from the AVT (Aachener Verfahrenstechnik) for sharing their experiences and the support regarding microfluidics. I also want to thank Thorsten Brands, Hans-Jürgen Koß, David Müller, Carsten Flake, Julia Thien, and others from the LTT (Institute of Technical Thermodynamics) for their help on Raman spectroscopy and indirect hard modeling. I always felt welcomed and luckily enjoyed the one or other coffee when measuring Raman at the LTT. I thank AK Wöll for their support regarding the confocal fluorescence microscopy measurements. Further, thanks go to the students Sonja Mürtz, Yannick Tschauder, and in particular my long-term student assistant Anna Meyer.

A tremendous thank you goes to my (extended) office mates Bine, Sarah, and Anne. I could not have imagined better – even the bad days became fun with you. I would like to thank the three of them and Frieda for the time we spent together in sports classes. I also thank Bine, Sarah, Anne, Frieda, Max, Monia, Eric, Steffen, Andrea S., Andrea M., Dominik, Christian, and the rest of AK Richtering and AK Wöll not only for great scientific discussions and the productive working atmosphere, but also for Friday after-work beers, spontaneous dinners, group trips, Christmas parties, and especially a lot of cakes.

I thank Silvia Centeno Benigno, Andrea Scotti, Thorsten Brands, and David Müller for critically reviewing the chapters concerning our joint projects and the chapter on Raman spectroscopy and microfluidics. I deeply thank Bine, Silke, and my mum for proofreading my thesis.

I thank everyone who has helped me in any way during this time and apologize if I forgot to mention someone personally. Finally, I want to thank my family and friends for the great and continuous support during my studies, my dissertation, and beyond.

– Thank you!

Publications

- Nothdurft, K.; Müller, D. H.; Mürtz, S. D.; Meyer, A. A.; Guerzoni, L. P. B.; Jans, A.; Kühne, A. J. C.; De Laporte, L.; Brands, T.; Bardow, A.; Richtering, W., Is the Microgel Collapse a Two-Step Process? Exploiting Cononsolvency to Probe the Collapse Dynamics of Poly-*N*-isopropylacrylamide (PNIPAM). *J. Phys. Chem. B* **2021**, *125*, 1503-1512.
- Kleinschmidt, D.; Nothdurft, K.; Anakhov, M. V.; Meyer, A. A.; Mork, M.; Gumerov, R. A.; Potemkin, I. I.; Richtering, W.; Pich, A., Microgel organocatalysts: modulation of reaction rates at liquid–liquid interfaces. *Mater. Adv.* **2020**, *1*, 2983-2993.
- Nothdurft, K.; Müller, D. H.; Brands, T.; Bardow, A.; Richtering, W., Enrichment of methanol inside PNIPAM gels in the cononsolvency-induced collapse. *Phys. Chem. Chem. Phys.* **2019**, *21*, 22811-22818.
- Jabłońska, M.; Nothdurft, K.; Nocuń, M.; Girman, V.; Palkovits, R., Redox-performance correlations in Ag–Cu–Mg–Al, Ce–Cu–Mg–Al, and Ga–Cu–Mg–Al hydrotalcite derived mixed metal oxides. *Appl. Catal. B* **2017**, *207*, 385-396.
- Thérien-Aubin, H.; Wang, Y.; Nothdurft, K.; Prince, E.; Cho, S.; Kumacheva, E., Temperature-Responsive Nanofibrillar Hydrogels for Cell Encapsulation. *Biomacromolecules* **2016**, *17*, 3244-3251.
- Dubbert, J.; Nothdurft, K.; Karg, M.; Richtering, W., Core–Shell–Shell and Hollow Double-Shell Microgels with Advanced Temperature Responsiveness. *Macromol. Rapid Commun.* **2015**, *36*, 159-164.

Conferences

- 2nd Joint Summer School SFB 985 & Georgia Institute of Technology, Monschau, *Poster presentation* (July 2018)
- 255th ACS National Meeting, New Orleans, USA, *Poster presentation* (March 2018)
- Kolloid-Tagung “Multiresponsive systems”, Garching, *Poster presentation* (October 2017)

Courses

October 2020	Project Management (Methods and Instruments of Project Management)
October 2020	2020 Virtual Symposium on Microgels
September 2019	Good Scientific Practice
April 2019	Grundlagen der BWL
January 2018 – January 2019	TANDEMdok mentoring program of RWTH Aachen University
December 2017	Grundlagen des wissenschaftlichen Vortragens
December 2017	Zeitmanagement und Planungstechniken für das Promotionsvorhaben
October 2017	Designing Interdisciplinary Research Processes

Supervised students

Anna Meyer – *Student assistant* (2019 – 2020, ~ 1.5 years), Synthesis of microgels with various compositions via microfluidics, size evaluation under equilibrium conditions and dynamic investigations of the cononsolvency-induced collapse

Sonja Mürtz – *Research project* (2019), Fluorescent microgels synthesized by microfluidics and their cononsolvency behavior

Yannick Tschauder – *Bachelor thesis* (2018), Microfluidic synthesis of microgels and their cononsolvency behavior

Eidesstattliche Erklärung

Katja Nothdurft erklärt hiermit, dass diese Dissertation und die darin dargelegten Inhalte die eigenen sind und selbstständig, als Ergebnis der eigenen originären Forschung, generiert wurden.

Hiermit erkläre ich an Eides statt:

1. Diese Arbeit wurde vollständig oder größtenteils in der Phase als Doktorand dieser Fakultät und Universität angefertigt;
2. Sofern irgendein Bestandteil dieser Dissertation zuvor für einen akademischen Abschluss oder eine andere Qualifikation an dieser oder einer anderen Institution verwendet wurde, wurde dies klar angezeigt;
3. Wenn immer andere eigene- oder Veröffentlichungen Dritter herangezogen wurden, wurden diese klar benannt;
4. Wenn aus anderen eigenen- oder Veröffentlichungen Dritter zitiert wurde, wurde stets die Quelle hierfür angegeben. Diese Dissertation ist vollständig meine eigene Arbeit, mit der Ausnahme solcher Zitate;
5. Alle wesentlichen Quellen von Unterstützung wurden benannt;
6. Wenn immer ein Teil dieser Dissertation auf der Zusammenarbeit mit anderen basiert, wurde von mir klar gekennzeichnet, was von anderen und was von mir selbst erarbeitet wurde;
7. Teile dieser Arbeit wurden zuvor veröffentlicht und zwar in:

Nothdurft, K.; Müller, D. H.; Brands, T.; Bardow, A.; Richtering, W., *Phys. Chem. Chem. Phys.* **2019**, *21*, 22811-22818.

Nothdurft, K.; Müller, D. H.; Mürtz, S. D.; Meyer, A. A.; Guerzoni, L. P. B.; Jans, A.; Kühne, A. J. C.; De Laporte, L.; Brands, T.; Bardow, A.; Richtering, W., *J. Phys. Chem. B* **2021**, *125*, 1503-1512.

Kleinschmidt, D.; Nothdurft, K.; Anakhov, M. V.; Meyer, A. A.; Mork, M.; Gumerov, R. A.; Potemkin, I. I.; Richtering, W.; Pich, A., *Mater. Adv.* **2020**, *1*, 2983-2993.